technische universität
dortmund

mpi

Biochemical studies of spindle assembly checkpoint components

Zur Erlangung des akademischen Grades
Doktor der Naturwissenschaften (Dr. rer. nat.)

der Fakultät für Chemie und Chemische Biologie
der Technischen Universität Dortmund

angefertigt am
Max-Planck-Institut für molekulare Physiologie

Dissertation

von

Claudia Verena Breit

November, 2015

Die vorliegende Arbeit wurde in der Zeit von November 2011 bis November 2015 am Max-Planck-Institut für molekulare Physiologie in Dortmund unter der Anleitung von Prof. Dr. Andrea Musacchio durchgeführt.

1. Gutachter: Prof. Dr. Andrea Musacchio
2. Gutachter: Prof. Dr. Daniel Rauh

In the context of this doctoral work the following article was accepted for publication

- Claudia Breit, Tanja Bange, Arsen Petrovic, John R. Weir, Franziska Müller, Doro Vogt & Andrea Musacchio. "Role of intrinsic and extrinsic factors in the regulation of the mitotic checkpoint kinase Bub1." *accepted for publication* (PLOS ONE, 2015).

Contents

List of Abbreviations

ADP	Adenosine-5'-diphosphate
AppNHp	Adenosine-5'-[(β,γ)-imido]-triphosphate
APS	Ammonium persulfate
ATP	Adenosine-tri-phosphate
ATPγS	Adenosine-5'-(3-thio)-triphosphate
BSA	Bovine serum albumine
DMSO	Dimethyl sulfoxide
DSS	Disuccinimidyl suberate
DTE	Dithioerythritol
EDTA	Ethylenediaminetetraacetic acid
EMSA	Electrophoretic mobility shift assay
EtOH	Ethanol
FCS	Fetal calf serum
FPLC	Fast protein liquid chromatography
HEPES	4-(2-Hydroxyethyl)-piperazine-1-ethanesulfonic acid
IPTG	Isopropyl-β-D-thiogalactopyranoside
mant	2'-/3'-O-(N'-Methylanthraniloyl)
MEF	Mouse embryonic fibroblast
MeOH	Methanol
MES	2-(N-morpholino)-ethanesulfonic acid
NaAc	Sodium acetate
OD	Optic density
PAGE	Polyacrylamide gelelectrophoresis
PBS	Phosphate buffered saline
PCR	Polymerase chain reaction

PEG	Polyethylene glycol
PMSF	Phenylmethylsulfonyl fluoride
SDS	Sodium dodecyl sulfate
Sf9	Spodoptera frugiperda
TAE	Tris-acetate-EDTA
TCEP	Tris-(2-carboxyethyl)-phosphine
TEMED	Tetramethylethylenediamine
TEV	Tobacco etch virus
TFA	Trifluoroacetic acid
TLS	Translation libration screw
Tnao38	Trichoplusia ni 38
Tris	Tris-(hydroxymethyl)-aminomethane
X-Gal	5-bromo-4-chloro-3-indolyl-β-D-galactopyranoside

Amino acids and nucleobases were consistently referred to as their respective one-letter or three-letter codes in compliance with the recommendations of the International Union of Pure and Applied Chemistry (IUPAC) and the International Union of Biochemistry and Molecular Biology (IUB).

Summary

During cell division cells must ensure that their chromatids are equally distributed onto the resulting daughter cells in order to maintain their ploidy. The spindle assembly checkpoint (SAC) is an intricate mechanism in mitosis that monitors correct attachment of the spindle apparatus to kinetochores, a complex protein structure on the centromeric region of chromosomes. Two components of the SAC machinery, the Bub1 and BubR1 kinases, are protein paralogs originating from a common ancestor gene that underwent gene duplication and was then subject to significant functional specialisation during evolution. Bub1 is a key player at the kinetochore due to its role in recruiting additional checkpoint proteins including BubR1. In contrast, BubR1 is an integral part of the SAC effector, the mitotic checkpoint complex (MCC). The kinase activity of Bub1 is further implied in regulating chromosome congression and alignment, while BubR1 kinase activity remains a matter of debate. The assessment of the mechanism of Bub1 regulation and the characterisation of Bub1 interactions at the kinetochore, particularly with respect to their implications for Bub1 kinase activity, formed the main focus of this dissertation.

The reconstitution of Bub1:Bub3 and BubR1:Bub3 complexes is reported in this thesis, along with a hydrodynamic characterisation that demonstrates both complexes to have 1:1 stoichiometry, without additional oligomerisation. As both dimeric complexes are shown to bind to each other, the resulting complex can be stably assembled on a phosphorylated fragment of Knl1, the kinetochore receptor of Bub1:Bub3. The work presented in this thesis also highlights the importance of a site in the middle region on Bub1 for the additional recruitment of another checkpoint component, Cdc20, which forms the basis for MCC assembly.

The comprehensive characterisation of the kinase domains of Bub1 and BubR1 described in this thesis resolves conflicting reports of kinase activity and shows that BubR1 kinase domain binds nucleotides, but is unable to deliver catalytic activity *in vitro*. Conversely, Bub1 is an active kinase that undergoes autophosphorylation on the P+1 substrate-binding loop, which is crucial in conferring Bub1 activity. Neither BubR1:Bub3 nor Knl1 modulate the kinase activity of Bub1 *in vitro*, suggesting the Bub1 kinase domain is regulated autonomously by autophosphorylation. The crystal structure of the phosphorylated Bub1 kinase domain presented here illustrates a hitherto unknown conformation of the P+1 loop docked into the active site of the Bub1 kinase. This conformation provides deeper insight into the mechanism of Bub1 kinase activation, which involves the structural rearrangement of the P+1 loop upon phosphorylation.

The work of this thesis is complemented with an analysis of the kinetochore substrates of Bub1 and for the first time identifies a common sequence motif on the substrates of Bub1 kinase. The discovery of highly conserved residues on Bub1 kinase indicates a functional surface implicated in substrate binding. Further findings suggest that DNA binding might additionally aid in directing Bub1 to nucleosomes. In the context of the current literature, the results reported in this dissertation contribute to a more profound understanding of Bub1 kinase activity from a structural and mechanistic point of view.

Zusammenfassung

Während der Zellteilung muss die Zelle sicherstellen, dass das genetische Material der Chromosomen, in Form von Chromatiden, gleichmäßig auf beide Tochterzellen aufgeteilt wird. Dieser Prozess ist entscheidend für die genetische Integrität der Zelle, da Ungleichverteilung der Chromatiden zu Zellanomalien und damit Störung des Organismus führen kann. Der mitotische Kontrollpunkt (englisch: *spindle assembly checkpoint, SAC*) bezeichnet einen komplexen zellulären Apparat dessen Aufgabe es ist zu gewährleisten, dass alle Chromosomen an der mitotischen Spindel angeheftet sind. Dies erfolgt über vielschichtige Proteinstrukturen, die sogenannten Kinetochore. Zwei essentielle Bestandteile der Kontrollpunkt-Maschinerie sind die Proteinkinasen Bub1 und BubR1, die funktionelle Paraloge darstellen, welche sich durch Genverdoppelung evolutiv in verschiedene Richtungen spezialisiert haben. Bub1 ist ein essentieller Grundbaustein der Kinetochorarchitektur, da es weitere Proteine, unter anderem BubR1, rekrutiert. Im Gegensatz dazu ist BubR1 ein Bestandteil des Kontrollpunkt-Effektorkomplex. Die enzymatische Aktivität von Bub1 ist wichtig für die Regulation der Zusammenkunft und Orientierung der Chromosomen am Zelläquator während der Mitose. Eine enzymatische Aktivität von BubR1 ist hingegen nicht eindeutig nachgewiesen. Den Umfang dieser Arbeit bilden die Untersuchung sowie Charakterisierung der Bub1 Regulationsmechanismen und Interaktionen am Kinetochor, insbesondere in Bezug auf deren Auswirkung auf die enzymatische Aktivität von Bub1.

Die in dieser Dissertation dargestellte Rekonstitution von Bub1:Bub3 und BubR1:Bub3 Proteinkomplexen ermöglichte deren Charakterisierung als stöchiometrische 1:1 Komplexe. Desweiteren konnte gezeigt werden, dass diese Proteinkomplexe sowohl aneinander binden, als auch an ihren Kinetochorrezeptor, das Protein Knl1, gekoppelt werden können. Ferner konnte eine Region innerhalb von Bub1 bestimmt werden, die ausschlaggebend für die Bindung von Cdc20 ist und damit die Grundlage für die Zusammensetzung des Effektorkomplexes des Kontrollpunkts darstellt.

Die detaillierte Beschreibung der Kinasedomänen von Bub1 und BubR1 ermöglichte die Auflösung der bestehenden Kontroverse bezüglich der Kinaseaktivität von BubR1; zwar bindet BubR1 Nukleotide, es kann aber kein Phosphat auf Substratproteine übertragen. Im Gegensatz dazu ist Bub1 eine aktive Kinase, die ihre Substratbindungsschleife (P+1 Schleife) intramolekular phosphoryliert, was den wesentlichen Schritt der Kinaseaktivierung darstellt. Weder BubR1:Bub3, noch Knl1 beeinflussen die Bub1 Kinaseaktivität *in vitro*, was nahelegt, dass die Bub1 Kinasedomäne allein durch Autophosphorylierung reguliert wird. Die Kristallstruktur der phosphorylierten Bub1 Kinasedomäne, die innerhalb dieser Dissertation beschrieben wird, zeigt eine bisher unbekannte Konformation der Substratbindungsschleife, wobei diese im aktiven Zentrum von Bub1 verankert ist. Diese Konformation erlaubt Rückschlüsse auf den Aktivierungsmechanismus von Bub1, der eine strukturelle Umordnung in Folge der Phosphorylierung des P+1 Segments beinhaltet.

Die Analyse von Bub1 Kinetochorsubstraten ermöglichte es, erstmalig ein spezifisches Aminosäuresequenzmotiv von Bub1 Substraten zu identifizieren. Die Oberfläche der Bub1 Kinase offenbart ferner evolutionär stark konservierte Aminosäuren, welche in die Interaktion mit Proteinsubstraten involviert sind. Im Kontext mit der aktuellen Literatur leisten die im Rahmen dieser Dissertation gewonnenen Ergebnisse einen fundamentalen Beitrag zu einem tiefergehenden Verständnis der strukturellen und mechanistischen Regulierung der mitotischen Kinase Bub1.

1 Introduction

Life in its simplest form originates from a single cell. During the course of evolution, a multitude of multicellular organisms and species developed by replication of cellular units into various highly differentiated cells. While the reproduction of single cells is required for germ line development and ultimately continuation of a species, the same species also possesses multiple somatic cells which need to proliferate in order to assemble an entire organism. Generally, cells differentiate and enter a state of quiescence, whereas continuous or uncontrolled cell duplication constitutes pathological behaviour, culminating in cancer. Remarkably, regardless of the actual cell type (somatic or germ line) or the number of cells constituting an organism, the mechanism by which cells propagate remains largely identical. Every single cell needs to comply with the same criteria in order to reproduce, which is controlled in a process called cell division or mitosis.

1.1 Basic principles of cell division

1.1.1 The cell cycle

Cell division is a highly regulated process, which poses an organisational challenge for the cell [1, 2] as it comprises the conversion of one cell into two, creating viable and genetically identical progeny. Division of a cell requires the precise duplication (S-phase) and segregation of genetic material (M-phase or mitosis) [1, 2], schematically depicted in Figure 1.1. The driving force of this process is the activity of tightly regulated **C**yclin-**d**ependent **k**inases (Cdks) that phosphorylate a number of targets, which results in pronounced changes in nuclear and cytoskeletal cell architecture. The activity of Cdks is controlled in a timely and ordered fashion by individual proteins (cyclins) that allow oscillating cell cycle-stage specific regulation at three distinct points of the cell cycle.

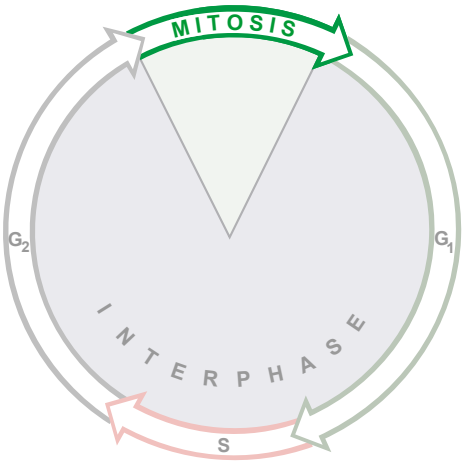

Figure 1.1: The cell cycle.
The phase termed interphase or G_0, shaded in grey, begins with a gap phase G_1, followed by S-phase where the cell duplicates its genetic material, gains size and replicates its genetic material and organelles, leading to another gap phase G_2, and ultimately to a phase of cell division (mitosis), creating two identical daughter cells. Importantly, both entry into S-phase and mitosis but also mitosis itself are controlled by cellular checkpoints ensuring the fidelity of cell division.

In vertebrates, cyclin E and A trigger and regulate the entry into synthesis (S-) phase; after passing a DNA damage checkpoint, the chromosomes replicate, producing two identical copies of the genetic material and its associated proteins. The gap phases G_1 and G_2 between S- and M-phase allow time for cell growth and metabolism, the duplication of organelles and monitoring of the external environment. Progressing through the G_2 checkpoint that selects for correctly duplicated chromosomes and favourable conditions is governed by cyclin B (see also Figure 1.8), which allows entry into mitosis (M-

phase). Mitosis is an elaborate multi-step process where chromosomes are segregated from each other, followed by cell division (cytokinesis) [3, 4]. Importantly, mitosis is also subject to a checkpoint, the mitotic checkpoint or spindle assembly checkpoint (see also Section 1.4). This checkpoint acts in metaphase, monitoring correct spindle assembly and chromosome attachment, thereby ensuring error-free cell division and maintenance of ploidy, which is a hallmark of genome stability.

1.1.2 Mitosis

Fibrillar structures of the spindle were first described in 1882 by the German anatomist Walther Flemming, which led to the term mitosis, derived from the greek μίτος (*mítos*, thread). Mitosis describes the process of nuclear division and has ever been a very active research topic in cell biology. It still strives to characterise the main players and general mechanisms that drive accurate chromosome segregation and define cell division.

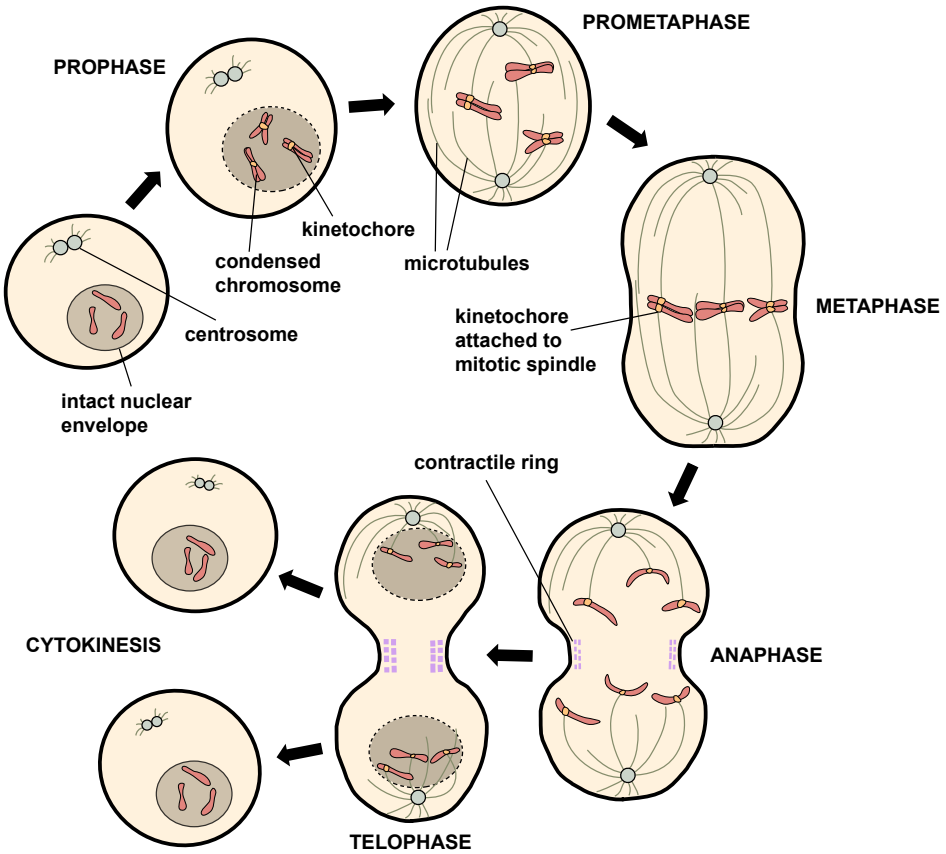

Figure 1.2: Schematic cycle of mitosis.
Mitotic division consists of 5 distinct phases followed by cytokinesis. They are defined by the condensation of sister chromatids (prophase) that become attached to the mitotic spindle after nuclear envelope breakdown (prometaphase). Chromosomes are bi-oriented and aligned on the spindle equator by the mitotic spindle (metaphase). Elimination of sister chromatid cohesion initiates movement of sister chromatids to opposite poles of the spindle (anaphase). Chromosomes are then packaged into separate nuclei while a contractile ring divides the cell in the final step of mitosis (telophase) resulting in two identical daughter cells (cytokinesis).

Mitosis can be divided into five distinct phases (Figure 1.2) and subsequent cytokinesis. In prophase, chromosomes are condensed into a compact shape by a protein complex called condensin [5], while the spindle apparatus starts forming from centrosomes. Prometaphase is defined by nuclear envelope breakdown and initiation of chromosome attachment to the spindle microtubules by large protein assemblies on the centromere, known as kinetochores. During metaphase, the chromosomes are aligned at the so-called metaphase plate between both spindle poles, allowing bi-orientation of chromosomes, which signifies that both sister chromatids are connected to spindle microtubules emanating from opposite spindle poles. Sister chromatids are held together by the protein complex cohesin [6] that is cleaved by separase, thus triggering anaphase and the segregation of chromosomes towards opposite spindle poles. At telophase, the two sets of chromosomes decondense and a new nuclear envelope is assembled, completing the process of mitosis. A contractile ring forms, leading to the division of the cytoplasm and ultimately to cytokinesis.
The accuracy of mitotic events is crucial for cell viability. Errors during the duplication and separation of chromosomes cause birth defects due to aberrations of the chromosome number (aneuploidy) in haploid germ cells. Aneuploidy can further contribute to the onset and progression of cancer in somatic cells [7, 8].

1.2 Kinetochore organisation and function

The first report of structures responsible for chromosome movement appeared in 1894, describing the *'Leitkörper'* ('the leading body') at the interface between chromosomes and the mitotic spindle in salamander spermatocytes [9]. This structure is now known as the kinetochore, which is derived from the greek κίνησις (*kinesis*, movement) and χώρος (*choros*, place or region). Kinetochores are characterised as the functional connection between two biological polymers, DNA and microtubules that is required to allow the partitioning of chromatids by the mitotic spindle apparatus.

1.2.1 The structural composition of kinetochores

Kinetochores are large assemblies of nearly 100 proteins that follow a hierarchical order to attain a connection of chromosomal DNA with spindle microtubules [12, 13]. The impressive number of protein components reflects the level of intricacy and versatility of the process of chromosome segregation. Kinetochores are molecular machines that are tightly regulated and largely conserved from yeast to mammals, highlighting that the kinetochore architecture and function are conserved [14, 15]. Studies mostly based on protein knock-down or ectopic localisation experiments were used to elucidate conserved pathways and hierarchy of kinetochore assembly that are now increasingly corroborated by direct interactions identified by biochemical experiments.

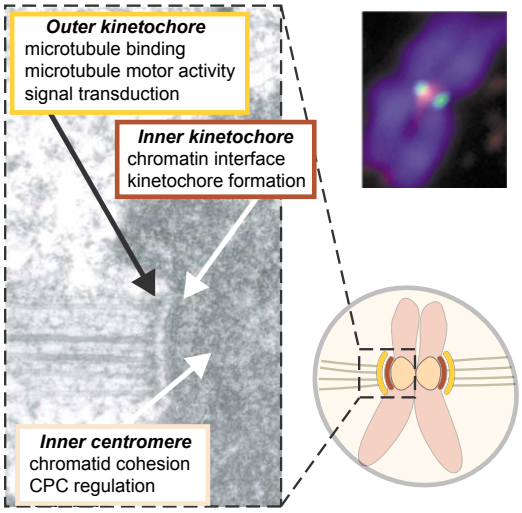

Figure 1.3: General structure of the centromere. Left, mitotic chromosome sectioned along the spindle plane axis, showing only one kinetochore attached to microtubules emanating from the left. Key structural elements are indicated by arrows. The inner centromere, locus of chromatid pairing, cohesion and error correction links outer kinetochore to chromatin via the inner kinetochore. The outer kinetochore, the site of microtubule binding, also regulates microtubule dynamics and checkpoint signalling. The interzone between inner and outer kinetochore is proposed to harbour tension receptors and contribute to checkpoint signalling; modified from [10]. Upper right: mitotic chromosome stained for DNA (blue), kinetochores (green) and cohesin (red), which is required for sister chromatid cohesion until anaphase [11]. Lower right: schematic view of a chromosome attached to the mitotic spindle.

In few organisms including some fungi and *Saccharomyces cerevisiae*, the kinetochore position is defined by a highly conserved 125 bp stretch of DNA, termed point-centromere [15, 16], which anchors a single microtubule [17]. This arrangement differs from the organisation in fission yeast or vertebrates, where centromeres span between kilo- to megabase regions (regional centromeres) [10, 18] that attach to a bundle of 15-20 microtubules [19] or expands along the entire chromosome length as in *Caenorhabditis elegans* (holocentric kinetochores) [20]. In the latter cases the location of the centromeres is thought to be determined by epigenetic marks or the centromere-specific histone CENP-A rather than specific DNA-sequences [21, 22].

The kinetochore is composed of several distinct layers that were first observed in the late 1960s by electron microscopy. A more detailed structure of kinetochores has been observed nearly 40 years later revealing a trilaminar structure [23], where the inner and outer layers are electron dense, separated by an electron-lucent mid-zone (Figure 1.3). This modular assembly (observed in Figure 1.3 and schematically depicted in Figure 1.4) is organised into larger functional sub-complexes that are commonly, yet tentatively, categorised into four parts.

(1) The inner centromere comprises microtubule-associated or -tracking proteins and an error correction module including the **c**hromosomal **p**assenger **c**omplex (CPC) [24, 25] that regulates kinetochore-microtubule attachments [26] in a tension-dependent manner (discussed in more detail in Sections 1.3 and 1.4).

(2) The inner kinetochore or **c**onstitutive **c**entromere **a**ssociated **n**etwork (CCAN), which contains proteins binding to DNA or nucleosomes persists throughout the cell cycle providing a platform for the assembly of other proteins [27, 28] (Section 1.2.2).

(3) The outer kinetochore or **K**NL1-**M**IS12-**N**DC80 (KMN) network physically bridges between the inner centromere and microtubules (Section 1.2.3); it is visible as discrete electron dense layer in Figure 1.3.

(4) An additional soluble fraction or fibrous corona, which presumably comprises proteins of the spindle assembly checkpoint, is only visible during mitosis at unattached kinetochores. This mechanism synchronises the state of correct kinetochore-microtubule attachment with cell cycle progression. It is a feedback control system that delays anaphase onset until all sister chromatids are properly attached to opposite spindle poles, a detailed description of this process can be found in Section 1.4.

1.2.2 The constitutive centromere associated network (CCAN)

The discovery of inner kinetochores was initiated with the finding that autoimmune sera from patients affected by **c**alcinosis, **R**aynaud's syndrome, **e**sophageal dysmotility, **s**clerodactyly and **t**elangiectasia (CREST) syndrome recognised the centromere region [29]. This was later confirmed to be the inner kinetochore or constitutive centromere associated network, in the following denoted as CCAN, which constitutes the innermost layer of kinetochores as shown in Figure 1.4. CCAN components lack enzymatic activity, being indicative of the main role of the CCAN as a structural platform for the assembly of structural and regulatory microtubule-binding entities of the kinetochore.
The CCAN is a large protein network consisting of at least 16 sub-complexes (Figure 1.4) that are commonly referred to as **cen**tromeric **p**roteins (CENP), individually assigned with a letter. Many of its members were initially identified by proteomics or sequence analysis [15, 27, 28, 30]. Later, these findings were complemented by biochemical experiments to find that the CCAN is organised in sub complexes that build an ordered hierarchical structure.
The conserved hallmark that specifies the centromere and therefore the position of the CCAN is the presence of the CENP-A protein. As a centromere-specific variant of the canonical histone H3 [31], CENP-A is found in multiple nucleosomes along the centromere [32, 33, 34]. Recruitment of all inner and outer kinetochore proteins relies on CENP-A [35], demonstrating the key importance of CENP-A

as the building block for kinetochore assembly.
CENP-A containing nucleosomes directly interact with two CCAN components, namely CENP-C, a highly elongated protein and essential structural CCAN component [10, 36, 37] and CENP-N [38]. CENP-C has been identified as a receptor for a CENP-H/I/K/M sub-complex [38, 39]. The CENP-H/I/K/M complex is in turn required to recruit a third sub-complex containing the CENP-O/P/Q/R/U subunits [28, 30, 39, 40]. The generality of this assembly mechanism, however, is unclear, as only few CCAN proteins have been identified so far in *Caenorhabditis elegans* and *Drosophila melanogaster*. In these organisms, the inner kinetochore assembly seems to rely fully on CENP-A and -C molecules, which is consistent with the observation that most other CCAN subunits are not essential in *Saccharomyces cerevisiae* [41]. CENP-C is further important in the maintenance of kinetochore localisation as it is involved in replenishing CENP-A in centromeric nucleosomes [28, 42].

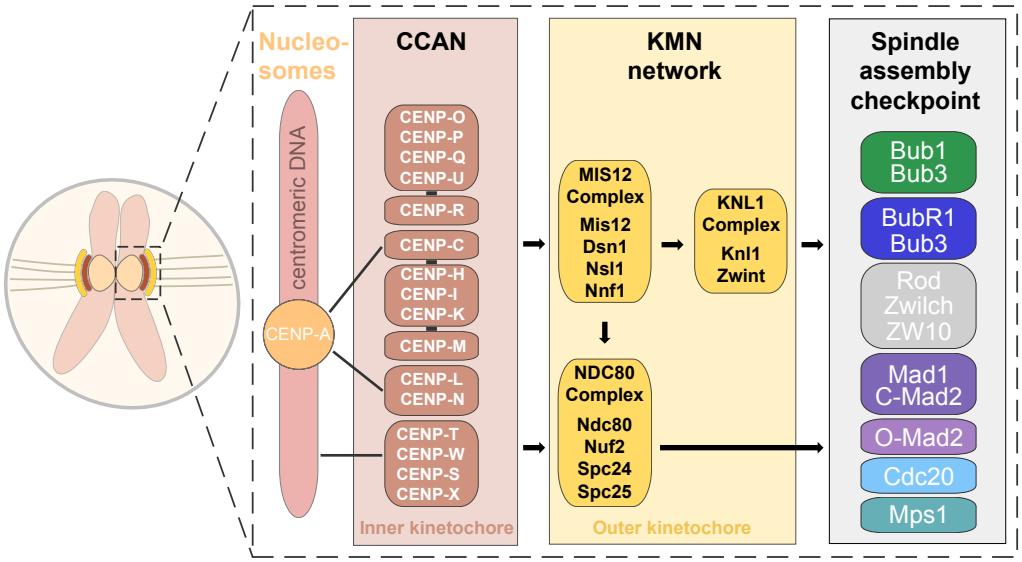

Figure 1.4: The modular organisation of the kinetochore structure.
Dashed lines indicate direct connections with centromeric DNA or chromatin. Continuous lines indicate recruitment dependencies. The composition of CCAN sub-complexes were inferred from reconstitution or from similarity of depletion phenotypes. For details see text, modified from [43].

The CENP-T/W/S/X complex consists of histone-fold domain-containing proteins that form a tightly interacting complex [27, 30] that is able to bind and supercoil DNA [44]. CENP-T and the CENP-H/I/K/M subunits were shown to be co-dependent for kinetochore localisation [30, 43, 45] placing them downstream of CENP-C. There is ongoing controversial discussion about whether the hierarchy of recruitment mostly relies on CENP-C or CENP-T [28, 30, 39, 40, 43, 45]. Speculatively, it is likely that the CENP-T and CENP-C pathway exhibit a certain degree of interdependence, which reconciles different hypotheses.
CENP-A, CENP-T/W, CENP-C, and CENP-H/I/K/M complexes were implicated to varying extents in contributing to the assembly of the outer kinetochore [30, 40, 46], as indicated in Figure 1.5. Both CENP-C and CENP-T are direct binders of nucleosomes or centromeric chromatin [36, 47] and interact with components of the outer kinetochore leading to a model where CENP-T and CENP-C

mediate outer kinetochore assembly from two different loci at the centromere in an interdependent pathway (Figure 1.5), which is described in more detail in Section 1.2.3.

1.2.3 The outer kinetochore KNL1-MIS12-NDC80 (KMN) network

The CCAN network provides a platform that specifically recognises the centromeric region of chromosomes, while the 10-subunit KMN (**K**NL1-**M**IS12-**N**DC80) network has been identified as the protein complex, which binds to this scaffold and allows direct interaction with kinetochore microtubules [48, 49]. Initial work was mostly performed in yeasts but shortly afterwards the KMN was shown to be highly conserved in other species as well [50, 51, 52, 53]. The main task of this network is to sustain and transmit forces emanating from microtubules of the mitotic spindle to the centromere and therefore to function as a tension-sensing machinery. Furthermore, this apparatus is able to monitor the microtubule attachment status and quality of attachment, in an effort to regulate the recruitment of both the correction machinery and the activation of the spindle assembly checkpoint [54, 55].

The KMN is linked to the inner kinetochore through direct interactions with the two CCAN components CENP-C and CENP-T that bind to the MIS12 complex and the NDC80 complex, respectively. In vertebrates, the conserved MIS12 complex localises to the inner plate of kinetochores, indistinguishable from CENP-A and -C [53], while Ndc80 localises to the outer plate (Figure 1.5). Thus, the arrangement of MIS12 complex and Ndc80 leads to a structure spanning from the inner centromere to the outer microtubule-binding interface.

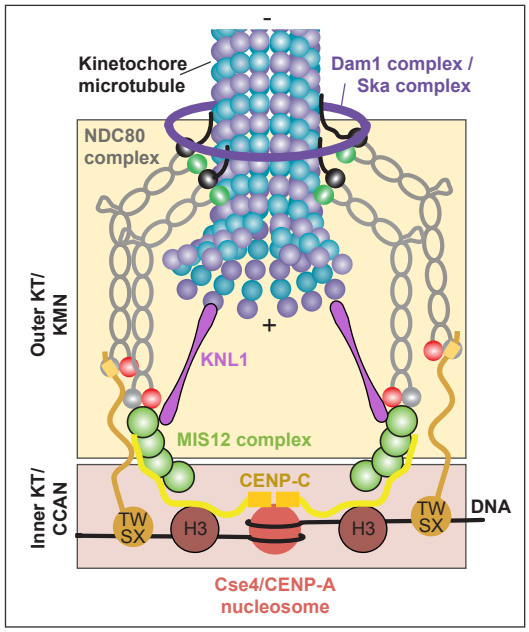

Figure 1.5: Schematic structural view of kinetochore architecture. The contributions of the constitutive centromere-associated network (CCAN) subunits CENP-A (Cse4), CENP-C and CENP-T to the recruitment of the outer kinetochore (KMN) are shown in detail. One microtubule-attachment site is shown for simplicity. CENP-C interacts directly with the CENP-A nucleosome and MIS12 complex. CENP-T binds centromeric chromatin and NDC80 complex. CENP-T and MIS12 complex are competing binding partners for NDC80 complex. Knl1 anchored via MIS12 complex and NDC80 are plus-end microtubule binders, thus act as interface for kinetochore-microtubule interaction. The yeast Dam1 complex and its supposed human homolog, Ska complex are thought to support these interactions. Modified from [41].

The MIS12 complex consists of the four subunits Dsn1, Mis12, Nnf1 and Nsl1 that form a rod-shaped elongated tetramer [53, 56, 57, 58] that localises to the inner kinetochore, establishing direct contact to CENP-C via the Nnf1 subunit [45, 59, 60]. The MIS12 complex is important for chromosome segregation as MIS12 mutants show both lower amounts of NDC80 complex at kinetochore and exhibit defects in establishing bi-orientation and tension across sister chromatids [56, 57]. These findings are in line with the role of MIS12 in outer kinetochore assembly where it serves as a structural platform for NDC80 and KNL1 complex binding [53, 58].

The NDC80 complex is a crucial organisational element of the outer kinetochore structure and contains the extended coiled-coil subunits Ndc80 (also known as Hec1), Nuf2, Spc24 and Spc25 [42, 61, 62, 63, 64, 65]. RNAi interference of Ndc80 leads to a kinetochore-null phenotype, highlighting its importance in the maintenance of stable kinetochore-microtubule attachments, kinetochore morphology and chromosome alignment as well as kinetochore localisation of mitotic checkpoint components [54, 64, 65, 66, 67, 68]. Structurally, the Spc24:25 dimers are oriented towards the kinetochore and bind the MIS12 (Nsl1) and KNL1 (Knl1) complexes [69, 70], the elongated structure of the complex presumably translating the tension from microtubules to the inner kinetochore [50, 51]. The N-terminal region of CENP-T interacts directly, in a phosphorylation-dependent manner, with the Spc24:25 dimer [45, 58, 71, 72, 73], which is mutually exclusive with the binding of Spc24:25 to MIS12 [71, 72, 73] (Figure 1.5). The head domains of Ndc80 and Nuf2 proteins bind to microtubules directly [51, 74, 75] and regulate the dynamics of kinetochore microtubules [52] (Section 1.3.1).
Some studies suggest a microtubule-dependent role for the Ndc80 complex in regulating the stable association of the checkpoint proteins Mad1:Mad2 and dynein with kinetochores [42, 54, 64, 68, 76]. Its role in checkpoint inactivation remains controversial but it emerges that spindle checkpoint signalling is abolished under conditions of complete removal of Ndc80 by RNAi [67]. This might be mediated by the interaction of the NDC80 complex with the checkpoint kinase Mps1, which is essential for checkpoint activity [54] (see also Section 1.4).

The KNL1 complex consists of a long protein Knl1 (also known as Blinkin, AF15q14, Spc105) and Zwint that binds to the C-terminus of Knl1 [40, 55, 58, 77]. Knl1 binds to microtubules via its N-terminus [51, 78] while its C-terminus is required for kinetochore localisation to the MIS12 complex [53, 58]. Knl1 has a role in the recruitment of spindle assembly checkpoint components, both directly (N-terminus) and indirectly (C-terminus) via Zwint, which is involved in the kinetochore recruitment of ZW10 [79]. ZW10 is a component of the Rod-Zwilch-ZW10 (RZZ) complex, that constitutes an integral part of the checkpoint, discussed comprehensively in Section 1.4. Additionally, the N-terminus of Knl1 is required for the recruitment of protein phosphatase 1 (PP1), an antagonist of Aurora B activity, that is involved in the regulation of kinetochore-microtubule attachments [55, 80] (see also Section 1.3.2) as well as mitotic checkpoint silencing [81] (see also Section 1.4.3). This role is consistent with a kinetochore-null phenotype, which can be observed when Knl1 is depleted, where cells fail to assemble a functional kinetochore-microtubule interface [77].

1.3 Control of kinetochore-microtubule attachment

The kinetochore is the interface between chromosomes and microtubules of the mitotic spindle. The ability of kinetochores to bind to growing or disassembling microtubules [82, 83] and stabilising the attached microtubules [82] is crucial for their role in monitoring and regulation of initial microtubule capture, achieving bi-orientation, and maintaining end-on attachments that generate the required force and tension for chromosome segregation.

1.3.1 The regulation of microtubule dynamics

In 1951, Inoue proposed the first model of dynamic equilibrium of spindle assembly and chromosome movement [84]. Microtubule structures are highly dynamic, characterised by a state termed "dynamic instability" that changes between states of spontaneous disassembly, pause and growth [85, 86]. Dynamic instability is a feature required to allow the correction of erroneous attachments of kinetochores (Figure 1.6) and also the stabilisation of correct, load-bearing kinetochore-microtubule attachments.

As the NDC80 complex is the principal microtubule-binding site, it is also a major site of regulation of microtubule-binding. The Dam complex from budding yeast and its possible functional homolog in humans, the Ska complex, also both bind microtubules and establish contacts with Ndc80, possibly enhancing the overall processivity of microtubule binding [87, 88, 89]. Ablation of Ska complex in cells displays a similar kinetochore-null phenotype as NDC80 inhibition [88, 90, 91] emphasising its role in mediating microtubule interaction.

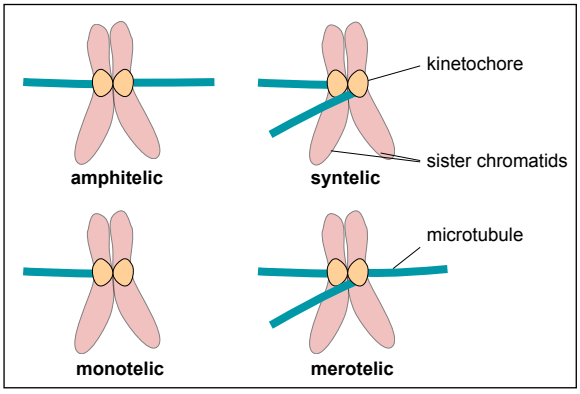

Figure 1.6: States of kinetochore-microtubule attachment.
Amphitelic orientation (correct attachment, bi-orientation), both sister kinetochores are bound to microtubules originating from proximal poles. Monotelic attachment, intermediate condition with only one kinetochore attached to the spindle. In syntelic attachment, both sisters connect to the same pole. Merotelic attachment, one sister is attached to both poles, a condition occuring frequently during mitosis.

The dynamics of kinetochore-microtubule interactions are mainly regulated by reversible phosphorylation events at the kinetochore, resulting from balanced kinase- and phosphatase activities, among which Aurora B kinase and PP2A phosphatase with its regulatory subunit B56 [92]. A number of KMN components are targets of Aurora B activity and exhibit reduced microtubule binding affinity upon phosphorylation [78]. In particular, Aurora B phosphorylates multiple sites on positively charged segments within the N-terminal tail of Ndc80 [75, 93], which neutralises the charges, hence decreases the microtubule-binding affinity *in vitro* and reduces the microtubule-induced clustering effects of the Ndc80 complex [51, 52, 75, 93]. In good agreement with these findings, the activity of Aurora B has been found to be crucial for kinetochore microtubule destabilisation and microtubule attachment error-correction *in vivo* [51, 52, 78, 94].

Additionally, Aurora B phosphorylation prevents premature stabilisation of erroneous attachments by negatively regulating the association of Ska complex with the NDC80 complex and microtubules [89, 95]. Aurora B is also known to phosphorylate Knl1, the Dsn1 subunit of the MIS12 complex and CENP-U at the inner kinetochore [78, 96]. However, the effects of these phosphorylation events on microtubule binding are still poorly characterised.

1.3.2 The error-correction machinery

Attachment errors, like monotelic, syntelic or merotelic attachments (Figure 1.6), are common [97] as microtubule filaments encounter kinetochores by chance. The ability to discriminate between correct and incorrect, labile microtubule attachments, thereby selectively stabilising the former and preventing the stabilisation of the latter is a crucial process for chromosome integrity that is achieved by a tension-sensitive apparatus of the cell [99, 100, 101].

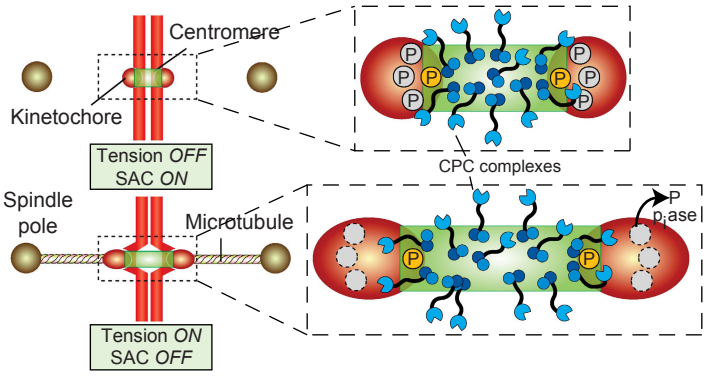

Figure 1.7: Error-correction in context of the spindle assembly checkpoint.
Schematic description of the relative arrangement of the centromere-kinetochore interface in the absence (above, OFF) and presence of tension (below, ON). Note that the absence of tension is coupled to SAC activity, which is silenced under conditions of tension. The magnification of the respective centromere-kinetochore interface demonstrates the change in phosphorylation status (P) of kinetochore substrates in response to tension. In the absence of tension, kinetochores are close to centromeres (green), where high kinase activity is present. In this configuration, substrates at the centromere (P, yellow circle) as well as the kinetochore (P, grey circle) are phosphorylated. Conversely, in the presence of tension, the distance of kinetochores from the centromere increases, allowing distal kinetochore substrate dephosphorylation by phosphatases ($p_i$ase), while phosphorylation of close centromere substrates persists; modified from [98].

Aurora B has been identified as key player in the destabilisation of erroneous attachments by phosphorylating KMN components described above (Section 1.3.1). Aurora B is a subunit of the **c**hromosomal **p**assenger **c**omplex (CPC), along with the proteins Incenp, Survivin, and Borealin [102, 103]. Attachment errors can be artificially stabilised if the activity of the Aurora B kinase is inhibited with a small molecule inhibitor [94, 104, 105, 106]. Re-activation of Aurora B, however, strikingly results in the correction of improper attachments after inhibitor washout [106]. Aurora B/Ipl1 mutants in yeast lead to massive chromosome missegregations because the release of kinetochore-microtubule attachments is impaired [107]. This highlights the importance of Aurora B as an essential component of the error-correction mechanism. The exact details of how incorrect attachments are sensed in a tension-dependent manner and how this is then translated to the differential activity of Aurora B remain unclear. Small molecule inhibitor studies also identified the

checkpoint kinase Mps1 to be implied in error-correction downstream of Aurora B [108].
According to the model presented in Figure 1.7, error correction is modulated by differential access of Aurora B to its kinetochore substrates. Faulty attachments are associated with lack of inter-kinetochore tension [26, 104], which allows Aurora B coupled to centromeres via the CPC [102, 103] to phosphorylate its kinetochore substrates [80] (Section 1.3.1).
Upon bi-orientation, the inter-kinetochore tension and -distance increase, leading to a displacement of centromere-bound Aurora B out of reach of its substrates [107]. This hypothesis was corroborated by elegant anchor-away experiments in which an Aurora B kinetochore substrate at a sufficiently large distance from the centromere became dephosphorylated upon microtubule attachment [26]. Furthermore, inter-kinetochore stretch, leading to a distance of 35-40 nm between kinetochores, was shown to be sufficient to satisfy and disable the spindle assembly checkpoint [109] (also schematically depicted in Figure 1.7).

Despite this sensible, though simplified model, it is conceptually unclear how stable attachments can initially be formed at the onset of mitosis, as the kinetochore substrate phosphorylation of Aurora B peaks in prometaphase, or when microtubules are depolymerised by nocodazole [80]. Importantly, Aurora B phosphorylation is counteracted by the activity of kinetochore-bound phosphatases, such as protein phosphatases 2A (PP2A) and 1 (PP1) [80, 92]. PP1 recruitment to the N-terminus of Knl1 in metaphase, which is negatively regulated by Aurora B activity, results in dephosphorylation of Aurora B substrates and stabilisation of kinetochore-microtubule attachments [80]. PP2A together with a B56 regulating unit promotes dephosphorylation of kinetochore substrates at unattached kinetochores to facilitate kinetochore-microtubule attachment and to maintain low phosphorylation levels on bi-oriented chromosomes. However, little is known about the PP2A- or PP1-specific substrates and how their activities are regulated at the kinetochore.
The mechanism of error correction is closely linked with the machinery of the spindle assembly checkpoint, as checkpoint proteins, such as Mps1, Bub1 and BubR1 and Polo-like kinase 1 (Plk1) [2] contribute to the regulation of kinetochore-microtubule attachment. The attachment is regulated in a feedback mechanism that influences both Aurora B and PP2A-B56 recruitment directly or indirectly. In particular, Aurora B targeting to centromeres depends on Bub1-mediated phosphorylation of histone H2A as well as Mps1 activity [110, 111, 112], whereas recruitment of PP2A-B56 to the kinetochore requires Plk1-dependent phosphorylation of BubR1 [113, 114]. This connection of error correction with spindle assembly checkpoint signalling is recapitulated by the fact that intra-kinetochore stretching couples both the spatial regulation of Aurora B activity and the state of checkpoint signaling [109] (Figure 1.7).

1.4 Molecular mechanisms of the spindle assembly checkpoint

During metaphase, erroneous attachments are destabilised and eliminated by the error correction machinery to promote bi-orientation of all chromosomes (see also Section 1.3.2) and induce activation of the spindle assembly checkpoint. This checkpoint (henceforth termed SAC) is a second safety mechanism of the cell, triggered by unattached or mono-oriented kinetochores, that consequently delays anaphase onset and exit from mitosis until all chromosomes are properly attached to the spindle [2, 98]. In the absence of SAC signalling, cohesin is cleaved, allowing exit from mitosis irrespective of kinetochore-microtubule attachments, which results in increased frequency of chromosome missegregation and aneuploidy [2, 7].

1.4.1 The assembly of a mitotic checkpoint complex

SAC proteins were first identified genetically by screens for mutants in *Saccharomyces cerevisiae* that fail to respond to improper microtubule attachments introduced by anti-microtubule drugs [115, 116]. Components of the SAC include the mitotic-arrest deficient (Mad) proteins Mad1, Mad2, and Mad3/BubR1 (human ortholog) [115], the budding uninhibited by benzimidazole (Bub) proteins Bub1 kinase and Bub3 [116, 117], monopolar spindle protein 1 (Mps1) kinase [118], Ipl1/Aurora B (human ortholog) kinase [119], and Sgo1 [120], all of which are highly conserved among eukaryotes. Despite knowing the identity of the main players, the exact molecular mechanism of how attachment errors at the kinetochore are converted into signals that inhibit anaphase onset remains insufficiently understood.

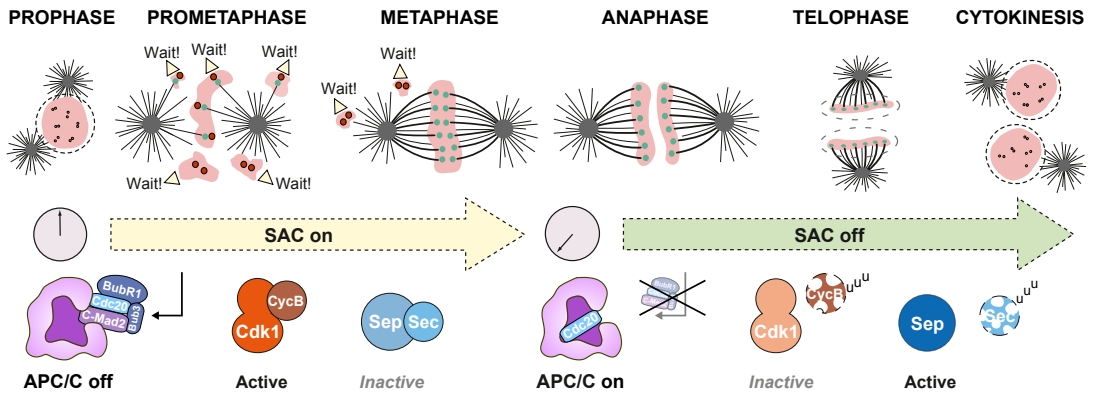

Figure 1.8: The spindle assembly checkpoint is a timing device to ensure faithful chromosome segregation. Schematic view of the sequential phases of mitosis (see Section 1.1.2 for details). Prometaphase starts after nuclear envelope breakdown (time zero). Unattached sister kinetochores (red dots) emit a "Wait!" signal, which arrests cells in mitosis. This signal corresponds to the production of MCC (BubR1, Bub3, Mad2, Cdc20) complexes by the SAC that inhibit the APC/C. This allows Cdk1–cyclin B (CycB) to remain active while separase (Sep) activity is restrained by securin (Sec). Chromosomes that fail to achieve correct attachment until metaphase continue to activate the SAC until all sister kinetochores are attached (green dots) to kinetochore fibers before anaphase. Upon full correct attachment, the SAC is satisfied, the APC/C becomes activated, cyclin B and securin are ubiquitylated (u) and destroyed in an APC/C-dependent manner. Separase is activated cleaving cohesin between sister chromatids, allowing anaphase onset while Cdk1 is inactivated ultimately leading to mitotic exit. Modified from [121, 122].

SAC proteins delay precocious chromosome segregation in anaphase through the inhibition of a complex of the E3 ubiquitin ligase known as the anaphase-promoting complex/cyclosome (APC) [123, 124] and its co-activator Cdc20 [125, 126]. APC/C^{Cdc20} catalyses the ubiquitination and destruction of cyclin B [127] and securin [128], leading to inactivation of the mitotic driver kinase Cdk1 and the release of active separase [129, 130, 131] (Figure 1.8). The proteolytic activity of separase cleaves cohesin and destroys the linkage between sister chromosomes, thus triggering anaphase and chromosome segregation.

The SAC inhibits APC/C^{Cdc20} activity by catalysing the formation of an inhibitory complex, referred to as the **m**itotic **c**heckpoint **c**omplex (MCC), which is a heterotetramer composed of Cdc20, Mad2, BubR1 and Bub3 [132, 133, 134] (Figure 1.9, 1.8). The individual contributions of the MCC components to APC/C^{Cdc20} inhibition remain controversially discussed as Mad2 and BubR1 bind to two distinct binding sites on Cdc20 [125, 135]. Some studies argue towards Mad2 binding to Cdc20 to have a dominant role [136], while others claim BubR1 provides the inhibitory activity of APC/C^{Cdc20} [137, 138]. The notion that BubR1 and Mad2 might act synergistically, reconciles this discrepancy [132, 133, 134, 136, 137, 138, 139, 140]. The sequestration of Cdc20 signifies a disruption of Cdc20 association with APC/C subunits [134] as BubR1 binding to Cdc20 blocks D-box sites in Cdc20 required for recognition by the APC/C [134, 141]. Moreover, the incorporation of Cdc20 into the MCC promotes APC/C-dependent autoubiquitylation of Cdc20, which reduces Cdc20 levels and allows for complete inhibition of the remaining Cdc20 pool by the SAC [142, 143]. The inhibition of APC/C^{Cdc20} by the SAC therefore stabilises securin and allows for time to correct errors in chromosome attachment and alignment (Figure 1.8).

Unattached kinetochores that delay a vertebrate cell for several hours in mitosis [144] represent the source of SAC signalling. Significantly, most SAC proteins, including Mps1, Bub1, Mad1, Mad2, BubR1, Bub3 and Cdc20, are shown to associate to unattached kinetochores (also depicted in Figure 1.9) and the majority is removed from kinetochores upon microtubule attachment [145]. Consistent with the central role of checkpoint proteins in initiating and maintaining mitotic arrest at unattached kinetochores, the recruitment of checkpoint kinase Mps1 to the kinetochore is required for mitotic arrest [146]. Conversely, elegant experiments show that constitutive kinetochore targeting of Mad1 is sufficient to sustain SAC signalling also at attached kinetochores since Mad1 removal from kinetochores is impaired [147].

Interestingly, although kinetochores are at the basis of SAC signalling, kinetochores are not absolutely essential for MCC formation. In human cells the MCC was shown to already be present during interphase, before kinetochore recruitment of SAC components [132]. The interphasic presence of the MCC was confirmed in yeast lacking functional kinetochores [148, 149, 150]. This soluble pool of MCC in human cells, however, is not sufficient to delay chromosome segregation when mitosis perturbed by microtubule poisons. Rather, the preformed MCC is thought to be required to set a minimum time for mitosis and for the inhibition of the APC/C in initial prometaphase, when kinetochores are still assembling and recruiting SAC proteins [67].

A key function in the kinetochore-based SAC signalling is the catalytic step of promoting the assembly of locally enriched MCC components into sub-complexes for final assembly, in particular Mad2:Cdc20 complexes [67, 133, 151] to interact with a constitutive BubR1:Bub3 complex [152, 153].

Mad2 exists in a "closed" conformer that is competent to bind Cdc20 and kinetochore receptor Mad1 and an "open" conformer that does not associate with Cdc20 [154, 155, 156, 157]. It is therefore crucial to convert the "open" into the "closed" conformer to allow the formation of inhibitory MCC complexes. The "Mad2 template" model postulates a mechanism for the Mad2 conversion that is catalysed by binding of closed Mad2 to kinetochore-localised Mad1 [151, 158]. This forms the source of closed Mad2 needed for the formation of Mad2-Cdc20 complexes (Figure 1.9). The molecular details of how Mad2:Cdc20 and BubR1:Bub3 sub-complexes then cooperate to form the final MCC still remain at issue. It has been shown that binding of Mad2 to Cdc20 is necessary for binding of BubR1 to Cdc20 and that BubR1 uses a lysine-glutamate-asparagine (KEN) sequence for Cdc20 binding [159]. Moreover, the crystal structure of a *Saccharomyces cerevisiae* MCC complex reveals a Mad2 bound to Cdc20, which also interacts with BubR1 and exposes Cdc20 for efficient BubR1 binding [134], thus lending support to previous assertions where Mad2-binding of Cdc20 was shown necessary for BubR1 binding [133, 159]. The actual composition of the MCC, particularly with regard to Bub3, is still unclear as in *Schizosaccharomyces pombe* Bub3 is not incorporated in the MCC [160]. An recent model [161] and other observations alluded to a role of a second molecule of Cdc20 binding to the MCC [150, 159, 162], the significance of which remains to be established.

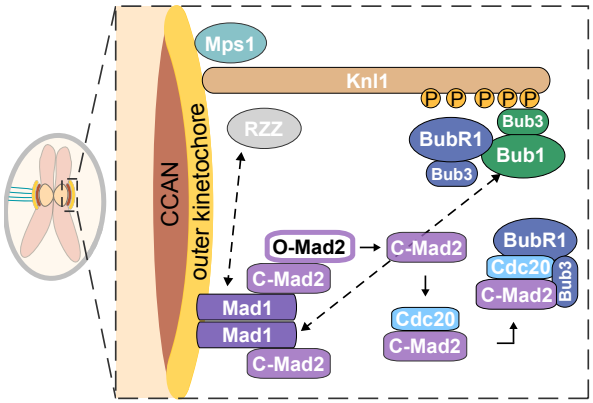

Figure 1.9: SAC activation at unattached kinetochores. Mps1 is recruited to kinetochores in an Aurora B dependent manner to phosphorylate Knl1. Phosphorylated Knl1 binds Bub1:Bub3 that in turn recruits BubR1:Bub3 complexes. In metazoans, Knl1-Zwint together also recruits the Rod-Zwilch-ZW10 (RZZ) complex, although the precise mechanism is unknown. These proteins collaborate to recruit a heterodimer of Mad1:Mad2 (in closed conformation) to the kinetochore. The Mad1:Mad2 complex catalyses the conversion of soluble open Mad2 into closed Mad2, which associates with Cdc20 in the cytoplasm. Mad2-Cdc20 complexes are then bound by BubR1:Bub3 to form the MCC that is competent to inhibit the APC/C.

It has been suggested recently that Mad2 released from the final inhibitory BubR1-Cdc20-Mad2 complex can then again facilitate the formation of additional MCC complexes [138]. This provides a model for MCC amplification from a kinetochore-derived Mad2-Cdc20 complex into the cytosol, implying that the major contribution for APC/C^{Cdc20} inhibition is provided by BubR1-Cdc20. Additionally, phosphorylation of Cdc20 by Bub1 kinase [163], of Mad2 by Mps1 kinase [164] or Aurora B dependent BubR1 phosphorylation [165] may also contribute to the efficient assembly of MCC complexes.

1.4.2 Activation of checkpoint signalling

The initiation of a checkpoint signal corresponding to the production of inhibitory MCC requires the recruitment of essential checkpoint components to unattached kinetochores [145]. Studies investigating recruitment dependencies of checkpoint proteins start to unravel the mechanism of SAC

activation to be a partly hierarchical but also an inter-dependent feedback pathway (Figure 1.9).
In the presence of microtubule-depolymerising drugs, Aurora B is required for the kinetochore recruitment of SAC proteins [67] and Aurora B or Mps1 inhibition severely impairs SAC signaling [104, 105, 108] placing both kinases upstream of the signalling pathway. The KMN network was shown to be essential for SAC signalling and SAC component recruitment in all eukaryotes examined [48, 49, 54, 63, 104, 108, 166]. This is in part explained by Aurora B-dependent phosphorylation of Ndc80, a protein which is implicated in the recruitment of the essential checkpoint kinase Mps1 [54, 166, 167], although the mechanism remains elusive (Figure 1.9). Additionally, the N-terminus of Knl1 was identified as a crucial hub for the establishment of checkpoint signalling [55, 168, 169, 170, 171]. Recent evidence shed light on the necessity of Mps1 activity in the checkpoint, in particular: Mps1 phosphorylates KNL1 at threonine residues within conserved MELT (M[D/E][I/L/V/M][S/T]) repeats [172, 173, 174, 175], thereby creating a docking site for Bub3 in complex with Bub1 (Figure 1.9). This Bub1:Bub3 complex in turn is necessary and sufficient for recruitment of the BubR1:Bub3 complex [176, 177, 178, 179, 180]. Evidence from yeast suggests that Bub1 is also directly implicated in the recruitment of Mad1:Mad2 [181, 182] while the dependence in human cells is less clear [183]. Further proteins are reported to provide further low-affinity binding sites as well, such as the NDC80 complex [54, 64] and the Rod-Zwilch-ZW10 (RZZ) complex [184], the latter being also dependent on Mps1 activity for its kinetochore targeting [108, 146, 185].
Collectively, SAC activation can be viewed as a two-branched model where checkpoint components localise to the Ndc80 complex (Mps1, Mad1:Mad2 and RZZ), whereas others associate with Knl1-Zwint (Bub1, BubR1 and Bub3). Mad1:Mad2 and RZZ might be stabilised by additional association with Knl1-bound Bub1 and Zwint, respectively (Knl1 branch highlighted in Figure 1.9). This configuration of SAC proteins is the foundation that leads to the generation of MCC inhibitory complexes, however, the mechanism of the interplay of Bub1:Bub3, BubR1:Bub3 complexes with Mad1:Mad2 and Cdc20 still remains to be established.

1.4.3 Silencing of checkpoint signalling

Progression through mitosis requires the mitotic checkpoint to be silenced upon achievement of bi-orientation and kinetochore attachment to the mitotic spindle. Continuation requires both the removal of mitotic checkpoint proteins from kinetochores, as any of them is able to sustain checkpoint activation [147, 186] and the disassembly of the MCC to allow activity of the APC/C. The APC/C activity in turn then leads to the ubiquitination and degradation of securin, thus activation of separase and sister chromosome separation (Figure 1.8).
As checkpoint activation is largely kinase-dependent, it is fair to assume that phosphatases play a central role in silencing. Indeed, the recruitment of PP1 to the N-terminus of Knl1 is implicated in checkpoint silencing on top of its role in regulating microtubule dynamics (Section 1.3.2), highlighting the close interplay of both processes [81, 187]. In particular, a Knl1 mutant deficient for PP1 binding shows higher levels of the checkpoint components Bub1 and BubR1 at kinetochores [188]. Furthermore, PP1 was shown to dephosphorylate MELT motifs in yeast and its overexpression reduces Bub1 levels at kinetochores [172]. In mammalian cells, PP2A-B56 was identified as a phos-

phatase removing Mps1-mediated Knl1 phosphorylation sites, which results in the removal of Bub1 and BubR1 from kinetochores [189].

The RZZ complex is proposed to contribute to SAC silencing, through the recruitment of Spindly upon microtubule attachment. Spindly localisation to kinetochores is in turn required for dynein-dynactin localisation [190, 191]. The dynein-dynactin complex is a minus end-directed motor protein that strips RZZ and bound Mad1:Mad2 complexes from kinetochores [192] in a process referred to as kinetochore shedding. This model, however, only applies for higher eukaryotes as neither RZZ nor Spindly have obvious homologs in yeast.

In a second branch, MCC disassembly is required to provide free Cdc20 in order to activate the APC/C. Additionally, in metazoans, the mitotic checkpoint silencing protein $p31^{comet}$ binds specifically to the closed form of Mad2 [193] and its overexpression results in less Mad2 bound to Cdc20 [194]. The AAA-ATPase TRIP13 is a direct binder of $p31^{comet}$ [195]. Depletion of TRIP13 delays the metaphase-to-anaphase transition and $p31^{comet}$ mediated mitotic checkpoint silencing. Recent evidence has emerged that the enzymatic activity of TRIP13 in cooperation with $p31^{comet}$ provides the energy required to disassemble stable MCC and to drive mitotic checkpoint silencing [195].

Moreover, the APC/C-dependent non-degradative autoubiquitylation of Cdc20 [143] promotes MCC disassembly and contributes to SAC silencing, thus leading to mitotic exit (also depicted in Figure 1.8). Discerning molecular mechanisms in order to characterise the interplay and connections between SAC kinase and phosphatase activity at the kinetochore, depending on the microtubule binding status, is the focus of current and future work.

1.5 Checkpoint kinases Bub1 and BubR1

Bub1 and BubR1 are essential and paralogous proteins at the core of the spindle assembly checkpoint machinery. Their domain architecture is remarkably similar (Figure 1.10) suggesting they evolved from the same progenitor gene [196, 197], however, their mitotic function is distinctly divergent. Several independent duplication events occurred during speciation, in all cases followed by substantial sub-functionalisation, resulting in their separate roles [196, 197].

1.5.1 The mitotic functions of Bub1 and BubR1

Bub1 and BubR1 were originally characterised as a conserved components of the SAC [115, 116, 145], recruited to kinetochores in response to unattached or misaligned kinetochores. More recently, Bub1 was also shown to play a role in chromosome alignment [177, 198] as well as BubR1 [196, 199]. Exactly how Bub1 and BubR1 perform their many functions on a molecular level, and whether all of its many interactions are phylogenetically conserved, is yet unclear.

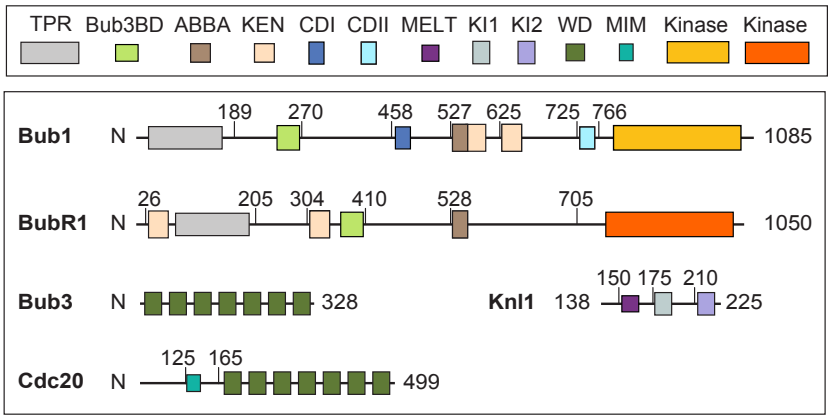

Figure 1.10: Domain structure of checkpoint components.
Domain positions and protein construct boundaries of a Knl1 fragment comprising the N-terminal MELT-motif and KI1 and KI2, are indicated by residue number. TPR-**t**etratrico**p**eptide **r**epeat, Bub3BD-Bub3 **b**inding **d**omain, ABBA-cyclin **A**, **B**ub1, **B**ubR1, **A**cm1 (ABBA) motif [200, 201] or F-box [202], KEN-lysine-glutamate-asparagine motif, CDI/II-**c**onserved **d**omain I/II (as defined in [183]), WD-tryptophan-aspartate, MIM-**M**ad2 **i**nteraction **m**otif.

Kinetochore recruitment of Bub1 and BubR1

Like its orthologs, human Bub1 possesses N-terminal **t**etratrico**p**eptide **r**epeats (TPR), followed by a binding motif for Bub3, two conserved motifs, and a C-terminal kinase domain. The overall organisation of BubR1 (Mad3 in yeast) is similar to Bub1, as shown in Figure 1.10 [183]. Bub1 as well as BubR1 each form a constitutive 1:1 complex with the checkpoint protein Bub3, a 7-bladed β-propeller, throughout the cell cycle [117, 135, 152, 203]. The interaction of Bub1 with Bub3 is mediated by its Bub3-binding domain (also referred to as GLEBS motif) [203]. The Bub3-binding domain is both necessary and sufficient for kinetochore localisation of Bub1 and BubR1 [66, 176]. The exact dependence of Bub3 binding on kinetochore recruitment is controversial, as in human cells, depletion of Bub3 does not affect Bub1 kinetochore recruitment although it might affect the localisation

of BubR1 [67]. Depletion of Bub1 or BubR1, however, was found to reduce kinetochore recruitment of Bub3 in *Xenopus* egg extracts [204] was shown to be required to recruit Bub3 to the kinetochores of fission yeast [176] and vertebrates [177, 204]. Biochemical studies initially identified the first 300 residues of the N-terminal region of murine Bub1 to be sufficient for kinetochore localisation [152] that comprises the TPR domain and the Bub3-binding domain. Further studies demonstrated that the Bub3-binding domain is sufficient for kinetochore localisation, which is consistent with the finding that mutations in the Bub3-binding domain prevent kinetochore localisation of Bub1 [183] and BubR1 [139, 205].

Bub1 recruitment was shown to be dependent on the phosphorylation of so-called MELT motifs on Knl1 by Mps1 [172, 173, 174, 175], which creates a docking site for Bub3 bound to Bub1, not however Bub3 bound to BubR1 [171, 179]. Indeed, Bub1 is required for kinetochore recruitment of BubR1 [66, 177, 206] and they directly interact in a region, which is immediately followed by their respective Bub3-binding domains [179].

In vertebrates, the kinetochore binding mechanism of Bub1 and BubR1 is more complex. The TPR domains of Bub1 and BubR1 interact with vertebrate Knl1 KI1 and KI2 motifs, respectively[199, 207, 208] (Figure 1.10). However, the TPR domains are dispensable for Bub1 or BubR1 recruitment to the kinetochore [152, 208]. This is consistent with the finding that the KI1 or KI2 motif on Knl1 is not required for Bub1 recruitment [173]. However, deletion or mutation of the KI motif or a TxxF/Y-motif preceding the MELT-sequence, that is also conserved only in vertebrates, strongly reduced the recruitment of the Bub1:Bub3 and BubR1:Bub3 *in vitro* and *in vivo*. Furthermore the deletion decreased the ability to mount a SAC response and led to impaired chromosome alignment, suggesting that this additional interaction stabilises the overall association of Bub1:Bub3 with Knl1 and promotes the subsequent recruitment of BubR1:Bub3 [171, 209].

Bub1 and BubR1 function at the kinetochore

The main contribution of Bub1 to checkpoint signalling constitutes its role as a scaffolding protein localising at kinetochores during early mitosis. Bub1 bound to kinetochores recruits downstream checkpoint components to the kinetochore, including BubR1 and Bub3 [177, 178, 179, 198, 204, 210] as well as the RZZ complex [180] and the Mad1:Mad2 complex [181, 182, 183, 211, 212].

Consistently, in yeast Bub1 and Mad1 have been shown to form a complex *in vitro* in the presence of Mad2 and Mps1 [211] while the complex formation of Bub1 and BubR1 was suggested by yeast-two hybrid assays [55, 199] and confirmed in human cells later *in vitro* and *in vivo* [179]. Molecular details of the interaction of both complexes are not available so far.

BubR1, unlike Bub1, contributes to the checkpoint directly, as it is a crucial component of the MCC together with Bub3, Mad2 and Cdc20 [132]. BubR1 contains two KEN boxes that have been implicated in Cdc20 binding and thus APC/C inhibition (Figure 1.10). Recent structural analysis of fission yeast MCC has revealed that BubR1/Mad3 uses its N-terminal KEN box, which precedes the TPR domain (and is absent in Bub1), to establish direct interactions with both Mad2 and Cdc20 [134, 138, 141, 199, 213]. The second KEN box is required to block substrate binding to the APC/C [139]. Additionally, the TPR domains of BubR1 also directly interact with Cdc20, consistent with the observation

that mutating the TPR or the KEN boxes of BubR1 disrupts its ability to bind Cdc20 and impairs SAC signaling [55, 139, 159].
More recently, an additional motif, present on cyclin **A**, **B**ub1, **B**ubR1 and **A**cm1 (hence termed ABBA motif or F-box, because it contains two conserved phenylalanines), was implicated in BubR1 binding to Cdc20 as well [200, 201, 202]. Cdc20 localisation was shown to depend on the ABBA motif of Bub1 [210], specific binding of Cdc20 was also attributed to contributions of the KEN motifs [214].
In addition to their essential role in SAC signalling, Bub1 and BubR1 also contribute to chromosome congression during prometaphase by stabilising correct kinetochore–microtubule interactions and destabilising erroneous contacts [106, 115, 152, 177, 205]. This regulation is mediated by BubR1-associated PP2A [113] and the intrinsic kinase activity of Bub1 [111, 176, 183, 215].

1.5.2 The role of Bub1 and BubR1 kinase activity

Protein kinases catalyse the phosphate transfer from ATP to protein substrates, a modification that can modulate the activity of an enzyme or regulate specific protein-protein interactions. Kinases are important enzymes representing two percent of the proteome, which corresponds to more than 500 different protein kinases. Pseudo-kinases are presumed to account for ten percent of the kinases encoded in the mammalian genome [216]. Protein kinases have evolved to work as highly dynamic molecular switches in signalling networks to allow quick responses to specific cues, for example the state of microtubule attachment to kinetochores.
Generally, protein kinases are thought to be maintained in a basal, inactive state and recruited only transiently upon different stimuli. Structurally, kinase activation is often associated with the release of an inhibitory domain allowing the dynamic assembly of hydrophobic regulatory spines (R-spines) [217] as a distinctive structural feature in kinases that is a prerequisite for kinase activity [216].
Both Bub1 and BubR1 possess a C-terminal kinase domain, yet the extent of BubR1 kinase activity is a matter of debate. It has been proposed previously that BubR1 kinase activity is required for SAC function or initiation [150, 218, 219] as well as SAC silencing. BubR1 involvement in SAC silencing was inferred from the inactivation of BubR1 kinase activity upon microtubule capture by the kinesin CENP-E [218, 219]. Additionally, BubR1 activity was implied in regulating chromosome alignment [213, 220, 221]. Other studies, however, demonstrated BubR1 kinase activity to be dispensable for the spindle checkpoint and chromosome alignment [150, 153, 159, 196, 222, 223]. More recently, it was proposed that BubR1 is an inactive pseudo-kinase whose kinase domain critically contributes to the overall stability of the protein [196]. This may explain previous discrepancies, in particular because it was shown that point mutations normally utilised to disrupt kinase activity largely decreased the overall structural stability of BubR1 [196] and is also in line with the fact that in other organisms as the yeasts *Saccharomyces cerevisiae* and *Schizosaccharomyces pombe* BubR1/Mad3 lack a kinase domain altogether.

Contrary to BubR1, Bub1 is a *bona fide* kinase [163, 214, 224]. Catalytically inactive Bub1 in mice exhibits increased chromosome segregation errors and aneuploidy [225]. The catalytic activity of Bub1 is believed to play a marginal role in the SAC [183, 204, 215, 226, 227, 228]. In contrast, Bub1

kinase activity is required for chromosome alignment and congression [111, 176, 183, 215, 226, 228] and was further shown to be important for error-correction [110, 225].
Two substrates of Bub1 activity aside from Bub1 itself have been identified in human cells, Cdc20 and histone 2A (H2A) [111]. Cdc20 has been implied in the contribution to checkpoint-dependent inhibition of APC/C [163], the significance of this contribution remains yet to be confirmed. The role of the phosphorylation on H2A has been studied more extensively. In mitosis, Bub1 phosphorylates T120 (S121 in yeast) on the C-terminal tail of H2A [110, 111, 229] promoting centromere accumulation of shugoshin (Sgo) [163, 227, 229, 230, 231] and PP2A [232, 233], which is instrumental in maintaining sister chromatid cohesion. Centromere-localised Sgo has been suggested to serve as an adaptor that facilitates the centromeric accumulation of Aurora B [110, 111]. Bub1 activity thus contributes to the Sgo-dependent recruitment of Aurora B kinase and also to the establishment and protection of centromeric cohesion [112, 225, 228, 234]. Aside from the function of Bub1 kinase activity, the molecular mechanism of substrate binding and Bub1 substrate specificity also remain unknown.

Despite the key function of Bub1 kinase activity, it remains largely unclear how its activity is regulated on a molecular level. Intra-molecular regulation by the N-terminal TPR domain (Figure 1.10) was shown to contribute to kinase activation [208, 225] using material immuno-precipitated from cells. This could not be confirmed by means of recombinant proteins in another study [224]. A crystal structure of the Bub1 kinase domain (PDB ID 4R8Q) reveals an N-terminal extension of the kinase wrapping around the N-lobe of the kinase domain in a cyclin-like manner, thus contributing to structural integrity of the kinase and constitution of an intact R-spine. Consistently, this extension is essential for kinase activity [214]. This crystal structure further demonstrates that the P+1 loop, a short motif following the activation loop that contributes to substrate recognition, creates a steric obstruction expected to prevent effective access of substrates to the active site [214]. The P+1 loop, however, undergoes a profound rearrangement following auto-phosphorylation, ultimately relieving the auto-inhibited conformation and activating Bub1 kinase [224] (PDB ID 4QPM). Conversely, there is no evidence that phosphorylation of the activation loop plays a role in the case of Bub1, which is crucial for the activation of many kinases [235, 236]. Very recently, evidence emerged that Bub1 auto-phosphorylation outside the kinase domain may contribute to its own kinetochore turnover [237], revealing an additional feature of kinase auto-regulation. A thorough characterisation of Bub1 kinase activity elucidating regulatory intramolecular properties of Bub1 or revealing control by other kinetochore proteins is missing so far.

2 Scope of the thesis

Bub1 is one of the crucial mitotic checkpoint proteins that govern cell division. Understanding the molecular regulation of Bub1 activity is of key importance to unravel the functional principles of chromosome segregation in general. Elucidating the factors involved in the activation and regulation of Bub1 upon kinetochore binding forms the major focus of this dissertation.

In this study, I set out to assess the mechanism of Bub1 regulation and thoroughly characterise known interactions of Bub1 and BubR1 at the kinetochore and their implications for Bub1 kinase activity *in vitro*. Towards this end, a combinatorial approach of biochemical and biophysical methods was used.

The Bub1:Bub3 and BubR1:Bub3 complexes were expressed and purified recombinantly in order to reconstitute kinetochore protein complexes *in vitro* for biochemical and functional analysis. Furthermore, Bub1 and BubR1 kinase domain were produced recombinantly to first allow the assessment of BubR1 and Bub1 activity and subsequently the kinetic characterisation of Bub1 kinase activity. Second, the use of X-ray crystallography allows structural analysis of the recombinant Bub1 kinase, which provides insight into the mechanisms and determinants involved in the regulation of kinase activity. A variety of kinetochore proteins were tested for their potential as a Bub1 substrate. The identified substrates were ultimately used for the determination of the Bub1 substrate specificity.

The results obtained by this thesis will advance the general understanding of the molecular regulation of Bub1 kinase activity and the physical relevance of the Bub1:Bub3 and BubR1:Bub3 complex at the kinetochore with regard to the recruitment of other checkpoint components during mitosis.

3 Results and Discussion

3.1 Biochemical characterisation of Bub1 and BubR1 complexes

The introduction illustrated the current understanding of Bub1 and BubR1 function at the kinetochore and the spindle assembly checkpoint. In order to study Bub1 and BubR1 interactions and function, I first set out to reconstitute these complexes *in vitro*.

3.1.1 Expression and purification of Bub1 and BubR1 constructs

Bub1 and BubR1 kinases have been suggested to have diverged from one progenitor gene into protein paralogs in a gene-duplication event. Both proteins independently underwent speciation and individual sub-functionalisation [196, 197], still, both share a similar overall domain architecture (Figure 3.1).

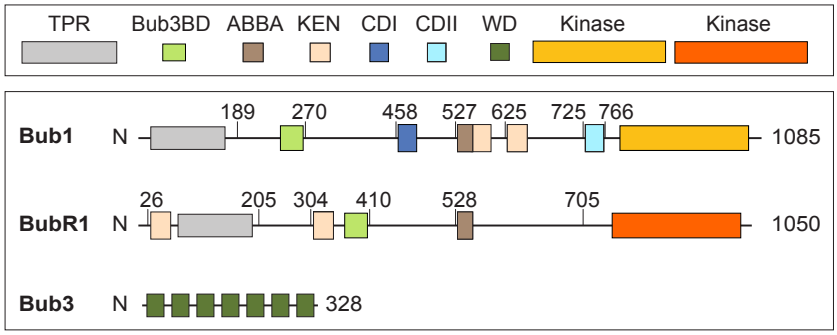

Figure 3.1: Domain architecture of Bub1, BubR1 and Bub3 proteins.
Domain positions and protein construct boundaries are indicated by residue number. TPR-tetratricopeptide repeat, Bub3BD-Bub3 binding domain, ABBA-ABBA-motif, KEN-lysine-glutamate-asparagine motif, CDI/II-conserved domain I/II, WD-tryptophan-aspartate.

The DNA sequences coding for full-length human Bub1 and BubR1 were cloned into custom pFH insect cell vectors that code for a TEV-protease cleavable His_6-tag to yield His_6-tagged proteins (sequences can be found in the Appendix Section 6.10). Bub3 was cloned into a second expression cassette on the vector, which allowed co-expression in one virus. It has previously been observed that Bub1 constructs exceeding amino acid 284 tend to be unstable, therefore co-expression of Bub3 was used for the stabilisation of longer Bub1 constructs *in vitro*. In contrast, BubR1 could be stably expressed and purified as a MBP-fusion without Bub3. Bub1 was also cloned into a pFG vector to obtain glutathione-S-transferase (GST)-tagged Bub1, along with Bub3 in a second expression cassette. The vector was recombined into a bacmid, then transfected in Sf9 insect cells where it was amplified and subsequently used for protein expression in Sf9 or Tnao38 cells. Individual steps are recapitulated in Sections 5.2.1 and 5.2.2.
Bub1 and BubR1 co-expressed with Bub3, henceforth termed Bub1:Bub3 and BubR1:Bub3, respectively, were obtained in a three-step purification using Ni-affinity, anion exchange and size exclusion chromatography, yielding both complexes in homogeneity (Figure 3.2, Section 5.2.2). GST-Bub1:Bub3 was purified equivalently using GSH-affinity chromatography.

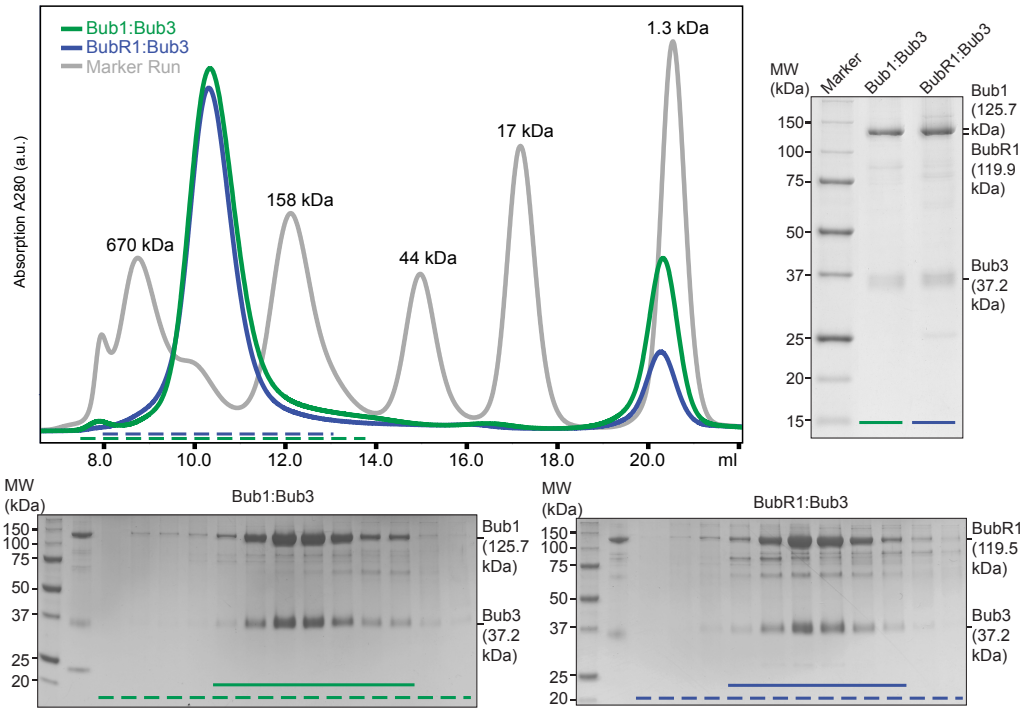

Figure 3.2: Bub1:Bub3 and BubR1:Bub3 complexes can be purified to homogeneity.
Size exclusion chromatogramme of His_6-Bub1:Bub3 and BubR1:Bub3 from a S200 10 300 column; a molecular weight standard is indicated in grey; green-Bub1:Bub3, blue-BubR1:Bub3. Below, SDS PAGE analysis of the fractions indicated by a dashed line in the chromatogramme. Right, the pooled fractions of the peaks indicated by a solid bar on the SDS PAGE gels below are analysed by SDS PAGE and Coomassie blue staining.

Both complexes exhibit nearly identical behaviour during purification and elute from gel filtration chromatography as single peaks that run at a molecular weight larger than their theoretical size. A point mutant of Bub1, D917N, that abrogates kinase activity has been constructed and purified in the same way. Bub1 D917N exhibits the same behaviour in purification while the mutation of K821R, that is also supposed to abolish kinase activity, was found to be expressed but is unstable in the course of purification. The typical yield for Bub1:Bub3 or BubR1:Bub3 complexes range from 0.5-1.5 mg per 1 l insect cell culture.

3.1.2 Bub1:Bub3 and BubR1:Bub3 form a complex and bind Knl1 in gel filtration

Bub1:Bub3 and BubR1:Bub3 complexes elute at higher molecular weight from gel filtration than expected from their theoretical mass, suggesting non-globular shapes, additional oligomerisation, or both. To investigate the effective state of the complexes, analytical ultracentrifugation experiments were performed. This method allows determination of the molecular weight and shape, hence the identification of the protein complex stoichiometry, derived from sedimentation velocities. Bub1:Bub3 and BubR1:Bub3 present nearly identical behaviour in sedimentation and the analysis of the sedimentation distribution curves c(S) concludes one predominant species. The calculated

molecular weights for the Bub1:Bub3 complex (150 kDa) and the BubR1:Bub3 complex (144 kDa) from the sedimentation analysis identified them as heterodimers (Figure 3.3 and Appendix Figure 6.1). The frictional ratio of 2.2 for both complexes is indicative of highly elongated structures, thus explaining the high apparent molecular weight in size exclusion chromatography.

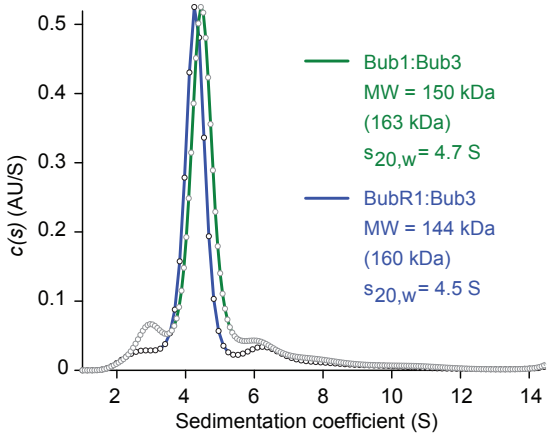

Figure 3.3: Sedimentation velocity analytical ultracentrifugation of Bub1:Bub3 and BubR1:Bub3. Normalised c(s) distribution curves for Bub1:Bub3 (green) and BubR1:Bub3 (blue). A predominant peak at 4.7 $S_{20,w}$ is apparent for Bub1:Bub3 and at 4.5 $S_{20,w}$ for BubR1:Bub3, indicating one dominant sedimenting species that corresponds to a theoretical molecular weight of 150 kDa and 144 kDa, respectively, the theoretical mass of a 1:1 complex is indicated for both in parentheses. Frictional ratios were determined as 2.16 for Bub1:Bub3 and 2.21 for BubR1:Bub3.

The direct interaction of Bub1 and BubR1 was suggested previously [206] and was more recently established and characterised [179, 180]. The complex of Bub1:Bub3 binds to the kinetochore protein Knl1, an interaction that is mediated by Bub3 binding to a phosphorylated MELT-motif on Knl1 [172, 173, 174, 175]. Bub1 contributes to this interaction by a short loop motif, whereas the same motif in BubR1 does not confer any binding affinity towards a phosphorylated MELT-motif. Therefore, the recruitment of BubR1:Bub3 may be directly mediated by dimerising with Bub1:Bub3 [175, 179].
In an effort to recapitulate these interactions *in vitro*, I set out to reconstitute the complex using full-length proteins. Indeed, Bub1:Bub3 and BubR1:Bub3 form a stable and homogenous complex in gel filtration as apparent from the peak shift and co-migrating bands on a SDS PAGE gel (Figure 3.4). The addition of MBP-Knl1$^{138-225}$, a fragment of Knl1 that corresponds to the first MELT-motif as well as the KI1 and KI2 motifs (Figure 3.8), pre-phosphorylated by Mps1, produces an additional peak shift of the complex (Figure 3.4). The binding of MBP-Knl1$^{138-225}$ also leads to a noticeable compaction of the peak (purple) in contrast to the corresponding peak of Bub1:Bub3-BubR1:Bub3 (black). SDS PAGE analysis of the peak fractions demonstrates that MBP-Knl1$^{138-225}$ is a stoichiometric component of the complex. In summary, these results lend strong support to a model in which Bub1:Bub3 is able to interact concomitantly with phosphorylated Knl1 and BubR1:Bub3 at the kinetochore.
The complex of MBP-Knl1$^{138-225}$-Bub1:Bub3-BubR1:Bub3 has a theoretical size of 375 kDa. It is conceivable that the conformation is rather stable, as Bub1 and BubR1 bind each other directly. Bub1 and BubR1 are also each both bound to Bub3, the protein which tethers Bub1 to Knl1. The TPR domains of BubR1 and Bub1 likely also interact with the respective KI2 and KI1 motifs on Knl1, perhaps strengthening the overall interaction. Unfortunately, attempts to crystallise this complex failed (summarised in Table 5.12), therefore I undertook initial attempts to characterise this complex by electron microscopy (EM). On EM grids, the complex is prone to disassembly and shows many small and heterogeneous species in negative stain EM. In preliminary tests, to circumvent the complex disassembly and to favour compact structures, the complex could be stabilised by complex cross-linking using glutaraldehyde in a glycerol gradient (GraFix).

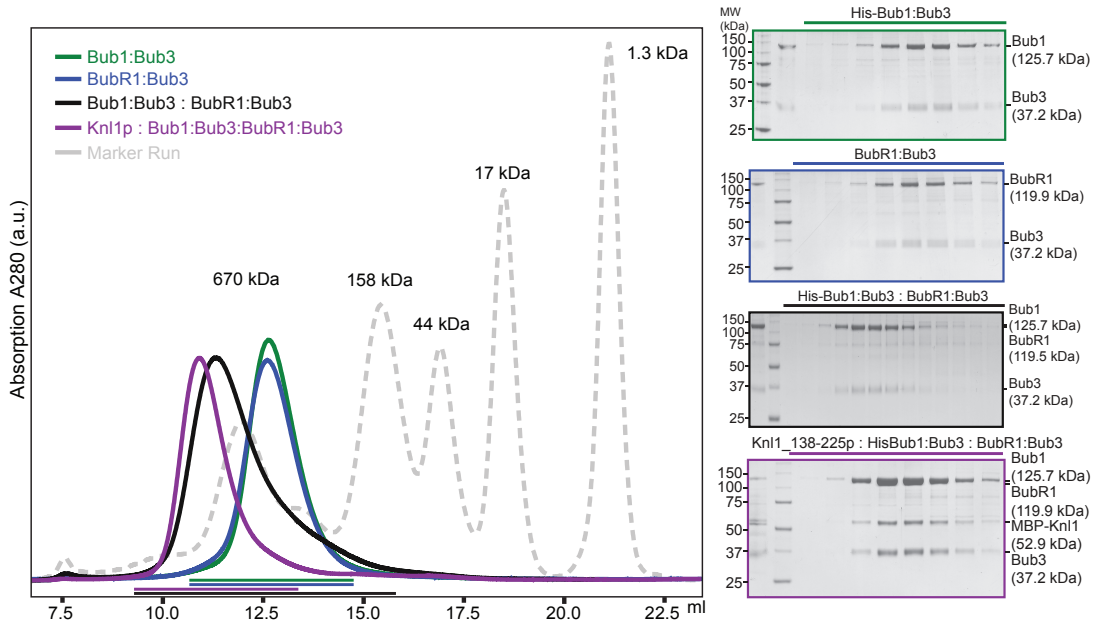

Figure 3.4: Assembly of a Bub1:Bub3-BubR1:Bub3 complex onto Knl1 in gel filtration.
Bub1:Bub3 (green) and BubR1:Bub3 (blue) form a stable complex in size exclusion chromatography (black) and can be assembled as a complex onto phosphorylated MBP-Knl1$^{138-225}$ (purple) on a S6 10 300 column. A marker run on this S6 10 300 column is shown as a dashed grey line. A bar of the respective colour indicates fractions of the formed complexes analysed by SDS PAGE and Coomassie blue staining (right).

Concurrently, in order to determine the stability of the MBP-Knl1$^{138-225}$-Bub1:Bub3-BubR1:Bub3 complex and obtain information regarding a complex suitable for structural studies, a limited proteolysis experiment was performed (Figure 3.5). MBP-Knl1$^{138-225}$-Bub1:Bub3-BubR1:Bub3 proved to be resilient to low concentrations of proteases (1:100). Upon incubation with higher concentrations of proteases, Bub1 and BubR1 are proteolysed, whereas Bub3 as well as Knl1, remain largely intact. This indicated that the Bub3 molecules and Knl1 may be organised in the centre of the complex or are otherwise shielded from proteolysis. Primarily the N-termini of Bub1 and BubR1 (Figure 3.1) are involved in complex assembly, whereas large parts towards the C-termini of Bub1 and BubR1 are probably rather flexible and prone to be proteolysed.

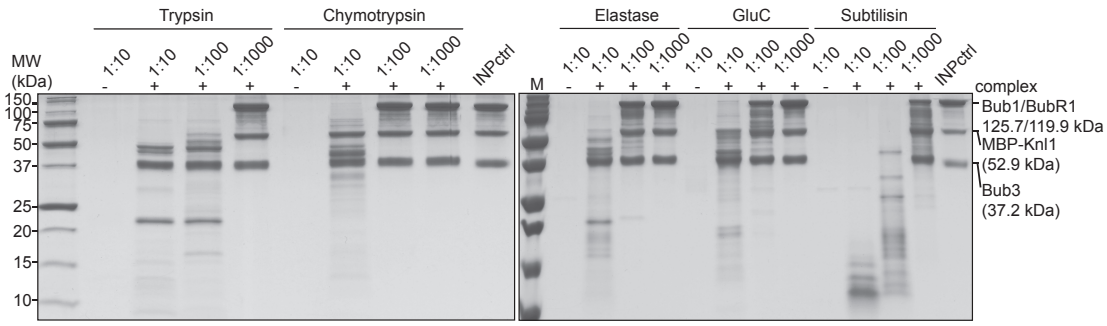

Figure 3.5: Limited proteolysis of the MBP-Knl1$^{138-225}$-Bub1:Bub3-BubR1:Bub3 complex.
The complex was digested with the indicated proteases for 30 min on ice, then quenched with SDS PAGE loading buffer and analysed by SDS PAGE stained with Coomassie blue.

Efforts to obtain structural insight into the overall organisation of this complex by EM are still ongoing, combined with the strategy to identify stable constructs suitable for crystallisation.

3.1.3 Bub1 assembles the MCC *in vitro*

Following the successful formation of the full-length Bub1:Bub3-BubR1:Bub3 complex on phosphorylated Knl1 (Section 3.1.2), we wondered whether this complex was the basis for the assembly of the mitotic checkpoint complex MCC that in addition to BubR1 and Bub3 consists of Cdc20 and Mad2. Both Bub1 and BubR1 possess KEN boxes and ABBA motifs (Figure 3.1) that confer Cdc20 binding [134, 139, 200, 201].
In order to test the assembly of the MCC on the Bub1:Bub3-BubR1:Bub3 complex, a pull-down assay using GST-Cdc20 as bait was implemented. GST-Cdc20 was incubated with Bub1:Bub3 and/or BubR1:Bub3 (Figure 3.6), the binding of the prey was assessed by SDS PAGE (Figure 3.6).

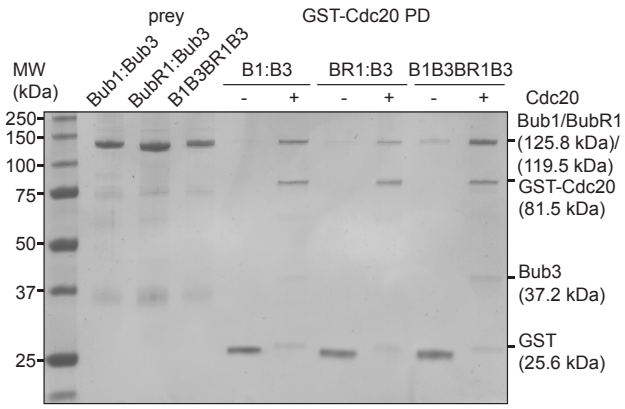

Figure 3.6: Bub1 assembles a complex of Bub1:Bub3-BubR1:Bub3 and Cdc20. GST-Cdc20 was used as bait to pull down Bub1:Bub3 or BubR1:Bub3, or both, as it was shown that they form a complex. Bub1 and BubR1 bind Cdc20 non-competitively. GST was used as a negative control bait. Protein input and pull down fractions were analysed by SDS PAGE and Coomassie blue staining. B1-Bub1; B3-Bub3 BR1-BubR1.

It is evident that GST-Cdc20 is able to pull down both Bub1:Bub3 and BubR1:Bub3 complexes individually. While GST-Cdc20-Bub1:Bub3 seems to be a stoichiometric and tight complex, the binding of GST-Cdc20 to BubR1:Bub3 seems to be less tight and substoichiometric. Importantly, Bub1:Bub3 binding to Cdc20 does not compete with complex formation of BubR1:Bub3-Cdc20 or binding of Bub1:Bub3 to BubR1:Bub3 as they associate into a 5-subunit complex (Figure 3.6). This suggests that Bub1 might be the initial receptor for Cdc20 binding and also for assembly of a Bub1:Bub3-BubR1:Bub3-Cdc20 complex as a precursor-MCC.

Given that Bub1:Bub3-BubR1:Bub3-Cdc20 is a stable complex, I opted to establish how the complex is organised on a molecular level. Since Bub1:Bub3 appeared to bind Cdc20 stoichiometrically compared to substoichiometric binding of BubR1:Bub3 to Cdc20 (Figure 3.6), I used mutants in both Bub1 KEN boxes (KEN to AAA), in combination with a mutation in the ABBA motif (FHVF to AHVA) in a GST-Cdc20 pull-down to assess which sites were required for efficient Cdc20 binding (Figure 3.7).
Bub1:Bub3 bound GST-Cdc20 in a stoichiometric complex as also shown in Figure 3.6. In contrast, both KEN1 and ABBA mutants show reduced binding to GST-Cdc20 as compared to wild-type

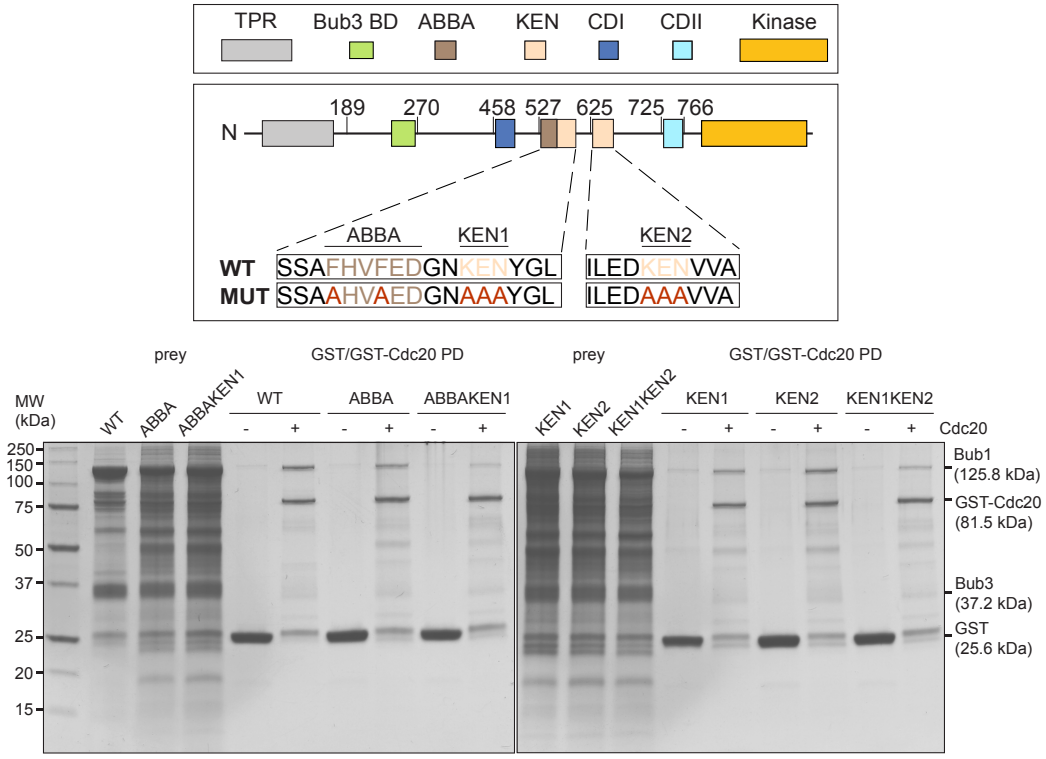

Figure 3.7: Mutation of the ABBA and KEN motifs of Bub1 affect Cdc20 binding.
Top, domain organisation of Bub1 with detailed view of the sequence of ABBA and KEN motifs and the mutations used in the particular motif. Below, affinity-purified Bub1:Bub3 constructs were used as prey for GST-Cdc20 immobilised on GSH affinity resin, GST was used as a negative control; protein input and bound complexes were analysed by SDS PAGE and Coomassie blue staining. KEN and ABBA refer to mutations in the respective motifs as indicated in the schematic drawing above; WT-wild-type.

Bub1:Bub3, whereas mutating KEN2 barely affected GST-Cdc20 binding. Additionally, the combination of ABBA and KEN1 mutations led to a further, more drastic reduction of Cdc20 binding. A stronger reduction of Cdc20 binding could also be observed with a KEN1/KEN2 double mutant, yet to a lesser extent. Likely, KEN1 and the preceding ABBA-motif represent a major binding site for Cdc20 although KEN2 also retains binding affinity or contributes to Cdc20 binding. It is therefore conceivable that Bub1 recruits Cdc20 via its ABBA-KEN1 motif, bringing Cdc20 into close proximity with BubR1:Bub3, which is also bound to Bub1, thus serving as a platform to build the MCC.

In order to deconvolute the organisation of the complex, I sought to investigate the interactions within the Bub1:Bub3-BubR1:Bub3-Cdc20 complex in more detail. To this end, the Bub1:Bub3-BubR1:Bub3-GST-Cdc20 complex was assembled onto MBP-Knl1$^{138-225}$, phosphorylated by Mps1. This assembly was subsequently subjected to cross-linking by disuccinimidyl suberate (DSS), a compound that covalently cross-links primary amines of lysine side chains within the vicinity of approximately 11 Å of each other. The cross-linked complex was proteolytically digested and analysed by mass spectrometry to determine sites of protein interaction (Figure 3.8). A comprehensive list of all identified cross-linked peptides can be found in the Appendix Tables 6.3 and 6.4.

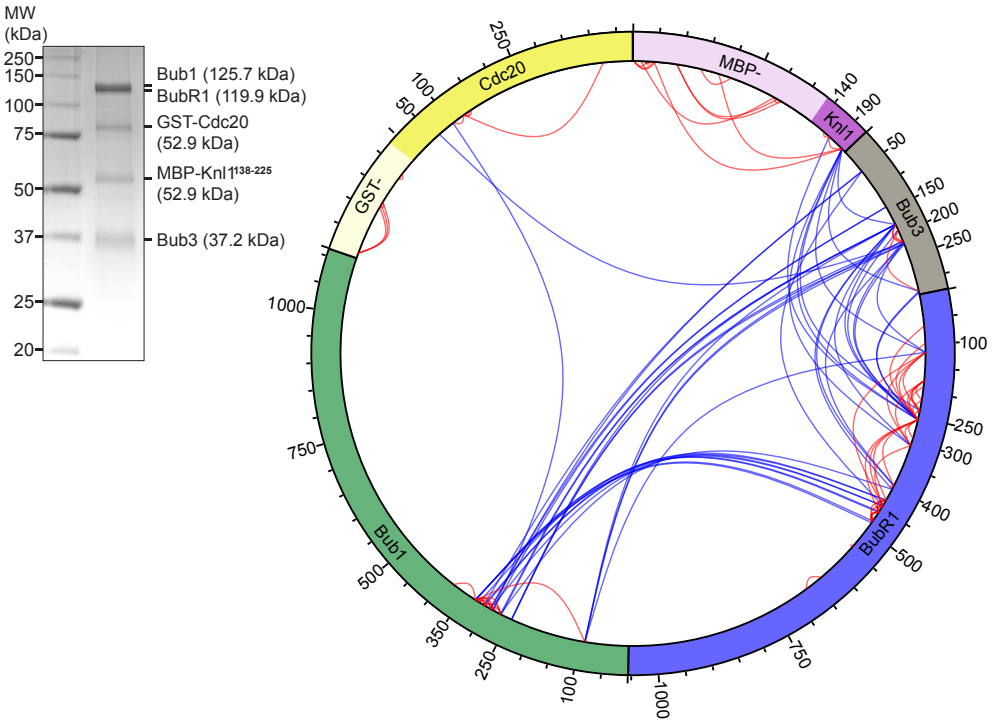

Figure 3.8: Cross-linking analysis of a Knl1$^{138-225}$-Bub1:Bub3-BubR1:Bub3-Cdc20 complex.
Left, the Knl1$^{138-225}$-Bub1:Bub3-BubR1:Bub3-Cdc20 complex was purified on a S6 10 300 column, pooled and analysed by SDS PAGE and Coomassie blue staining. Right, visualisation of complex interactions after cross-linking with DSS, proteolytic digest and analysis of resulting peptides by mass spectroscopy. Intramolecular cross-links are depicted in red, intermolecular cross-links in blue; the residue numbers of the constructs are indicated on the outer circle. The GST-/MBP-tag of Cdc20 (yellow) or Knl1 (purple) are represented in a lighter shade of yellow and purple, respectively. Note that Bub1 (green) and BubR1 (blue) both bind Bub3 and that the central Bub3 (grey) in the scheme most likely represents two molecules of Bub3.

As Bub1 and BubR1 were both found to be bound to Bub3 in the Bub1:Bub3-BubR1:Bub3-GST-Cdc20 complex, in all likelihood the complex contains two molecules of Bub3. These two distinct Bub3 molecules are indistinguishable by cross-linking and thus are represented as one Bub3 in Figure 3.8. Bub3 appears to be a central component that establishes contacts to all other proteins in the complex. The main interactors of Bub3 are the N-termini of Bub1 and BubR1, which share cross-links with Bub3. The sites of interaction on Bub1 and BubR1 are distributed around the Bub3-binding site of Bub1 (residues 235-255) and BubR1 (residues 395-405). This site on Bub1 and BubR1 is immediately followed by a region of direct interaction between Bub1 and BubR1, which is in perfect agreement with our recent definition of a minimal Bub1:Bub3-BubR1:Bub3 interaction site [179]. This Bub1-BubR1 binding site analysis allows to define the region of interaction more closely to residues 280-330 for Bub1 and 430-480 for BubR1. Cross-links appear exclusively in the N-terminal half of Bub1 and BubR1. Interaction of their TPR domains with Knl1 can only be observed for BubR1, not Bub1. Cdc20 appears to be tethered to the complex by the Bub1:Bub3 complex, as also alluded to in the previous paragraphs and Figures 3.6 and 3.7. The identified interaction by cross-link here suggests that the N-terminus of Cdc20 (before the start of the propeller) contacts Bub1 in the same region where also Bub3 and BubR1 bind to Bub1. This could in turn also account for the observed

cross-link between Cdc20 and Bub3 as well as be the basis for Cdc20 delivery to BubR1, as this is a site of close contact for all three proteins, Bub1, BubR1 and Cdc20.

It should be noted that the absence of cross-links does not signify lack of interaction. In the case of MBP-Knl1$^{138-225}$, the presence of intramolecular cross-links between Knl1$^{138-225}$ and the MBP-tag might indicate that the MBP-tag partly shields the Knl1 fragment from binding other proteins, particularly the TPR domains of Bub1 or BubR1. Conversely, an interaction present in the complex but not visible by cross-linking might be restricting access of the cross-linking agent DSS.

Taken together, we conclude that the ABBA-KEN1 motif is required for Bub1-Cdc20 interaction, as shown in Figure 3.7. Additionally, cross-linking analysis suggests that the N-terminus of Cdc20 might also engage in contacting Bub1. This is intriguing for two reasons: First, the identified Bub1-Cdc20 cross-link is located in a region immediately preceding the Cdc20-Mad2 interaction site, which puts yet another MCC component (besides Bub3 and BubR1) at the same site of interaction. Second, the N-terminus of Cdc20 has also been reported to be phosphorylated by Bub1 [163]. The direct interaction of Bub1-Cdc20 now places the N-terminus of Cdc20 in direct reach of the kinase activity of Bub1.

The MBP-Knl1$^{138-225}$-Bub1:Bub3-BubR1:Bub3-GST-Cdc20 complex is the basis of how we could envision the mitotic effector complex to be formed. The prevailing question that arises is how the MCC complex is then released from kinetochore-bound Bub1 to bind and inhibit the APC/C.

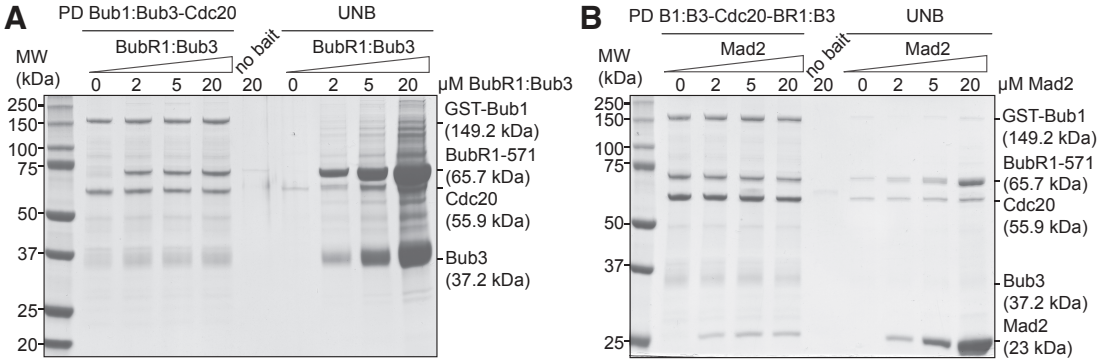

Figure 3.9: Formation of a soluble MCC complex.
(A) The complex of GST-Bub1:Bub3-Cdc20 is preformed and bound to beads. Addition of increasing amounts of BubR1$^{1-571}$:Bub3 leads to a stoichiometric bound complex, with only the excess of BubR1$^{1-571}$:Bub3 in the soluble fractions. (**B**) The complex of GST-Bub1:Bub3-BubR1$^{1-571}$:Bub3-Cdc20 binds Mad2, using an excess of Mad2 leads to the solubilisation of MCC components. GSH-beads without bait were used as a control for unspecific binding. Soluble fractions and fractions bound to beads were analysed by SDS PAGE and Coomassie blue staining.

In a pull-down assay using GST-Bub1:Bub3 as prey, Cdc20 and BubR1$^{1-571}$:Bub3 form a complex on GST-Bub1:Bub3 (Figure 3.9 A). The complex cannot be displaced from Bub1 and solubilised by adding an excess of BubR1$^{1-571}$:Bub3, as revealed by the SDS PAGE analysis. Only BubR1$^{1-571}$:Bub3, which is added in excess, is present in the soluble (UNB in Figure 3.9 A) fractions. These data suggest that BubR1:Bub3 addition to a GST-Bub1:Bub3-Cdc20 complex is not sufficient for the release of Cdc20-BubR1:Bub3 from the complex on Bub1.

Since BubR1:Bub3 is incapable of competing Cdc20 off Bub1, we reasoned that Mad2, as fourth MCC component, could be the releasing factor. By using the same setup as in Figure 3.9 A, we assembled Cdc20 and BubR1$^{1-571}$:Bub3 on GST-Bub1:Bub3 and then titrated Mad2 onto the complex (Figure 3.9 B). In the GST-Bub1:Bub3-bound fractions, we identify the components of the MCC bound to Bub1. Upon the addition of increasing concentrations of Mad2, a soluble pool (UNB in Figure 3.9 B) of MCC protens is detectable, which is reflected in the decrease of bound BubR1$^{1-571}$. However, the quantity of Mad2 required to produce soluble MCC amounts to a 20-fold excess over the other MCC components (Figure 3.9). The fact that the majority of the MCC proteins is still bound to Bub1 argues that other release factors are still missing. A possible contributor facilitating MCC formation and not being part of the experimental setup used above is Mad1, an essential protein of the checkpoint response [125, 238, 154]. Furthermore, a second molecule of Cdc20 might be essential for the formation of the MCC, or more specifically, the release of Cdc20 from Bub1, as it could compete for Bub1 binding resulting in the liberation of a BubR1-Cdc20 complex. Another alternative for catalysing the formation of the MCC could be the kinase activity of Bub1, whose contribution to checkpoint signalling remains doubtful and debatable, but was nevertheless also claimed to be of importance [163, 214]. Cdc20 has been reported to be phosphorylated by Bub1, resulting in the inhibition of the APC/C^{Cdc20}[163]. Also Bub1 itself is a substrate for Bub1 kinase activity, although the effect of these autophosphorylations remains uncertain.

3.2 Biochemical characterisation of Bub1 and BubR1 kinase activity

It was alluded to in the introduction that the extent and role of Bub1 as well as BubR1 kinase activity remains ambiguous. In order to address this controversial issue, I set out to methodically establish and characterise the degree of Bub1 and BubR1 kinase activity *in vitro*. Various BubR1 kinase domain constructs were generated, in order to answer the prevailing question. In the following, the most commonly used BubR1 construct encompassing residues 705-1050 will be referred to as BubR1^{kinase}. The corresponding construct of Bub1 kinase domain containing amino acids 725-1085 will be named Bub1^{kinase} for ease of reference (Figure 3.10 A).

3.2.1 Expression and purification of Bub1 and BubR1 kinase constructs

BubR1^{kinase}was cloned into a pFH vector, expressed and purified as described in Sections 5.2.1 and 5.2.2; along with Bub1^{kinase}, which was already available in a pFG vector. Both constructs were purified by affinity chromatography (Ni^{2+} for BubR1^{kinase}, GSH for Bub1^{kinase}), followed by anion exchange (Bub1^{kinase} was collected as a practically pure protein from the flow-through) and size exclusion chromatography. The proteins were pooled after size exclusion chromatography, as depicted in Figure 3.10 B and C.

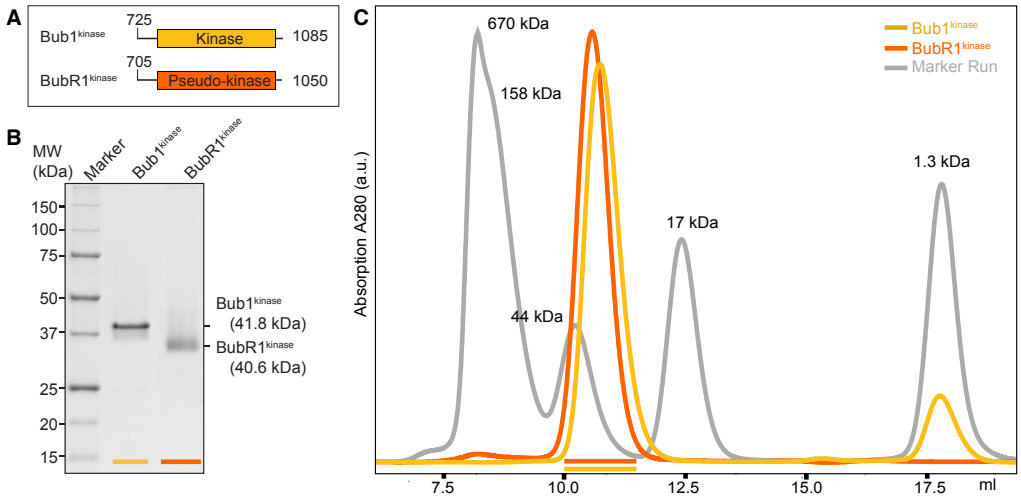

Figure 3.10: Bub1 kinase and BubR1 pseudo-kinase are purified to homogeneity.
(**A**) Bub1 and BubR1 kinase domain organisation with indicated construct boundaries. (**B**) Purified Bub1^{kinase} and BubR1^{kinase} were separated by SDS-PAGE and analysed by Coomassie blue staining. Their respective sizes are indicated on the right. (**C**) Bub1^{kinase} (yellow) and BubR1^{kinase} (orange) elute as pure and globular proteins in size exclusion chromatography. Pooled fractions are indicated by a bar of the respective colour. A molecular weight standard is given in grey.

BubR1^{kinase} and Bub1^{kinase} eluted as globular proteins from gel filtration, as monomers of around 40 kDa. SDS PAGE analysis reveals the homogeneity of the final protein pools (Figure 3.10 B). As an initial indication for kinase activity, Bub1^{kinase} and BubR1^{kinase} were assessed with regard to their potential to undergo autophosphorylation. Therefore, Bub1^{kinase} and BubR1^{kinase} were incubated with ATP and $MgCl_2$, any change in mass after the reaction was analysed by ESI-MS (Figure 3.11).

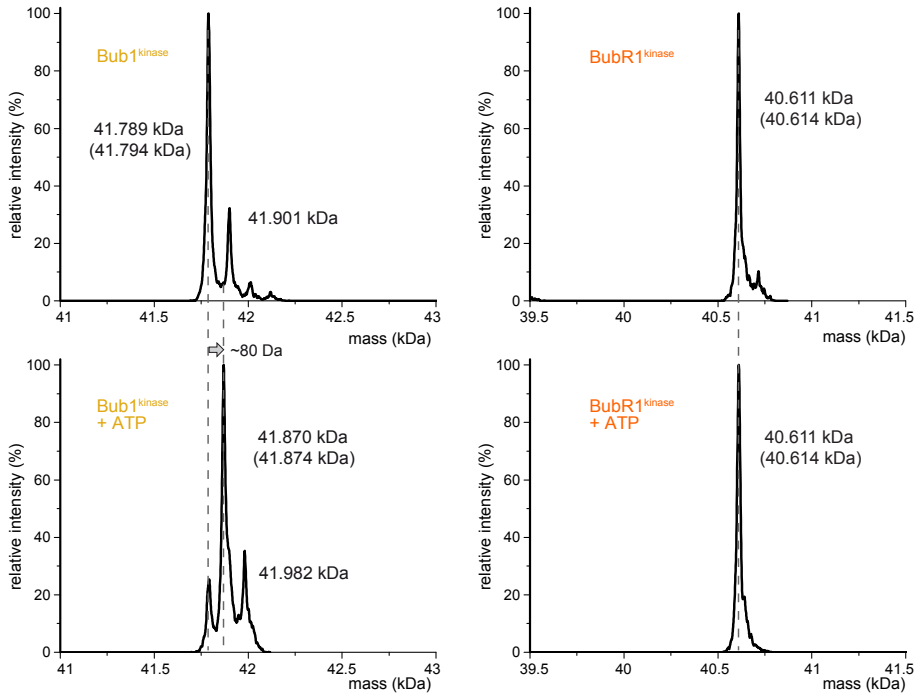

Figure 3.11: ESI-MS of Bub1^{kinase} and BubR1^{kinase}.
The mass of BubR1^{kinase} before and after incubation with ATP reflects its theoretical unmodified mass 40.6 kDa (upper and lower right) whereas Bub1^{kinase} autophosphorylates in the presence of ATP (upper and lower left). The theoretical weight is given in parentheses.

BubR1^{kinase} does not autophosphorylate, as demonstrated by its mass, being the theoretical size of approximately 40611 Da, irrespective of the presence or absence of ATP. In contrast, an evident increase in mass could be observed for Bub1^{kinase}, from 41789 Da to 41870 Da upon incubation with ATP. The shift of the peak to a higher mass corresponds to the addition of one phosphate (80 Da) shown in Figure 3.11. A small fraction of Bub1^{kinase} remained unphosphorylated, which is apparent from the small persisting peak at 41789 Da. Furthermore, the sample contains a small but significantly larger species of Bub1 (41901 Da), which correlates with other autophosphorylation products. This observation leads to the elementary conclusion that while Bub1^{kinase} is able to autophosphorylate, BubR1^{kinase} is not.

3.2.2 Nucleotide binding of Bub1^{kinase} and BubR1^{kinase} *in vitro*

I next asked whether the absence of autophosphorylation of BubR1^{kinase}, as opposed to Bub1^{kinase}, reflected a lack of nucleotide binding ability of BubR1^{kinase}. To address this question I took advantage of fluorescent properties of mant-ATP [239] a nucleotide-analog whose emission at 450 nm changes upon alteration of the fluorophore environment (as the incorporation into the kinase active site).
I performed a titration experiment where I titrated mant-ATP up to 1 mM, then added 1 µM Bub1^{kinase} or BubR1^{kinase} to all conditions. The resulting change in fluorescence of free mant-ATP to bound mant-ATP-kinase complex is plotted against total mant-ATP concentration (Figure 3.12).

In this setting, BubR1^{kinase} exhibited the same degree of mant-ATP binding as Bub1^{kinase}, with K_D in the range of 300-400 µM. This indicates that BubR1^{kinase}, despite the lack of kinase activity, is still able to bind nucleotides (Figure 3.12).

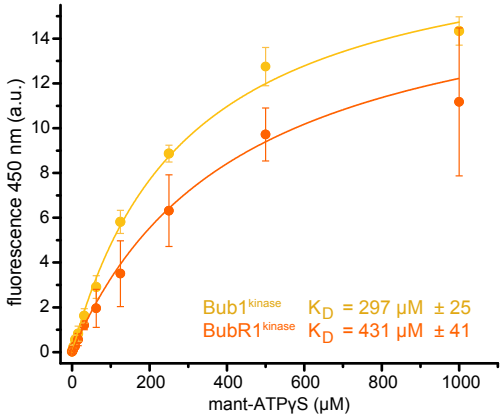

Figure 3.12: Bub1^{kinase} and BubR1^{kinase} are mant-nucleotide-binding proteins.
Fluorescence emission (excitation: 340 nm) of Bub1^{kinase} (yellow) or BubR1^{kinase} (orange) and mant-ATP alone were subtracted from the emission of Bub1^{kinase}/BubR1^{kinase} with mant-ATP. The change in fluorescence emission at 450 nm was plotted as a function of total mant-ATP concentration (1-1000 µM) using 1 µM Bub1^{kinase}/BubR1^{kinase} in all measurements. The data were fitted with a one-site binding equation using Origin 9.0 to obtain a K_D of 297 µM for Bub1^{kinase} and 431 µM for BubR1^{kinase}.

The relatively low affinity of BubR1^{kinase} and Bub1^{kinase} for mant-ATP, in comparison to previous measurements with other kinases (for example reference [240]), could reflect an unfavourable interaction of the mant group with the kinase scaffold, thereby reducing the overall binding affinity for the modified nucleotide. Nevertheless, I could verify that mant-ATP is a substrate of Bub1 (Appendix Figure 6.3), therefore the similarity of binding affinity for Bub1^{kinase} and BubR1^{kinase} suggests that they are both competent to bind nucleotides.

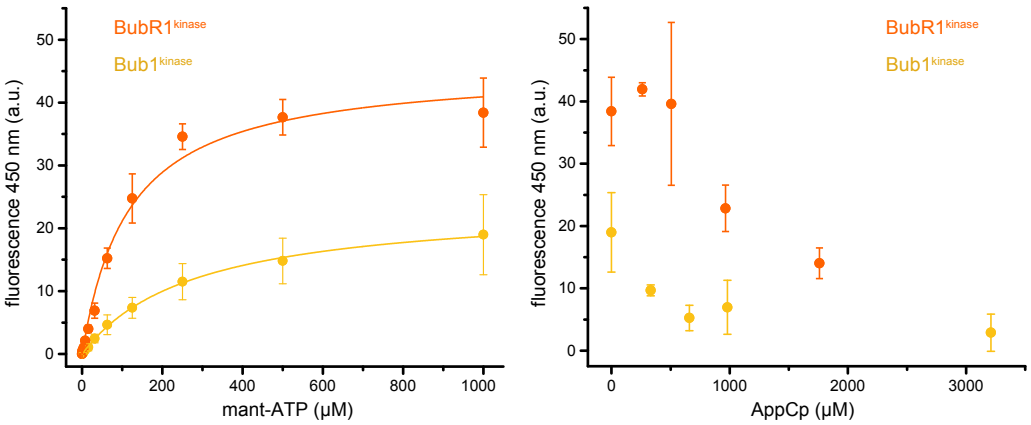

Figure 3.13: Nucleotide-binding of Bub1^{kinase} and BubR1^{kinase} is specific.
Titration of mant-ATP to Bub1^{kinase} (yellow) or BubR1^{kinase} (orange) as in Figure 3.12, (left). After achieving maximal binding of mant-ATP (1 mM), an ATP analog, AppCp, was added at the indicated concentrations, resulting in dose-dependent reduction of the mant-ATP fluorescence signal (right). (excitation: 340 nm, emission: 450 nm)

To further confirm the specificity of nucleotide-binding and exclude unspecific binding of mant-ATP, I performed a competition experiment by titrating an unlabeled uncleavable ATP analog, AppCp,

onto the putative complex of Bub1^{kinase}-mant-ATP, or BubR1^{kinase}-mant-ATP, respectively. Upon increasing concentrations of AppCp, the fluorescence signal of bound mant-ATP dropped in a dose-dependent manner, which is consistent with mant-ATP being replaced by AppCp in the active site (Figure 3.13). Thus, this experiment confirms that mant-ATP specifically binds to the ATP-binding site of both kinases.

3.2.3 BubR1 is an inactive pseudo-kinase

Given that BubR1^{kinase}proved capable of nucleotide binding, I wanted to investigate whether it was also able to phosphorylate protein substrates. The kinase activity of BubR1^{kinase} and full-length BubR1:Bub3 was tested on MBP, histone H1 and the Borealin:Survivin complex, all of which are proteins that are used as surrogate kinase substrates for lack of known and established BubR1 substrates. The phosphorylation reactions were then analysed by SDS PAGE and phosphostaining using the Pro-Q® Diamond Phosphoprotein Gel Stain (Figure 3.14).

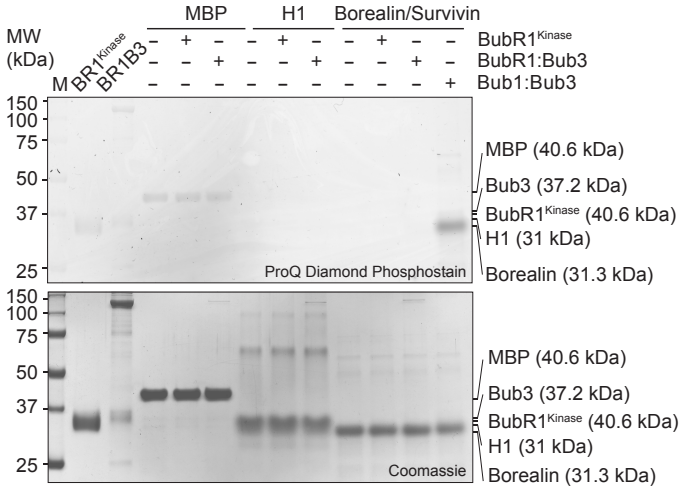

Figure 3.14: BubR1 is not an active kinase.
Maltose binding protein (MBP), histone H1 and Borealin/Survivin were incubated with 50 nM BubR1 constructs and ATP, then analysed by SDS PAGE and Coomassie blue staining (below). Phosphates were visualised using the Pro-Q®Diamond Phosphoprotein Gel Stain (above). 10 nM Bub1:Bub3 was used as a positive control. BR1–BubR1, BR1B3–BubR1:Bub3, M–protein marker.

BubR1 failed to hydrolyse nucleotides or phosphorylate MBP, histone H1 or Borealin in this assay. In contrast, Bub1 successfully phosphorylated Borealin at five-fold lower kinase-to-substrate ratio (Figure 3.14, last lane). Presumably, the BubR1 kinase domain containing the formerly functionally relevant residues was preserved due to structural reasons [196]. Protein stability is a particularly plausible argument with regard to our finding that Bub1 protein stability depends upon the integrity of the kinase as well, as seen in a disruptive K821R kinase mutant. The ability of BubR1 to still bind nucleotides might have a similar stabilising purpose. We cannot entirely exclude that there are substrates actually phosphorylated by BubR1, or that there is a missing factor required for activating BubR1, a role that has been suggested for CENP-E [218, 219]. However, our findings in combination with the fact that the catalytic motifs in BubR1 are divergent from the kinase consensus [196] provide compelling evidence that although Bub1^{kinase} and BubR1^{kinase} are both ATP-binding proteins, only Bub1^{kinase} is an active, phosphorylating enzyme. BubR1 will therefore in the following be regarded and depicted as a pseudo-kinase.

3.2.4 Kinetic characterisation of Bub1 kinase activity

Bub1 is known to be an active kinase, as confirmed in the preceding section. However, a comprehensive characterisation and determination of regulating factors of Bub1 kinase activity are still missing. In order to quantify kinase activity in more detail, I used the ADP-Glo^{TM} Kinase Assay. This assay detects ADP generated in a phosphorylation reaction, which is linearly correlated with a luminescent signal created in a subsequent reaction. This relation thus permits the quantification of kinase activity, the plot of an ADP-standard is shown in Figure 6.2 (Appendix). The detailed protocol can be found in Section 5.2.4, the working principle of the assay is schematically depicted in Figure 5.1.

Bub1 activity is not regulated by Bub1 domains outside the kinase domain

To date, the role of molecular regulation of Bub1 by intrinsic (intramolecular domains, autophosphorylation) and extrinsic (binding proteins, phosphatases) factors remains unclear. The N-terminal TPR domain (Figure 3.1) has previously been shown to have an essential role in sustaining kinase activity, as determined in kinase assays performed with immuno-precipitates from HeLa cells or MEFs [208, 225]. This could not be confirmed *in vitro* [224], using recombinant Bub1 with a deleted TPR domain and full-length Bub1. To address this discrepancy, both Bub1^{kinase} and full-length Bub1:Bub3 were tested for their ability to phosphorylate H2A or Borealin (Figure 3.15 A-B) and assessed for their

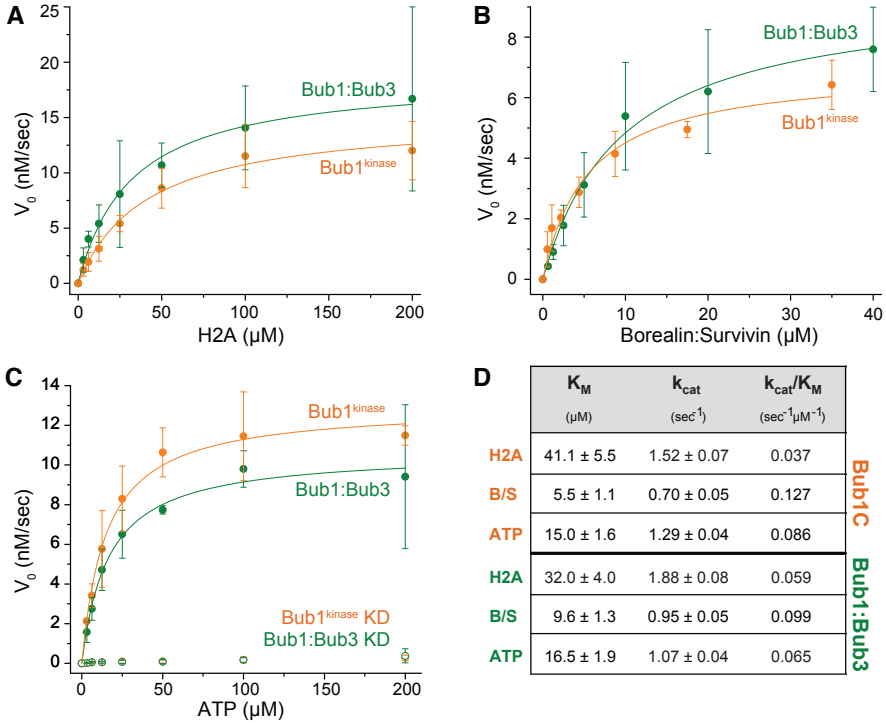

	K_M (μM)	k_{cat} (sec^{-1})	k_{cat}/K_M ($sec^{-1}\mu M^{-1}$)
H2A	41.1 ± 5.5	1.52 ± 0.07	0.037
B/S	5.5 ± 1.1	0.70 ± 0.05	0.127
ATP	15.0 ± 1.6	1.29 ± 0.04	0.086
H2A	32.0 ± 4.0	1.88 ± 0.08	0.059
B/S	9.6 ± 1.3	0.95 ± 0.05	0.099
ATP	16.5 ± 1.9	1.07 ± 0.04	0.065

Figure 3.15: Kinetic characterisation of Bub1 complexes.
(**A**-**C**) Bub1^{kinase} and Bub1:Bub3 (each 10 nM) exhibit the same catalytic activity towards H2A (**A**) and Borealin (**B**), both also hydrolyse ATP at the same rate (**C**). The mutation D917N abrogates ATPase activity, H2A was used as a substrate; KD-kinase dead. (**C**). The kinase activity was determined using the ADP-Glo^{TM} Kinase Assay and is plotted as a function of substrate concentration to allow fitting with the Michaelis-Menten equation using Origin 9.0 with R^2=0.99 (Bub1^{kinase} on Borealin/Survivin (B/S) R^2=0.97). Error bars are SD of a mean of at least two independent experiments. (**D**) Kinetic parameters of the Michaelis-Menten fits as determined in (**A**-**C**).

potential in ATP hydrolysis (Figure 3.15 C) by the ADP-Glo^{TM} Kinase Assay. The initial reaction velocities were obtained from the amount of ADP generated in a time-course of the phosphorylation reaction and they are shown as a function of substrate concentration in Figure 3.15. The data were fitted using Origin 9.0 (OriginLab Corp., Northampton, USA) and by means of the Michaelis-Menten equation described in Equation 5.1.

We find that Bub1^{kinase} and Bub1:Bub3 are equally able to phosphorylate H2A and Borealin efficiently using substoichiometric amounts of kinase (Figure 3.15 A-B). Furthermore, the rate of ATP-hydrolysis of Bub1^{kinase} and Bub1:Bub3 is equivalent. Kinase activity can be specifically and efficiently inhibited by mutating the catalytic aspartate (D917) in Bub1^{kinase} and the full-length protein. Both, Bub1^{kinase} and Bub1:Bub3 showed very similar catalytic properties in terms of K_M and k_{cat}/K_M values that are measures of substrate affinity and efficiency of phosphorylation, respectively (Figure 3.15 D). The lack of any striking difference argues that Bub1 activity is not regulated intramolecularly or by Bub3. Of note, with reference to the K_M value and the catalytic efficiency (k_{cat}/K_M), H2A is found to be a worse substrate for Bub1 than Borealin. Although the maximal velocity of the reaction and therefore k_{cat} is rather high, the overall efficiency is lowered due to a low K_M for H2A.

Bub1 binding to nucleosomes enhances its affinity towards H2A

We were surprised to see that Borealin seemed to be a better substrate than H2A *in vitro*. We wondered whether Bub1 activity could be directed on a level of substrate specificity and asked if phosphorylation of nucleosomes rather than H2A alone was a more efficient process. For this purpose, I incubated reconstituted nucleosomes containing either histone H3 or its centromere variant CENP-A with Bub1:Bub3 or Bub1^{kinase}. Phosphorylation was assessed by SDS PAGE using the Pro-Q® Diamond Phosphoprotein Gel Stain (Figure 3.16 A).

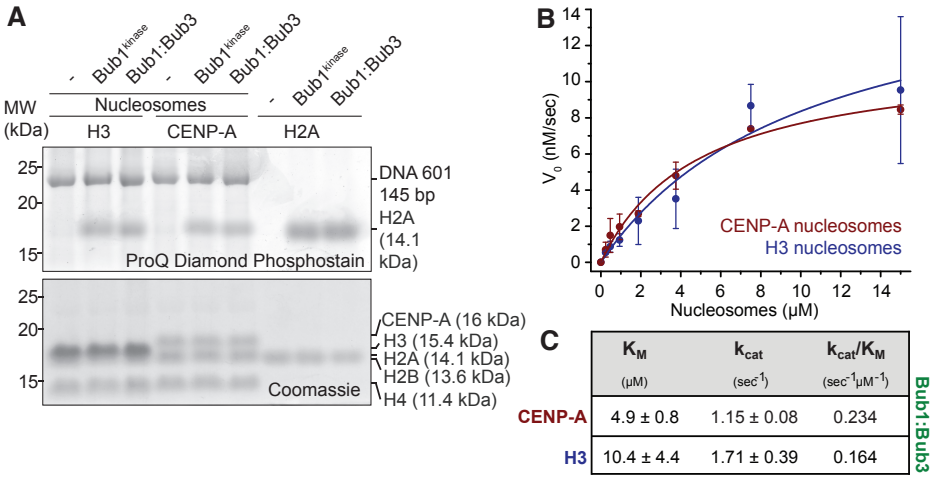

Figure 3.16: Bub1 does not discriminate between H2A incorporated in H3- or CENP-A nucleosomes.
(**A**) H2A or H2A contained in H3- or CENP-A nucleosomes is efficiently phosphorylated by Bub1^{kinase} kinase domain and Bub1:Bub3 full-length complex (each 10 nM). Kinase reactions were analysed by SDS PAGE and Coomassie blue staining (right), phosphates were visualised using the Pro-Q® Diamond Phosphoprotein Gel Stain (left). Note that DNA is also stained by this compound. (**B**) The kinase activity of 10 nM Bub1:Bub3, is plotted as a function of substrate concentration that allows fitting with the Michaelis-Menten equation using Origin 9.0 with R^2=0.95 (H3) and 0.99 (CENP-A). Error bars represent SD of a mean of at least two independent experiments. (**C**) Kinetic parameters of the Michaelis-Menten fits obtained in (**B**).

We observe that H2A is efficiently phosphorylated by Bub1^{kinase} and Bub1:Bub3 regardless of its incorporation into nucleosomes. Conversely, a subtle difference manifests when comparing the kinetics of the phosphorylation of H2A contained in nucleosomes to free H2A as measured by the ADP-Glo^{TM} Kinase Assay. The K_M of the reaction (a measure of substrate affinity) improves to 5-10 µM as compared to 30 µM for H2A, which leads to a four-fold enhanced overall catalytic efficiency k_{cat}/K_M (Figure 3.16 C, 3.15 D). The increase in catalytic efficiency argues that nucleosomes are a better substrate for Bub1 than H2A alone. This might suggest that H2A by itself lacks features implicated in recognition by Bub1 and that the phosphorylation of H2A could be enhanced by nucleosome binding of Bub1.
The notion that Bub1 directly binds to nucleosomes was tested in an electrophoretic mobility shift assay (EMSA). Both, autophosphorylated and dephosphorylated Bub1^{kinase} were compared in their ability to bind to CENP-A- or H3-nucleosomes, or free DNA. Upon mixing Bub1^{kinase} with nucleosomes, I observe a band shift to higher molecular weight with increasing amounts of Bub1^{kinase}, indicating complex formation.

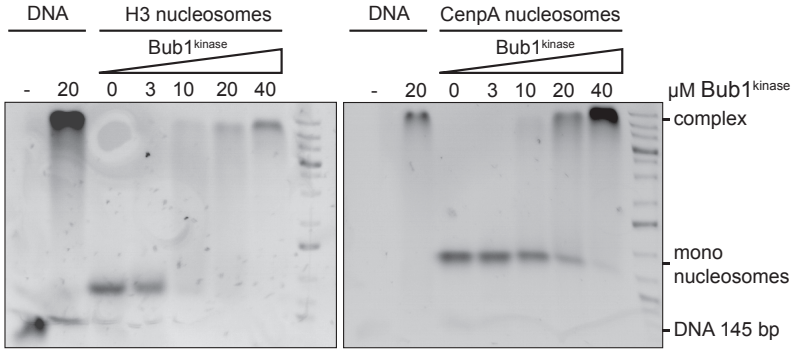

Figure 3.17: Bub1^{kinase} binding to H3- and CENP-A containing nucleosomes.
EMSA showing DNA and nucleosome binding of Bub1^{kinase} and H3- or CENP-A nucleosomes. The right lane of each agarose gel shows a DNA ladder as reference.

We note that Bub1^{kinase} binds both CENP-A- and H3-nucleosomes with similar apparent affinity (Figure 3.17), which is consistent with Bub1 phosphorylating H2A in both CENP-A- and H3 containing nucleosomes (Figure 3.16). Furthermore, binding of nucleosomes was found to be independent of the phosphorylation status of Bub1^{kinase} as shown in Appendix Figure 6.4. However, Bub1^{kinase} also readily binds to DNA at least in this experimental setting (Figure 3.17), providing a potential explanation for improved binding of Bub1 to nucleosomes as compared to free H2A (Figure 3.15 and 3.16).

Bub1 activity is not regulated by extrinsic factors

Having established that Bub1 kinase activity is not regulated by other domains within Bub1, we wondered whether there were other extrinsic factors modulating kinase activity. We successfully expressed and purified Bub1:Bub3 and BubR1:Bub3 complexes recombinantly (as described in Section 3.1.1 and 3.1.2). The reconstitution of different Bub1 complexes allowed us to test whether BubR1 or addition of Knl1 would alter kinase activity of Bub1 as measured by the ADP-Glo^{TM} Assay (Figure 3.18).

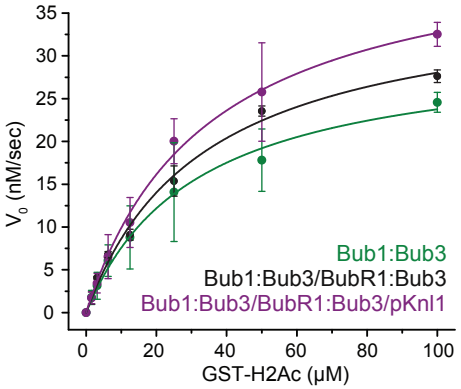

GST-H2Ac

K_M (μM)	k_{cat} (sec^{-1})	k_{cat}/K_M (sec^{-1} μM^{-1})	
31.2 ± 4.1	3.12 ± 0.17	0.100	Bub1:Bub3
33.3 ± 4.3	3.74 ± 0.2	0.112	Bub1:Bub3/ BubR1:Bub3
34.4 ± 3.6	4.39 ± 0.19	0.128	Bub1:Bub3/ BubR1:Bub3/ pKnl1

Figure 3.18: Complexes of Bub1 exhibit the same kinase activity toward a GST-H2A substrate.
The kinase activity is plotted as a function of substrate concentration to allow fitting with the Michaelis-Menten equation using Origin 9.0 with R^2=0.99. Error bars represent SD of a mean of at least two independent experiments. (D) Kinetic parameters of the Michaelis-Menten fits as determined in (C). a.u.-arbitrary units. 10 nM kinase complex was consistently used in all experiments.

Kinase activity was tested against the H2A tail-peptide as substrate, using full-length H2A with the ADP-Glo^{TM} Kinase Assay yielded similar results (Appendix Figure 6.5, 3.15). We could not detect any effect on Bub1 activity upon formation of the Bub1:Bub3-BubR1:Bub3 complex, with or without Knl1, which is also largely consistent with previous findings [224]. Collectively, our results argue that Bub1 kinase activity is not regulated by extrinsic factors, neither on an intra- nor intermolecular level.

3.2.5 Bub1 is an autophosphorylated kinase

It has been suggested recently that Bub1 undergoes autophosphorylation and thereby regulates its own activity [224]. When incubated with 1 mM ATP for 16 hours, Bub1^{kinase} indeed autophosphorylates (Figure 3.11 and 3.19 A) and LC-MS/MS confirmed S969 on the substrate binding loop (P+1 loop) to be the phosphorylated residue. We then asked if phosphorylation of S969 was a prerequisite for kinase activity. To this end, we created alanine (S969A), glutamate (S969E) and aspartate (S969D) mutants of S969 in Bub1^{kinase} (Figure 3.19 B and C).
After incubation with ATP and subsequent SDS PAGE analysis, no phosphorylation-dependent shift could be detected for the Bub1^{kinase} mutations or dephosphorylated Bub1^{kinase}. Importantly however, a phosphorylation-dependent shift is clearly discernible for wild-type Bub1^{kinase} (Figure 3.19 B), strongly suggesting that S969 is the major autophosphorylation site within the kinase domain.
As Bub1 activity did not seem to be regulated by extrinsic factors, we wondered whether we could confirm an intramolecular effect of kinase regulation by autophosphorylation. We assessed the activity of the S969A and S969D mutants on H2A using the ADP-Glo^{TM} Kinase Assay and found that, while the phospho-mimicking mutation S969D is able to phosphorylate H2A efficiently, the S969A mutation markedly reduced kinase activity (Figure 3.19 D and E). Consistently, also S969E rescues kinase activity (Appendix Figure 6.6).

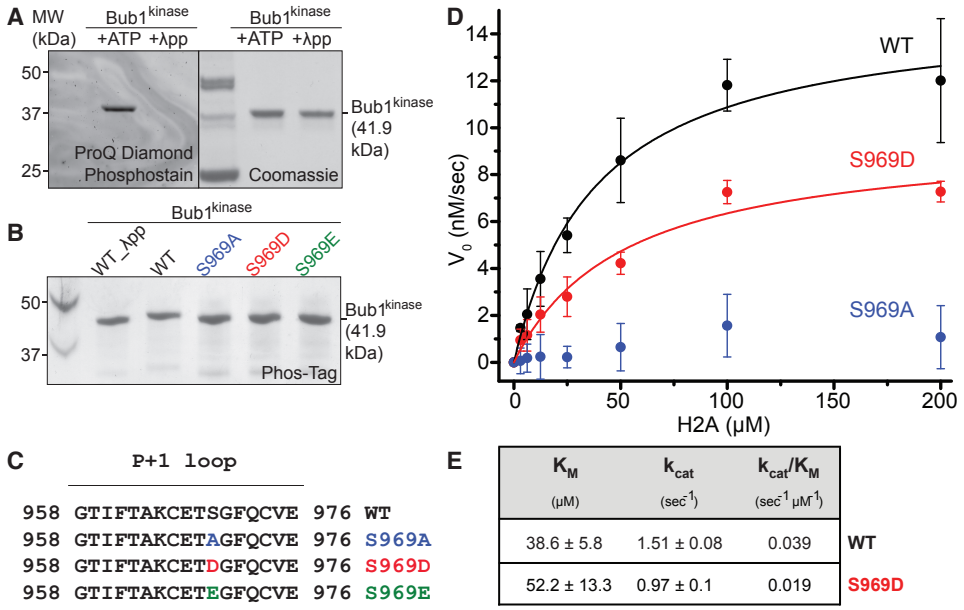

Figure 3.19: Bub1 autophosphorylates at S969, a phosphorylation site that confers kinase activity.
(**A**) Bub1^{kinase} undergoes autophosphorylation, which is reversible by treatment with λ-phosphatase. Bub1 samples were analysed by SDS PAGE and Coomassie blue staining (right). Phosphorylation was visualised using the Pro-Q® Diamond Phosphoprotein Gel Stain (left). (**B**) Bub1^{kinase} wild-type (WT), S969A, S969D and S969E were incubated with ATP or λ-phosphatase (λ-pp) and analysed by SDS PAGE and Coomassie blue staining using Phos-tag to detect a phosphorylation-specific shift. (**C**) Amino acid sequence of the Bub1 P+1 loop with mutations of S969 highlighted in blue (S969A), red (S969D) and green (S969E). (**D**) The phosphomimetic S969D restores kinase activity while S969A is catalytically inactive. The kinase activity plotted as a function of substrate concentration allows fitting with the Michaelis-Menten equation with R^2=0.99 (WT), R^2=0.97 (S969D). Error bars represent SD of a mean of at least 2 independent experiments. 10 nM kinase was consistently used in all experiments. (**E**) Kinetic parameters of the Michaelis-Menten fits as determined in (**D**).

In conclusion, our results confirm that autophosphorylation at S969 is required for efficient catalysis while other domains within Bub1, namely the TPR, or binding partners such as BubR1, Bub3 or Knl1 do not affect kinase activity. We see, however, that the composition of substrates, particularly in the case of H2A, can influence the kinase affinity and hence the phosphorylation efficiency. This represents an advanced possibility to subtly tune kinase activity.

3.3 Structure of a phosphorylated Bub1 kinase domain

The structure of unphosphorylated Bub1 kinase (Bub1$^{724-1085}$) [214] is known. In this structure, the P+1 loop is obstructing the active site, leaving Bub1 in a conformation that was incompatible with substrate binding (see Figure 3.22 left). As we have shown that S969 is both a prerequisite for Bub1 kinase activity (Figure 3.19) and a site of autophosphorylation, we were intrigued to see the structural and mechanistic consequences of this phosphorylation.
Bub1^{kinase} was preparatively autophosphorylated and subjected to co-crystallisation with ADP (Figure 3.20). The initial conditions and strategy are summarised in Section 5.2.5.

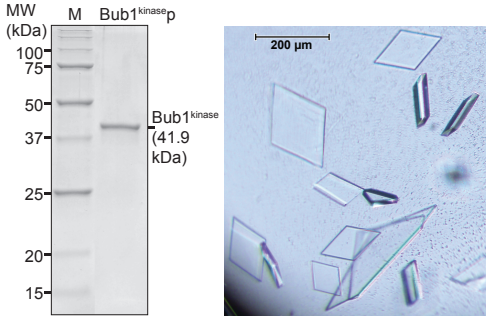

Figure 3.20: Crystallising phosphorylated Bub1^{kinase}.
Autophosphorylated Bub1^{kinase} was analysed by SDS PAGE and Coomassie blue staining (left) and co-crystallised with ADP. After 48 h, diamond-shaped crystals grew to full size of 200 µm diameter in a refined crystallisation condition of 15 % PEG 3500 and 0.2 M NaCl at 4°C using the sitting-drop vapour diffusion method (right). M-molecular weight standard.

3.3.1 Phosphorylated Bub1^{kinase} structure determination by X-ray crystallography

We obtained diffracting crystals and determined the structure by using the structure of unphosphorylated Bub1$^{724-1085}$ (PDB ID: 3E7E) [214] as a reference model for molecular replacement. Note that the structure deposited with PDB code 3E7E, is now superseded by the structure with the PDB code 4R8Q. This later structure is the result of a re-refinement where ATP, which had been originally modeled in the structure [214], was replaced with ADP and a second Mg^{2+} ion [224]. Surprisingly, our final structure of phosphorylated Bub1^{kinase} is remarkably similar to the structure of unphosphorylated Bub1, although the cell parameters and space group of both structures are different (Figure 3.21, Figure 3.22). Bub1$^{724-1085}$ crystallises with one molecule per asymmetric unit, while the asymmetric unit for the final model of phosphorylated Bub1^{kinase} comprises two monomers of Bub1^{kinase}. The table containing collected diffraction data and refinement statistics can be found in the Appendix Table 6.1.

The refined structure showed clear, inconspicuous density for both the phosphorylated residue S969p and the entire P+1 loop (Figure 3.21). The phosphate of S969 points directly toward the co-crystallised ADP molecule and further resides in space that would be occupied by a substrate residue (Figure 3.21, Figure 6.9). The position of S969p and its immediate proximity to the gamma-phosphate of a putative ATP molecule led us to suspect that this conformation represents the autophosphorylation-intermediate immediately following ATP hydrolysis. This conformation is likely stabilised by contacts of symmetry mates in the crystal. The phosphate faces a highly negatively charged environment (Appendix Figure 6.7), composed of the directly neighboring residues E967 and D917N (Figure 3.21) that would be expected create a repulsive force towards the phosphate.

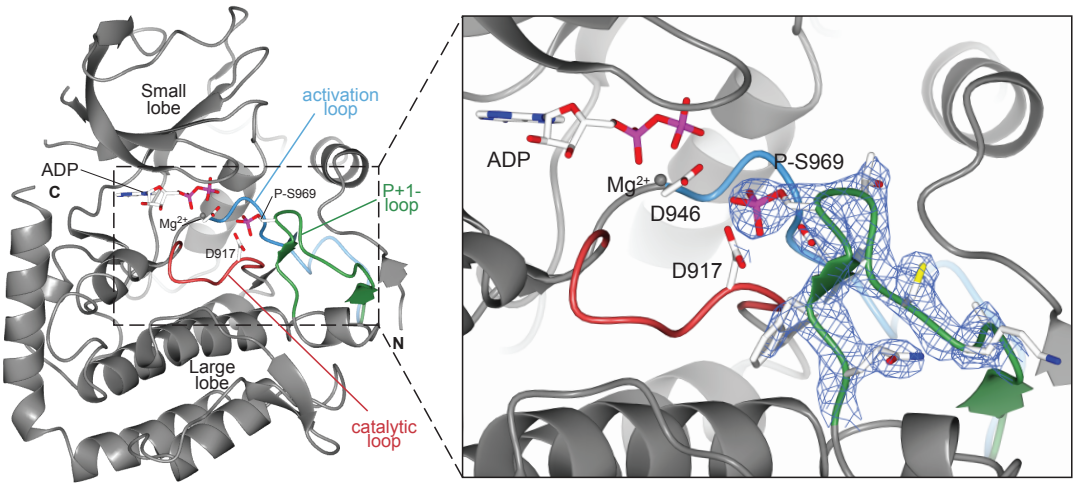

Figure 3.21: The structure of phosphorylated Bub1^{kinase}.
Left, ribbon diagramme showing a phosphorylated structure of Bub1^{kinase}. N and C indicate the N- and C-termini, respectively. The P+1 loop harbouring the phosphorylated S969 is highlighted in green. The activation loop is depicted in blue and the catalytic loop Residues D946, D917, S969 and ADP are shown as sticks, one Mg^{2+} atom is represented by a grey sphere. Right, detailed view of the active site of Bub1 showing S969p pointing towards the catalytic aspartate D917 and ADP. The electron density around the P+1 loop is represented by the $2F_o$-F_c map and contoured at 1.5 σ as a blue mesh. The structure was published with the PDB ID 5DMZ. All images were created with CCP4MG.

It seems plausible that the electrostatic repulsion would lead to a conformational change of the phosphorylated P+1 loop as demonstrated in the recently published structure of phosphorylated Bub1$^{740-1085}$ [224] (Figure 3.22). This published Bub1$^{740-1085}$ construct is very similar to Bub1^{kinase} but lacks 14 amino acids (725-739) at the beginning of the N-terminal kinase extension, a segment that is involved in establishing contacts with the activation segment. The structure of phosphorylated Bub1$^{740-1085}$ might represent an "open" and active conformation of the P+1 loop, as it provides the necessary space to accommodate a substrate peptide at the active site in contrast to phosphorylated Bub1^{kinase} (Figure 3.26 and 6.9).

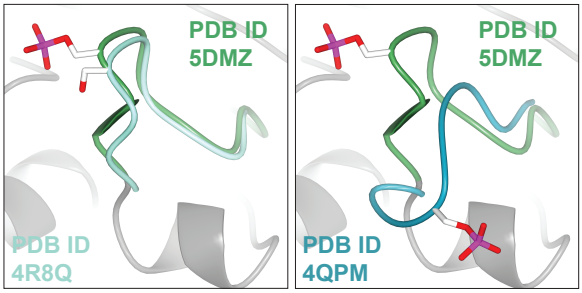

Figure 3.22: Overlay of Bub1 P+1 loop conformations. phosphorylated Bub1^{kinase} (PDB ID: 5DMZ, grey) with unphosphorylated Bub1$^{724-1085}$ (PDB ID: 4R8Q, left) and phosphorylated Bub1$^{740-1085}$ (PDB ID: 4QPM, right).
The P+1 loop of 4R8Q and 4QPM is coloured in shades of blue, the loop of 5DMZ in green. Both images were created with CCP4MG.

3.3.2 Validation of the phosphorylated Bub1^{kinase} structure

To verify the actual positions and electron density of the respective P+1 loops of phosphorylated and unphosphorylated Bub1 structures, I used the structure factors of unphosphorylated Bub1^{kinase} and

phosphorylated Bub1$^{740-1085}$ (PDB IDs: 4R8Q, 4QPM) and reprocessed the data. In the reprocessing, our phosphorylated Bub1^{kinase} was used as a model for molecular replacement. The resulting models were refined to R_{free} factors below 0.3 for qualitative assessment (Figure 3.23).

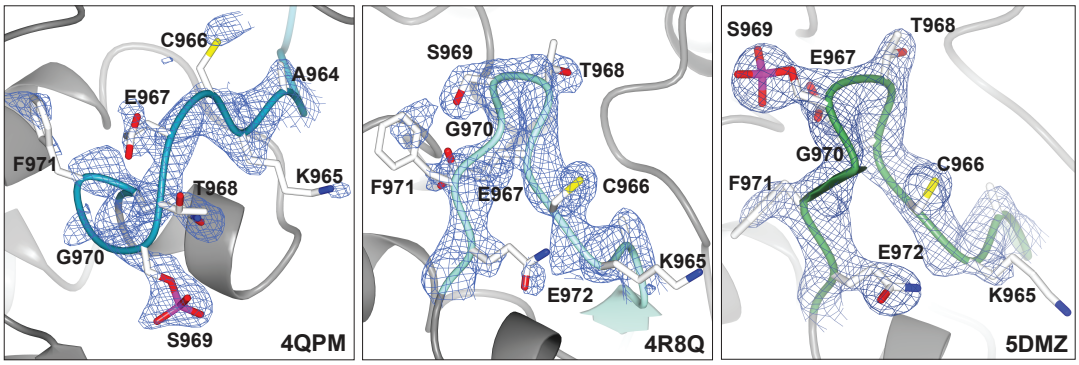

Figure 3.23: Bub1 structures have a clearly defined density around the P+1 loop.
Detailed view of the P+1 loop of phosphorylated Bub1$^{740-1085}$ (4QPM, blue), unphosphorylated Bub1$^{724-1085}$ (4R8Q, turquoise) and Bub1^{kinase} (5DMZ, green), the side chains are shown as sticks. The electron density around the P+1 loop for 4QPM and 4R8Q has been rebuilt and refined from the structure factors and is represented by the $2F_o$-F_c map, contoured at 1.5 σ as a blue mesh for all structures. All images were created with CCP4MG.

In fact, by rebuilding the models we were able to authenticate the published positions of the P+1 loop of unphosphorylated Bub1 (covering the active site) and phosphorylated Bub1$^{740-1085}$ (undergoing structural rearrangement). Therefore, the three Bub1 kinase structures likely represent Bub1 each at a different state of the phosphorylation process.

3.3.3 Bub1^{kinase} autophosphorylation does not influence nucleotide binding

We have demonstrated that S969p is a crucial site for kinase activity, as shown in Figure 3.19, where the mutation S969A disrupts activity. To account for the importance of S969p, we could envision two scenarios where S969 either plays a role in the binding of ATP or a substrate peptide. To test whether S969p had an impact on nucleotide binding of Bub1^{kinase}, we compared the ATP binding of phosphorylated and dephosphorylated Bub1^{kinase} by titrating mant-ATPγS against phosphorylated and dephosphorylated Bub1 (Figure 3.24).

Bub1^{kinase} and phosphorylated Bub1^{kinase} did not show a significant difference in the dissociation constants (K_D) of ATP (Figure 3.24), thus we conclude that S969p does not affect ATP binding. This is initially at odds with our structure, which appears incompatible with binding of an ATP molecule but rather provides more evidence, that the position of the P+1 loop we have crystallised is not the conformation of active Bub1^{kinase}. However, as S969 is located in the substrate-binding loop (Figure 3.21, 3.19 B) we hypothesise that phosphorylation of this residue induces a conformational rearrangement of the P+1 loop that is required for substrate-peptide binding.

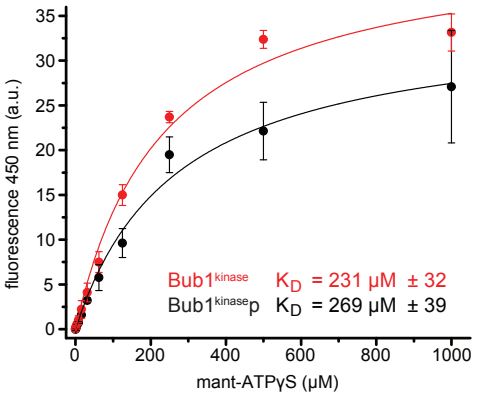

Figure 3.24: S969p does not interfere with ATP binding of Bub1^{kinase}.
The change in fluorescence emission of mant-ATPγS at 450 nm (excitation: 340 nm) upon mixing with Bub1^{kinase} (red) or phosphorylated Bub1^{kinase} (black) is plotted as a function of total mant-ATPγS concentration. The data were fitted with a one-site binding equation using Origin 9.0 with R^2=0.99. Error bars represent SD of a mean of at least two independent experiments. a.u.-arbitrary units.

3.3.4 Substrate binding of phosphorylated Bub1^{kinase}

Crystallisation attempts of substrate-bound Bub1

The available structures of phosphorylated and unphosphorylated Bub1 kinase domain only allow speculation as to how and where a peptide substrate might bind. In order to obtain a crystal structure of a substrate-bound Bub1, I followed two strategies: First, co-crystallisation of phosphorylated Bub1^{kinase} with peptides of human or *xenopus laevis* H2A$^{115-126}$ were tested (Figure 3.25 (a)). Peptides encompassing residues 115-126 of the human and *xenopus laevis* H2A sequence were synthesised by Sascha Gentz with either wild-type sequence or a mutation in the phosphorylation site T120 (T120A). These peptides were co-crystallised with phosphorylated Bub1^{kinase} and yielded crystals very similar in shape to crystals of phosphorylated Bub1^{kinase} (Figure 3.20) but in crystallising conditions that were significantly different. The most promising condition for co-crystallisation found during screening was 0.1 M Tris pH 7.0 and 20 % PEG MME 2000, that reproducibly gave rise to crystals in refinement conditions around pH values of 7.0-7.2 and PEG MME 2000 concentrations ranging from 20-22 %. An initial positive screening result was found with the wild-type H2A$^{115-126}$ peptide in 0.1 M Hepes pH 7.5 and 20 % PEG 10000 but this result could not be reproduced. The crystals co-crystallised with T120A peptides from refinement screens show X-ray diffraction and had very similar space group and cell parameters as phosphorylated Bub1^{kinase} without peptide. Upon refining of the models it became evident that there was no additional density for a bound peptide, neither was the position of the P+1 loop clearly defined. Unfortunately, the addition of higher concentrations of peptide (up to 100-times excess) to increase the peptide occupancy in the phosphorylated Bub1^{kinase} crystal, caused the crystal quality to drop and the diffraction was lost.

In a parallel attempt, I designed a direct fusion of Bub1^{kinase} and H2A, where the H2A$^{115-130}$ peptide was added with a triple or quadruple glycine-serine repeat (named GS_3 and GS_4, respectively) to link the peptide sequence to the C-terminal helix of Bub1^{kinase}. The H2A sequence was inserted directly after E1079 omitting the last Bub1 residues to introduce less flexibility of the H2A peptide. The GS_3 construct was also constructed as a T120A (GS_3TA) mutant. The proteins were expressed, purified and autophosphorylated in the same manner as the wild-type Bub1^{kinase}, they also behaved similarly, were obtained in comparable yields (1 mg/l insect cell culture) and show the same homogeneity (Figure 3.25 (b)).

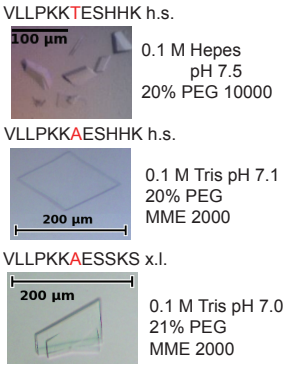

(a) Co-crystallisation of phosphorylated Bub1^{kinase} with H2A peptides.

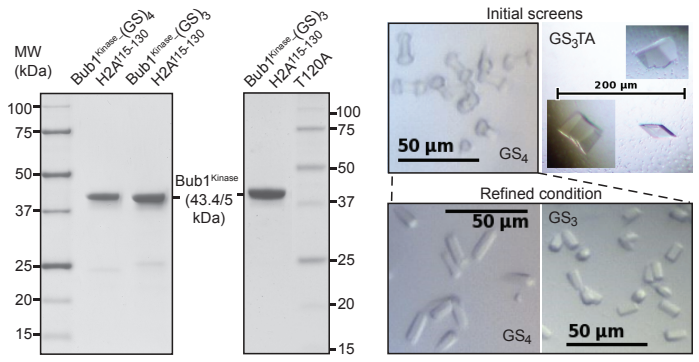

(b) Crystals obtained from a phosphorylated Bub1^{kinase}-GS$_x$H2A$^{115-130}$ fusion approach.

Figure 3.25: Crystallisation attempts for phosphorylated Bub1^{kinase} with a H2A substrate peptide.
(a) The crystallising condition yielding the crystal is indicated on the right, the peptide sequence is indicated on the top of each image with the phosphorylated residue T120 or its mutation T120A highlighted in red. h.s.-homo sapiens; x.l.-*xenopus laevis*. (b) Left, SDS PAGE analysis of phosphorylated Bub1^{kinase}-GS$_x$H2A$^{115-130}$ proteins, right, crystals of the different constructs as indicated in the images in different crystallising conditions. All crystal conditions were obtained in sitting drop vapour diffusion at 4°C.

The three protein constructs were screened for crystallising conditions with one direct hit (0.1 M MES pH 6, 10 % glycerol, 30 % PEG 600, 5 % PEG 1000; for the GS$_3$TA construct, Figure 3.25(b) upper right) that could not be reproduced. A second promising condition yielded quasi-crystals for the GS$_3$ and GS$_4$ construct (0.2 M NaCl, 0.1 M Na acetate pH 4.5, 40 % PEG 300; Figure 3.25(b) upper left) that could be optimised with the addition of 3 % methanol (Figure 3.25(b), lower two panels)
In spite of numerous attempts and screened additives (summarised in Table 5.12), no condition yielded crystals larger than 30 µm (as depicted in Figure 3.25(b)). Furthermore, none of the tested crystals showed diffraction neither at the in-house X-ray source nor at the synchrotron. It is unclear whether the lack of X-ray diffraction was a result of the crystal size or an inherent quality of the substrate-bound phosphorylated Bub1^{kinase} crystals, as also observed for co-crystallised phosphorylated Bub1^{kinase}.
Nevertheless, a promising advance towards a crystal structure of Bub1 with a substrate peptide could thus far be achieved by finding crystallising conditions for a Bub1 construct linked with a substrate peptide. Further attempts to optimise the diffraction or the constructs by increasing linker length and producing a GS$_4$TA construct are currently in progress.

Conservation mapping discerns a substrate binding surface on the Bub1 kinase domain

Comprehensive attempts to crystallise Bub1^{kinase} with substrate peptides have not been successful in yielding diffracting crystals to date. In spite of the lack of structural information, we wanted to validate the substrate binding specificity by modeling a substrate peptide onto the Bub1 structure. The structure of phosphorylated Bub1^{kinase} presented in Section 3.3 does not qualify for the modeling of substrate binding because the active site is obstructed (Appendix Figure 6.9). Therefore, the phosphorylated Bub1$^{740-1085}$ structure (PDB ID: 4QPM) was superposed with the structure of PKA (PDB ID: 1APM) kinase that was co-crystallised with an inhibitor peptide (Figure 3.26).

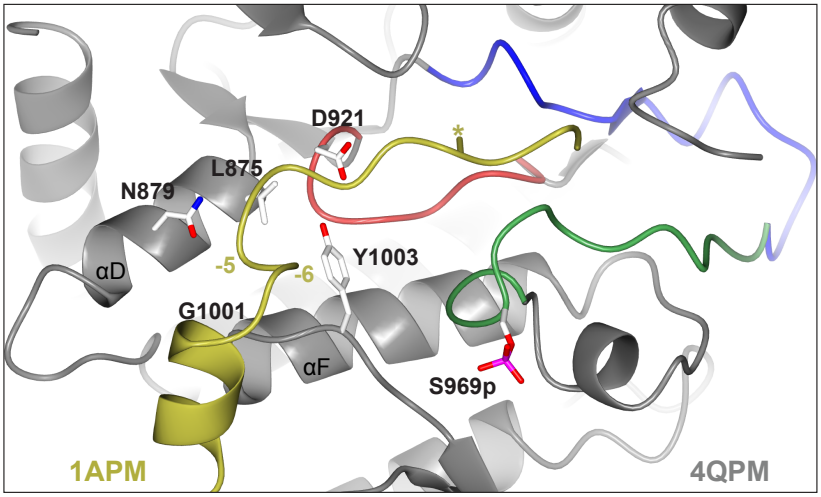

Figure 3.26: Superposition of PKA, with a bound substrate or inhibitor peptide and Bub1$^{740-1085}$.
Only Bub1$^{740-1085}$ (PDB ID: 4QPM, grey) and the co-crystallised pseudo-substrate inhibitor of PKA (PDB ID: 1APM, yellow) are shown. The activation loop is depicted in blue, the P+1 loop in green, the catalytic loop is coloured red. S969p and putative residues involved in substrate recognition are depicted as sticks. The position of the phosphorylated substrate residue (Ala in 1APM peptide) is denoted with a yellow asterisk, the -5 and -6 positions on the peptide are indicated in yellow.

In order to determine the conservation of residues on the surface of Bub1^{kinase} and to identify a possible substrate-binding surface, I aligned Bub1 sequences from 12 organisms from yeast to human using the MUSCLE algorithm [241]. The ConSurf programme [242] then allowed to elucidate the extent of sequence and structure conservation in the kinase domain of Bub1. The complete alignment can be found in the Appendix Figure 6.10.
Mapping the conservation on the surface of Bub1^{kinase} highlights a conserved patch around the active site (magenta), which is expected for catalytic residues. Strikingly, the conservation also extends beyond this site (Figure 3.27). The ribbon view in Figure 3.27 accentuates the positions of the conserved residues outside the catalytic cleft, that reside on helices of the C-lobe of Bub1^{kinase}, forming the surface of the C-lobe. Interestingly, the combined extent of conservation and position of substrate peptide binding, as modeled in Figure 3.26, suggests residues L875, N879 (αD helix), D921, G1001 and Y1003 are likely to be candidates involved in stabilising or conceivably conferring specificity for substrate binding.

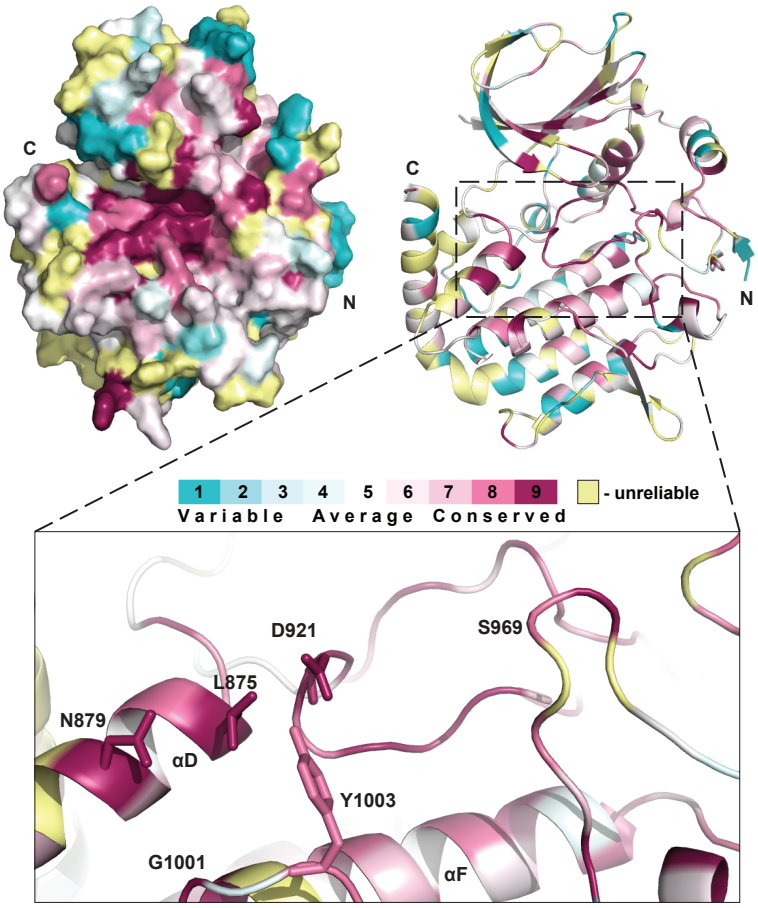

Figure 3.27: Bub1^{kinase} sequence and structure conservation of the C-lobe.
Conservation was determined by aligning Bub1^{kinase} from 14 organisms with ConSurf [242], the scoring legend is depicted in the center. Above, the kinase surface representation and ribbon diagramme are shown, the N- and C-termini are indicated. Below, detailed view of the site of high conservation, the αD and αF helices are indicated. The conserved residues exposed to the surface shown as sticks (L875, N879, D921, G1001 and Y1003) correspond to the same residues shown in Figure 3.26. Conservation scores are considered to be unreliable if they were obtained for positions in the alignment that had less than 6 un-gapped amino acids or if the computed confidence intervals for the rate of a specific position spans 4 or more colour grades. Such positions are colored light yellow in the graphic visualisation output. Images were created with CCP4MG and Pymol.

Mutation analysis of these conserved kinase residues was used to shed light on the role of this surface on the kinase. To this end L875 and N879 on the αD helix, as well as G1001 and Y1003 on the loop following the αF helix were mutated to alanine residues (LN mutant, GY mutant). Another mutant was generated harbouring all four mutations (LNGY mutant). The kinase activity of these proteins was assessed using the ADP-Glo^{TM} Kinase Assay and by SDS PAGE with phosphostaining analysis of the individual kinase reactions (Figure 3.28).
The Bub1 kinase mutants LN, GY and LNGY all proved stable and were also able to autophosphorylate to comparable levels as the wild-type Bub1 kinase (Appendix Figure 6.8). However, when tested on their ability to phosphorylate H2A, the mutants exhibit considerably lower ATP hydrolysis (Figure 3.28 A) and H2A phosphorylation in contrast to Bub1 wild-type (Figure 3.28 B). These results lend strong support to the claim that both the αD helix as well as the residues of the loop succeeding the αF

helix are implicated in substrate recognition. The positions of L875, N879, G1001 and Y1003 are at an ample distance to the active site of Bub1 and the P+1-loop, which corroborates the proposed model where these residues likely confer binding to substrate residues preceding the phosphorylation site (Figure 3.26).

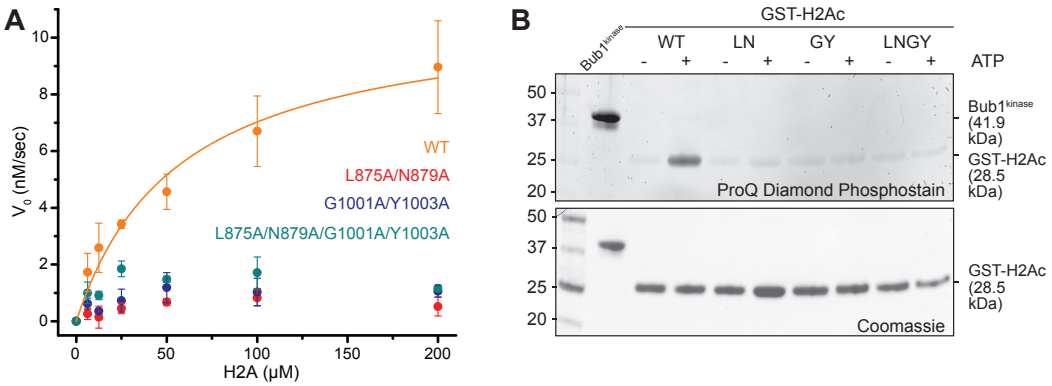

Figure 3.28: Mutation of the conserved surface of Bub1^{kinase} abrogates phosphorylation of H2A.
(**A**) The mutation of L875A/N879A (red), G1001A/Y1003A (blue) and the combined mutation L875A/N879A/G1001A/Y1003A (teal) abolishes phosphorylation of H2A in comparison to the wild-type (WT, yellow). The kinase activity as obtained by the ADP Glo Assay plotted as a function of substrate concentration allows fitting with the Michaelis-Menten equation with R^2=0.97 (WT). Error bars represent SD of a mean of at least 2 independent experiments. 10 nM kinase was consistently used for all experiments. (**B**) The activity of the L875A/N879A (LN), G1001A/Y1003A (GY), and L875A/N879A/G1001A/Y1003A (LNGY) mutants on GST-H2A C-terminal tail (GST-H2Ac) was compared to that of wild type Bub1^{kinase}. GST-H2Ac was incubated with 30 nM Bub1 constructs, with (+) and without (-) ATP, then analysed by SDS PAGE and Coomassie blue staining (below). Phosphates were visualised using the Pro-Q® Diamond Phosphoprotein Gel Stain (above). Phosphorylated Bub1^{kinase} was used as a positive control for phosphostaining. Note that in all phosphorylation reactions the auto-phosphorylation of the Bub1kinase domain was not observed because the kinase was added is amounts that make it undetectable in this assay (~40 ng kinase against 2 µg substrate were used).

In conclusion, we propose that the requirement for phosphorylation of S969 in Bub1 activity signifies an indirect effect. S969p is not directly involved in establishing or stabilising interactions with the substrate peptide, based upon the molecular model of peptide binding to Bub1 kinase (Figure 3.26). Rather, we conceive the role of S969p to be the main driving force that causes the conformational change from an inaccessible active site to a state that allows substrate binding, hence “activating” the kinase. The conserved surface on the C-lobe of the Bub1 kinase domain has a crucial role in recognising substrate peptides, as mutation of specific residues constituting this surface leads to a significant loss of substrate phosphorylation but not autophosphorylation.

3.4 Towards a structure of the BubR1 kinase domain

The structure of BubR1 kinase domain is hitherto unknown. Especially with regard to the fact that it is catalytically inactive, it would be very insightful to know if and how the inactivity can be explained from a structural point of view. In the course of this work, I attempted to obtain structural information on the BubR1 kinase domain.

3.4.1 Identification and design of BubR1 kinase constructs

BubR1$^{543-1050}$ was expressed and purified, then subjected to limited proteolysis in order to obtain stable and minimal kinase constructs suitable for crystallography (Figure 3.29A). A prominent band of approximately 40 kDa was observed, which when excised from the gel and identified by mass spectroscopy, corresponded to the C-terminal domain of BubR1. By performing N-terminal sequencing of this proteolysis fragment, a short sequence was identified that corresponds to the region around residue 700 of BubR1. This corresponds to the size of the Bub1 kinase domain (Bub1^{kinase}) with its N-terminal extension and also fits with secondary structure predictions obtained for BubR1 using the online secondary structure prediction servers Phyre2 [243] and PSIPRED [244] (analyses can be found in the Appendix Figure 6.12 and Figure 6.11).

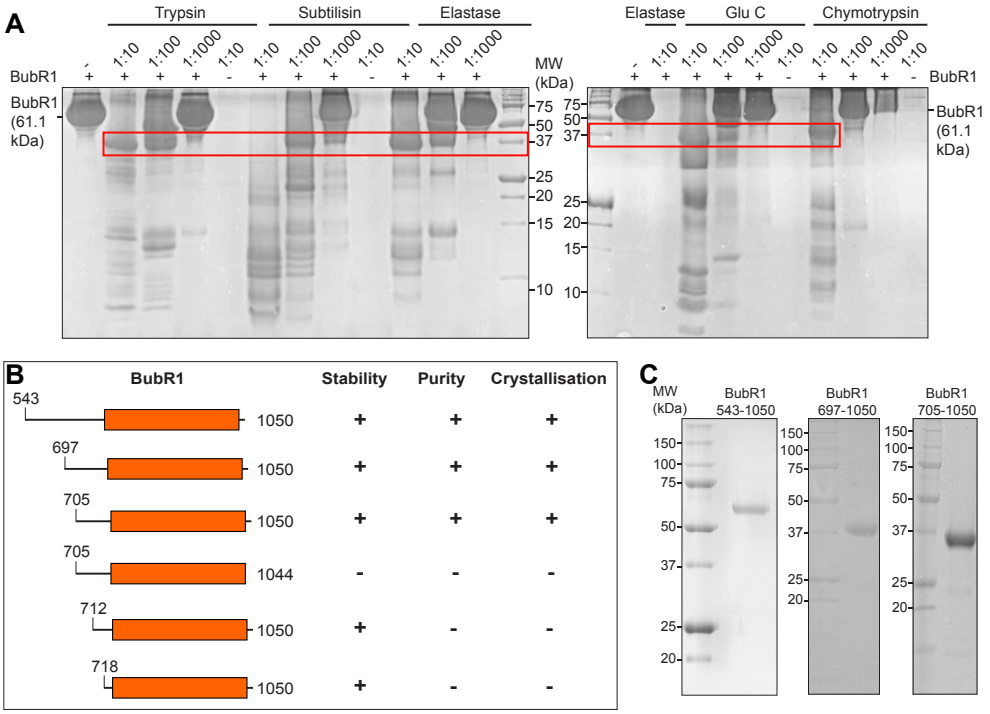

Figure 3.29: Designing constructs of BubR1 kinase domain suitable for crystallogenesis.
(**A**) Coomassie blue stained SDS PAGE analysis of a limited proteolysis performed on BubR1$^{543-1050}$ with different proteases as indicated on top. Boxed in red is a recurring stable fragment of BubR1 of ~40 kDa, which fits the size of the kinase domain. (**B**) Constructs designed following limited proteolysis, mass spectroscopic analysis and N-terminal sequencing, high stability and purity of the purified proteins is indicated by a + sign, only if both is present, the construct was used for crystallogenesis (+). (**C**) Purified constructs of BubR1 kinase were analysed by SDS PAGE and Coomassie blue staining and used for crystallogenesis.

Consequently, five additional constructs of BubR1 were designed (Figure 3.29B), starting at different positions N-terminally of the kinase domain (residues 697, 705, 712, 718). The BubR1$^{705-1044}$ construct additionally contained a C-terminal truncation to exclude the possibility that the very C-terminal residues impede crystallisation. All of the BubR1 constructs were cloned as His_6-tagged proteins and tested for expression. BubR1$^{705-1044}$ proved not to be stable, suggesting that an intact C-terminus is required for protein stability. Furthermore, residues 1044-1049 may fold into a helix as suggested by secondary structure predictions using Phyre2 [243] (Figure 6.12). BubR1 constructs starting at amino acids 697, 705, 712, 718 proved to be expressable, soluble and stable. However, the expression of BubR1$^{712-1050}$ and BubR1$^{718-1050}$ was significantly lower and the following purification did not yield pure protein. Subsequently, BubR1$^{543-1050}$, BubR1$^{697-1050}$ and BubR1$^{705-1050}$ were purified to homogeneity and ultimately subjected to crystallogenesis (Figure 3.29B-C).

3.4.2 Crystallisation attempts of BubR1 kinase constructs

The constructs described in Figure 3.29B were subjected to diverse crystallisation trials, a comprehensive summary of the crystallisation strategies and can be found in Section 5.2.5 and Table 5.12. In brief: The protein constructs (BubR1$^{543-1050}$, BubR1$^{697-1050}$ and BubR1$^{705-1050}$) were purified to homogeneity. Of note, BubR1$^{543-1050}$ was phosphorylated in the course of expression in insect cells. Phosphates were removed prior to crystallogenesis to allow for a homogenous sample, BubR1$^{697-1050}$ and BubR1^{kinase} were not phosphorylated during expression (see also Figure 3.11). The constructs did not yield any spherulites or quasi-crystals from any condition of the screens tested (Table 5.12) that seemed promising for further refinement. Reductive lysine methylation [245, 246], a method used to increase surface hydrophobicity did not increase the propensity of proteins to crystallise. The screens were each set up using varying concentrations of protein and with different additives including ADP, ATPγS, AppNHp. For further crystallisation trials, other additives, potential binding partners or different temperatures could be tested and optimised.
In conclusion, two minimal constructs of BubR1 kinase, BubR1$^{697-1050}$ and BubR1$^{705-1050}$ were found to be stable, nonetheless, a condition for successful crystallisation yet needs to be identified.

3.5 Characterisation of Bub1 substrates

In addition to the kinase substrate interaction as discussed in Section 3.3.4, the range and number of Bub1 kinase substrates and their specific characteristics remain largely unknown. In the course of my work, I also set out to test several kinetochore proteins as substrates for Bub1 kinase *in vitro* with the aim to discern a common substrate sequence pattern and identify novel targets of Bub1 kinase activity.

3.5.1 Screening identifies novel kinetochore substrates of Bub1

Kinetochore and centromere proteins were tested as potential substrates in phosphorylation reactions with Bub1^{kinase}. Among the proteins tested were histone H1, H3 and H2A (which has already been shown to be a Bub1 substrate), Borealin:Survivin complex, Knl1, and the RZZ complex.
The phosphorylation reactions were analysed by SDS PAGE using Pro-Q® Diamond Phosphoprotein Gel- and Coomassie staining, shown in Figure 3.30. H1 and RZZ were not obvious substrates and were not included.

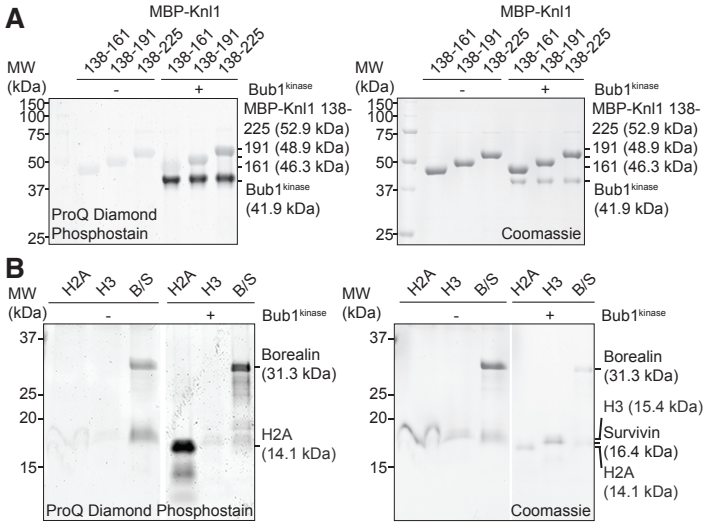

Figure 3.30: Kinetochore proteins were tested for their potential of being a Bub1 substrate. Knl1$^{138-161}$, Knl1$^{138-191}$ and Knl1$^{138-225}$ (**A**) as well as H2A, H3, and the Borealin:Survivin (B/S) in (**B**) complex were incubated with ATP and with (+) or without (-) Bub1^{kinase}. The reactions were then analysed by SDS PAGE and Coomassie blue staining (**A**,**B** right), phosphates were specifically stained using Pro-Q® Diamond Phosphoprotein Gel Stain (**A**,**B** left).

Along with the established substrate H2A, the known kinetochore receptor of Bub1, Knl1, Borealin and Bub1 itself were revealed as targets of Bub1 activity as they could be identified by phosphorylation staining. Histone H3 did not show any phosphorylation, highlighting that Bub1 phosphorylation on histones is specific for H2A. This specificity is also compatible with H2B and H4 not being phosphorylated either, consistent with observations in phosphorylation reactions using reconstituted nucleosomes (Figure 3.16 A). Phosphorylation on Knl1 reveals that while Knl1$^{138-161}$ does not appear to be phosphorylated, by increasing the length of the Knl1 construct to Knl1$^{138-191}$ or Knl1$^{138-225}$, phosphorylation staining occurs and intensifies (Figure 3.30 A). This points towards Bub1 phosphorylation sites being present in the region between 161 and 191 or beyond, corresponding to the position of the KI1 and KI2 motifs (domain structure in Figure 3.8), the known interaction sites of the Bub1 and BubR1 TPR domains with Knl1. Borealin is a part of the chromosomal passen-

ger complex and reported to be highly phosphorylated, which is functionally important in its role to anchor Aurora B at centromeres [247, 248, 249]. The role of these phosphorylation sites and their relevance *in vivo* still remains to be established.

3.5.2 Phosphorylation sites of substrates reveal a consensus sequence

The proteins histone H2A, Borealin, Knl1 and also full-length Bub1 were identified to be Bub1 substrates (Section 3.5.1). They were further evaluated by LC-MS/MS to determine the specific sites of phosphorylation or, in the case of Bub1, auto-phosphorylation. Alignment of the specific phosphorylation sites of these substrates allowed the identification of a putative kinase consensus motif (Figure 3.31).

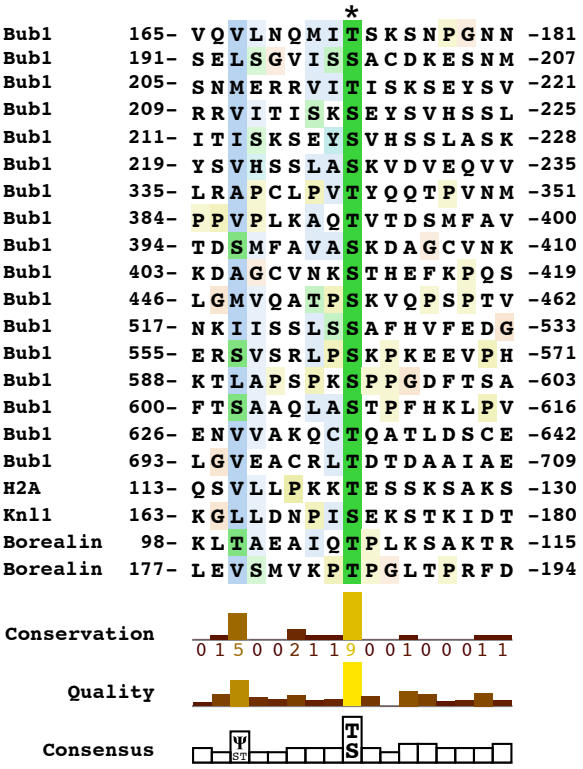

Figure 3.31: Alignment of phosphorylation sites found in Bub1-dependent phosphorylation reactions using Jalview [250].
Phosphosphorylation sites were identified by LC MS/MS and the sequences of the substrates comprising Bub1 itself, H2A, Knl1 and Borealin were aligned at the site of the phosphorylation, which is denoted with an asterisk. Numbers correspond to protein boundaries; the conservation of residues is highlighted using the Clustalx coloring scheme in the sequence alignment and numbers from 0-9 in the bar diagramme. The -6 position is occupied by a hydrophobic residue indicated by Ψ in the consensus below. In a few cases this position is filled by S or T. Note that also in between the phosphorylated residue and the -6 position, the occurrence of aliphatic residues is increased.

The identified consensus predicts the presence of an hydrophobic residue at position -6 relative to the acceptor, a site that is often followed by further aliphatic residues that may also contribute to specific recognition by Bub1 kinase. This motif can be described as ψ-(x)$_5$-T/S where ψ is an aliphatic residue and x is any amino acid (Figure 3.31). The position of the conserved hydrophobic residue of the substrate is structurally consistent with being in the immediate proximity of the highly conserved surface of Bub1$^{\text{kinase}}$ as depicted in Figure 3.26 and 3.27.

3.5.3 A consensus sequence mediates H2A-Bub1 specificity

The discovery of a well conserved sequence feature of Bub1 substrates led us to hypothesise that these residues might be important in substrate-kinase specific interactions. To test this idea, we mutated the H2A residues non-conservatively to V115D, L116N, L117N. To dissect the potential of this 'DNN' mutant as a Bub1 substrate *in vitro*, individual phosphorylation reactions were analysed by SDS PAGE and Pro-Q® Diamond Phosphoprotein Gel staining (Figure 3.32).

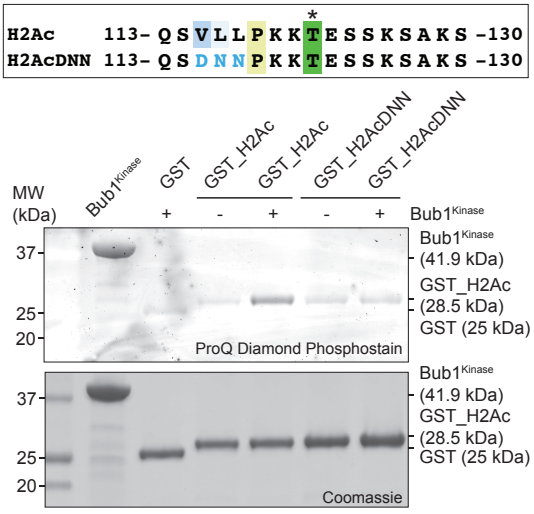

Figure 3.32: Bub1-dependent phosphorylation of H2A can be strongly reduced by mutating residues V115D, L116N, L117N on H2A.
Above, sequence of wild-type H2Ac and the H2AcDNN mutant, the phosphorylated T is indicated with an asterisk. Below, GST-H2A constructs as wild-type (H2Ac) and mutated (H2AcDNN), 2 µg each, were incubated with 10 nM Bub1^{kinase} and ATP, then analysed by SDS PAGE and Coomassie blue staining (lower gel), phosphates were specifically stained using Pro-Q® Diamond Phosphoprotein Gel Stain (upper gel). Autophosphorylation of Bub1^{kinase} was used as a positive control for activity and phosphorylation staining.

Strikingly, the Bub1^{kinase} phosphorylation efficiency of the H2A DNN-mutant is distinctly reduced compared to the wild-type sequence.

Taken together, I was able to identify Borealin and Knl1 as previously unrecognised Bub1 kinase substrates, which in combination with phosphorylation sites on H2A and Bub1 itself, reveal a novel consensus sequence for Bub1 activity. This aliphatic sequence indeed contributes in mediating Bub1 kinase specificity, as corroborated by the reduced phosphorylation of the H2A consensus sequence mutant. The determination of this motif might prove a useful tool in the verification of or screening for other presumptive Bub1 substrates.

The requirement of this substrate sequence is in excellent agreement with the identification of a highly conserved surface on the C-lobe of the Bub1 kinase domain (Section 3.3.4). Bub1 residues L875, N879, G1001 and Y1003 that form this surface are modeled to contact the substrate peptide at the -5 to -6 position, corresponding to the V115 and L116 residues on Bub1. Convincingly, mutation of either, the conserved residues on Bub1 or on H2A was shown to result in a significant decrease in phosphorylation.

4 Conclusion and Perspectives

In this study, I have presented a biochemical and structural characterisation of the mitotic checkpoint proteins Bub1 and BubR1. I have identified BubR1 to be a pseudo-kinase and defined the role of autophosphorylation in the regulation of Bub1 kinase activity. The reconstitution of Bub1:Bub3 and BubR1:Bub3 complexes allowed me to disclose an unprecedented role of Bub1 in assembly of the mitotic checkpoint complex and therefore expands its role as a scaffold protein in checkpoint signalling.

4.1 The role of Bub1:Bub3 and BubR1:Bub3 complexes at the kinetochore

Bub1 and BubR1 reflect sub-functionalisations of paralogs generated by gene duplication [196, 197]. With regard to the distinct functions of Bub1 and BubR1, it is of extreme interest that several independent duplication and sub-functionalisation events might have taken place in the course of evolution [196, 197]. To what extent the biochemical evolution of the components of the paralog pairs that were created by these distinct duplications followed similar or different paths, is currently unclear. The investigation of this intriguing question may contribute to the understanding of how the SAC network constrains the evolution of its components. Thus, encouraged by the desire to shed light on this question, I set out to investigate in biochemical detail the regulation of human Bub1 and BubR1.

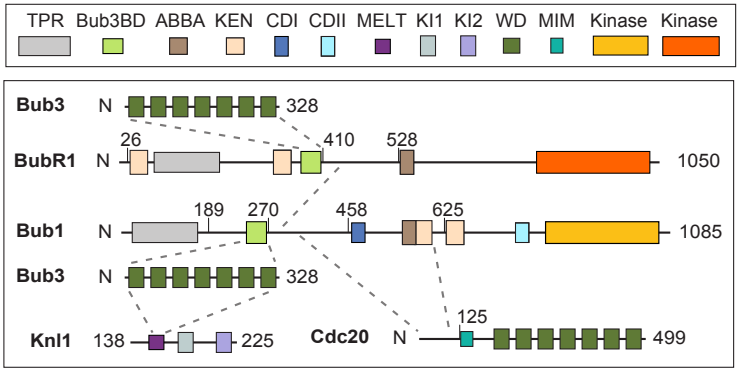

Figure 4.1: The molecular interactions of Knl1, Bub3, Bub1, BubR1 and Cdc20.
The regions or domains of interaction as determined in pull down assays or shown by cross-linking analysis are depicted as grey dashed lines. Domain positions and protein construct boundaries are indicated by residue number. TPR-tetratricopeptide repeat, Bub3BD-Bub3 binding domain, ABBA-ABBA-motif, KEN-lysine-glutamate-asparagine motif, CDI/II-conserved domain I/II, WD-tryptophan-aspartate. The interaction of TPR domains with KI1 (Bub1) and KI2 (BubR1), respectively, is omitted.

The similarity of Bub1 and BubR1 is reflected in the comparable domain organisation of both proteins (Figure 4.1). As shown in the previous section, however, their respective domains behave significantly differently. Hydrodynamic analysis demonstrates for the first time that both Bub1:Bub3 and BubR1:Bub3 form stable, monodisperse 1:1 complexes devoid of further oligomerisation. The Bub1:Bub3 and BubR1:Bub3 complexes interact with a segment of Knl1 containing a single (Mps1-generated) phosphorylated MELT repeat and two previously identified KI motifs, which interact with the TPR regions of Bub1 and BubR1 [208, 55, 171, 251] leading to a tight complex. Importantly, BubR1:Bub3 binding depends upon the presence of Bub1:Bub3.

Little was known thus far about the molecular nature of the interactions that lead to efficient MCC catalysis. The complex of Bub1:Bub3-BubR1:Bub3 on Knl1 was capable of stably binding Cdc20, leading to a network of protein interactions as determined by cross-linking analysis and pull-down experiments (Figure 4.1). The complex of Knl1-Bub1:Bub3-BubR1:Bub3-Cdc20 could form the basis for the MCC, but it remains to be shown whether this composition actually occurs within a cell. Although binding of Cdc20 appears to preferentially bind to Bub1 rather than BubR1, as corroborated by the cross-linking data, it is not evident where the Cdc20 molecule binds in this complex. The Cdc20 binding motifs are divergent between Bub1 and BubR1. This is reflected in the fact that Bub1:Bub3 readily binds to Cdc20 whereas BubR1:Bub3 binds to a much lesser extent, supporting the idea that BubR1-Cdc20 binding is Mad2-dependent [159, 133, 134]. The fact that Mad2 *in vitro* was not sufficient to efficiently generate MCC complexes further argues in favour of a model where the pre-formation of Mad2-Cdc20 is essential in order to build a complex with BubR1:Bub3.

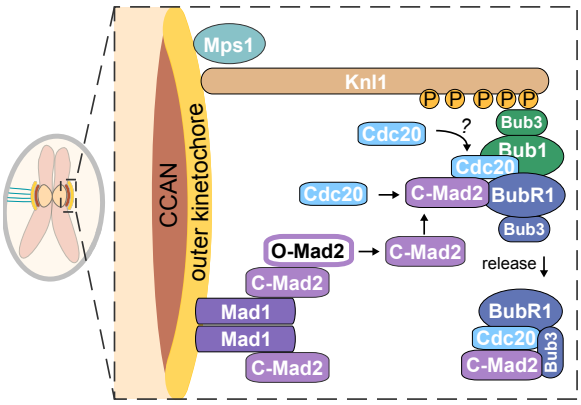

Figure 4.2: Model for Bub1 as a scaffold for MCC assembly. Bub1:Bub3 is recruited to Knl1 phosphorylated by Mps1 and binds a complex of BubR1:Bub3. Bub1 is also a receptor of Cdc20, which can bind as single protein or possibly in a complex with closed Mad2 (C-Mad2). This assembly on Bub1 allows close contact of BubR1:Bub3 and Mad2-Cdc20 complexes that consequently have to be released to form the soluble MCC competent to inhibit the APC/C. The precise mechanism of MCC release is yet unknown, it might involve a second Cdc20 wedging in between Bub1 and evanescent MCC complexes (marked "?") [162, 159, 150] or the activity of a checkpoint kinase, especially Bub1, which was shown to phosphorylate Cdc20 *in vitro* [163].

The ABBA motif as a second independent binding site on BubR1 may account for why BubR1 binds Cdc20 in the absence of Mad2, as observed in previous studies [150, 159, 162]. However, whether a second Cdc20 molecule is effectively required for checkpoint signalling remains uncertain. Possibly, Bub1 is initially a better binder of Cdc20 as it combines the affinity of ABBA motif (further confirmed in [210]) and KEN1, which is spatially further apart in BubR1, although this hypothesis needs to be tested.

Collectively, our findings lend support to a hypothesis where Bub1 is a recruiting scaffold at the kinetochore. Upon kinetochore binding, BubR1:Bub3 and Cdc20 are recruited, where they intersect with Mad2 to form the MCC. A model of this process that correlates very well with other recent studies [179, 180, 210] is shown in Figure 4.2. Concerning the interplay between Bub1:Bub3 and Mad1:Mad2, further biochemical analysis will be crucial to dissect stoichiometries as well as the mechanism of MCC complex formation, taking into account the putative second Cdc20 molecule. Additionally, structural information of this complex will be extraordinarily valuable in terms of revealing individual molecular contributions with regard to understanding the overall mechanism of MCC assembly and signalling.

4.2 The structural basis of kinase regulation

4.2.1 Molecular basis of Bub1 activity and BubR1 inactivity

In order to resolve conflicting reports of kinase activity, I compared Bub1 and BubR1 activities and established that BubR1 is not an active kinase. This finding is consistent with a recent report also demonstrating BubR1 to be an inactive pseudo-kinase [196]. In extension of this previous study, I could further show that the BubR1 kinase domain binds to nucleotides with a binding affinity comparable to that of Bub1. This is surprising, as the residues of the Gly-rich loop, a region of kinases in the upper N-lobe, which is implicated in the stabilisation of nucleotide binding, are highly divergent from a common kinase consensus. Another recent study found BubR1 to be incapable of nucleotide binding [252], thus contradicting our finding. This discrepancy is probably due to the different methodologies employed to investigate nucleotide binding. Still, significant sequence divergence from active kinases in the Gly-rich loop of BubR1, previously indicated as a possible cause of loss of activity [196], may not affect the ability of BubR1 to bind nucleotides. This suggests that divergence of BubR1 from Bub1 at other regions of the kinase domain, possibly in the catalytic loop [196], may be the predominant cause of its impaired activity. The well-established kinase-inactivating mutation, such as K821R in Bub1, resulted in dramatically reduced yields of expressed and purified Bub1 proteins. This is in compliance with findings in BubR1 (K795R mutation [196]), which confirms the idea that these kinase mutations are critical for kinase stability [196], transcending their potentially deleterious effects on enzymatic activity. Mutation of the catalytic aspartate in Bub1 to asparagine (D917N mutant), however, did not apparently perturb the stability of Bub1 but led to a loss of enzymatic activity. Collectively, based on the results obtained in this thesis that BubR1 is inactive and binds to Bub1, we hypothesise that the kinase activity associated with BubR1 precipitates in previous studies can be attributed to Bub1 [218, 196]. Furthermore, as BubR1 is known to bind to PP2A, the assumed effects of BubR1 kinase activity in chromosome congression could be explained by co-precipitation of PP2A [113, 253]. Bub1, on the other hand, is an active kinase that hydrolyses ATP for phosphoryl-transfer to a variety of substrates. Moreover, catalytic properties of Bub1 kinase activity, reported here by their turnover rate (k_{cat}) and catalytic efficiency (k_{cat}/K_M), are similar to those reported for many other kinases [254].

4.2.2 Extrinsic regulation of Bub1 kinase activity

One of the motivations behind this thesis was to explore whether the interactions of Bub1 with its most direct binding partners in the kinetochore, Bub3, Knl1, and BubR1, imposes an extrinsic level of regulation on Bub1 kinase activity. Kinase regulation by binding partners is common, specifically in the sense of relieving an auto-inhibitory feature of the kinase. The release of an inhibitory loop also occurs in the case of Bub1, where the P+1 loop blocks substrate access to the active site. However, in conclusion from the analysis presented here, this may not be true, at least when reconstituting the Bub1 interactions with recombinant material *in vitro*. Another study, using deletion constructs in HeLa cells, reaches similar conclusions [237] in support of the findings presented here. Previously, independent reports described that the TPR region of Bub1 may also extrinsically contribute to the regulation of Bub1 kinase activity [208, 225]. While the analysis of this dissertation seems inconsis-

tent with the earlier claim, it remains possible that the discrepancy may be generated by inherent differences in the Bub1 material utilised in these assays. Previous studies have used a precipitated form of Bub1 from either HeLa cells [208] or mouse embryonic fibroblasts [225] as the source of kinase activity, whereas it was purely recombinant protein here. In agreement with the findings presented above, where Bub1 kinase exhibits the same degree of activity as full-length Bub1, a recent study also failed to identify differences in the kinase activity of full-length Bub1 compared to a TPR-deleted construct [224].

4.2.3 Intrinsic regulation of Bub1 kinase activity

Activation of many kinases involves the phosphorylation of their activation loop [235, 236] thereby inducing a structural rearrangement, leading to the activation of the kinase. This process might involve an activating phosphorylation by another kinase or autophosphorylation. In Bub1, phosphorylation takes place on the P+1 loop that is in the region of the activation segment following the acceptor site (P-loop) and involved in substrate recognition. In agreement with a recent study [224], an auto-phosphorylation site on the substrate-binding P+1 loop of Bub1 is identified in this study (S969p), which represents an atypical position for an activating auto-phosphorylation in kinases.

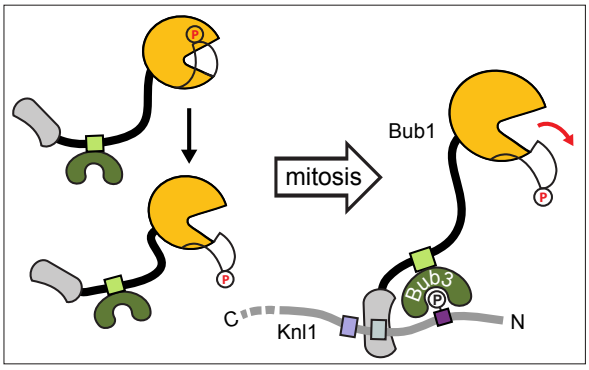

Figure 4.3: Bub1 intramolecular activation and recruitment to the kinetochore.
Bub1 kinase domain (orange) autophosphorylates (denoted by a P) in the cytoplasm (left), which leads to its activation by rearrangement of the substrate binding loop to relieve obstruction of the active site. In mitosis Bub1 becomes recruited to the kinetochore by Knl1 where Bub3 recognises a MELT sequence (purple box) that is phosphorylated by Mps1, further interaction of the TPR domain (grey) with KI1 (light-grey box) on Knl1 might strengthen the binding. The intramolecular activation and kinetochore recruitment allows Bub1 to reach its substrates at the kinetochore and centromere.

This dissertation introduces a crystal structure of the phosphorylated Bub1 kinase where the P+1 loop is captured in a conformation that creates a steric blockade to the active site. The phosphate is attached to the side chain of S969, pointing towards the nucleotide-binding pocket of Bub1. This structure adds to two previous structures of the catalytic domain of Bub1 with an unphosphorylated, or a phosphorylated and rearranged P+1 loop [214, 224]. The unphosphorylated Bub1 structure displays the same “closed” arrangement of the P+1 loop that seems unsuitable for binding of a substrate peptide. In contrast, the phosphorylated Bub1 structure presents an “open” conformation where the phosphate on S969 points towards the solvent (Figure 4.3). The structure presented here appears to be an intermediate conformation of the P+1 loop after phosphate transfer but before extrusion from the active site (Figure 4.3), providing insight into the activation mechanism of Bub1 kinase.

The obtained results show that S969 is most likely the only phosphorylation site on Bub1 kinase.

Phosphorylation of S969 is also critical for Bub1 activity, as the S969A mutant exhibits strongly reduced kinase activity while the S969D or S969E mutation still supports kinase activity. This finding strongly argues in favour of the necessity of a negatively charged residue at the 969 position, as the process of P+1 loop re-arrangement is likely to be driven by electrostatic repulsion from predominantly negatively charged residues in the direct environment of S969 (Appendix Figure 6.7). In particular, the catalytic residue D917 and E967 on the P+1 loop directly oppose the negatively charged phosphate, thereby creating the driving force for the structural rearrangement of the P+1 loop. The fact that the phosphorylation of the P+1 loop does to interfere with nucleotide binding of Bub1, advocates that it rather affects substrate peptide binding, which may be facilitated by "opening" the active site of Bub1.

The conservation of S969 lends further support to this hypothetical mechanism. In other organisms as yeasts, *Drosophila melanogaster*, or *Caenorhabditis elegans*, the serine is replaced by an aspartate or glutamate at the equivalent position (Appendix Figure 6.10), circumventing a requirement for phosphorylation. With regard to the apparent lack of extrinsic regulation of Bub1 kinase activity, it remains unclear why other organisms rely on seemingly dispensable and redundant phosphorylation of the P+1 loop in order to activate Bub1 kinase.

4.2.4 Bub1 as a constitutively active kinase

Collectively, the structural and biochemical analysis of Bub1 indicates that it is a constitutively active kinase. This is corroborated by the presence of an intact regulatory spine (R-spine), a structural motif within the kinase domain that is a hallmark for kinase activity (Figure 4.4) [216, 217]. The presence of this hydrophobic spine implies the correct positioning of both the catalytic loop and Mg-binding loop as they form the lower part of the spine, as well as the positioning of the integral αC helix and the β4 strand shaping the upper part of the spine. Even though the catalytic motif and Mg-binding loop of Bub1 deviate from common kinase consensus sequences, the catalytic motif being HGD (consensus HRD) while the Mg-binding segment is

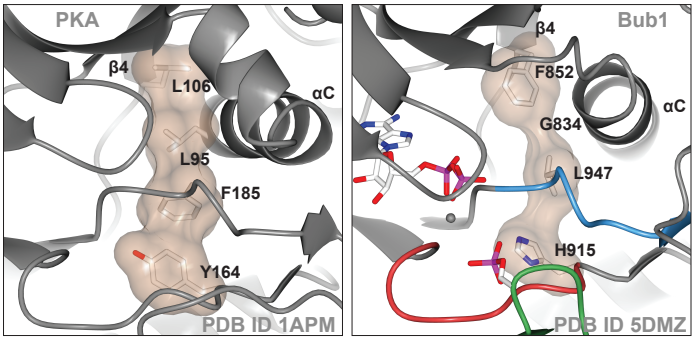

Figure 4.4: Bub1 kinase has an organised R-spine.
Protein kinase A (PKA) (PDB ID: 1APM, left) and phosphorylated Bub1^{kinase} (PDB ID: 5DMZ, right) are shown with the residues forming the R-spine and ADP and S969 in Bub1 are shown as sticks, the Mg^{2+} ion is depicted as a grey sphere. The molecular surface around the R-spine is highlighted in brown. The P+1 loop of Bub1 is coloured in green, the catalytic loop in red (H915 is part of the HRD (HGD in Bub1) motif), the activation loop is depicted in blue (L947 is part of the Mg-binding DFG (DLG in Bub1) motif). The upper two residues of the R-spine emanate from the αC helix and the beginning of the β4 strand, respectively. The R-spine residues are partly degenerated in Bub1, specifically G834 in the αC helix, still they form an intact hydrophobic spine. Both images were created with CCP4MG.

DLG (consensus DFG), they align in a functional hydrophobic spine. Another unique aspect of this conformation is the lack of a hydrophobic residue at the third position of the spine that is occupied by L95 in protein kinase A (PKA), used as a reference model kinase here, but by G834 in Bub1. Likely, the conformation of F852 that points downward in the Bub1 structure partly compensates for G834, resulting in an altered, yet fully formed constitutive R-spine.

The fact that in other eukaryotes the 969 position is occupied by an aspartate, which embodies a constantly active kinase conformation, strongly argues in favour of Bub1 being a constitutively active kinase. This argument is substantiated by the finding that the level of phosphorylation of S969 does not appear to change during the cell cycle [224]. Even being inherently active, Bub1 may need to be specifically recruited to kinetochores in prometaphase in a Bub3- and Knl1-dependent manner. Timely kinetochore recruitment of Bub1 is required in order to phosphorylate the physiologically relevant Bub1 substrates at the kinetochore and centromere, implying spatial and temporal control of its kinase activity (Figure 4.3). As a result of localisation to Knl1 during mitosis, Bub1 is positioned in close proximity to its substrates. Indeed, H2A as a centromere substrate of Bub1 is only found to be phosphorylated in mitosis [111, 229]. Furthermore, the overall levels of Bub1 have been shown to drop rapidly after mitosis [206, 255], insinuating that its regulation may also be controlled by protein degradation. Very recent evidence revealed another autophosphorylation site on Bub1 outside its kinase domain that may contribute to the turnover of Bub1 at kinetochores [237], representing an additional feature of the extent of Bub1 auto-regulation. Checkpoint silencing has been connected to the activity and kinetochore recruitment of phosphatases [81, 189]. Therefore, an increased level of phosphatase activity at the kinetochore could also lead to the inactivation of Bub1 by tipping the balance towards dephosphorylation of S969p.

4.3 Bub1 kinase substrates and specificity

4.3.1 Specific features of Bub1 substrates

Aside from H2A very little is known about the kinetochore substrates of Bub1, much less about the functional consequence of Bub1 phosphorylation. Cdc20 was also reported to be a substrate of Bub1, the phosphorylation predicted to be involved in APC/C inhibition. The presence of this phosphorylation [163], however, could not be identified in cells [214]. Numerous other kinetochore substrates have been reported for Bub1 kinase, amongst which are Mad1, Bub3, Incenp, and Bub1 itself [117, 224, 234, 237, 256]. The relevance of these phosphorylation events remains partly debatable. It is shown here that Knl1, the kinetochore receptor of Bub1 and Borealin, a component of the chromosomal passenger complex, are also substrates of Bub1 kinase activity *in vitro*. The phosphorylation sites on Knl1 are intriguing because they precede the KI1 motif of Knl1, that is known to bind the TPR domain of Bub1 [55, 171, 208, 251]. Whether this phosphorylation of Knl1 influences the binding of the Bub1 TPR domain is a question that needs to be answered. The role of Bub1 in its own recruitment has gained attention in light of recent findings where the activity of Bub1 was implicated in its own kinetochore localisation [237]. Borealin, which is required to anchor Aurora B at centromeres, is strongly phosphorylated in mitosis by numerous kinases [247, 248, 249], but the role of these phosphorylation sites and their relevance *in vivo* remains largely elusive. Conceivably, Bub1-phosphorylation sites on Borealin might cooperate with phosphorylation on H2A to recruit Sgo in order to localise the CPC at centromeres.

Another facet of Bub1 substrates was discovered upon comparison of phosphorylation of free H2A and H2A within the nucleosomal complex, where the latter was a significantly preferred substrate. Notably, the *in vitro* binding of Bub1 to DNA might assist in recognising H2A as a substrate at the centromere.

The analysis of the individual phosphorylation sites reveals that Bub1 substrates share a common sequence motif up to 6 residues upstream of the phosphorylated residue. Particularly the -6 position seems to preferentially be occupied by an aliphatic residue. The results presented here disclose that mutations at the -6 to -4 positions in H2A are sufficient to abolish phosphorylation by Bub1. It would be revealing to see whether this consensus prediction held true for other substrates as well and to show that the hydrophobic residues preceding the phosphorylation site, at the -6 position in particular, are crucial for the recognition by Bub1 kinase.

4.3.2 Substrate recognition on Bub1

The identification of distinct Bub1 substrate features, that might determine their affinity or specificity for Bub1, led to the assumption that similar distinct features must be discernible on the Bub1 kinase domain. In lack of a structure of Bub1 with a bound substrate, an overlay with PKA co-crystallised with a bound inhibitor peptide was used to disclose residues on the C-lobe of Bub1 kinase that would indicate a putative substrate-binding site (Section 3.26). The importance of residues L875/N879 or G1001/Y1003 is corroborated by our finding that their mutation considerably diminishes Bub1 activity towards substrates. It is tempting to hypothesise that the residues L875, N879, G1001 and Y1003 form a hydrophobic groove that allows the selective binding of substrates thus

conferring specificity. Notably, the residues identified are highly conserved among Bub1 proteins. Additionally, based on the structural alignment, G1001 and Y1003 might also contact the -5 or -6 position on the substrate peptide, which was consensually found to be a hydrophobic residue (Figure 3.31).

D921 is a fully conserved amino acid on the catalytic loop of Bub1 and the only acidic residue that might contribute to the putative substrate-binding surface. Its orientation is not entirely clear from the electron density as it could be both facing outwards or stabilising a water molecule that is involved in coordinating the Mg^{2+} ion, which in turn would also account for its conservation. Whether the catalytic function can be uncoupled from the regulatory role is an important question for determining kinase specificities in general. Y1003 could be required for the establishment of hydrophobic contacts whereas G1001 is much more likely to be a gate for substrate entry with its position at the end of a loop. As an aromatic residue, Y1003 is further at a position of kinases that is in general highly conserved in kinases. Moreover, a proline is usually present at the position of G1001, accentuating the structural conservation of this loop arrangement [257].

A recent study used a computational approach aimed at identifying residues that determine kinase specificity but are not necessarily directly involved in substrate binding. Thus, they identified two residues on the αC helix (named αC-1 and αC-3 positions) that confer specificity for the second residue following the phosphorylation site (P+2) on kinase substrates [257]. Although the arrangement of the αC helix in Bub1 is different from other kinases, as it is held in place by the essential N-terminal extension, the corresponding αC-1 residue (N827 in Bub1) points out towards the substrate-binding loop, making it an attractive candidate for conferring specificity. With this computational approach the study further identifies the seventh residue preceding the APE motif (APE-7) at the end of the P+1 loop of kinases (CVE in Bub1) to be implicated in substrate recognition at the P+1 position of the substrate [257]. In Bub1, this APE-7 residue is equivalent to T968, immediately preceding the autophosphorylation site S969. Furthermore, in the structure presented in [224], T968 is in a position consistent with the accommodation of the P+1 residue of a substrate. Hence, the APE-7 position identified in [257] is in excellent agreement with the findings of this thesis highlighting the importance of correct positioning of the P+1 loop in mediating substrate binding for efficient kinase activity.

In conclusion, efficient catalytic activity in the case of Bub1 requires on one hand autophosphorylation of S969, which rearranges the P+1 loop, leading to a conformation suitable for substrate binding. On the other hand, highly conserved residues on the C-lobe of Bub1 (L875/N879 and G1001/Y1003) contribute to conferring specificity of the phosphorylation of kinetochore substrates.

4.4 Perspectives

Bub1 has multiple functions during mitosis and is an important regulator in the spindle assembly checkpoint. Bub1 is critical to localise the chromosomal passenger complex and to recruit the cohesin protector, Sgo1, to kinetochores by phosphorylating histone H2A. Bub1 further regulates the recruitment of other checkpoint components, such as BubR1, Cdc20 and Mad1 to kinetochores. It is therefore important to understand the mechanism of how Bub1 acts on its substrates and how Bub1 activity is regulated during the cell cycle. Within the scope of this dissertation, I aimed to answer these questions by providing potential substrate determinants of Bub1 kinase and also generating a possible substrate consensus sequence. Additionally, I set out to establish the role of autophosphorylation of Bub1 kinase while excluding regulation by Bub1 binding partners at the kinetochore. Finally, my obtained results add to the understanding of the recruitment mechanism of BubR1 and Cdc20 to the kinetochore.

Most evidence advancing our knowledge of kinetochore machinery is derived from observations in cells, of phenotypes associated with protein mutations *in vivo*, an approach which is limited in inferring molecular mechanisms. Biochemical reconstitution of spindle checkpoint complexes building upon a Knl1-Bub1:Bub3 scaffold will be revealing in determining direct dependencies and interactions. Structural work on a Knl1-Bub1:Bub3-BubR1:Bub3-Cdc20 complex by electron microscopy would allow determination of the recruitment process. The investigation of smaller protein constructs, notably around the interface of Bub1:Bub3-BubR1:Bub3, possibly in complex with Cdc20, using X-ray crystallography would be very valuable as well.

Further structural studies will also be insightful for the analysis of the Bub1 substrate-binding mechanism. Attaching a substrate peptide to the N-terminus of Bub1 rather than the C-terminus might be of use. Alternatively, coupling of a nucleotide to a substrate peptide mimicking a phosphoryl-transfer transition state could prove a promising approach. It would be advantageous to further assess the role of individual residues within the recognition motif of Bub1 substrates, which may be useful also for the identification or characterisation of further Bub1 substrates. Although extensive attempts have already been made here to obtain a crystal structure of the human BubR1 kinase, it might be worthwhile making use of the BubR1 kinase domain from a different organism for crystallographic purposes. A crystal structure might shed light on the molecular basis of kinase inactivity as well as the evolutionary development of Bub kinases in general.

The concept of Bub1 as a constitutively active kinase has several implications for its regulation at the kinetochore. Bub1 autophosphorylation is required for its activation but is most likely also involved in mediating its own kinetochore turnover [237]. Therefore, it is crucial to ascertain how Bub1 activity is silenced and Bub1 is removed from those kinetochores that are correctly attached to microtubules. Mechanisms that ensure the timely inactivation of a mitotic kinase are crucial to guarantee faithful cell division. This might be achieved by phosphatase activity counterbalancing kinase activity. It is appealing to identify an antagonistic *bona fide* phosphatase for Bub1 substrates and Bub1 itself. In particular, whether phosphorylated S969 on the kinase itself could also be a phosphatase target is an intriguing question. Particularly with regard to the presence of an acidic residue in this position

in other eukaryotes, the identification of a phosphatase could reveal a difference in Bub1 regulation between distinct species. Mutational studies of constitutively active Bub1 mutants (S969D) in human cell lines, or the artificial introduction of a serine in the corresponding position in yeast could shed more light on this mechanism. On the other hand, aside from phosphorylation, other post-translational modifications might be used as a Bub1 degradation or inactivation signal. Ultimately, the factors that mediate and control Bub1 kinase silencing or removal are yet unknown. Elucidating the factors and mechanisms that regulate kinase activity downstream of mitotic signalling will contribute to a more general grasp of mitotic mechanisms and advance our understanding of upstream cell cycle control.

In conclusion, this study significantly contributes to unraveling the elaborate mechanism of spindle assembly checkpoint signalling by Bub1, Bub3, BubR1 and Cdc20 checkpoint proteins and to unveiling molecular details of the regulation of Bub1 activity. Understanding how these molecular interactions are orchestrated and supervised in the larger framework of the kinetochore and spindle assembly checkpoint in the effort to govern cell division, remains a challenge for future studies.

5 Materials and Methods

5.1 Materials

5.1.1 Chemicals and Reagents

The chemicals and reagents used in this thesis were obtained in the highest purity possible, they are summarised together with used kits, enzymes and molecular weight standards in Table 5.1.

Table 5.1: List of enzymes, kits and chemicals consistently used for the preparation of this manuscript.

ENZYMES / REAGENTS	SUPPLIER
Acetic acid	Sigma-Aldrich, St. Louis, USA
Acetonitrile	LGC Promochem Wesel, Germany
Acrylamide (30 %, Mix 37.5 : 1)	AppliChem GmbH, Darmstadt, Germany
Adenosine-5'-diphosphate (ADP)	Jena Bioscience GmbH, Jena, Germany
Adenosine-5'-triphosphate (ATP)	Sigma-Aldrich, St. Louis, USA
Adenosine-5'-[(β,γ)-imido]triphosphate (AppNHp)	Jena Bioscience GmbH, Jena, Germany
Adenosine-5'-(3-thio)-triphosphate (ATPγS)	Jena Bioscience GmbH, Jena, Germany
ADP-Glo^{TM} Kinase Assay	Promega Corp., Madison, USA
Agarose ultrapure	Invitrogen^{TM} Life Technologies, Carlsbad, USA
Agarose LE (low electroendosmosis)	Roche Applied Science, Penzberg, Germany
Ammoniumperoxosulfate (APS)	Serva Electrophoresis GmbH, Heidelberg, Germany
Ampicillin	Serva Electrophoresis GmbH, Heidelberg, Germany
β-Mercaptoethanol	Serva Electrophoresis GmbH, Heidelberg, Germany
Bovine Serum Albumine (BSA)	Carl Roth Chemie GmbH, Karlsruhe, Germany
Bradford Protein Assay	Bio-Rad Laboratories Inc., Hercules, USA
Bromophenol blue	Sigma-Aldrich, St. Louis, USA
Coomassie G250/R250	Serva Electrophoresis GmbH, Heidelberg, Germany
Dimethylsulfoxide (DMSO)	Serva Electrophoresis GmbH, Heidelberg, Germany
Dithioerythritol (DTE)	Serva Electrophoresis GmbH, Heidelberg, Germany
DNA Polymerases Q5®/Phusion®, DNA ligase T4	New England Biolabs, Ipswich, USA
AccuPrime^{TM} Taq DNA Polymerase	Invitrogen^{TM} Life Technologies, Carlsbad, USA
DNA ladder GeneRuler^{TM} 1kb	Fermentas, St. Leon-Rot, Germany
Ethanol (EtOH)	Thermo Fisher Scientific, Waltham, USA
Ethylenediaminetetraacetic acid (EDTA)	Gerbu Biotechnik GmbH, Heidelberg, Germany
Fetal Calf Serum (FCS)	Gibco® Life Technologies, Carlsbad, USA
FuGENE® HD Transfection reagent	Promega Corp., Madison, USA
Gentamycine	Serva Electrophoresis GmbH, Heidelberg, Germany
Glycerol	Gerbu Biotechnik GmbH, Heidelberg, Germany, Sigma-Aldrich, St. Louis, USA
Hydrochloric acid (HCl)	AppliChem GmbH, Darmstadt, Germany
4-(2-Hydroxyethyl)-piperazine-1-ethanesulfonic acid (HEPES)	Sigma-Aldrich, St. Louis, USA

Table 5.1 continued

Imidazole	Merck KGaA, Darmstadt, Germany/ Sigma-Aldrich, St. Louis, USA
Isopropyl-β-D-thiogalactopyranoside (IPTG)	Carl Roth Chemie GmbH, Karlsruhe, Germany
Kanamycine	Gerbu Biotechnik GmbH, Heidelberg, Germany
Laboratory Film - Parafilm	Bemis Company Inc., Neenah, USA
Lactose	Sigma-Aldrich, St. Louis, USA
L-Glutathione reduced	AppliChem GmbH, Darmstadt, Germany
λ-Phosphatase	Dortmund Protein Facility (DPF), Dortmund, Germany
Magnesium chloride ($MgCl_2$)	J.T.Baker Chemicals, Center Valley, USA
N-methylanthraniloyl-(mant)-adenosin-5'-triphosphate-gamma-S (mantATPγS)	Jena Bioscience GmbH, Jena, Germany
Methanol (MeOH)	Sigma-Aldrich, St. Louis, USA
Midori Green	Nippon Genetics, Düren, Germany
2-(N-morpholino)-ethanesulfonic acid (MES)	Sigma-Aldrich, St. Louis, USA
N, N, N', N'-Tetramethylethylenediamine (TEMED)	Carl Roth Chemie GmbH, Karlsruhe, Germany
NucleoSpin® Plasmid Isolation	Macherey-Nagel, Düren, Germany
Phenylmethylsulfonylfluorid (PMSF)	Serva Electrophoresis GmbH, Heidelberg, Germany
Phos-tag™ Acrylamide AAC-107	Wako Pure Chemical Industries, Ltd., Osaka, Japan
Polyethylenglycol (PEG) 300, 3350, MME 550, 2000	Sigma-Aldrich, St. Louis, USA
Potassium Chloride (KCl)	Sigma-Aldrich, St. Louis, USA
Potassium dihydrogenphosphate (K_2HPO_4)	AppliChem GmbH, Darmstadt, Germany
Precision Plus Protein Unstained/Stained Standards	Bio-Rad Laboratories Inc., Hercules, USA
Pro-Q® Diamond Phosphoprotein Gel Stain	Invitrogen™ Life Technologies, Carlsbad, USA
Proteases (TEV, PreScission)	Dortmund Protein Facility (DPF), Dortmund, Germany
Proteases (Trypsin, Chymotrypsin, Elastase, GluC, Subtilisin)	Promega Corp., Madison, USA
Protease Inhibitor Mix HP Plus	Serva Electrophoresis GmbH, Heidelberg, Germany
Restriction Endonucleases	New England Biolabs (NEB), Ipswich, USA
Crystallisation Suites (JCSG Core I – IV JCSG+, Classics, PACT, PEG I + II, ProComplex,AmSO4)	Qiagen, Hilden, Germany
Crystallisation-Additive Screen HT	Hampton Research Aliso Viejo, USA
Sodium acetate (NaAc)	Sigma-Aldrich, St. Louis, USA
Sodium Chloride (NaCl)	Sigma-Aldrich, St. Louis, USA
Sodium dodecyl sulfate (SDS)	Carl Roth Chemie GmbH, Karlsruhe, Germany
Sodium hydroxide (NaOH)	Waldeck GmbH & Co. KG, Münster, Germany
Tetracycline	Serva Electrophoresis GmbH, Heidelberg, Germany
Tris-(hydroxymethyl)-aminomethane (Tris)	Sigma-Aldrich, St. Louis, USA
Tris-(2-carboxyethyl)-phosphine (TCEP)	Sigma-Aldrich, St. Louis, USA
Triton X-100	Serva Electrophoresis GmbH, Heidelberg, Germany
Wizard® SV Gel and PCR Clean-Up System	Promega Corp., Madison, USA
5-bromo-4-chloro-3-indolyl-β-D-galactopyranoside (X-Gal)	Thermo Fisher Scientific, Waltham, USA

DNA oligonucleotides were exclusively ordered from Eurofins-MWG Operon (Ebersberg, Germany), desalted and lyophylised. They were dissolved in TE or H_2O to a stock solution of 100 pmol/µl and diluted in H_2O to 5 µM prior to use. An overview of the plasmids is given in Table 5.2. A comprehensive list of oligonucleotides can be found in Table 6.2 (Appendix).

Table 5.2: Protein constructs and corresponding vectors created and used in the course of this work.

ENCODED PROTEIN	CONSTRUCT VECTOR NAME	SOURCE
Borealin 1-280, Survivin 1-142	pGEX-2rbs-BorealinSurvivin	Musacchio lab
Bub1 1-1085, Bub3 1-328	pFG-Bub1:Bub3	this manuscript
Bub1 1-1085, Bub3 1-328	pFH-Bub1:Bub3	this manuscript
Bub1 1-1085 D917N, Bub3 1-328	pFH-Bub1_D917N:Bub3	this manuscript
Bub1 1-1085 K821R, Bub3 1-328	pFH-Bub1_K821R:Bub3	this manuscript
Bub1 1-1085 (KEN535-537AAA), Bub3 1-328	pFH-Bub1:Bub3_KEN1^{mut}	this manuscript
Bub1 1-1085 (F527A, F530A KEN535-537AAA), Bub3 1-328	pFH-Bub1:Bub3_ABBA^{mut}KEN1^{mut}	this manuscript
Bub1 1-1085 (KEN535-537AAA, KEN625-627AAA), Bub3 1-328	pFH-Bub1:Bub3_KEN1^{mut}KEN2^{mut}	this manuscript
Bub1 1-1085 (KEN625-627AAA), Bub3 1-328	pFH-Bub1:Bub3_KEN2^{mut}	this manuscript
Bub1 1-1085 (F527A, F530A), Bub3 1-328	pFH-Bub1:Bub3_ABBA^{mut}	this manuscript
Bub1 740-1085	pFH-Bub1C_740	this manuscript
Bub1 726-1085	pFG-Bub1C	Musacchio lab
Bub1 726-1085, D917N	pFG-Bub1C_D917N	this manuscript
Bub1 726-1085, S969D	pFG-Bub1C_S969D	this manuscript
Bub1 726-1085, S969E	pFG-Bub1C_S969E	this manuscript
Bub1 726-1085, S969A	pFG-Bub1C_S969A	this manuscript
Bub1 726-1085, L875A, N879A	pFG-Bub1C_LN	this manuscript
Bub1 726-1085, G1001A, Y1003A	pFG-Bub1C_GY	this manuscript
Bub1 726-1085, L875A, N879A, G1001A, Y1003A	pFG-Bub1C_LNGY	this manuscript
Bub1 726-1085, H2A 115-130	pFG-Bub1C_$(GS)_3$H2Ac	this manuscript
Bub1 726-1085, H2A 115-130 T120A	pFG-Bub1C_$(GS)_3$H2AcTA	this manuscript
Bub1 726-1085, H2A 115-130	pFG-Bub1C_$(GS)_4$H2Ac	this manuscript
BubR1 1-1050, Bub3 1-328	pFH-BubR1:Bub3	this manuscript
BubR1 543-1050	pFH-BubR1C-543	Musacchio lab
BubR1 697-1050	pFH-BubR1C-697	Musacchio lab
BubR1 705-1050	pFH-BubR1C-705	this manuscript
BubR1 705-1043	pFH-BubR1C-705ΔC	this manuscript
BubR1 712-1050	pFH-BubR1C-712	this manuscript
BubR1 718-1050	FH-BubR1C-718	this manuscript
Cdc20 1-499	pFG-Cdc20	Musacchio lab
H2A 1-130	pET3-H2A	Musacchio lab
H2A 115-130	pGEX-2rbs-H2Ac	this manuscript
H2A 115-130 V114D, L115N, L116N	pGEX-2rbs-H2AcDNN	this manuscript
Knl1 138-161	pGEX-MBP-Knl1-MELT1	Musacchio lab
Knl1 138-191	pGEX-MBP-Knl1-MELT1KI1	Musacchio lab
Knl1 138-225	pGEX-MBP-Knl1-MELT1KI1,2	Musacchio lab

5.1.2 Media and Solutions

Table 5.3 and Table 5.4 give an overview of media, solutions and buffers frequently used during the production of this manuscript.

Table 5.3: Media for bacterial and insect cell culture. Bacterial media and agar plates were prepared by the in-house media kitchen facility.

MEDIA	RECIPE / SUPPLIER
Luria Bertani (LB)	10 g tryptone, 5 g yeast extract, 10 g NaCl ad 1 l H_2O, pH 7.4 (media kitchen facility)
LB agarose plates	10 g tryptone, 5 g yeast extract, 10 g NaCl ad 1 l H_2O, pH 7.4 + 1,5% agar (media kitchen facility)
Terrific broth (TB)	12 g tryptone, 24 g yeast extract, 4 ml glycerol (ad 900 ml H_2O), 2,31 g KH_2PO_4 (0,17 M), 12,54 g K_2HPO_4 (0,72 M), ad 100 ml H_2O (media kitchen facility)
Sf-900 III Serum-free medium	Gibco® Life Technologies, Carlsbad, USA

Table 5.4: Buffers and solutions frequently used for the preparation of this manuscript. All buffers were prepared using ddH_2O.

SOLUTIONS	RECIPE
Coomassie Staining Solution	10 % acetic acid, 50 % ethanol, 2.5 % Coomassie G250, 2.5 % Coomassie R250
Phosphate buffered saline (PBS)	8 g/l NaCl, 0.2 g/l KCl, 0.2 g/l Na_2HPO_4, 0.2 g/l K_2HPO_4
Protein sample loading buffer	50 mM Tris-HCl, 4 % SDS, 10 % glycerol, 0.02 % bromophenol blue, 1 % β-mercaptoethanol
SDS PAGE cathode buffer	0.1 M Tris pH 8.25, 0.1 M Tricine, 3.5 mM SDS
SDS PAGE anode buffer	0.2 M Tris pH 8.9
SDS PAGE gel buffer 4 x	3 M Tris pH 8.45, 10 mM SDS
Tris-Acetate-EDTA buffer (TAE)	1 mM Tris, 1.14 ml glacial acetic acid, 10 mM EDTA (pH 8)

5.1.3 *E. coli* and insect cell cloning and expression strains

DNA sequences coding for recombinant proteins were cloned and amplified using Omnimax cells, then further overexpressed using either C41 or BL21 strains. Bacmids for insect cell expression were recombined in *E. coli* EmBACY cells and then used for virus production and amplification in Sf9 cells. Protein expression was subsequently carried out in Sf9 or Tnao38 cells.

Table 5.5: Insect cell lines and bacterial strains used for the preparation of this manuscript.

CELL STRAIN	SUPPLIER
E. coli One Shot® OmniMAX^{TM}2 T1 Phage-Resistant Cells	Invitrogen^{TM} Life Technologies, Carlsbad, USA
E. coli OverExpress^{TM}C41 DE3	Lucigen® Corporation, Middleton, USA
E. coli BL21-CodonPlus (DE3)-RIL Competent Cells	Agilent Technologies, Santa Clara, USA
E. coli DH10*Multi*Bac^{Turbo}	ACEMBL Expression System Series *Multi*bac^{Turbo}, ATG:biosynthetics, Merzhausen, Germany
Spodoptera frugiperda 9 (Sf9)	Invitrogen^{TM} Life Technologies, Carlsbad, USA
Trichoplusia ni 38 (Tnao38)	Gift from Gary W. Blissard [258]

5.1.4 Equipment and Tools

Tables 5.6,5.7 and 5.8 comprise a list of the instruments, software and online tools used for the preparation of this manuscript.

Table 5.6: Equipment frequently used for the preparation of this manuscript.

APPLICATION/ITEM	INSTRUMENT	MODEL	MANUFACTURER
Agarose gel electrophoresis	Agarose gel electrophoresis system		Carl Roth Chemie GmbH, Karlsruhe, Germany
Biological Safety Cabinet	Heraeus HERAsafe®	HS12	Thermo Fisher Scientific, Waltham, USA
Cell Counting	Scepter^{TM}		Merck Millipore KGaA, Darmstadt, Germany
	Neubauer counting chamber		Marienfeld-Superior, Lauda-Königsfeld, Germany
Cell lysis	Sonifier® Cell Disruptor		Branson Ultrasonics Corp., Danbury, USA
Centrifuges	Universal Centrifuge	320 R	Hettich Lab Technology, Tuttlingen, Germany
	Sorvall centrifuge	RC3BP+	Thermo Fisher Scientific, Waltham, USA
	Microcentrifuge	5418 R	Eppendorf AG, Hamburg, Germany
	Avanti centrifuge	J-30I	Beckman Coulter, Brea, USA
	Analytical: ProteomeLab^{TM}	XL-A	Beckman Coulter, Brea, USA
Concentrators	Amicon Ultra, MWCO 3, 10, 50 kDa		Merck KGaA Millipore, Darmstadt, Germany
	Documentation		
- DNA	Transilluminator	2.0	Thermo Fisher Scientific, Waltham, USA
	Bioprint DS Videodocumentation		LTT Labortechnik Tasler GmbH, Würzburg, Germany
- Fluorescence/ Luminescence	Microplate reader Infinity	M200	Tecan, Männedorf, Switzerland
	Typhoon	3.0	Amersham Biosciences Europe GmbH, Freiburg, Germany

Table 5.6 continued

- Vis-Photometer	BioPhotometer®		Eppendorf AG, Hamburg, Germany
Filter units	Whatman™ Membrane filters 0.2 µm	ME24	GE Healthcare, Chalfont St. Giles, UK
	Filtropur S syringe filters 0.2 µm		Sarstedt AG & Co, Nümbrecht, Germany
	Rotilabo® syringe filters 0.8 µm		Carl Roth Chemie GmbH, Karlsruhe, Germany
Fast protein liquid chromatography (FPLC)			
- System	ÄKTA	Purifier, Prime plus	GE Healthcare, Chalfont St. Giles, UK
- Affinity	GSTrap™	FF 5 ml	GE Healthcare, Chalfont St. Giles, UK
	Amintra Glutathione Resin		Expedeon Inc., San Diego, USA
	HisTrap™	FF 5 ml	GE Healthcare, Chalfont St. Giles, UK
	Nickel-NTA-Superose Beads		GE Healthcare, Chalfont St. Giles, UK
	HiTrap Heparin	HP 5 ml	GE Healthcare, Chalfont St. Giles, UK
- Anion-exchange	Resource Q	6 ml	GE Healthcare, Chalfont St. Giles, UK
- Size exclusion	HiLoad Superdex	75 PG, 200 PG	GE Healthcare, Chalfont St. Giles, UK
	Superdex 75, Superdex 200, Superose 6	10/300 GL	GE Healthcare, Chalfont St. Giles, UK
Glass Beads	Glass beads (2.85-3.45mm)		Carl Roth GmbH, Karlsruhe, Germany
Incubator Shaker	Multritron®	Version 2	Infors AG, Bottmingen, Switzerland
Mass spectrometry	Finnigan LCQ Advantage Max Spectrometer		Thermo Fisher Scientific, Waltham, USA
	EASY-nLC 1000 HPLC system		Thermo Fisher Scientific™, Odense, Denmark
	Quadrupole Orbitrap mass spectrometer (Q Exactive™)		Thermo Scientific™, Odense, Denmark
Microscopes	CX41 with camera Olympus DP21	RF200	Olympus Corporation, Tokyo, Japan
	Leica with power supply KL1500 LCD	M125	Leica Microsystems, Wetzlar, Germany
Mixer	Vortex-Genie®	2	Scientific Industries, Inc., Bohemia, USA
	Magnetic stirrer IKA® RH	Basic 2	IKA®-Werke GmbH & CO. KG, Staufen, Germany
	Programmable rotator	Bio RS-24	BioSan, Riga, Latvia
	Thermomixer	Comfort	Eppendorf AG, Hamburg, Germany
PCR	Professional Trio Thermocycler		Analytik Jena AG, Jena, Germany

Table 5.6 continued

Pipettes	Eppendorf research pipettes		Eppendorf AG, Hamburg, Germany
	Tips: 2-10 µl, 2-200 µl, 100-1000 µl		Sarstedt AG & Co, Nümbrecht, Germany
	Multichannel: RAININ Pipet-lite	XLS	Mettler Toledo, Columbus, USA
pH-meter	Basic Meter	PB-11	Sartorius, Göttingen, Germany
Plasticware	Cuvettes, 15 ml-, 50 ml tubes		Sarstedt AG & Co, Nümbrecht, Germany
	Half-volume 96-well plates, white		Cayman Chemical Company, Ann Arbor, USA
	Reaction tubes 0.5 ml, 1.5 ml, 2 ml, 5 ml		Eppendorf AG, Hamburg, Germany
Power Supply Unit	Power Pac	300	Bio-Rad Laboratories Inc., Hercules, USA
	Protein Crystallography		
- Imaging System	Rock Imager	1000	Formulatrix Inc.,Waltham, USA
- Manual Pipetting Aid	Liquidator^{96}		Steinbrenner Laborsysteme GmbH, Wiesenbach, Germany
- Crystallisation Robot	Mosquito® Nanodispenser		TTP LabTech Ltd., Melbourn, UK
- Anode	MICROSTAR		Bruker AXS Corp., Billerica, USA
- Detector	Mar Image Plate Detector	345	Marresearch, Norderstedt, Germany
- Screening	Corning® 3550 Protein Crystallisation Plate		Corning Inc., New York, USA
	Crystalquick plate 96 well		Greiner Bio-One GmbH, Frickenhausen, Germany
	96-well Microplate V-Shape		Greiner Bio-One GmbH, Frickenhausen, Germany
	Crystalgen SuperClear^{TM} Plates, pregreased		Jena Bioscience GmbH, Jena, Germany
	Cryschem Plate 24 well, sitting drop		Hampton Research, Aliso Viejo, USA
Quantification DNA/protein	Nanodrop	1000	Thermo Fisher Scientific, Waltham, USA
Scales	Deltarange®	PM 480	Mettler Toledo, Columbus, USA
	Standard	BA3100P	Sartorius, Göttingen, Germany
	Standard	CP225D	Sartorius, Göttingen, Germany
SDS PAGE	Mini-PROTEAN® system		Bio-Rad Laboratories Inc., Hercules, USA
Thermostat	Metal Thermostat Dri-Block	DB2A	Bibby Scientific, Stone
Water-filtration unit	Millipore Synergy Desalting Unit		Merck KGaA, Darmstadt, Germany

Table 5.7: Online services used for the preparation of this manuscript.

ONLINE TOOLS	APPLICATION	WEBSITE
ConSurf	Conservation mapping	http://consurf.tau.ac.il
MolProbity	Structure validation	http://molprobity.biochem.duke.edu
Phyre2	Secondary structure prediction	http://www.sbg.bio.ic.ac.uk/phyre2/html/page.cgi?id=index [243]
ProtParam	Protein parameter calculation	http://web.expasy.org/protparam/
PSIPRED	Secondary structure prediction	http://bioinf.cs.ucl.ac.uk/psipred/ [244]
Reverse Complement	DNA sequence inverting	http://www.bioinformatics.org/sms/rev_comp.html
Sednterp	Parameters for AUC analysis	http://sednterp.unh.edu/#
Sequence Alignment	Protein sequence alignment	http://www.ebi.ac.uk/Tools/msa/muscle/
TLSMD	TLS parameter determination	http://skuld.bmsc.washington.edu/ [259]
Uniprot	Protein sequences	http://www.uniprot.org/uniprot/

Table 5.8: Software used for the preparation of this manuscript.

SOFTWARE	VERSION	PROVIDER
Clone Manager	9.0	Scientific & Educational Software, Morrisville, USA
Gimp	2.6	GNU General Public License, www. gimp.org
Illustrator CS4	14.0.0	Adobe Systems Inc., San Jose, USA
ImageJ	1.46r	Public License, N.I.H., http://imagej.nih.gov/ij/
JalView	14.0	http://www.jalview.org [250]
MagTran		[260]
MaxQuant	1.5.2.18	[261]
Office Suite	14.1.0	Microsoft Corp., Redmond, USA
Origin	9.0	OriginLab Corp., Northampton, USA
Phenix	1.9-1692	PHENIX Industrial Consortium, Berkeley, USA
Pymol	1.4	Schrödinger LLC, Cambridge, UK [262]
CCP4MG	2.9.0	http://www.ccp4.ac.uk/MG/index.html [263]
SedFit	14.4d	Center for Information Technology N.I.H, Bethesda, USA
Unicorn Control Software	5.31	GE Healthcare, Chalfont St. Giles, UK
Xcalibur		Thermo Fisher Scientific, Waltham, USA
XDS Program Package		Max-Planck-Institut für medizinische Forschung, Heidelberg, Germany

5.2 Methods

5.2.1 Molecular biology methods

Polymerase chain reaction (PCR)

The polymerase chain reaction (PCR) was used for preparative production of DNA. Two primers with restriction sites specific to the target vector that anneal at the 3' and 5' end of the desired sequence of a gene of interest are used to create a PCR product. The standard protocol used for PCR is depicted in Table 5.9. The cloning of DNA sequences was either performed using enzymatic restriction or restriction-free cloning as described below.

Table 5.9: Preparative PCR procedure.

REACTION MIX	PCR PROGRAMME		
45 ng DNA template	30 s	98 °C	
10 µM complementary oligonucleotides	15 s	98 °C	20 cycles
5 µl 10x Polymerase buffer	20 s	58 °C	
0.5 µl AccuPrime^{TM} Taq DNA Polymerase	20 s	68 °C	
3 % DMSO	10 min	68 °C	
H_2O ad 50 µl	∞	4 °C	

Restriction cloning

Sequence-specific cutting of PCR fragments could be obtained using restriction enzymes (New England Biolabs, Ipswich, USA). The DNA was supplemented with enzyme buffer and enzymes in ratios according to the manufacturer's recommendations, incubated at 37 °C for 4 h and further purified by agarose gel electrophoresis (Section 5.2.1). The target DNA-plasmid was digested by the corresponding enzymes creating compatible overhangs with the addition of shrimp alkaline phosphatase (New England Biolabs, Ipswich, USA) to prevent re-ligation of the plasmid. The digested PCR product and plasmid were ligated in a molar ratio of 2:1 for 4 h with T4-DNA-ligase (New England Biolabs, Ipswich, USA) at 20 °C or overnight at 4 °C. This reaction was subsequently transformed in competent bacteria *E. coli* Omnimax by applying a 42 °C heat shock for 30 sec and immediately plating the mix on selective media containing the respective antibiotics. Positive clones were confirmed by DNA-restriction and verified by DNA sequencing (Beckman Coulter Genomics; Takeley, UK).

DNA extraction and purification

Agarose gel electrophoresis is used for the separation of nucleic acids according to their size. For the preparation of this manuscript, 0.9 % agarose in 1x TAE buffer was used supplemented with the DNA-binding dye Midori Green. DNA samples were mixed with DNA loading buffer (Table 5.4), loaded in the wells of the gel and then separated by applying a constant voltage of ~100 V. The nucleic acid standard GeneRuler^{TM} 1kb DNA Ladder (Fermentas, St. Leon-Rot, Germany) served as a reference for the size of the DNA fragments. DNA fragments of appropriate sizes were excised from the gel and were extracted using the Wizard® SV Gel and PCR Clean-Up System (Promega Corp., Madison, USA). For the amplification of plasmids, ~100 ng were transformed in competent *E. coli* Omnimax

and incubated at 37 °C in 4 ml LB-medium overnight. The plasmid DNA was then isolated using the NucleoSpin® Plasmid Isolation Kit (Macherey-Nagel, Düren, Germany).

Restriction-free cloning

This method involves PCR amplification of the gene region encoding the desired amino acid sequence to produce a "megaprimer". This megaprimer was produced to possess compatible overhangs with the target vector where it was subsequently integrated in a second PCR reaction (http://rf-cloning.org). The following constructs were obtained by restriction-free cloning (see also Table 5.2): pFH-Bub1$^{740-1085}$, pFG-Bub1$^{726-1085}$-$(GS)_{3/4}$H2A$^{115-130}$, pFG-Bub1$^{726-1085}$-$(GS)_{3/4}$H2A$^{115-130}$T120A, pGEX-2rbs-H2Ac.

Site-directed mutagenesis of DNA

Site-directed mutagenesis was used to introduce single- or multiple-base substitution into a DNA sequence of choice to achieve amino acid mutations. All single-amino acid mutants were generated using the QuikChange site-directed mutagenesis instructions (Stratagene, La Jolla, USA).

DNA Sequencing

The verification of cloned plasmid DNA sequences was carried out by the sequencing service offered at MPI Dortmund (Dortmund, Germany) or by Beckman-Coulter Genomics (Takeley, UK).

Generation of infectious baculoviruses

The baculoviral expression system is a means of expressing recombinant proteins in a eukaryotic system, insect cells. To this end, all protein constructs were cloned into Multibac vectors (pFG, pFH, modified after [264, 265]) recombined in a bacmid using *E. coli* DH10*Multi*Bac^{Turbo} cells following the manufacturer's protocol (ATG:biosynthetics GmbH, Merzhausen, Germany). Recombined and precipitated bacmids were resuspended in 30 µl TE and then used to generate recombinant baculoviruses in insect Sf9 cells using the FuGENE system (Stratagene, La Jolla, USA), according to the manufacturer's instructions.

5.2.2 Protein biochemical methods

Protein expression and purification

Recombinant baculoviruses encoding the His_6-tagged Bub1 and untagged Bub3 were generated using the FuGENE (Stratagene) system 5.2.1. After two rounds of virus amplification (4 days each) Sf9 or Tnao38 (see Table 5.5) cells were infected at a multiplicity of infection of 1/20-1/50 and harvested 72 hours after infection (15 min at 1165 x g, 20 °C, rotor H6000A, Sorvall centrifuge RC3BP+, Thermo Fisher Scientific). Insect cells are grown in suspension at 27.5 °C, 110 rpm in an incubator shaker Multitron® (Infors AG, Bottmingen, Switzerland).
For proteins produced in bacteria, the constructs have been transformed in competent *E. coli* (5.5), grown overnight to inoculate cultures at OD_{600} of 0.05 in TB media supplemented with 0.2 % lactose and the corresponding antibiotic. Cells were then initially grown for 4 h, 37 °C at 150 rpm in an incubator shaker Multitron® (Infors AG, Bottmingen, Switzerland), then temperature was reduced to 25 °C for another 20-24 h of expression before cells were harvested (20 min at 5895 x g, 20 °C, rotor H6000A, Sorvall centrifuge RC3BP+, Thermo Fisher Scientific).
Pelleted cells were either stored at -80 °C or immediately resuspended in lysis buffer at 4 °C (50 mM Tris pH 8, 300 mM KCl, 2 mM $MgCl_2$ and 2 mM PMSF or 1x protease inhibitor mix HP plus (Serva Electrophoresis GmbH, Heidelberg, Germany)), sonicated (Sonifier® Cell Disruptor, Branson Ultrasonics Corp., Danbury, USA) and cleared by centrifugation at 108800 x g, 4 °C (Rotor JA 30.50, Avanti J-30I, Beckman Coulter Inc., Brea, USA) and filtration of the lysate using Rotilabo® syringe filters 0.45-0.8 µm (Carl Roth Chemie GmbH, Karlsruhe, Germany).
The cleared lysate was passed on 1 ml Nickel-NTA-Superose-/GSH beads (GE Healthcare, Amintra Glutathione Resin Expedeon Inc., San Diego, USA) or a 5 ml HisTrap FF/GSTrap FF (GE Healthcare, Chalfont St. Giles, UK) depending on the affinity tag of the protein. The bound complex was washed with lysis buffer to eliminate unspecifically bound proteins followed by a one-step elution in 300 mM imidazole (Ni-affinity) or 25 mM glutathione (GSH-affinity).
The eluted protein was diluted to 50 mM KCl and either directly purified by anion exchange chromatography (Resource Q 6 ml), or first incubated with TEV protease (all pFH constructs) or PreScission (pFG constructs) overnight or for 4 h for complete tag-cleavage. The cut protein solution was passed over the respective affinity resin to remove the protease and affinity tag before applying the protein on the anion exchange column. Unspecifically bound proteins were removed from the column in a washing step followed by elution in a linear gradient to 500 mM NaCl/KCl. The fractions containing the protein were monitored by UV (245 nm, 280 nm), analysed on SDS PAGE (Section 5.2.3), then pooled, concentrated (Section 5.2.2) and passed on a gel filtration column, the respective buffers are listed in Table 5.10. Proteins not exceeding 70 kDa in size were passed on a HiLoad Superdex 75 PG or Superdex 75 10/300 GL, for complexes of bigger sizes a Superdex 200 10/300, HiLoad Superdex 200 PG or Superose 6 10/300 GL was used (all anion exchange and gel filtration columns: GE Healthcare, Chalfont St. Giles, UK). Each of the purification steps has been carried out at 4 °C using the ÄKTA Purifier, or Prime plus systems (GE Healthcare, Chalfont St. Giles, UK).
The pH of the purification buffers was adjusted to the theoretical isoelectric point of the specific protein, an overview of the gel filtration buffers for specific protein constructs can be found in Table 5.10. $MgCl_2$ was added to lysis and gel filtration buffers of protein kinases, NaCl or KCl was added

to buffers in different amounts depending on the protein.
Point mutants of amino acids or short protein truncations were expressed and purified equally to the wild-type protein. The purification of MBP-Knl1 138-225 was carried out as described [179] with the exception of changing the desalting column to a gelfiltration step.

Table 5.10: Protein constructs, their expression system and gel filtration buffers consistently used in the preparation of this manuscript.
Amino acid mutants and truncations of proteins were purified under the same conditions.

CONSTRUCT	EXPRESSION	ION EXCHANGE BUFFER	GEL FILTRATION BUFFER
Borealin:Survivin	*E. coli* C41	A: 25 mM HEPES pH 7.4, 125 mM NaCl, 1 mM DTE B: 25 mM HEPES pH 7.4, 2 M NaCl, 1 mM DTE	25 mM HEPES pH 7.4, 150 mM NaCl, 1 mM DTE, 5 % glycerol
Bub1:Bub3, BubR1:Bub3	Sf9, Tnao38	A: 50 mM Tris pH 8, 50 mM KCl, 2 mM DTE B: 50 mM Tris pH 8, 1 M KCl, 2 mM DTE	50 mM Tris pH 8, 150 mM KCl, 2 mM DTE, 2 mM $MgCl_2$
$Bub1^{kinase}$, $Bub1^{kinase}$-$H2A^{115-130}$	Tnao38	A: 50 mM Tris pH 8, 50 mM NaCl, 2 mM DTE B: 50 mM Tris pH 8, 1 M NaCl, 2 mM DTE	25 mM HEPES pH 7.6, 100 mM NaCl, 2 mM TCEP, 5 mM $MgCl_2$
$BubR1^{kinase}$	Tnao38	A: 50 mM HEPES pH 7.4, 50 mM KCl, 2 mM TCEP, 1 mM EDTA B: 50 mM HEPES pH 7.4, 1 M KCl, 2 mM TCEP	20 mM HEPES pH 7.4, 150 mM sodium citrate/KCl, 2 mM TCEP
Cdc20	Sf9	-	50 mM Mes pH 6.5, 250 mM NaCl, 2 mM TCEP, 1 mM $MgCl_2$, 5 % glycerol
$H2A^{115-130}$	*E. coli* C41	-	50 mM Tris pH 8, 100 mM KCl, 2 mM DTE
$Knl1^{138-225}$	*E. coli BL21 RIL*	-	50 mM Tris pH 8, 150 mM KCl, 2 mM TCEP

Concentrating protein solutions

All protein solutions were concentrated using Amicon Ultra-0.5, Ultra-4 or Ultra-15 Centrifugal concentrators, 3, 10 or 50 kDa MWCO, at 4 °C. The Ultra-4 and -15 concentrators were used at 1520 x g (Universal Centrifuge 320 R, Hettich Lab Technology, Tuttlingen, Germany), the Ultra-0.5 centrifugal filter devices at 5500 x rcf (Microcentrifuge 5418 R, Eppendorf AG, Hamburg, Germany). Purified protein was concentrated in the gel filtration buffer, then flash frozen in liquid nitrogen and stored at -80 °C.

Preparative protein phosphorylation and -dephosphorylation

In order to generate fully auto-phosphorylated ($Bub1^{kinase}$) or dephosphorylated purified samples, the protein solution was pooled after affinity chromatography and supplemented with 1 mM ATP and 10 mM $MgCl_2$ or λ-phosphatase and 10 mM $MnCl_2$, respectively, then incubated at 4 °C overnight. Excess of ATP or λ-phosphatase was removed in an subsequent anion-exchange chromatography step.

Preparation of histone H2A and mononucleosomes

Histone H2A was used as a Bub1 kinase substrate and expressed in *E. coli* from a pET3 vector and further purified by isolation from inclusion bodies as previously described [266].
The reconstitution and purification of histone H3 and CENP-A containing nucleosomes, which consist of either H3 or CENP-A and H4, H2A, H2B and a short sequence of centromeric DNA, was produced with slight modifications for CENP-A containing nucleosomes as published before [267, 266]. Briefly, the single histones H2A and H2B are mixed in equimolar amounts to obtain a dimer while CENP-A and H4 are mixed to obtain a tetramer. A digested centromeric DNA with eight repeats of the 601-145 bp sequence was combined with H2A/H2B dimer and CENP-A/H4 tetramer to obtain CENP-A nucleosomes. Histone purification and nucleosome reconstitution was largely implemented by Doro Vogt and Federica Basilico.

5.2.3 Analytical and biophysical methods

SDS Polyacrylamide gel electrophoresis (PAGE)

SDS Polyacrylamide gel electrophoresis (SDS PAGE) is a method to separate proteins on a gel according to their size [268]. The protein sample is mixed with a 5x SDS-sample buffer (see Table 5.4), reduced and boiled at 95 °C. The proteins and a molecular weight standard (Precision Plus Protein Unstained/Stained Standards, Bio-Rad Laboratories Inc., Hercules, USA) were subsequently separated on a SDS PAGE gel (see Table 5.11) by gel electrophoresis using SDS-PAGE buffers (see Table 5.4) at 100 V for around 45 min.

Table 5.11: Composition of SDS gels used in this manuscript. The amounts are calculated for two 10 % gels.

SOLUTION	STACKING GEL	SEPARATING GEL
4x buffer (Table5.4)	0.38 ml	2.5 ml
Acrylamide 4K solution (30 %)	0.5 ml	3.2 ml
APS (10 %)	50 µl	100 µl
TEMED	5 µl	10 µl
ddH_2O	2.1 ml	3.9 ml

The protein bands were visualised by staining with heated Coomassie staining solution (Table 5.4) followed by background destaining with 10 % (v/v) acetic acid and 20 % (v/v) ethanol.

Determination of protein and DNA concentrations

Concentrations of both protein and DNA solutions were measured with a Nanodrop 1000 (Thermo Fisher Scientific, Waltham, USA) UV-Vis spectrophotometer.

Limited proteolysis

Limited proteolysis is a means to determine stable protein fragments that are potential candidates for further structural or biochemical characterisation. A protein or complex of interest is incubated

with low amounts of proteases that cut in intrinsically unstructured or flexible regions of a polypeptide chain. This yields smaller cleavage products that can be further analysed by mass spectrometry or N-terminal peptide sequencing.
In this manuscript proteins or complexes were subjected to digestion by proteases with different site specificities: Trypsin (R, K), Elastase (A, V), Chymotrypsin (large hydrophobics), Glu C (E) and Subtilisin (large uncharged residues). 3 µg of protein or protein complex was incubated with 3 µl of protease (1 mg/ml stock diluted 1:10, 1:100 and 1:1000 in protease dilution buffer, 20 mM HEPES pH 7.5, 50 mM NaCl, 10 mM $MgSO_4$), for 30 minutes at 4 °C. The reaction was quenched with protein sample loading buffer, then analysed by SDS PAGE (see 5.2.3) using undigested protein and protease of the highest concentration as references.

Non-equilibrium binding experiments

Qualitative binding of proteins was tested in GST-pull down experiments using GST-tagged bait protein coupled to GSH beads. Beads were blocked with BSA and washed prior to use to prevent unspecific binding of prey proteins. Beads were incubated with 1 µM protein, rotating for 1 h at 4 °C, then washed three times with binding buffer (50 mM Tris pH 8, 100 mM KCl, 0.05 % Tween-20) to remove unbound protein. The bound bait was then incubated with 3 µM prey protein, rotating for 1 h at 4 °C and washed again to remove unbound or unspecifically bound protein. Alternatively, bait and prey were premixed and bound in one single step. Analysis of bound proteins was carried out by SDS PAGE (see Section 5.2.3) loading bait and prey alone as input reference.

Electrophoretic Mobility Shift Assay (EMSA)

The electrophoretic mobility shift assay (EMSA) is a technique for determining and visualising of DNA-protein interactions. This method exploits the fact that protein species bound to DNA migrate more slowly than free DNA when subjected to agarose gel electrophoresis. Moreover, it allows to resolve different complex assemblies dependent upon their conformation or stoichiometry. Here, protein binding to nucleosomes was studied by EMSA using 0.5 µM nucleosomes, 22.5 mM HEPES pH 7.5, 90 mM NaCl, 1.8 mM TCEP, 4.5 mM $MgCl_2$, 1 mM AppNHp in a final volume of 20 µl. Different concentrations of protein (0-40 µM) were added, incubated for 30 min on ice before adding 2.2 µl loading dye (20 mM TEA, 1 mM EDTA, 20 % glycerol). The mix was subjected to agarose gel electrophoresis using a 0.7 % agarose gel (Agarose LE, Roche Applied Science, Penzberg, Germany), run in 0.2 % TBE, at 20 mA for about 2 h using free DNA and unbound protein as references. Staining and analysis as in Section 5.2.1.

Analytical ultracentrifugation

The molecular mass and stoichiometry of protein complexes was assessed by measuring the sedimentation velocity of a protein species in analytical ultracentrifugation. Protein complexes were used in concentrations corresponding to a molecular absorption at 280 nm of 0.6 using the individual

extinction coefficients as determined by ProtParam (http://web.expasy.org/protparam/). Sedimentation velocity experiments were performed in an Optima XL-A analytical ultracentrifuge with Epon charcoal-filled double-sector quartz cells and an An-60 Ti rotor (all Beckman Coulter, Brea, USA). Samples were dialysed against buffer (50 mM Tris pH 8, 150 mM KCl, 3 mM $MgCl_2$, 2 mM TCEP) that was used as a reference. Samples were centrifuged at 203,000 x g at 20 °C and 500 radial absorbance scans at 280 nm were collected with a time interval of 1 min. The obtained data was further analysed in terms of continuous distribution function of sedimentation coefficients (c(S)) using SedFit [269] with fitting parameters for the protein partial specific volume, buffer viscosity and density as determined by SEDNTERP. Data were plotted using the program GUSSI comprised in the SedFit software [269].

Electrospray ionisation mass spectrometry (ESI-MS)

Electrospray ionisation mass spectrometry (ESI-MS) [270] is a method for the accurate determination of the molecular weight of molecules. The application of an electrical field allows the enrichment of ions of the same charge, which are collected in an ion trap, where they are separated and detected according to their sizes by applying an altering electric field. For the analysis of protein samples, 0.5 nmol protein were desalted via HPLC on a C_4 column (HPLC system LC1100, Agilent Technologies, Santa Clara, USA) and eluted a combination of 0.1 % TFA (trifluoroacetic acid) in H_2O (buffer A) and 0.08 % TFA in acetonitrile (buffer B) using a linear gradient to 20 % buffer A and 80 % buffer B. The mass analysis of the samples was performed using a Finnigan LCQ Advantage MAX mass spectrometer (Thermo Fisher Scientific, Waltham, USA). The software Xcalibur and MagTran [260] were used for analysis and deconvolution of mass spectra; the accuracy of the weight determination of proteins via ESI-MS is estimated to be approximately 7 Da.

Phosphorylation-site analysis

Liquid chromatography coupled with mass spectrometry was used to assess the phosphorylation status or novel phosphorylation sites. The proteins of interest (~10 µg) were incubated with 10 nM kinase in buffer (25 mM Tris pH 7.6, 10 mM $MgCl_2$, 150 mM NaCl, 5 mM TCEP) and 0.5 mM ATP for at least 4 h at 25 °C. Samples were then digested with LysC/Trypsin and/or GluC and prepared for LC-MS/MS analysis as previously described [271]. 100 ng of peptides were separated on a Thermo Scientific™ EASY-nLC 1000 HPLC system (Thermo Fisher Scientific™, Odense, Denmark); in an one hour gradient from 5-60 % acetonitrile with 0.1 % formic acid and directly sprayed via a nano-electrospray source in a quadrupole Orbitrap mass spectrometer [272] (Q Exactive™, Thermo Fisher Scientific™) . The Q Exactive™ was operated in data-dependent mode acquiring one survey scan and subsequently ten MS/MS scans [273]. Resulting raw files were processed with the MaxQuant software (version 1.5.2.18) using a reduced database containing only the proteins of interest for the search and giving phosphorylation on serine, threonine and tyrosine as variable modification [261]. A false discovery rate cut off of 1 % was applied at peptide and protein levels and the phosphorylation site decoy fraction. Proteolysis and phospho-peptide analysis was kindly performed by Franziska Müller and Tanja Bange.

Cross-linking analysis coupled with mass spectrometry

This method was used to identify potential sites of protein-protein interaction of larger protein assemblies. Experiments of cross-linking coupled with mass spectrometry were carried out and analysed in collaboration with Dr. Franz Herzog's laboratory at the Ludwig Maximilian University in Munich [274, 275].

5.2.4 Kinetic characterisation of kinase constructs

The kinetic parameters of the studied proteins were determined either by measuring the change in fluorescence of a 2'-/3'-O-(N'-Methylanthraniloyl) (mant) [239] labeled nucleotide or using the ADP-Glo^{TM} Kinase Assay. Reaction temperature for all experiments was 27 °C. The different methods will be explained in more detail below.

Determination of catalytic parameters (ADP Glo Assay)

The ADP-Glo^{TM} Kinase Assay was implemented to allow for the quantitative measurement of ADP produced in the kinase reaction. The schematic working principle is depicted in Figure 5.1. The kinase reaction was carried out by mixing in a total volume of 45 µl, a first substrate (concentrations from 0 to 200 µM) with a second substrate (saturating concentration 200 µM) in kinase buffer (25 mM Tris pH 7.6, 10 mM $MgCl_2$, 150 mM NaCl, 5 mM TCEP) and starting the reaction by the addition of 10 nM kinase. For each time point (0, 3, 7, 14 min) 8 µl were taken from the mix and quenched in ADP-Glo reagent and incubated for ≥ 45 min in 8 µl ADP Glo reagent already present in a white half-volume 96-well plate. Kinase detection reagent (16 µl) was added and the mix further incubated for 30 min. Luminescence of the detection reaction was recorded using the plate reader Infinity M200 (Microplate reader M200, Tecan, Männedorf, Switzerland).

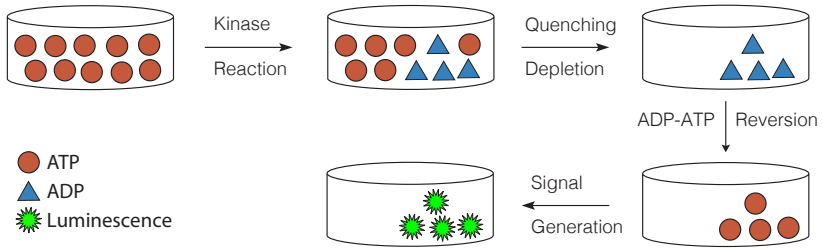

Figure 5.1: Working principle of the ADP-Glo^{TM} Kinase Assay.
The assay was performed in two steps: after completion of the kinase reaction, the first reagent (ADP Glo reagent) was added to quench the activity and deplete the remaining ATP; in a second step another reagent was added, which reverts the remaining ADP into ATP to be detected by a luciferase/luciferin reaction. The luminescent signal produced is linearly correlated to the amount of ADP produced in the kinase reaction and therefore a readout for kinase activity. Modified from ADP-Glo^{TM} Kinase Assay Technical Manual (Promega Corp., Madison, USA).

The catalytic parameters K_M and k_{cat} could be determined by means of measuring velocities from time course experiments using different substrate concentrations. Plotting the initial reaction ve-

locities ν_0 as a function of the substrate concentrations used [S], considering the enzyme concentration [E], obtained the kinetic parameters K_M and k_{cat} from the relation known in enzymology as Michaelis-Menten equation (equation 5.1).

$$\frac{\nu_0}{[E]} = \frac{[S]\,k_{cat}}{[S] + K_M}. \tag{5.1}$$

ν_0	initial reaction velocity (nM sec^{-1})
[E]	enzyme concentration (nM)
[S]	substrate concentration (µM)
k_{cat}	turnover number (sec^{-1})
K_M	Michaelis-Menten constant (µM)

The obtained data plots were fitted and analysed using the Origin 9.0 software (OriginLab Corp., Northampton, USA).

Fluorescence anisotropy

The binding of nucleotides to the studied kinases was carried out as described in reference [240]. Mant-labeled nucleotide was titrated from 0-1 mM to the kinase using 1 µM kinase in all measurements. Fluorescence emission at 450 nm (excitation at 340, detection 450 nm) was recorded using a microplate reader Infinity M200 (Tecan, Männedorf, Switzerland); the emission of mant-nucleotide alone was subtracted from the emission of the complex to obtain a binding isotherm. Data were fitted to a one site binding model equation using the Origin 9.0 software (OriginLab Corp., Northampton, USA) to determine binding parameters.

5.2.5 X-ray crystallography

X-ray crystallography is a method that allows to determine the structure of a molecule, like a protein, on atomic level. To this end the molecule needs to be obtained as a crystal that is subjected to x-ray and the diffracted rays are collected on a detector as a diffraction pattern. This diffraction pattern is characteristic for each crystal and allows the determination of the electron density in the crystal, which can then be used as a model to build a 3-dimensional structure of the molecule. In this manuscript the structure of phosphorylated Bub1 kinase (726-1085) was solved. Initial crystallising conditions were obtained using 5 g/l protein and 2 mM ADP, a Mosquito® Nanodispenser (TTP LabTech Ltd., Melbourn, UK), Corning® 3550 Protein Crystallisation Plates (Corning Inc., New York, USA) and the Core I-IV crystallisation solutions (Qiagen, Hilden, Germany). The conditions were refined to obtain diffraction-quality diamond-shaped crystals of 200 µm diameter after two days at 4 °C, in a sitting drop vapour diffusion Cryschem plate 24 well (Hampton Research, Aliso Viejo, USA). The reservoir solution contained 15 % PEG 3350 and 0.2 M NaCl, crystals were cryo-protected in this reservoir solution supplemented with 20 % (v/v) glycerol and then flash-frozen in liquid nitrogen. Different crystals of varied conditions were initially tested for diffraction at the Max-Planck-Institute (MICROSTAR x-ray source, Bruker AXS Corp., Billerica, USA; Mar345 Image Plate Detector, Marresearch GmbH, Norderstedt, Germany).

Exhaustive attempts have been performed unsuccessfully to obtain crystals of the BubR1 kinase domain. Initial crystallising attempts of the MBP-Knl1$^{138-225}$-Bub1:Bub3-BubR1:Bub3 complex failed as well as the comprehensive effort to obtain crystals of sufficient diffraction quality of phosphorylated Bub1^{kinase} co-crystallised- or as a direct fusion with H2A peptide (amino acids 115-128). Crystals could be obtained for phosphorylated Bub1^{kinase} by co-crystallisation with an H2A peptide but the obtained electron density map showed no apparent density for either a bound peptide or the substrate binding loop of Bub1. A summary of these protein constructs and crystallisation strategy used can be found in Table 5.12.

Table 5.12: Protein constructs and crystallisation strategies.
Indicated for the crystallisation of BubR1 kinase domain, the Knl1-Bub1:Bub3-BubR1:Bub3 complex and the crystallisation of phosphorylated Bub1 with a H2A peptide in fusion or co-crystallisation attempts. All successful crystallisation conditions were obtained at 4 °C.

CONSTRUCT	STRATEGY	PROTEIN CONDITIONS	CRYSTALLISING CONDITION
BubR1$^{543-1050}$	JCSG Core I-IV, Classics, PACT, PEGs I-II (Qiagen, Hilden, Germany)	8 g/l	– none –
BubR1$^{697-1050}$	JCSG Cores I-IV, JCSG+, ComPAS, $AmSO_4$, Anions, Cations, ClassicsI-II, Cryos, MPD, PACT, PEGsI-II, ProComplex (Qiagen, Hilden, Germany), Methylation [245, 246]	10 g/l, 1 mM ADP/AppCp, 5 % glycerol	– none –
BubR1$^{705-1050}$		8-10 g/l, 150 mM sodium citrate / 1M KCl / 150 mM KCl	– none –
BubR1$^{705-1044}$ BubR1$^{712-1050}$	expressed by DPF, not stable		– none –
BubR$^{718-1050}$	expressed by DPF, insufficient purity		– none –
Knl1-B1:B3-BR1:B3	JCSG Core I-IV (Qiagen, Hilden, Germany)	4 g/l	– none –
Bub1$^{740-1085}$	co-crystallisation with H2A peptide, amino acids 115-128 (human, T120A)	5 g/l, 2 mM ADP, autophosphorylated	– none –
Bub1$^{726-1085}$	co-crystallisation with H2A peptide, amino acids 115-128 (human, human T120A, or xenopus laevis), 20 °C, 4 °C	5 g/l, 2 mM ADP / ATPγS / AppNHp, autophosphorylated	0.1 M Tris pH 7.0-7.2, 20-23 % PEG MME 2000 (by seeding)
	co-crystallisation with H2A/H2B	5 g/l, 15 g/l H2A/H2B, BeF_3 / $NaVO_4$, autophosphorylated	– none –
Bub1^{kinase}-$GS_{3/4}$H2A$^{115-130}$ Bub1^{kinase}-$GS_{3/4}$H2A$^{115-130}$_T120A	JCSG Core I-IV, Opti Salts (Qiagen, Hilden, Germany), Crystallisation-Additive Screen HT (Hampton Research Aliso Viejo, CA, USA)	4-5 g/l, 2-5 mM ADP/ATPγS/AppNHp	0.1 M Na-acetate pH 4.4-4.6, 0.2 M NaCl, 40 % PEG 300, 3 % MeOH/EtOH, 2-5 mM ADP (no diffraction)

Data collection and processing

Diffraction data were collected from crystals cooled to 100 K at the X-ray source X10SA of the Swiss Light Source (Paul Scherrer Institute, Villigen, Switzerland) at a wavelength of 1 Å. Images were recorded on a Pilatus 6M detector, indexed and integrated using XDS and scaled using XSCALE [276]

in the CCP4 programme suite. Based on the unit cell volume the Matthews Coefficient suggested two copies of phosphorylated Bub1^{kinase} per asymmetric unit. The crystal diffracted to a minimum Bragg spacing of 2.4 Å and exhibited space group $P2_1$ with cell parameters a= 62 Å, b=66 Å, c=107, β=98. Data collection statistics and cell parameters are listed in Table 6.1 (Appendix).

Structure Solution and Refinement

Initial phases of the phosphorylated Bub1^{kinase} were obtained by molecular replacement using the programme PHASER [277]. The coordinates of human Bub1 kinase (PDB ID: 3E7E, [214]) were used as initial search model. Note, that these coordinates have later been re-refined with ADP and a second Mg ion instead of ATP in the electron density of the active site, which was then resubmitted with the PDB ID 4R8Q. The initial structure of the Bub1^{kinase} was further refined using rigid-body refinement and iterative rounds of restrained refinement using PHENIX [278] with TLS parameters [259] to better account for anisotropic observed B factors, interspersed with manual rebuilding using Coot [279, 280]. The final model was validated using MolProbity [281, 282]. Graphical representation or movies were generated using CCP4MG 2.9.0 [263] or Pymol [262].

6 Appendices

Table 6.1: Data collection and refinement statistics for phosphorylated Bub1 ^{kinase} (PDB ID 5DMZ).

DATA COLLECTION	
Wavelength (Å)	1.0000 Å
Resolution range (Å)	43.3 - 2.4 (2.486 - 2.4)
Space group	P 1 21 1
Unit cell (a, b, c, α, β, γ)	62.38 66.34 106.54
	90 98.34 90
Total reflections	233252 (23340)
Unique reflections	33866 (3332)
Multiplicity	6.9 (7.0)
Completeness (%)	99.85 (99.70)
Mean I/σ (I)	11.24 (1.03)
Wilson B-factor	56.36
R_{merge}	0.1133 (2.202)
R_{meas}	0.1227 (2.620)
CC1/2	0.999 (0.592)
CC*	1 (0.863)
REFINEMENT STATISTICS	
Reflections used for R-free	1694
R_{work}	0.211 (0.386)
R_{free}	0.245 (0.406)
Number of non-hydrogen atoms	5606
Macromolecules	5526
Ligands	56
Water	24
Protein residues	680
Missing residues	A/B: 726-734; 807-815; 1084-1085
RMS (bonds)	0.004
RMS (angles)	0.853
Ramachandran favoured (%)*	98
Ramachandran outliers (%)*	0
Clashscore*	4.49
Average B-factor	78.6
Macromolecules	78.9
Ligands	63.1
Solvent	50.6

Data for the highest-resolution shell are given in parentheses.
$R_{\text{merge}} = 100\Sigma_h \Sigma_i |I_{h,i} - \langle I_h \rangle| / \sum_h \sum_i I_{h,i}$, where the outer sum (h) is over the unique reflections and the inner sum (i) is over the set of independent observations of each unique reflection.
$R_{\text{work}} = \Sigma_{hkl} ||F_{obs}| - |F_{calc}|| / \sum F_{obs}$, where F_{obs} and F_{calc} are the observed and calculated structure factors of the respective reflexes hkl.
R_{free} was determined corresponding to R_{work} for random 5 % of the reflexes, which have been excluded from use in the refinement.
* As defined by MolProbity [281]

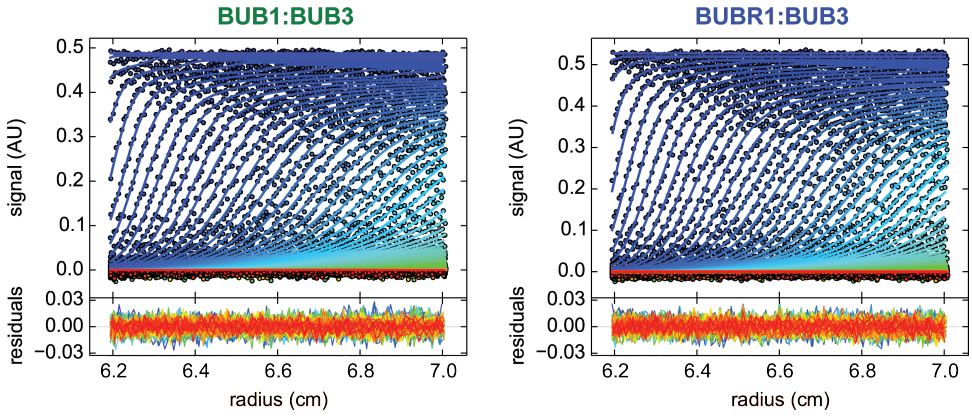

Figure 6.1: Sedimentation velocity absorption profiles.
Radial signals of the sedimentation velocity absorption profiles of the Bub1:Bub3 (left) and BubR1:Bub3 (right) complexes and the corresponding residuals of the fits showing the deviation of the c(S) model from the observed signals.

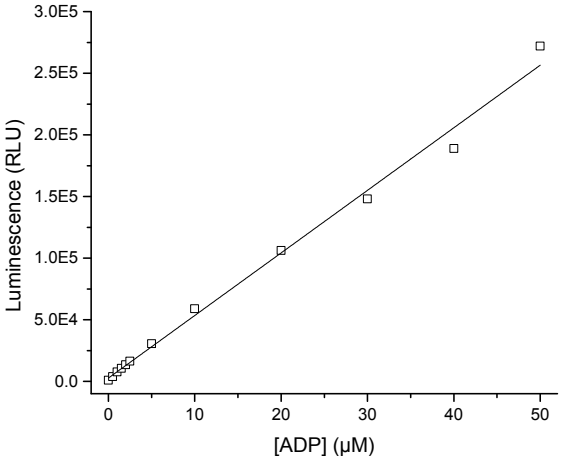

Figure 6.2: ADP standard used for the quantification of kinase activity performed with the ADP-Glo^{TM} Kinase Assay.
The amount of ADP (µM) is linearly correlated to the luminescence (RLU) generated in a kinase reaction by the ADP-Glo^{TM} Kinase Assay (Promega). The slope of the curve was determined in a linear curve fit as 5077 (RLU/µM) with R^2=0.99.

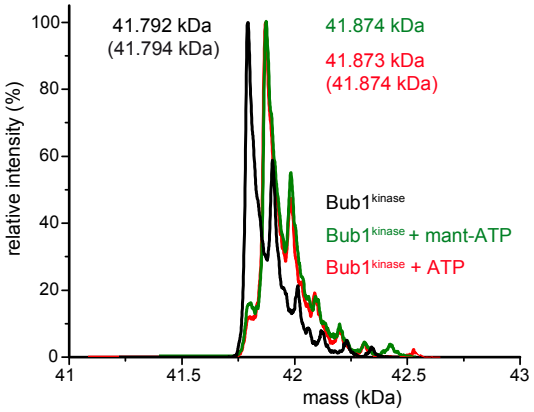

Figure 6.3: Mant-ATP is a substrate of Bub1^{kinase}.
Unphosphorylated Bub1^{kinase} (black) efficiently autophosphorylates using ATP (red) as well as mant-ATP (green) as a substrate. The autophosphorylation reaction with and without mant-ATP was analysed by ESI-MS. The theoretical weight of the unphosphorylated and phosphorylated protein is given in parentheses.

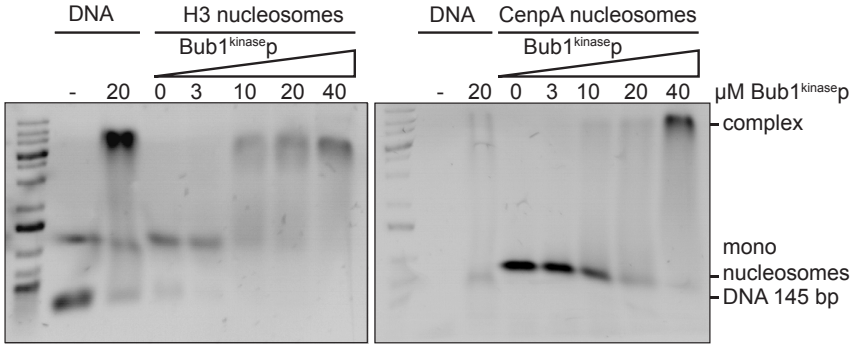

Figure 6.4: Nucleosome binding of phosphorylated Bub1^{kinase}.
EMSA showing DNA and nucleosome binding of phosphorylated Bub1^{kinase} and H3- or CENP-A nucleosomes.

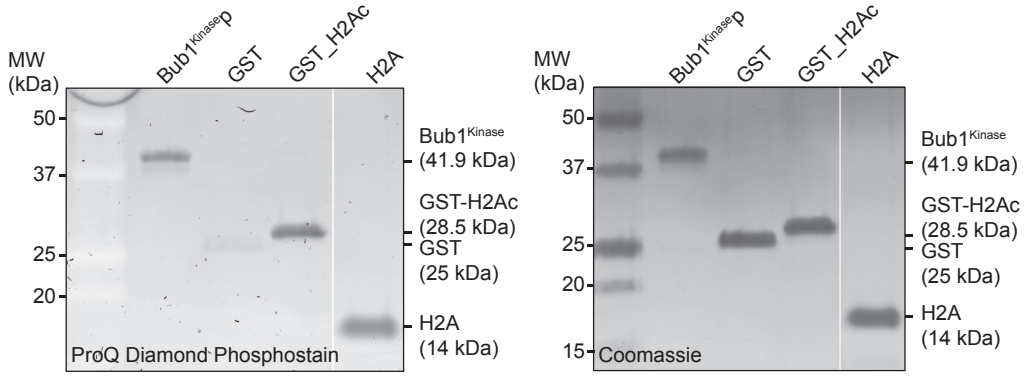

Figure 6.5: GST-H2Ac (H2A$^{113-130}$) and not GST is a substrate of Bub1 kinase.
GST, GST-H2Ac and H2A were incubated with 30 nM Bub1^{kinase} and ATP, then analysed by SDS PAGE and Coomassie blue staining (right). Phosphates were visualised using the Pro-Q® Diamond Phosphoprotein Gel Stain (left). Phosphorylated Bub1^{kinase} was used as a positive control for phosphostaining.

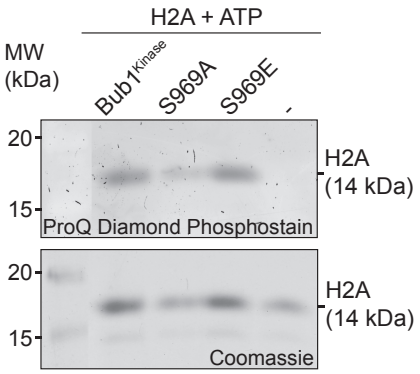

Figure 6.6: Bub1^{kinase} S969E is an active enzyme while S969A is catalytically inefficient.
H2A phosphorylation was analysed on SDS PAGE after incubation with Bub1^{kinase} or Bub1^{kinase} S969E/A and ATP using Pro-Q®Diamond Phosphoprotein Gel Stain. The figure has been cropped showing only the relevant lanes.

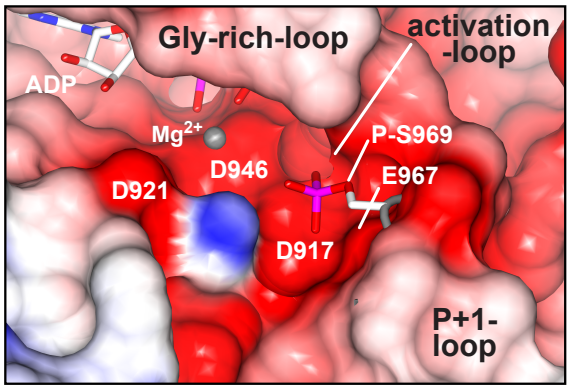

Figure 6.7: The electrostatic potential of the surface of Bub1^{kinase} shows a highly negatively charged cleft opposing S969p.
The electrostatic potential was drawn around Bub1^{kinase}, the residues contributing to the negative electrostatic potential are indicated; S969, ADP and Mg are shown as sticks or sphere, respectively. The position of Gly-rich loop, activation loop and P+1 loops is marked. The image was created with CCP4MG.

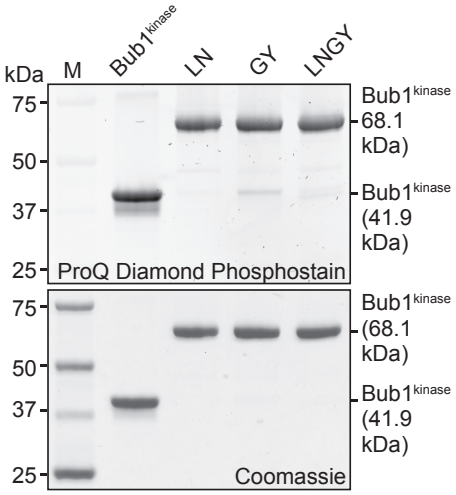

Figure 6.8: Bub1^{kinase} mutants LN, GY, LNGY are active enzymes that autophosphorylate.
Autophosphorylation was analysed on SDS PAGE after incubation of Bub1^{kinase} proteins with ATP using Pro-Q®Diamond Phosphoprotein Gel Stain. Note, the mutant proteins are tagged with GST, leading to a higher mass. LN- L875A/N879A, GY- G1001A/Y1003A, LNGY- L875A/N879A/G1001A/Y1003A. M- Molecular weight protein marker, indicated in kDa on the left.

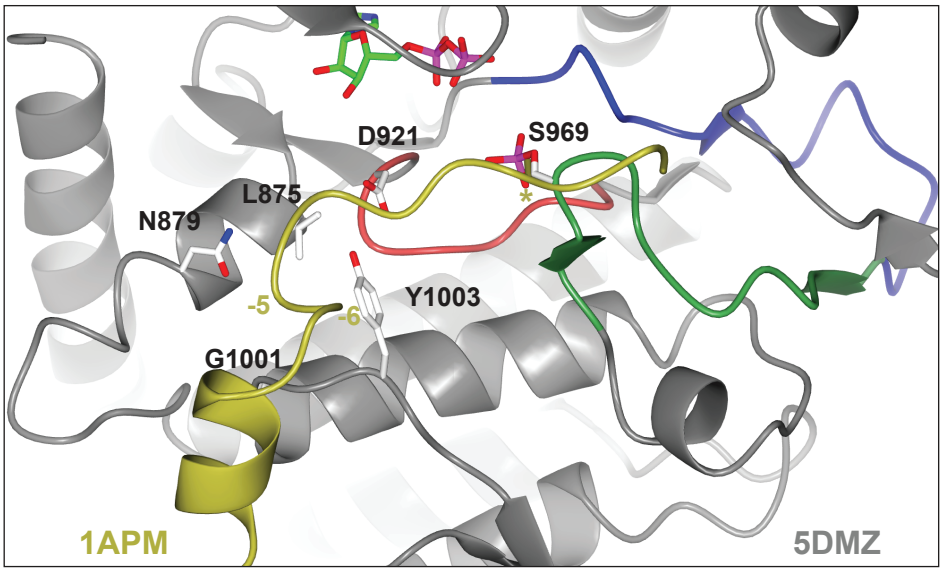

Figure 6.9: The position of S969p is incompatible with substrate binding.
Superposition PKA with a bound substrate inhibitor peptide and Bub1^{kinase} (PDB IDs: 1APM, 5DMZ) showing only Bub1^{kinase} (grey) and the co-crystallized peptide of PKA (yellow). The activation loop is shown in blue, the P+1 loop in green, the catalytic loop is coloured red. ADP, S969p and putative residues involved in substrate recognition are depicted as sticks. The position of the phosphorylated substrate residue (Ala in 1APM peptide) is denoted with a yellow asterisk, the -5 and -6 positions on the peptide are indicated in yellow. The image was created with CCP4MG.

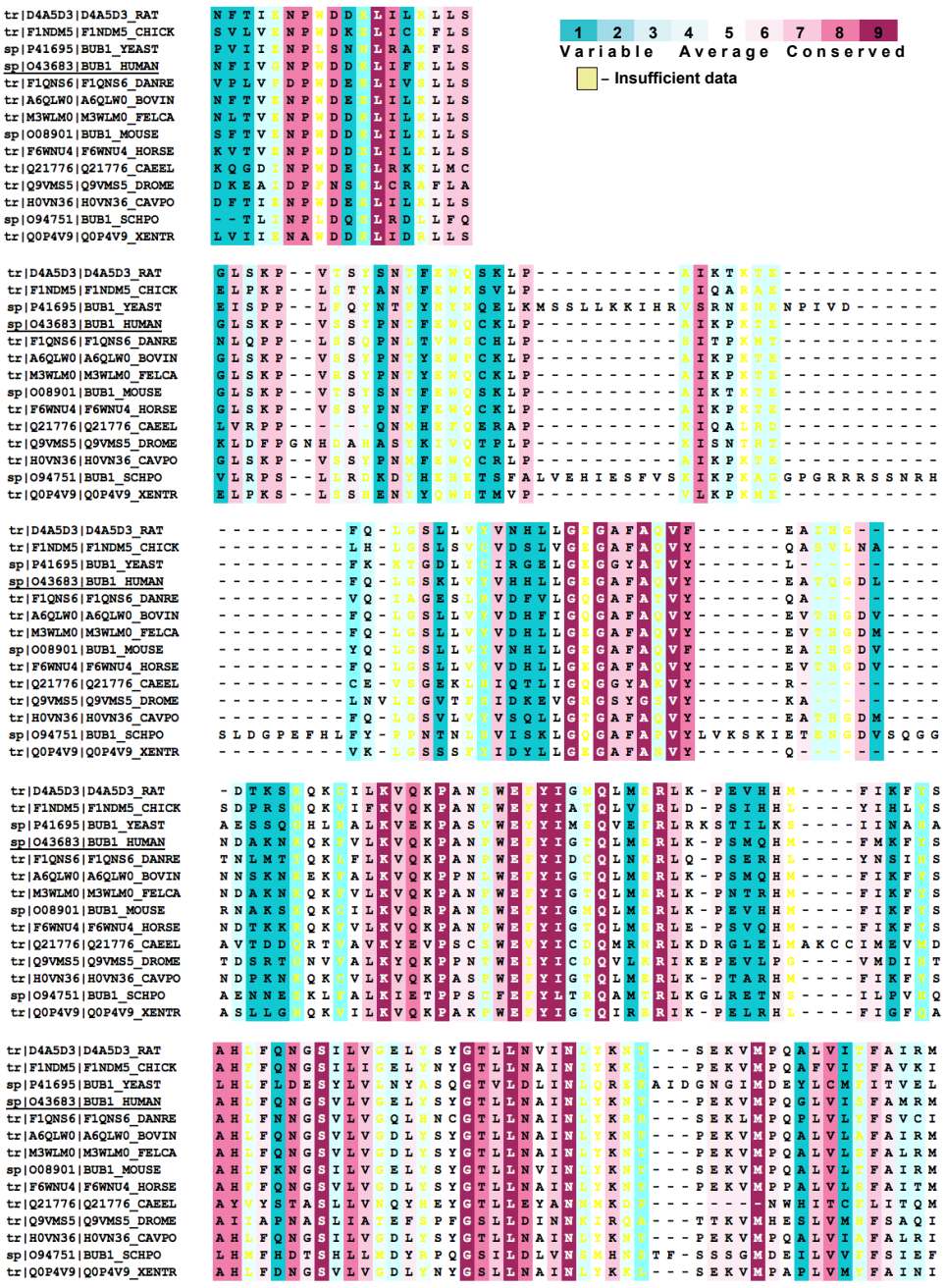
tr|D4A5D3|D4A5D3_RAT
tr|F1NDM5|F1NDM5_CHICK
sp|P41695|BUB1_YEAST
sp|O43683|BUB1_HUMAN
tr|F1QNS6|F1QNS6_DANRE
tr|A6QLW0|A6QLW0_BOVIN
tr|M3WLM0|M3WLM0_FELCA
sp|O08901|BUB1_MOUSE
tr|F6WNU4|F6WNU4_HORSE
tr|Q21776|Q21776_CAEEL
tr|Q9VMS5|Q9VMS5_DROME
tr|H0VN36|H0VN36_CAVPO
sp|O94751|BUB1_SCHPO
tr|Q0P4V9|Q0P4V9_XENTR
1 2 3 4 5 6 7 8 9
Variable Average Conserved
– Insufficient data

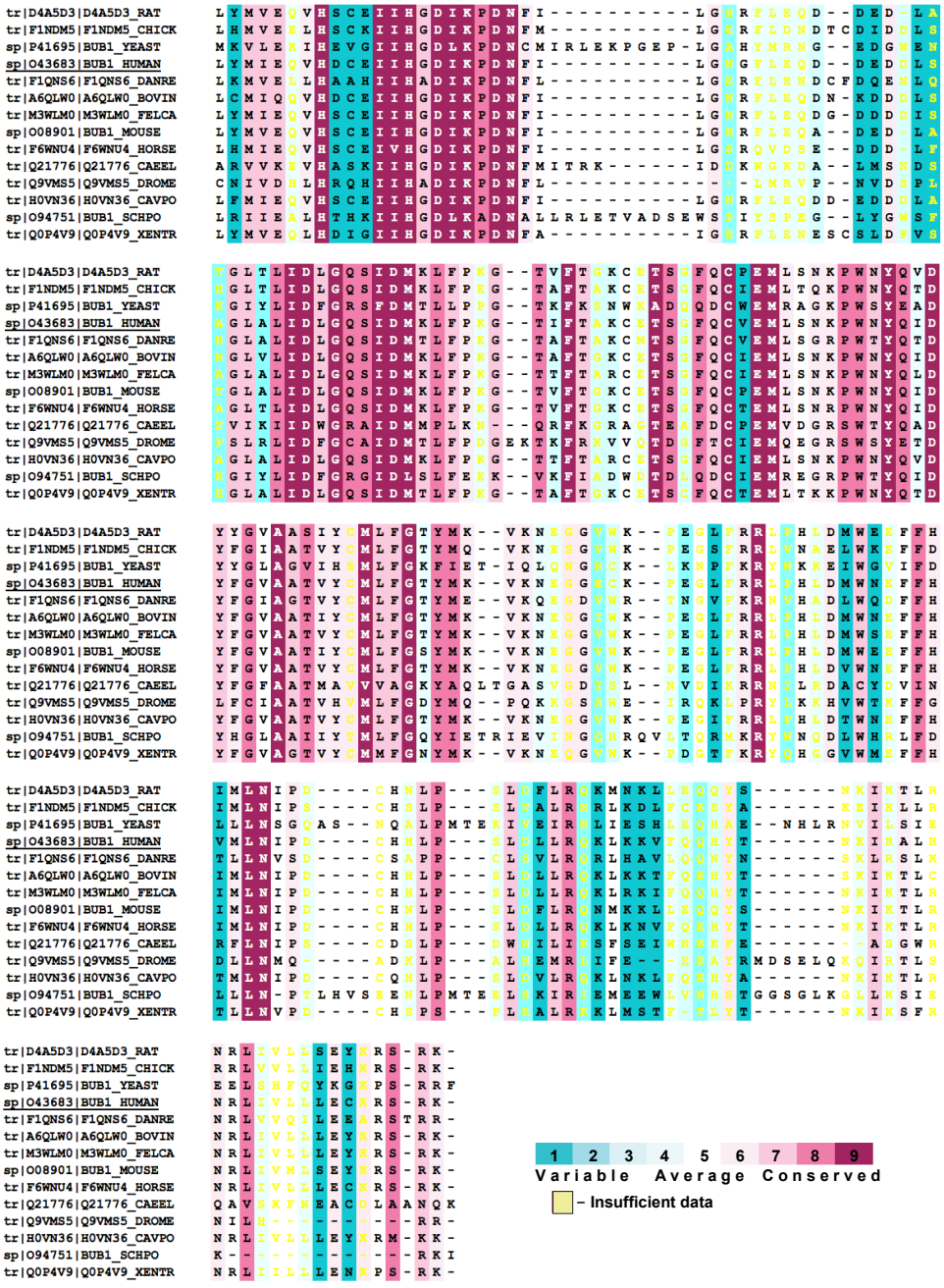

Figure 6.10: Alignment of Bub1 kinase domains from 12 organisms ranging from yeast to human.
The sequence alignment was produced by the MUSCLE server [241] and analysed for conservation using the ConSurf tool [242]. The conservation score is indicated in colours ranging from blue (variable) to magenta (conserved). Conservation scores are considered to be unreliable if they were obtained for positions in the alignment that had less than 6 un-gapped amino acids or if the computed confidence intervals for the rate of a specific position spans 4 or more colour grades. Such positions are colored light yellow in the graphic visualisation output.

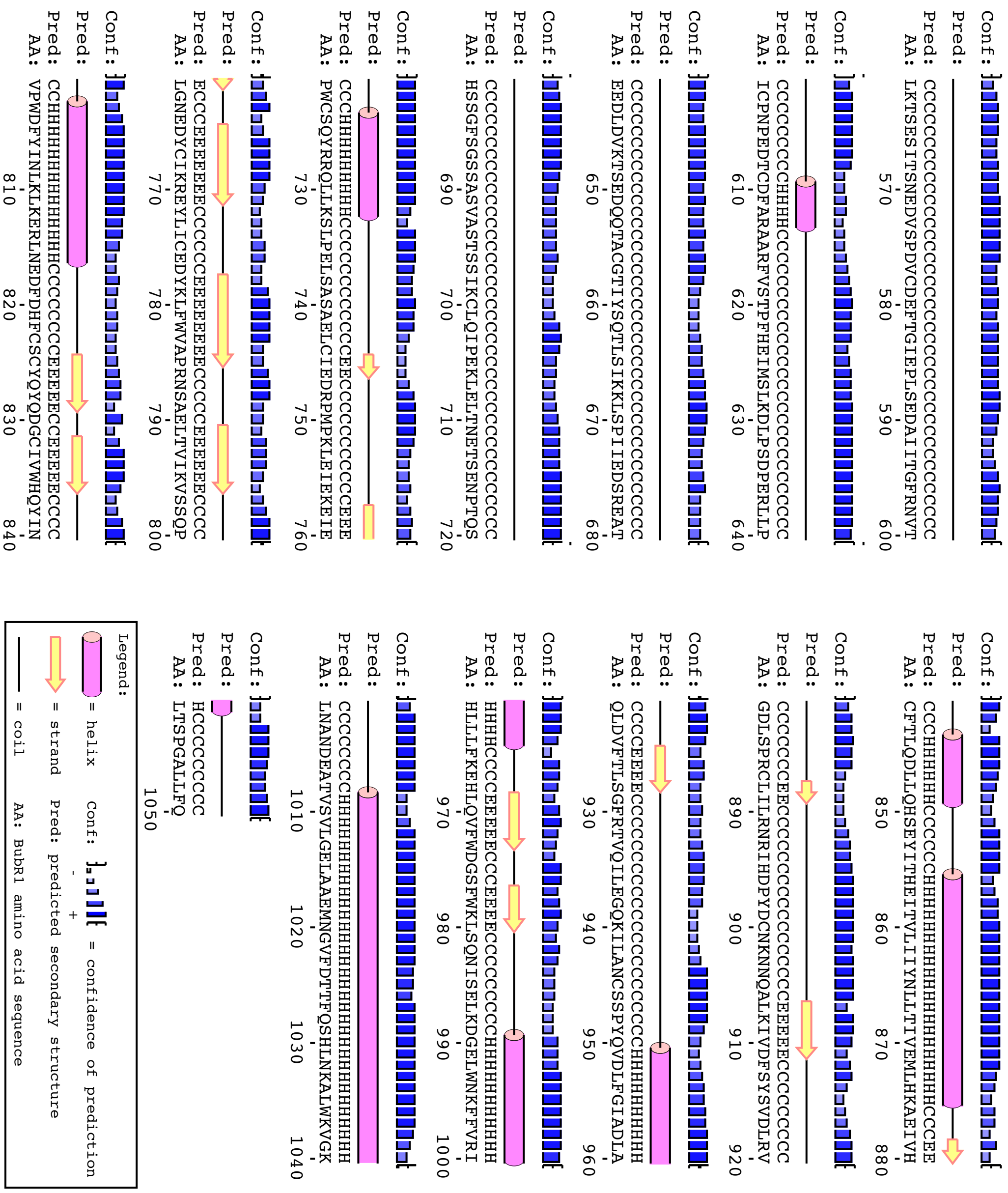

Figure 6.11: Secondary structure prediction of BubR1$^{543-1050}$ by PSIPRED ([244]).
Only residues 561-1050 are shown, a legend is indicated in the figure.

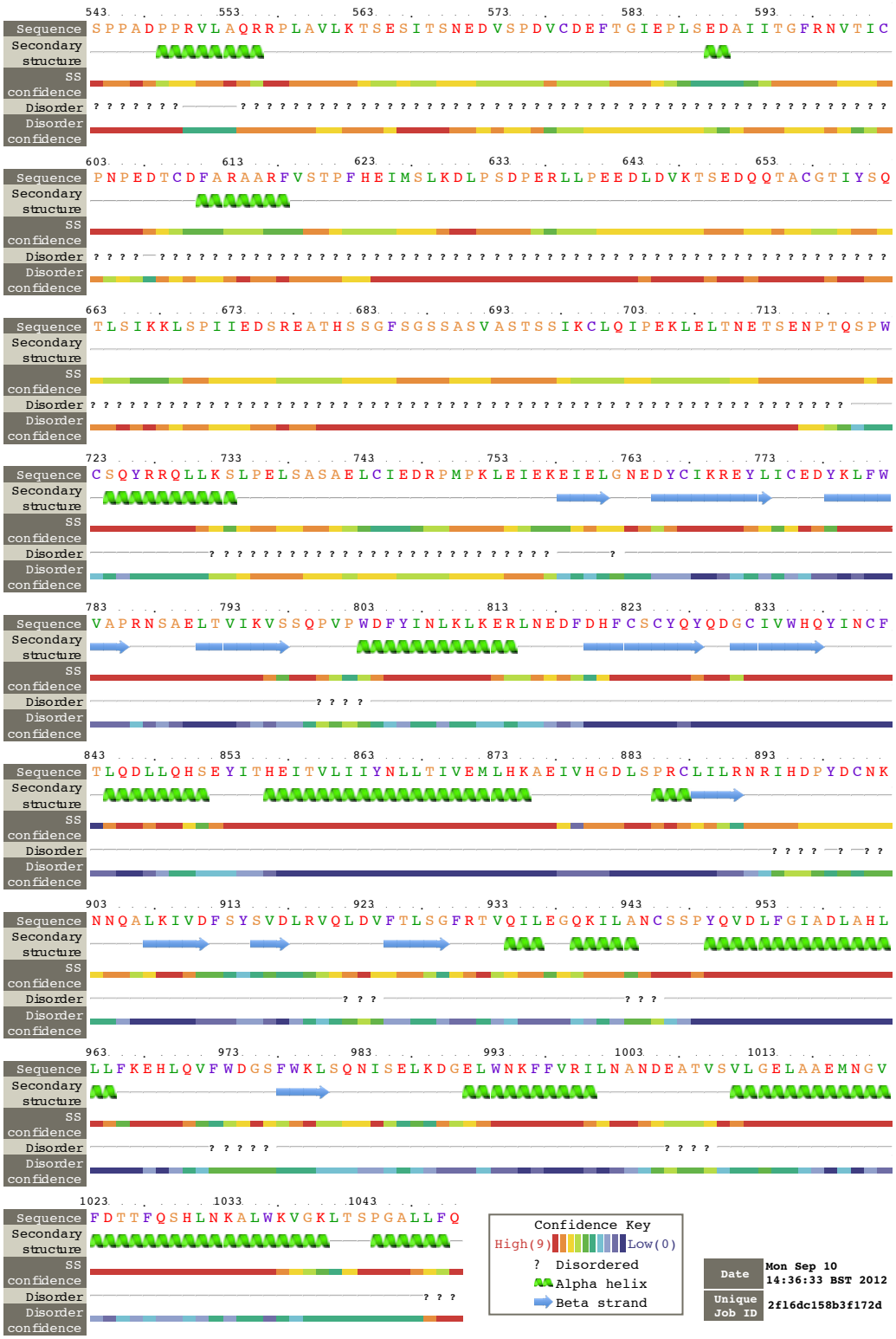

Figure 6.12: Secondary structure prediction of BubR1$^{543-1050}$ by Phyre2 ([243])
A legend is indicated in the figure.

Table 6.2: DNA oligonucleotides used for the preparation of this manuscript.

TARGET	NAME	DESCRIPTION	SEQUENCE (5'-3')
BubR1	CB019	BR1Trc2BamHIf	GATCATGGATCCAGTCCTCCTGCAGATCCCCCACGAG
BubR1	CB022	BR1SalIrev	GATCAT GTCGAC TTATCACTGAAAGAGCAAAGCCCC
BubR1	CB023	BR1 S697	GATCATGGATCCTCCATGAAATGTCTTCAAATTCCTGAGAAAC
BubR1	CB024	BR1 E705	GATCATGGATCCGAGAAACTAAGAACTTACTAATGAGACTTC
BubR1	CB025	BR1S697C700S	GATCATGGATCCTCCATGAAATCTCTTCAAATTCCTGAGAAAC
BubR1	CB027	BR1S697C700S*	GATCATGGATCCTCCATCAAATCTCTTCAAATTCCTGAGAAAC
BubR1	CB028	BR1 Trc3 E705*	GATCATGGATCCGAGAAACTAGAACTTACTAATGAGACTTC
Bub1	CB029	Qc_Bub1FL_f	CCTGATATTTCTGATGACAAAGATGAATGGC
Bub1	CB030	Qc_Bub1FL_r	GCCATTCATCTTTGTCATCAGAAATATCAGG
Bub1	CB037	Bub1_d189fwd	GATCATGGATCCGGTTCAGAGCTTTCTGGAGTGATATCTTCAGC
Bub1	CB038	Bub1_d189rev	GATCATGTCGACTTATTTTCGTGAACGCTTACATTCTAAGAGCAGTAC
Bub3	CB039	Bub3QCfix	GCTATGCATCAGCTGCTAGCTCAAGTACATGGTGACTTGGG
Bub3	CB040	Bub3QCfix	CCCAAGTCACCATGTACTTGAGCTAGCAGCTGATGCATAGC
Bub3	CB041	Bub3NheIrev	GATCATGCTAGCTCAAGTACATGGTGACTTGGGTTTTGTTTCTGC
Bub3	CB042	Bub3QCfix2f	GGTGACTTGGGTTTTGTTTCTGCATCTGTCACTTGGCG
Bub3	CB043	Bub3QCfix2r	CGCCAAGTGACAGATGCAGAAACAAAACCCAAGTCACC
Bub1	CB044	Bub1D917Nf	GACTGTGAAATCATTCATGGAAACATTAAACCAGACAATTTC
Bub1	CB045	Bub1D917Nr	GAA ATT GTC TGG TTT AAT GTT TCC ATG AAT GAT TTC ACA GTC
BubR1	CB046	BR1 E712	GATCATGGATCCGAGACTTCAGAAAACCCTACTCAG
BubR1	CB047	BR1 T718	GATCATGGATCCACTCAGTCACCATGGTGTTCACAG
BubR1	CB048	BR1 S724	GATCATGGATCCTCACAGTATCGCAGACAGCTACTG
BubR1	CB049	BR1 REVΔC7	ATCATGGTCGACTTATCAACTAGTTAACTTCCCTACC
Bub1	CB050	B1mutAut1F	GCTGATTTTCAAACTTTTAGCTGGGCTTTCTAAACCAGTGAGTTCC
Bub1	CB051	B1mutAut1R	GGAACTCACTGGTTTAGAAAGCCCAGCTAAAAGTTTGAAAATCAGC
Bub1	CB054	B1S969Afwd	CAGCAAAGTGTGAAACAGCTGGTTTTCAGTGTGTTGAG
Bub1	CB055	B1S969Arev	CTCAACACACTGAAAACCAGCTGTTTCACACTTTGCTG
Bub1	CB056	B1S955Afwd	GCTGATTTTCAAACTTTTAGCTGGGCTTGCTAAACCAGTGAGTTCC
Bub1	CB057	B1S955Arev	GGAACTCACTGGTTTAGCAAGCCCAGCTAAAAGTTTGAAAATCAGC
Bub1	CB058	Bub1BamQCf	CTGTTCCAGGGGCCCATGGGATCCATGGACACCC
Bub1	CB059	Bub1BamQCr	GGGTGTCCATGGATCCCATGGGCCCCTGGAACAG
H2A	CB060	H2ACtopMALf	TGGCTGATGAGAATCTTTATTTTCAGTGCCATCAGTCCGTGCTGCTGCCC
H2A	CB061	H2ACtopMALr	CTGGGATTTAGGTGACACTATAGAATACTCAAGCTTTCACTTGCTCTTG GCCGACTTG
H2A	CB062	H2ACtopGEXf	GGAAGTTCTGTTCCAGGGGCCCCAGTCCGTGCTGCTGCCC
H2A	CB063	H2ACtopGEXr	GCTCAGATCTATCTCCTTCTTAAAGTTAAACAAAATTATTACTAGTGTTCACTTGCTCTTGGCCGACTTG
H2A	CB064	H2AVLLDNNqc	GGGCGGGGTCCTGCCCAACATCCAGTCCGACAACAACCCCAAGAAAACCGAGAGTTCCAAGTCGGCC
B1/H2A	CB065	B1C3GS_H2Acf	GGGCCCTACGTAATAGGCTAATTGTACTGCTCTTAGAAGGTTCCGGTTCAGGTTCCCAGTCCGTGCTGCTGCCC
B1/H2A	CB066	B1CH2Acr	TGGTACCGCATGCCTCGAGTTATCACTTGCTCTTGGCCGACTTG
B1/H2A	CB067	B1C4GS_H2Acf	GGGCCCTACGTAATAGGCTAATTGTACTGCTCTTAGAAGGTTCCGGTTCTGGTTCAGGTTCCCAGTCCGTGCTGCTGCCC
H2A	CB068	H2AT121-Ala	CATC CAGTC CGTGCTGCTG CCCAAGAAAG CCGAGAGTTC CAAGTCGGCC AAGAGCAAGT GA
Bub1	CB069	B1CS969E	CAGCAAAGTGTGAAACAGAAGGTTTTCAGTGTGTTGAG
H2A	CB070	H2AcVLLDNN1	GGAAGTTCTGTTCCAGGGGCCCCAGTCCACAACAACCCCAAGAAAACCGAG AGTTCCAAGTCGGCC
H2A	CB071	H2AcVLLDNN2	GGAAGTTCTGTTCCAGGGGCCCCAGTCCGACAACAACCCCAAGAAAACCGAGAGTTCCAAGTCGGCC
Bub1	CB072	B1CS969D	CAGCAAAGTGTGAAACAGACGGTTTTCAGTGTGTTGAG
Bub1	CB073	Bub1KEN1AAA	GCTTTTCATGTGTTTGAAGATGGAAACGCAGCAGCTTATGGATTACCACAG CCTAAAAATAAACCC
Bub1	CB074	Bub1KEN2AAA	GGAGTCAGTGCACATTTTAGAAGATGCAGCAGCTGTGGTAGCAAAACAGT GTACCCAGGCG
Bub1	CB075	Bub1C740pFHf	CGACCGAAAACCTGTATTTTCAGGGCAACCCATGGGATGATAAGCTGATTT TCAA
Bub1	CB076	Bub1C740pFHr	CGCGACTAGTGAGCTCGTCGACTTATTTTCGTGAACGCTTACATTCTAAGA GCAG
Bub1	CB077	Bub1PheboxAA	GTCAATAAGATCATCTCTTCTTTGTCATCTGCTGCTCATGTGGCTGAAGATG GAAACGCAGC
Bub1	CB078	Bub1FboxA	GTCAATAAGATCATCTCTTCTTTGTCATCTGCTGCTCATGTGGCTGAAGATGG AAACAAAG
Bub1	CB079	Bub1FboxA2	GATCATCTCTTCTTTGTCATCTGCTGCTCATGTGGCTGAAGATGGAAACAAA GAAAATTATGG

Table 6.3: Intermolecular cross-links of the MBP-Knl1$^{138-225}$-Bub1:Bub3-BubR1:Bub3-GST-Cdc20 complex observed in the presence of DSS.
Mz- mass to charge ratio. n_seen- number of fragment ion spectra assigned to the cross-link in entire dataset. TIC- fraction of total ion current of fragment ion spectrum assigned to cross-link. Note that the Cdc20 and Knl1$^{138-225}$ used for cross-linking were tagged with GST or MBP, which is omitted in the table.

Cross-linked peptides	Protein 1	Protein 2	Abs Pos1	Abs Pos2	Mz	z	Error [ppm]	n_ seen	TIC	lD-Score
KHEQWVNEDR-KLKEQR-a1-b3	Bub1	BubR1	292	430	570.553	4	-0.3	4	0.51	40.32
RKHEQWVNEDR-LKEQR-a2-b2	Bub1	BubR1	292	430	462.246	5	0.6	8	0.45	39.16
RLKTGHHHHHH-AVEALQGEKR-a3-b9	Knl1	BubR1	470	118	659.354	4	1.2	54	0.62	38.38
AVEALQGEKR-LKTGHHHHHH-a9-b2	BubR1	Knl1	118	470	620.328	4	0.9	319	0.69	38.36
VQSHQQASEEKK-YAFKCHR-a11-b4	BubR1	Bub3	397	222	630.064	4	0.8	34	0.5	38.23
KLHQVVETSHEDLPASQER-LKEIQTTQQER-a1-b2	Bub1	BubR1	327	459	929.234	4	0.6	23	0.46	37.63
RKHEQWVNEDR-KLKEQR-a2-b3	Bub1	BubR1	292	430	487.865	5	0.2	5	0.53	35.55
KLHQVVETSHEDLPASQER-KLKEIQTTQQER-a1-b3	Bub1	BubR1	327	459	961.259	4	1.8	13	0.41	34.22
KLHQVVETSHEDLPASQER-KLKEIQTTQQER-a1-b1	Bub1	BubR1	327	457	769.208	5	1.6	6	0.44	34.09
LKTGHHHHHH-STLAELKSK-a2-b7	Knl1	BubR1	470	236	471.656	5	-0.3	8	0.6	33.26
AVEALQGEKR-KYHNDPR-a9-b1	BubR1	Bub1	118	89	434.232	5	0.5	1	0.41	33.2
HYMKR-LKEQR-a4-b2	Bub1	BubR1	305	430	386.965	4	-1.6	1	0.4	32.84
VQSHQQASEEKK-KYAFKCHR-a11-b5	BubR1	Bub3	397	222	662.087	4	0.1	4	0.4	32.66
KEANAFEEQLLK-EAELLTSAEKR-a1-b10	Bub1	BubR1	307	443	935.162	3	-0.7	9	0.57	32.57
LKTGHHHHHH-RESSLKYQTR-a2-b6	Knl1	Bub3	470	179	529.877	5	-0.4	3	0.27	32.46
LKTGHHHHHH-ESSLKYQTR-a2-b5	Knl1	Bub3	470	179	623.07	4	0.5	5	0.31	32.08
EANAFEEQLLKQK-EAELLTSAEKR-a11-b10	Bub1	BubR1	318	443	977.849	3	-0.2	3	0.38	31.63
VGGALKAPSQNR-RLKTGHHHHHH-a6-b3	BubR1	Knl1	255	470	547.096	5	-0.3	5	0.38	31.52
VDVEQVVMYCKEK-RESSLKYQTR-a11-b6	Bub1	Bub3	267	179	758.637	4	0.4	2	0.6	31.3
KYHNDPR-YAFKCHR-a1-b4	Bub1	Bub3	89	222	410.405	5	0.3	1	0.46	31.23
VQSHQQASEEKK-RESSLKYQTR-a11-b6	BubR1	Bub3	397	179	701.615	4	1.4	4	0.46	31.21
ESSLKYQTR-MMYCKEK-a5-b5	Bub3	BubR1	179	405	746.693	3	1.5	6	0.3	31.17
VAVEYLDPSPEVQKK-AVEALQGEKR-a14-b9	Bub3	BubR1	216	118	735.649	4	0.4	1	0.39	31.05
VQSHQQASEEKK-ESSLKYQTR-a11-b5	BubR1	Bub3	397	179	662.59	4	1.3	11	0.23	30.99
RKEANAFEEQLLK-EAELLTSAEKR-a2-b10	Bub1	BubR1	307	443	592.721	5	-0.7	4	0.42	30.88

Table 6.3 continued

VITISKSEYSVHSSLASK-YAFKCHR-a6-b4	Bub1	Bub3	244	222	764.397	4	-2.3	5	0.36	30.48
KLHQVVETSHEDLPASQER-TGDQQEETMPTKETTK-a1-b12	Bub1	BubR1	327	480	833.608	5	1.2	4	0.49	30.3
ESSLKYQTR-EKLIR-a5-b2	Bub3	Bub1	179	269	636.358	3	-1.3	1	0.23	29.88
AFPNKQGYVLSSIEGR-VGGALKAPSQNR-a5-b6	Bub3	BubR1	191	255	1034.225	3	1.2	1	0.46	29.54
KEANAFEEQLLKQK-EAELLTSAEKR-a12-b10	Bub1	BubR1	318	443	1020.547	3	-0.2	7	0.37	29.52
VGGALKAPSQNR-LKTGHHHHHH-a6-b2	BubR1	Knl1	255	470	515.876	5	-1.4	16	0.23	29.28
VITISKSEYSVHSSLASK-ESSLKYQTR-a6-b5	Bub1	Bub3	244	179	796.925	4	1	3	0.28	29.22
VDVEQVVMYCKEK-ESSLKYQTR-a11-b5	Bub1	Bub3	267	179	959.145	3	-1	2	0.44	28.63
RLKTGHHHHHH-QVTDAETKPK-a3-b8	Knl1	Bub3	470	322	530.882	5	2.5	2	0.31	28.52
VGGALKAPSQNR-RESSLKYQTR-a6-b6	BubR1	Bub3	255	179	651.358	4	1.2	4	0.26	27.85
VITISKSEYSVHSSLASK-VAVEYLDPSPEVQKK-a6-b14	Bub1	Bub3	244	216	944.508	4	0.4	2	0.68	27.68
AKENELQAGPWNTGR-ESSLKYQTR-a2-b5	BubR1	Bub3	309	179	973.825	3	0.1	2	0.37	27.55
AKENELQAGPWNTGR-LKTGHHHHHH-a2-b2	BubR1	Knl1	309	470	762.884	4	1.8	2	0.4	27.54
KLHQVVETSHEDLPASQER-ETTKLQIASESQK-a1-b4	Bub1	BubR1	327	484	951.493	4	0.6	2	0.29	26.39
RESSLKYQTR-KYHNDPR-a6-b1	Bub3	Bub1	179	89	467.647	5	2.8	1	0.32	26.24
VGGALKAPSQNR-QVTDAETKPK-a6-b8	BubR1	Bub3	255	322	817.78	3	1.6	6	0.38	25.88
IDTTSFLANLKLHTEDSR-VGGALKAPSQNR-a11-b6	Knl1	BubR1	434	255	849.702	4	-1.8	5	0.31	25.85
LKYQHTGAVLDCAFYDPTHAW SGGLDHQLK-KHEQWVNEDR-a2-b1	Bub3	Bub1	52	292	701.77	7	0.3	4	0.38	25.58
VAVEYLDPSPEVQKK-VGGALKAPSQNR-a14-b6	Bub3	BubR1	216	255	759.916	4	0.8	1	0.49	25.52
LKTGHHHHHH-QVTDAETKPK-a2-b8	Knl1	Bub3	470	322	499.661	5	1.8	7	0.24	25.29
MMYCKEK-EKLIR-a5-b2	BubR1	Bub1	405	269	446.983	4	-1.2	2	0.26	25.08
LKYQHTGAVLDCAFYDPTHAW SGGLDHQLK-EAELLTSAEKR-a2-b10	Bub3	BubR1	52	443	963.279	5	-1.9	5	0.37	25.08
VGGALKAPSQNR-YAFKCHR-a6-b4	BubR1	Bub3	255	222	579.805	4	-2.3	1	0.3	24.74
TPCNAGTFSQPEKVYTLSVSGDR-AQKYNQR-a13-b3	Bub3	Bub1	139	286	890.436	4	-1.8	2	0.34	24.72

Table 6.3 continued

TPCNAGTFSQPEKVYTLSVSGDR-RKHEQWVNEDR-a13-b2	Bub3	Bub1	139	292	830.404	5	0.2	1	0.34	24.68
ENQPENSQTPTKK-AQKYNQR-a12-b3	Cdc20	Bub1	340	286	509.86	5	1.1	2	0.32	24.06
TPCNAGTFSQPEKVYTLSVSGDR-KHEQWVNEDR-a13-b1	Bub3	Bub1	139	292	998.726	4	-2	2	0.28	23.64
QVTDAETKPKSPCT-VGGALKAPSQNR-a10-b6	Bub3	BubR1	324	255	724.877	4	0.5	1	0.33	22.92
VAVEYLDPSPEVQKK-KYHNDPR-a14-b1	Bub3	Bub1	216	89	692.863	4	0.6	2	0.35	22.4
VQSHQQASEEKKEK-YAFKCHR-a11-b4	BubR1	Bub3	397	222	555.68	5	0.5	2	0.27	22.3
RVITISKSEYSVHSSLASK-VAVEYLDPSPEVQKK-a7-b14	Bub1	Bub3	244	216	787.027	5	-0.2	3	0.46	22.23
LKYQHTGAVLDCAFYDPTHAW SGGLDHQLK-KEANAFEEQLLK-a2-b1	Bub3	Bub1	52	307	997.899	5	1	4	0.26	22.15
VQTTPSKPGGDR-YAFKCHRLK-a7-b4	Cdc20	Bub3	304	222	521.275	5	-4	1	0.18	20.53

Table 6.4: Intramolecular cross-links of the MBP-Knl1$^{138-225}$-Bub1:Bub3-BubR1:Bub3-GST-Cdc20 complex observed in the presence of DSS.
Mz- mass to charge ratio. n_seen- number of fragment ion spectra assigned to the cross-link in entire dataset. TIC- fraction of total ion current of fragment ion spectrum assigned to cross-link. Note that the Cdc20 and Knl1$^{138-225}$ used for cross-linking were tagged with GST or MBP, which is omitted in the table.

Cross-linked peptides	**Protein 1**	**Protein 2**	**Abs Pos1**	**Abs Pos2**	**Mz**	**z**	**Error [ppm]**	**n_ seen**	**TIC**	**lD-Score**
IAYSKDFETLK-IKGLVQPTR-a5-b2	Cdc20	Cdc20	113	11	616.602	4	-0.1	2	0.61	41.05
VTVEHPDKLEEK-LKTGHHHHHH-a8-b2	Knl1	Knl1	43	470	561.091	5	-0.4	57	0.54	40.68
RKHEQWVNEDR-AQKYNQR-a2-b3	Bub1	Bub1	292	286	509.06	5	-0.3	3	0.54	40.06
KHEQWVNEDR-AQKYNQR-a1-b3	Bub1	Bub1	292	286	597.047	4	-1.6	8	0.52	39.99
KADAIFQEGIQQK-VGGALKAPSQNR-a1-b6	BubR1	BubR1	175	255	937.512	3	1.3	14	0.52	39.96
AKENELQAGPWNTGR-AVEALQGEKR-a2-b9	BubR1	BubR1	309	118	727.879	4	0.4	6	0.53	39.13
AVEALQGEKR-STLAELKSK-a9-b7	BubR1	BubR1	118	236	738.75	3	0.3	6	0.65	39.1
VGGALKAPSQNR-STLAELKSK-a6-b7	BubR1	BubR1	255	236	771.104	3	-0.3	6	0.5	38.47
GYNGLAEVGKK-FEKDTGIK-a10-b3	Knl1	Knl1	26	30	553.299	4	0.9	22	0.69	38.25
KRIEAIPQIDK-YLKSSK-a1-b3	Cdc20	Cdc20	181	194	544.071	4	0	5	0.54	38.15
VQSHQQASEEKK-MMYCKEK-a11-b5	BubR1	BubR1	397	405	505.843	5	0	12	0.64	37.92
VGGALKAPSQNR-AVEALQGEKR-a6-b9	BubR1	BubR1	255	118	812.453	3	2.1	7	0.51	37.47
KLHQVVETSHEDLPASQER-KHEQWVNEDR-a1-b1	Bub1	Bub1	327	292	920.959	4	2.4	5	0.43	37.45

Table 6.4 continued

KFEKDTGIK-MKIEEGK-a4-b2	Knl1	Knl1	30	2	510.029	4	-0.8	4	0.54	37.42
KADAIFQEGIQQK-SKGKK-a1-b2	BubR1	BubR1	175	238	720.74	3	1.3	4	0.57	36.17
LKEIQTTQQER-KLKEQR-a2-b1	BubR1	BubR1	459	428	463.265	5	-0.3	4	0.25	35.77
RESSLKYQTR-KYAFK-a6-b1	Bub3	Bub3	179	218	516.034	4	-1.3	8	0.43	35.38
KEANAFEEQLLK-KHEQWVNEDR-a1-b1	Bub1	Bub1	307	292	725.117	4	0.2	3	0.46	35.36
VTVEHPDKLEEK-RLKTGHHHHHH-a8-b3	Knl1	Knl1	43	470	592.31	5	-2.2	15	0.48	35.29
RESSLKYQTR-YAFKCHR-a6-b4	Bub3	Bub3	179	222	597.308	4	-0.4	16	0.64	34.82
KLHQVVETSHEDLPASQER-RKHEQWVNEDR-a1-b2	Bub1	Bub1	327	292	640.324	6	-0.6	6	0.45	34.78
ESSLKYQTR-YAFKCHR-a5-b4	Bub3	Bub3	179	222	558.283	4	0.2	32	0.29	34.49
LKTGHHHHHH-IDFNDFIKR-a2-b8	Knl1	Knl1	470	467	509.866	5	1.4	6	0.63	34.48
ESSLKYQTR-KYAFK-a5-b1	Bub3	Bub3	179	218	477.009	4	-0.3	7	0.36	34.43
AKENELQAGPWNTGR-EAELLTSAEKR-a2-b10	BubR1	BubR1	309	443	1018.858	3	3	2	0.44	34.03
KLHQVVETSHEDLPASQER-AQKYNQR-a1-b3	Bub1	Bub1	327	286	812.668	4	0.8	9	0.4	33.89
ESSLKYQTR-KYAFKCHR-a5-b5	Bub3	Bub3	179	222	590.307	4	0.8	9	0.35	33.88
KLHQVVETSHEDLPASQER-HYMKR-a1-b4	Bub1	Bub1	327	305	615.717	5	1.5	8	0.52	33.69
KLKEIQTTQQER-LKEQR-a3-b2	BubR1	BubR1	459	430	578.83	4	0.6	3	0.28	33.6
LSGKPQNAPEGYQNR-LKVLYSQK-a4-b2	Cdc20	Cdc20	367	380	694.377	4	0.4	4	0.49	33.55
KADAIFQEGIQQK-STLAELKSK-a1-b7	BubR1	BubR1	175	236	863.81	3	0.4	3	0.43	33.5
KEANAFEEQLLK-AQKYNQR-a1-b3	Bub1	Bub1	307	286	822.1	3	0.2	5	0.28	33.34
VDFLSKLPEMLK-IKGLVQPTR-a6-b2	Cdc20	Cdc20	125	11	642.877	4	-0.1	4	0.54	33.33
VGGALKAPSQNR-LKEQR-a6-b2	BubR1	BubR1	255	430	502.789	4	1.1	4	0.36	33.06
LKEIQTTQQER-LKEQR-a2-b2	BubR1	BubR1	459	430	546.805	4	-1.3	3	0.29	32.97
ETTKLQIASESQK-LKEIQTTQQER-a4-b2	BubR1	BubR1	484	459	744.15	4	0.8	1	0.35	32.95
KLKEIQTTQQER-VGGALKAPSQNR-a3-b6	BubR1	BubR1	459	255	709.897	4	0.6	1	0.44	32.78
DFETLKVDFLSK-IKGLVQPTR-a6-b2	Cdc20	Cdc20	119	11	648.368	4	-0.6	3	0.6	32.64
GPSVPFSIFDEFLLSEKK-NKSPPADPPR-a17-b2	BubR1	BubR1	544	547	814.681	4	1.8	22	0.48	32.57
ETTKLQIASESQK-KLKEIQTTQQER-a4-b1	BubR1	BubR1	484	457	776.172	4	-1.9	1	0.35	32.46
IDTTSFLANLKLHTEDSR-LKTGHHHHHH-a11-b2	Knl1	Knl1	434	470	688.554	5	-0.3	8	0.49	32.37
ETTKLQIASESQK-KLKEIQTTQQER-a4-b3	BubR1	BubR1	484	459	776.172	4	-1.2	3	0.36	32.15

Table 6.4 continued

VDFLSKLPEMLK-IAYSKDFETLK-a6-b5	Cdc20	Cdc20	125	113	718.643	4	0.7	2	0.53	32.08
RESSLKYQTR-KYAFKCHR-a6-b5	Bub3	Bub3	179	222	629.331	4	-2.1	5	0.61	31.87
TGDQQEETMPTKETTK-LKEIQTTQQER-a12-b2	BubR1	BubR1	480	459	834.415	4	0.8	2	0.38	31.86
AEMQKQIEEMEK-KLKEIQTTQQER-a5-b3	BubR1	BubR1	449	459	783.904	4	0.4	4	0.49	31.83
EAELLTSAEKR-KLKEQR-a10-b3	BubR1	BubR1	443	430	729.078	3	0	8	0.54	31.79
VGGALKAPSQNR-EAELLTSAEKR-a6-b10	BubR1	BubR1	255	443	861.137	3	0.5	3	0.38	31.78
EKLIRGESEFSFEELR-AQKYNQR-a2-b3	Bub1	Bub1	269	286	603.514	5	0.1	5	0.43	31.57
RAEMQKQIEEMEK-KLKEIQTTQQER-a6-b3	BubR1	BubR1	449	459	822.929	4	-0.1	5	0.37	31.5
AKENELQAGPWNTGR-VGGALKAPSQNR-a2-b6	BubR1	BubR1	309	255	1002.523	3	-0.7	4	0.47	31.33
LVIWINGDKGYNGLAEVGK-DKPLGAVALK-a9-b2	Knl1	Knl1	16	298	799.453	4	1.5	2	0.54	31.32
DTGIKVTVEHPDKLEEK-GYNGLAEVGKK-a5-b10	Knl1	Knl1	35	26	1070.903	3	0.9	4	0.32	31.1
LKTGHHHHHH-YENGKYDIK-a2-b5	Knl1	Knl1	470	176	502.252	5	-0.9	10	0.24	30.99
KEANAFEEQLLK-HYMKR-a1-b4	Bub1	Bub1	307	305	764.401	3	0.4	5	0.36	30.94
AEMQKQIEEMEK-EAELLTSAEKR-a5-b10	BubR1	BubR1	449	443	720.112	4	0.1	8	0.59	30.86
TGDQQEETMPTKETTK-KLKEIQTTQQER-a12-b3	BubR1	BubR1	480	459	693.351	5	-1.5	5	0.35	30.79
FVSTPFHEIMSLKDLPSDPER-KLSPIIEDSR-a13-b1	BubR1	BubR1	634	673	748.791	5	0.1	4	0.42	30.53
KLHQVVETSHEDLPASQER-KEANAFEEQLLK-a1-b1	Bub1	Bub1	327	307	940.736	4	-0.1	3	0.42	30.42
KHEQWVNEDR-EKLIR-a1-b2	Bub1	Bub1	292	269	428.03	5	0.3	5	0.31	30.14
EAELLTSAEKR-LKEQR-a10-b2	BubR1	BubR1	443	430	686.38	3	-0.1	4	0.42	30.11
LSGKPQNAPEGYQNR-VAELKGHTSR-a4-b5	Cdc20	Cdc20	367	671	724.13	4	2.1	2	0.46	29.75
KYHNDPR-EFLDKK-a1-b5	Bub1	Bub1	89	87	369.996	5	-1.3	4	0.36	29.66
LKEIQTTQQER-QIEEMEKK-a2-b7	BubR1	BubR1	459	456	849.112	3	0.4	5	0.33	29.08
KLHQVVETSHEDLPASQER-EKLIR-a1-b2	Bub1	Bub1	327	269	500.606	6	0.2	2	0.38	29.03
EAELLTSAEKR-LKEIQTTQQER-a10-b2	BubR1	BubR1	443	459	690.121	4	-1.2	4	0.45	29
STLAELKSK-GKKTAR-a7-b3	BubR1	BubR1	236	241	592.02	3	0.4	1	0.44	28.59
DKPLGAVALKSYEEELAK-AFQDKLYPFTWDAVR-a10-b5	Knl1	Knl1	306	89	989.52	4	0.9	5	0.31	28.38
LSGKPQNAPEGYQNR-VLYSQKATPGSSR-a4-b6	Cdc20	Cdc20	367	386	798.163	4	0	5	0.47	28.23

Table 6.4 continued

VTVEHPDKLEEKFPQVAATGDGPDIIF WAHDR-MKIEEGK-a8-b2	Knl1	Knl1	43	2	765.724	6	0.2	2	0.37	28.09
AKENELQAGPWNTGR-KADAIFQEGIQQK-a2-b1	BubR1	BubR1	309	175	821.674	4	0.6	4	0.36	27.81
KLKEIQTTQQER-EAELLTSAEKR-a3-b10	BubR1	BubR1	459	443	962.525	3	0.4	2	0.36	27.78
TGDQQEETMPTKETTK-KLKEIQTTQQER-a12-b1	BubR1	BubR1	480	457	866.438	4	0.7	3	0.45	27.75
TGDQQEETMPTKETTK-EAELLTSAEKR-a12-b10	BubR1	BubR1	480	443	1069.857	3	-0.5	4	0.37	27.73
KLHQVVETSHEDLPASQER-RKEANAFEEQLLK-a1-b2	Bub1	Bub1	327	307	784.011	5	0.3	1	0.37	27.61
RKEANAFEEQLLK-QKMDELHK-a2-b2	Bub1	Bub1	307	320	549.093	5	1.3	2	0.42	27.1
YISWTEQNYPQGGKESNMSTLLER-VGGALKAPSQNR-a14-b6	BubR1	BubR1	99	255	1042.272	4	1.1	3	0.38	26.73
APCLPVTYQQTPVNMEKNPR-KLHQVVETSHEDLPASQER-a17-b1	Bub1	Bub1	381	327	937.472	5	-0.4	2	0.51	26.58
QTLLALEKEEEEEVFESSVPQR-VGGALKAPSQNR-a8-b6	BubR1	BubR1	215	255	1309.016	3	3.6	6	0.37	26.29
EANAFEEQLLKQK-MDELHKK-a11-b6	Bub1	Bub1	318	326	862.446	3	-2.5	3	0.34	26.03
VGGALKAPSQNR-VQSHQQASEEKK-a6-b11	BubR1	BubR1	255	397	684.114	4	2.2	2	0.35	25.85
RKHEQWVNEDR-EKLIR-a2-b2	Bub1	Bub1	292	269	459.251	5	0	2	0.19	25.72
KLHQVVETSHEDLPASQER-QKMDELHK-a1-b2	Bub1	Bub1	327	320	562.289	6	1.4	3	0.38	25.68
VTVEHPDKLEEKFPQVAATGDGPDIIF WAHDR-MKIEEGK-a12-b2	Knl1	Knl1	47	2	918.665	5	-1.8	2	0.32	25.63
RKEANAFEEQLLK-RKHEQWVNEDR-a2-b2	Bub1	Bub1	307	292	642.735	5	0	2	0.32	25.53
IMSTLQGALAQESACNNTLQQQKR-VGGALKAPSQNR-a23-b6	BubR1	BubR1	64	255	1007.022	4	0	2	0.43	25.4
RESSLKYQTR-KKYAFK-a6-b2	Bub3	Bub3	179	218	548.058	4	0.4	1	0.3	25.25
KADAIFQEGIQQKAEPLER-VGGALKAPSQNR-a13-b6	BubR1	BubR1	187	255	877.226	4	1.7	1	0.3	25.2
EKLIR-HYMKR-a2-b4	Bub1	Bub1	269	305	510.626	3	0.1	2	0.34	24.91
AFPNKQGYVLSSIEGR-VAVEYLDPSPEVQKK-a5-b14	Bub3	Bub3	191	216	901.98	4	1.4	2	0.42	24.84
EAELLTSAEKR-AVEALQGEKR-a10-b9	BubR1	BubR1	443	118	828.784	3	2.5	1	0.32	24.15
DKPLGAVALKSYEEELAKDPR-AFQDKLYPFTWDAVR-a18-b5	Knl1	Knl1	314	89	865.455	5	1.7	2	0.36	24

Table 6.4 continued

AFPNKQGYVLSSIEGR-QVTDAETKPK-a5-b8	Bub3	Bub3	191	322	1007.197	3	0	2	0.29	23.66
NKHMNADTDYSIAEAAFNK-TWEEIPALDKELK-a2-b10	Knl1	Knl1	203	138	962.973	4	0	3	0.53	23.38
QTLLALEKEEEEEVFESSVPQR-KADAIFQEGIQQK-a8-b1	BubR1	BubR1	215	175	1401.713	3	-3	6	0.32	23.14
TGDQQEETMPTKETTK-LKEQR-a12-b2	BubR1	BubR1	480	430	659.33	4	0.7	2	0.25	23.13
KHEQWVNEDR-QKMDELHK-a1-b2	Bub1	Bub1	292	320	627.309	4	-1.3	3	0.18	23.06
EAELLTSAEKRAEMQK-KLKEIQTTQQER-a10-b1	BubR1	BubR1	443	457	868.966	4	2.2	1	0.3	22.08
IDTTSFLANLKLHTEDSR-GLLDNPISEKSTK-a11-b10	Knl1	Knl1	434	420	900.728	4	2.6	1	0.48	22.06
RAEMQKQIEEMEK-KLKEQR-a6-b3	BubR1	BubR1	449	430	647.844	4	-0.2	1	0.22	21.84
KLHQVVETSHEDLPASQER-KYHNDPR-a1-b1	Bub1	Bub1	327	89	654.734	5	2.7	2	0.55	21.61
EFLENYLLTDEGLEAVNKDKPLGAVALK-SYEEELAKDPR-a20-b8	Knl1	Knl1	298	314	913.476	5	2.1	1	0.18	21.55
LSGKPQNAPEGYQNR-ENQPENSQTPTKK-a4-b12	Cdc20	Cdc20	367	340	824.911	4	1.3	4	0.47	21.52
AEMQKQIEEMEKK-EAELLTSAEKR-a5-b10	BubR1	BubR1	449	443	752.137	4	1.9	1	0.55	20.45
ITVFDENADEASTAELSKPTVQPWIAPPMPR-VGGALKAPSQNR-a18-b6	BubR1	BubR1	294	255	1187.115	4	2	4	0.3	20.13

Protein sequences

Bub1 (homo sapiens)

```
   1 MDTPENVLQM LEAHMQSYKG NDPLGEWERY IQWVEENFPE NKEYLITLLE 50
  51 HLMKEFLDKK KYHNDPRFIS YCLKFAEYNS DLHQFFEFLY NHGIGTLSSP 100
 101 LYIAWAGHLE AQGELQHASA VLQRGIQNQA EPREFLQQQY RLFQTRLTET 150
 151 HLPAQARTSE PLHNVQVLNQ MITSKSNPGN NMACISKNQG SELSGVISSA 200
 201 CDKESNMERR VITISKSEYS VHSSLASKVD VEQVVMYCKE KLIRGESEFS 250
 251 FEELRAQKYN QRRKHEQWVN EDRHYMKRKE ANAFEEQLLK QKMDELHKKL 300
 301 HQVVETSHED LPASQERSEV NPARMGPSVG SQQELRAPCL PVTYQQTPVN 350
 351 MEKNPREAPP VVPPLANAIS AALVSPATSQ SIAPPVPLKA QTVTDSMFAV 400
 401 ASKDAGCVNK STHEFKPQSG AEIKEGCETH KVANTSSFHT TPNTSLGMVQ 450
 451 ATPSKVQPSP TVHTKEALGF IMNMFQAPTL PDISDDKDEW QSLDQNEDAF 500
 501 EAQFQKNVRS SGAWGVNKII SSLSSAFHVF EDGNKENYGL PQPKNKPTGA 550
 551 RTFGERSVSR LPSKPKEEVP HAEEFLDDST VWGIRCNKTL APSPKSPGDF 600
 601 TSAAQLASTP FHKLPVESVH ILEDKENVVA KQCTQATLDS CEENMVVPSR 650
 651 DGKFSPIQEK SPKQALSSHM YSASLLRLSQ PAAGGVLTCE AELGVEACRL 700
 701 TDTDAAIAED PPDAIAGLQA EWMQMSSLGT VDAPNFIVGN PWDDKLIFKL 750
 751 LSGLSKPVSS YPNTFEWQCK LPAIKPKTEF QLGSKLVYVH HLLGEGAFAQ 800
 801 VYEATQGDLN DAKNKQKFVL KVQKPANPWE FYIGTQLMER LKPSMQHMFM 850
 851 KFYSAHLFQN GSVLVGELYS YGTLLNAINL YKNTPEKVMP QGLVISFAMR 900
 901 MLYMIEQVHD CEIIHGDIKP DNFILGNGFL EQDDEDDLSA GLALIDLGQS 950
 951 IDMKLFPKGT IFTAKCETSG FQCVEMLSNK PWNYQIDYFG VAATVYCMLF 1000
1001 GTYMKVKNEG GECKPEGLFR RLPHLDMWNE FFHVMLNIPD CHHLPSLDLL 1050
1051 RQKLKKVFQQ HYTNKIRALR NRLIVLLLEC KRSRK
```

Bub3 (homo sapiens)

```
   1 MTGSNEFKLN QPPEDGISSV KFSPNTSQFL LVSSWDTSVR LYDVPANSMR 50
  51 LKYQHTGAVL DCAFYDPTHA WSGGLDHQLK MHDLNTDQEN LVGTHDAPIR 100
 101 CVEYCPEVNV MVTGSWDQTV KLWDPRTPCN AGTFSQPEKV YTLSVSGDRL 150
 151 IVGTAGRRVL VWDLRNMGYV QQRRESSLKY QTRCIRAFPN KQGYVLSSIE 200
 201 GRVAVEYLDP SPEVQKKKYA FKCHRLKENN IEQIYPVNAI SFHNIHNTFA 250
 251 TGGSDGFVNI WDPFNKKRLC QFHRYPTSIA SLAFSNDGTT LAIASSYMYE 300
 301 MDDTEHPEDG IFIRQVTDAE TKPKSPCT
```

BubR1 (homo sapiens)

```
   1 MAAVKKEGGA LSEAMSLEGD EWELSKENVQ PLRQGRIMST LQGALAQESA 50
  51 CNNTLQQQKR AFEYEIRFYT GNDPLDVWDR YISWTEQNYP QGGKESNMST 100
 101 LLERAVEALQ GEKRYYSDPR FLNLWLKLGR LCNEPLDMYS YLHNQGIGVS 150
 151 LAQFYISWAE EYEARENFRK ADAIFQEGIQ QKAEPLERLQ SQHRQFQARV 200
 201 SRQTLLALEK EEEEEVFESS VPQRSTLAEL KSKGKKTARA PIIRVGGALK 250
 251 APSQNRGLQN PFPQQMQNNS RITVFDENAD EASTAELSKP TVQPWIAPPM 300
 301 PRAKENELQA GPWNTGRSLE HRPRGNTASL IAVPAVLPSF TPYVEETAQQ 350
 351 PVMTPCKIEP SINHILSTRK PGKEEGDSLQ RVQSHQQASE EKKEKMMYCK 400
 401 EKIYAGVGEF SFEEIRAEVF RKKLKEQREA ELLTSAEKRA EMQKQIEEME 450
 451 KKLKEIQTTQ QERTGDQQEE TMPTKETTKL QIASESQKIP GMTLSSSVCQ 500
 501 VNCCARETSL AENIWQEQPH SKGPSVPFSI FDEFLLSEKK NKSPPADPPR 550
 551 VLAQRRPLAV LKTSESITSN EDVSPDVCDE FTGIEPLSED AIITGFRNVT 600
 601 ICPNPEDTCD FARAARFVST PFHEIMSLKD LPSDPERLLP EEDLDVKTSE 650
 651 DQQTACGTIY SQTLSIKKLS PIIEDSREAT HSSGFSGSSA SVASTSSIKC 700
 701 LQIPEKLELT NETSENPTQS PWCSQYRRQL LKSLPELSAS AELCIEDRPM 750
 751 PKLEIEKEIE LGNEDYCIKR EYLICEDYKL FWVAPRNSAE LTVIKVSSQP 800
 801 VPWDFYINLK LKERLNEDFD HFCSCYQYQD GCIVWHQYIN CFTLQDLLQH 850
 851 SEYITHEITV LIIYNLLTIV EMLHKAEIVH GDLSPRCLIL RNRIHDPYDC 900
 901 NKNNQALKIV DFSYSVDLRV QLDVFTLSGF RTVQILEGQK ILANCSSPYQ 950
 951 VDLFGIADLA HLLLFKEHLQ VFWDGSFWKL SQNISELKDG ELWNKFFVRI 1000
1001 LNANDEATVS VLGELAAEMN GVFDTTFQSH LNKALWKVGK LTSPGALLFQ 1050
```

References

[1] S. Santaguida and A. Musacchio. "The life and miracles of kinetochores". In: *EMBO J.* 28.17 (2009), pp. 2511–2531.

[2] E. A. Foley and T. M. Kapoor. "Microtubule attachment and spindle assembly checkpoint signalling at the kinetochore". In: *Nat. Rev. Mol. Cell Biol.* 14.17 (2013), pp. 25–37.

[3] D. Coudreuse and P. Nurse. "Driving the cell cycle with a minimal CDK control network". In: *Nature* 468.7327 (Dec. 2010), pp. 1074–1079.

[4] D. O. Morgan. *The Cell Cycle: Principles of Control.* New Science Press, 2007.

[5] T. Hirano. "Condensins: universal organizers of chromosomes with diverse functions". In: *Genes Dev.* 26.15 (Aug. 2012), pp. 1659–1678.

[6] I. C. Waizenegger, S. Hauf, A. Meinke, and J. M. Peters. "Two distinct pathways remove mammalian cohesin from chromosome arms in prophase and from centromeres in anaphase". In: *Cell* 103.3 (Oct. 2000), pp. 399–410.

[7] C. Lengauer, K. W. Kinzler, and B. Vogelstein. "Genetic instabilities in human cancers". In: *Nature* 396.6712 (Dec. 1998), pp. 643–649.

[8] D. J. Gordon, B. Resio, and D. Pellman. "Causes and consequences of aneuploidy in cancer". In: *Nat. Rev. Genet.* 13.3 (Mar. 2012), pp. 189–203.

[9] R. Metzner. "Beiträge zur Granulalehre. I. Kern und Kerntheilung." In: *Verlag von Veit, Leipzig* (1894), pp. 309–348.

[10] D. W. Cleveland, Y. Mao, and K. F. Sullivan. "Centromeres and kinetochores: from epigenetics to mitotic checkpoint signaling". In: *Cell* 112.4 (Feb. 2003), pp. 407–421.

[11] T. J. Mitchison and E. D. Salmon. "Mitosis: a history of division". In: *Nat. Cell Biol.* 3.1 (Jan. 2001), pp. 17–21.

[12] T. Wittmann, A. Hyman, and A. Desai. "The spindle: a dynamic assembly of microtubules and motors". In: *Nat. Cell Biol.* 3.1 (Jan. 2001), pp. 28–34.

[13] C. E. Walczak and R. Heald. "Mechanisms of mitotic spindle assembly and function". In: *Int. Rev. Cytol.* 265 (2008), pp. 111–158.

[14] K. Kitagawa and P. Hieter. "Evolutionary conservation between budding yeast and human kinetochores". In: *Nat. Rev. Mol. Cell Biol.* 2.9 (Sept. 2001), pp. 678–687.

[15] P. Meraldi, A. McAinsh, E. Rheinbay, and P. Sorger. "Phylogenetic and structural analysis of centromeric DNA and kinetochore proteins". In: *Genome Biology* 7.3 (2006), R23.

[16] L. Clarke and J. Carbon. "Isolation of a yeast centromere and construction of functional small circular chromosomes". In: *Nature* 287.5782 (Oct. 1980), pp. 504–509.

[17] M. Winey, C. L. Mamay, E. T. O'Toole, D. N. Mastronarde, T. H. Giddings, K. L. McDonald, and J. R. McIntosh. "Three-dimensional ultrastructural analysis of the Saccharomyces cerevisiae mitotic spindle." In: *J. Cell Biol.* 129.6 (1995), pp. 1601–1615.

[18] Y. Chikashige, N. Kinoshita, Y. Nakaseko, T. Matsumoto, S. Murakami, O. Niwa, and M. Yanagida. “Composite motifs and repeat symmetry in S. pombe centromeres: direct analysis by integration of NotI restriction sites”. In: *Cell* 57.5 (June 1989), pp. 739–751.

[19] B. F. McEwen, G. K. Chan, B. Zubrowski, M. S. Savoian, M. T. Sauer, and T. J. Yen. “CENP-E is essential for reliable bioriented spindle attachment, but chromosome alignment can be achieved via redundant mechanisms in mammalian cells”. In: *Mol. Biol. Cell* 12.9 (Sept. 2001), pp. 2776–2789.

[20] P. S. Maddox, K. Oegema, A. Desai, and I. M. Cheeseman. “"Holo"er than thou: chromosome segregation and kinetochore function in C. elegans”. In: *Chromosome Res.* 12.6 (2004), pp. 641–653.

[21] B. A. Sullivan and G. H. Karpen. “Centromeric chromatin exhibits a histone modification pattern that is distinct from both euchromatin and heterochromatin”. In: *Nat. Struct. Mol. Biol.* 11.11 (Nov. 2004), pp. 1076–1083.

[22] B. E. Black, D. R. Foltz, S. Chakravarthy, K. Luger, V. L. Woods, and D. W. Cleveland. “Structural determinants for generating centromeric chromatin”. In: *Nature* 430.6999 (July 2004), pp. 578–582.

[23] B. F. McEwen, C. E. Hsieh, A. L. Mattheyses, and C. L. Rieder. “A new look at kinetochore structure in vertebrate somatic cells using high-pressure freezing and freeze substitution”. In: *Chromosoma* 107.6-7 (Dec. 1998), pp. 366–375.

[24] F. Wang, J. Dai, J. R. Daum, E. Niedzialkowska, B. Banerjee, P. T. Stukenberg, G. J. Gorbsky, and J. M. Higgins. “Histone H3 Thr-3 phosphorylation by Haspin positions Aurora B at centromeres in mitosis”. In: *Science* 330.6001 (Oct. 2010), pp. 231–235.

[25] A. E. Kelly, C. Ghenoiu, J. Z. Xue, C. Zierhut, H. Kimura, and H. Funabiki. “Survivin reads phosphorylated histone H3 threonine 3 to activate the mitotic kinase Aurora B”. In: *Science* 330.6001 (Oct. 2010), pp. 235–239.

[26] D. Liu, G. Vader, M. J. Vromans, M. A. Lampson, and S. M. Lens. “Sensing chromosome biorientation by spatial separation of aurora B kinase from kinetochore substrates”. In: *Science* 323.5919 (Mar. 2009), pp. 1350–1353.

[27] D. R. Foltz, L. E. Jansen, B. E. Black, A. O. Bailey, J. R. Yates, and D. W. Cleveland. “The human CENP-A centromeric nucleosome-associated complex”. In: *Nat. Cell Biol.* 8.5 (May 2006), pp. 458–469.

[28] M. Okada, I. M. Cheeseman, T. Hori, K. Okawa, I. X. McLeod, J. R. Yates, A. Desai, and T. Fukagawa. “The CENP-H-I complex is required for the efficient incorporation of newly synthesized CENP-A into centromeres”. In: *Nat. Cell Biol.* 8.5 (May 2006), pp. 446–457.

[29] Y. Moroi, C. Peebles, M. J. Fritzler, J. Steigerwald, and E. M. Tan. “Autoantibody to centromere (kinetochore) in scleroderma sera”. In: *Proc. Natl. Acad. Sci. U.S.A.* 77.3 (Mar. 1980), pp. 1627–1631.

[30] T. Hori, M. Amano, A. Suzuki, C. B. Backer, J. P. Welburn, Y. Dong, B. F. McEwen, W.-H. Shang, E. Suzuki, K. Okawa, I. M. Cheeseman, and T. Fukagawa. "CCAN Makes Multiple Contacts with Centromeric DNA to Provide Distinct Pathways to the Outer Kinetochore". In: *Cell* 135.6 (2008), pp. 1039–1052.

[31] D. K. Palmer, K. O'Day, H. L. Trong, H. Charbonneau, and R. L. Margolis. "Purification of the centromere-specific protein CENP-A and demonstration that it is a distinctive histone". In: *Proc. Natl. Acad. Sci. U.S.A.* 88.9 (May 1991), pp. 3734–3738.

[32] M. D. Blower, B. A. Sullivan, and G. H. Karpen. "Conserved Organization of Centromeric Chromatin in Flies and Humans". In: *Dev. Cell* 2.3 (2002), pp. 319–330.

[33] A. P. Joglekar, D. Bouck, K. Finley, X. Liu, Y. Wan, J. Berman, X. He, E. Salmon, and K. S. Bloom. "Molecular architecture of the kinetochore-microtubule attachment site is conserved between point and regional centromeres". In: *J Cell Biol.* 181.4 (2008), pp. 587–594.

[34] O. J. Marshall, A. T. Marshall, and K. A. Choo. "Three-dimensional localization of CENP-A suggests a complex higher order structure of centromeric chromatin". In: *J Cell Biol.* 183.7 (2008), pp. 1193–1202.

[35] K. A. Collins, A. R. Castillo, S. Y. Tatsutani, and S. Biggins. "De novo kinetochore assembly requires the centromeric histone H3 variant". In: *Mol. Biol. Cell* 16.12 (Dec. 2005), pp. 5649–5660.

[36] H. Saitoh, J. Tomkiel, C. A. Cooke, H. Ratrie, M. Maurer, N. F. Rothfield, and W. C. Earnshaw. "CENP-C, an autoantigen in scleroderma, is a component of the human inner kinetochore plate". In: *Cell* 70.1 (July 1992), pp. 115–125.

[37] C. W. Carroll, K. J. Milks, and A. F. Straight. "Dual recognition of CENP-A nucleosomes is required for centromere assembly". In: *J. Cell Biol.* 189.7 (June 2010), pp. 1143–1155.

[38] C. W. Carroll, M. C. Silva, K. M. Godek, L. E. Jansen, and A. F. Straight. "Centromere assembly requires the direct recognition of CENP-A nucleosomes by CENP-N". In: *Nat. Cell Biol.* 11.7 (July 2009), pp. 896–902.

[39] K. Klare, J. R. Weir, F. Basilico, T. Zimniak, L. Massimiliano, N. Ludwigs, F. Herzog, and A. Musacchio. "CENP-C is a blueprint for constitutive centromere-associated network assembly within human kinetochores". In: *J. Cell Biol.* 210.1 (July 2015), pp. 11–22.

[40] I. M. Cheeseman, T. Hori, T. Fukagawa, and A. Desai. "KNL1 and the CENP-H/I/K complex coordinately direct kinetochore assembly in vertebrates". In: *Mol. Biol. Cell* 19.2 (Feb. 2008), pp. 587–594.

[41] S. Westermann and A. Schleiffer. "Family matters: structural and functional conservation of centromere-associated proteins from yeast to humans". In: *Trends Cell Biol.* 23.6 (June 2013), pp. 260–269.

[42] T. Hori, T. Haraguchi, Y. Hiraoka, H. Kimura, and T. Fukagawa. "Dynamic behavior of Nuf2-Hec1 complex that localizes to the centrosome and centromere and is essential for mitotic progression in vertebrate cells". In: *J. Cell. Sci.* 116.Pt 16 (Aug. 2003), pp. 3347–3362.

[43] F. Basilico, S. Maffini, J. R. Weir, D. Prumbaum, A. M. Rojas, T. Zimniak, A. De Antoni, S. Jeganathan, B. Voss, S. van Gerwen, V. Krenn, L. Massimiliano, A. Valencia, I. R. Vetter, F. Herzog, S. Raunser, S. Pasqualato, and A. Musacchio. "The pseudo GTPase CENP-M drives human kinetochore assembly". In: *Elife* 3 (2014), e02978.

[44] T. Nishino, K. Takeuchi, K. E. Gascoigne, A. Suzuki, T. Hori, T. Oyama, K. Morikawa, I. M. Cheeseman, and T. Fukagawa. "CENP-T-W-S-X forms a unique centromeric chromatin structure with a histone-like fold". In: *Cell* 148.3 (Feb. 2012), pp. 487–501.

[45] K. E. Gascoigne, K. Takeuchi, A. Suzuki, T. Hori, T. Fukagawa, and I. M. Cheeseman. "Induced ectopic kinetochore assembly bypasses the requirement for CENP-A nucleosomes". In: *Cell* 145.3 (Apr. 2011), pp. 410–422.

[46] S. E. McClelland, S. Borusu, A. C. Amaro, J. R. Winter, M. Belwal, A. D. McAinsh, and P. Meraldi. "The CENP-A NAC/CAD kinetochore complex controls chromosome congression and spindle bipolarity". In: *The EMBO Journal* 26.24 (2007), pp. 5033–5047.

[47] M. Amano, A. Suzuki, T. Hori, C. Backer, K. Okawa, I. M. Cheeseman, and T. Fukagawa. "The CENP-S complex is essential for the stable assembly of outer kinetochore structure". In: *J. Cell Biol.* 186.2 (July 2009), pp. 173–182.

[48] C. Janke, J. Ortiz, J. Lechner, A. Shevchenko, A. Shevchenko, M. M. Magiera, C. Schramm, and E. Schiebel. "The budding yeast proteins Spc24p and Spc25p interact with Ndc80p and Nuf2p at the kinetochore and are important for kinetochore clustering and checkpoint control". In: *EMBO J.* 20.4 (Feb. 2001), pp. 777–791.

[49] P. A. Wigge and J. V. Kilmartin. "The Ndc80p complex from Saccharomyces cerevisiae contains conserved centromere components and has a function in chromosome segregation". In: *J. Cell Biol.* 152.2 (Jan. 2001), pp. 349–360.

[50] I. M. Cheeseman, S. Niessen, S. Anderson, F. Hyndman, J. R. Yates, K. Oegema, and A. Desai. "A conserved protein network controls assembly of the outer kinetochore and its ability to sustain tension". In: *Genes Dev.* 18.18 (Sept. 2004), pp. 2255–2268.

[51] I. M. Cheeseman, J. S. Chappie, E. M. Wilson-Kubalek, and A. Desai. "The conserved KMN network constitutes the core microtubule-binding site of the kinetochore". In: *Cell* 127.5 (Dec. 2006), pp. 983–997.

[52] J. G. DeLuca, W. E. Gall, C. Ciferri, D. Cimini, A. Musacchio, and E. D. Salmon. "Kinetochore microtubule dynamics and attachment stability are regulated by Hec1". In: *Cell* 127.5 (Dec. 2006), pp. 969–982.

[53] C. Obuse, O. Iwasaki, T. Kiyomitsu, G. Goshima, Y. Toyoda, and M. Yanagida. "A conserved Mis12 centromere complex is linked to heterochromatic HP1 and outer kinetochore protein Zwint-1". In: *Nat. Cell Biol.* 6.11 (Nov. 2004), pp. 1135–1141.

[54] S. Martin-Lluesma, V. M. Stucke, and E. A. Nigg. "Role of Hec1 in spindle checkpoint signaling and kinetochore recruitment of Mad1/Mad2". In: *Science* 297.5590 (Sept. 2002), pp. 2267–2270.

[55] T. Kiyomitsu, C. Obuse, and M. Yanagida. "Human Blinkin/AF15q14 is required for chromosome alignment and the mitotic checkpoint through direct interaction with Bub1 and BubR1". In: *Dev. Cell* 13.5 (Nov. 2007), pp. 663–676.

[56] G. Goshima, T. mitsu, K. Yoda, and M. Yanagida. "Human centromere chromatin protein hMis12, essential for equal segregation, is independent of CENP-A loading pathway". In: *J. Cell Biol.* 160.1 (Jan. 2003), pp. 25–39.

[57] S. L. Kline, I. M. Cheeseman, T. Hori, T. Fukagawa, and A. Desai. "The human Mis12 complex is required for kinetochore assembly and proper chromosome segregation". In: *J. Cell Biol.* 173.1 (Apr. 2006), pp. 9–17.

[58] A. Petrovic, S. Pasqualato, P. Dube, V. Krenn, S. Santaguida, D. Cittaro, S. Monzani, L. Massimiliano, J. Keller, A. Tarricone, A. Maiolica, H. Stark, and A. Musacchio. "The MIS12 complex is a protein interaction hub for outer kinetochore assembly". In: *J. Cell Biol.* 190.5 (Sept. 2010), pp. 835–852.

[59] M. R. Przewloka, Z. Venkei, V. M. Bolanos-Garcia, J. Debski, M. Dadlez, and D. M. Glover. "CENP-C is a structural platform for kinetochore assembly". In: *Curr. Biol.* 21.5 (Mar. 2011), pp. 399–405.

[60] E. Screpanti, A. De Antoni, G. M. Alushin, A. Petrovic, T. Melis, E. Nogales, and A. Musacchio. "Direct binding of Cenp-C to the Mis12 complex joins the inner and outer kinetochore". In: *Curr. Biol.* 21.5 (Mar. 2011), pp. 391–398.

[61] P. De Wulf, A. D. McAinsh, and P. K. Sorger. "Hierarchical assembly of the budding yeast kinetochore from multiple subcomplexes". In: *Genes Dev.* 17.23 (Dec. 2003), pp. 2902–2921.

[62] S. Westermann, I. M. Cheeseman, S. Anderson, J. R. Yates, D. G. Drubin, and G. Barnes. "Architecture of the budding yeast kinetochore reveals a conserved molecular core". In: *J. Cell Biol.* 163.2 (Oct. 2003), pp. 215–222.

[63] M. L. McCleland, R. D. Gardner, M. J. Kallio, J. R. Daum, G. J. Gorbsky, D. J. Burke, and P. T. Stukenberg. "The highly conserved Ndc80 complex is required for kinetochore assembly, chromosome congression, and spindle checkpoint activity". In: *Genes Dev.* 17.1 (Jan. 2003), pp. 101–114.

[64] R. Bharadwaj, W. Qi, and H. Yu. "Identification of two novel components of the human NDC80 kinetochore complex". In: *J. Biol. Chem.* 279.13 (Mar. 2004), pp. 13076–13085.

[65] J. G. DeLuca, Y. Dong, P. Hergert, J. Strauss, J. M. Hickey, E. D. Salmon, and B. F. McEwen. "Hec1 and nuf2 are core components of the kinetochore outer plate essential for organizing microtubule attachment sites". In: *Mol. Biol. Cell* 16.2 (Feb. 2005), pp. 519–531.

[66] E. S. Gillett, C. W. Espelin, and P. K. Sorger. "Spindle checkpoint proteins and chromosome-microtubule attachment in budding yeast". In: *J. Cell Biol.* 164.4 (Feb. 2004), pp. 535–546.

[67] P. Meraldi, V. M. Draviam, and P. K. Sorger. "Timing and checkpoints in the regulation of mitotic progression". In: *Dev. Cell* 7.1 (July 2004), pp. 45–60.

[68] M. L. McCleland, M. J. Kallio, G. A. Barrett-Wilt, C. A. Kestner, J. Shabanowitz, D. F. Hunt, G. J. Gorbsky, and P. T. Stukenberg. "The vertebrate Ndc80 complex contains Spc24 and Spc25 homologs, which are required to establish and maintain kinetochore-microtubule attachment". In: *Curr. Biol.* 14.2 (Jan. 2004), pp. 131–137.

[69] R. R. Wei, P. K. Sorger, and S. C. Harrison. "Molecular organization of the Ndc80 complex, an essential kinetochore component". In: *Proc. Natl. Acad. Sci. U.S.A.* 102.15 (Apr. 2005), pp. 5363–5367.

[70] X. Wan, R. P. O'Quinn, H. L. Pierce, A. P. Joglekar, W. E. Gall, J. G. DeLuca, C. W. Carroll, S. T. Liu, T. J. Yen, B. F. McEwen, P. T. Stukenberg, A. Desai, and E. D. Salmon. "Protein architecture of the human kinetochore microtubule attachment site". In: *Cell* 137.4 (May 2009), pp. 672–684.

[71] A. Schleiffer, M. Maier, G. Litos, F. Lampert, P. Hornung, K. Mechtler, and S. Westermann. "CENP-T proteins are conserved centromere receptors of the Ndc80 complex". In: *Nat. Cell Biol.* 14.6 (June 2012), pp. 604–613.

[72] F. Malvezzi, G. Litos, A. Schleiffer, A. Heuck, K. Mechtler, T. Clausen, and S. Westermann. "A structural basis for kinetochore recruitment of the Ndc80 complex via two distinct centromere receptors". In: *EMBO J.* 32.3 (Feb. 2013), pp. 409–423.

[73] T. Nishino, F. Rago, T. Hori, K. Tomii, I. M. Cheeseman, and T. Fukagawa. "CENP-T provides a structural platform for outer kinetochore assembly". In: *EMBO J.* 32.3 (Feb. 2013), pp. 424–436.

[74] R. R. Wei, J. Al-Bassam, and S. C. Harrison. "The Ndc80/HEC1 complex is a contact point for kinetochore-microtubule attachment". In: *Nat. Struct. Mol. Biol.* 14.1 (Jan. 2007), pp. 54–59.

[75] C. Ciferri, S. Pasqualato, E. Screpanti, G. Varetti, S. Santaguida, G. Dos Reis, A. Maiolica, J. Polka, J. G. De Luca, P. De Wulf, M. Salek, J. Rappsilber, C. A. Moores, E. D. Salmon, and A. Musacchio. "Implications for kinetochore-microtubule attachment from the structure of an engineered Ndc80 complex". In: *Cell* 133.3 (May 2008), pp. 427–439.

[76] J. G. DeLuca, B. Moree, J. M. Hickey, J. V. Kilmartin, and E. D. Salmon. "hNuf2 inhibition blocks stable kinetochore-microtubule attachment and induces mitotic cell death in HeLa cells". In: *J. Cell Biol.* 159.4 (Nov. 2002), pp. 549–555.

[77] A. Desai, S. Rybina, T. Muller-Reichert, A. Shevchenko, A. Shevchenko, A. Hyman, and K. Oegema. "KNL-1 directs assembly of the microtubule-binding interface of the kinetochore in C. elegans". In: *Genes Dev.* 17.19 (Oct. 2003), pp. 2421–2435.

[78] J. P. Welburn, M. Vleugel, D. Liu, J. R. Yates, M. A. Lampson, T. Fukagawa, and I. M. Cheeseman. "Aurora B phosphorylates spatially distinct targets to differentially regulate the kinetochore-microtubule interface". In: *Mol. Cell* 38.3 (May 2010), pp. 383–392.

[79] D. A. Starr, R. Saffery, Z. Li, A. E. Simpson, K. H. Choo, T. J. Yen, and M. L. Goldberg. "HZwint-1, a novel human kinetochore component that interacts with HZW10". In: *J. Cell. Sci.* 113 (Pt 11) (June 2000), pp. 1939–1950.

[80] D. Liu, M. Vleugel, C. B. Backer, T. Hori, T. Fukagawa, I. M. Cheeseman, and M. A. Lampson. "Regulated targeting of protein phosphatase 1 to the outer kinetochore by KNL1 opposes Aurora B kinase". In: *J. Cell Biol.* 188.6 (Mar. 2010), pp. 809–820.

[81] J. S. Rosenberg, F. R. Cross, and H. Funabiki. "KNL1/Spc105 recruits PP1 to silence the spindle assembly checkpoint". In: *Curr. Biol.* 21.11 (June 2011), pp. 942–947.

[82] T. Mitchison, L. Evans, E. Schulze, and M. Kirschner. "Sites of microtubule assembly and disassembly in the mitotic spindle". In: *Cell* 45.4 (May 1986), pp. 515–527.

[83] C. L. Rieder and E. D. Salmon. "The vertebrate cell kinetochore and its roles during mitosis". In: *Trends Cell Biol.* 8.8 (Aug. 1998), pp. 310–318.

[84] S. Inoue and K. Dan. "Birefringence of the living cell. " In: *J Morph* 89 (1951), pp. 423–456.

[85] T. Mitchison and M. Kirschner. "Dynamic instability of microtubule growth". In: *Nature* 312.5991 (1984), pp. 237–242.

[86] R. A. Walker, E. T. O'Brien, N. K. Pryer, M. F. Soboeiro, W. A. Voter, H. P. Erickson, and E. D. Salmon. "Dynamic instability of individual microtubules analyzed by video light microscopy: rate constants and transition frequencies". In: *J. Cell Biol.* 107.4 (Oct. 1988), pp. 1437–1448.

[87] S. Westermann, H. W. Wang, A. Avila-Sakar, D. G. Drubin, E. Nogales, and G. Barnes. "The Dam1 kinetochore ring complex moves processively on depolymerizing microtubule ends". In: *Nature* 440.7083 (Mar. 2006), pp. 565–569.

[88] J. P. Welburn, E. L. Grishchuk, C. B. Backer, E. M. Wilson-Kubalek, J. R. Yates, and I. M. Cheeseman. "The human kinetochore Ska1 complex facilitates microtubule depolymerization-coupled motility". In: *Dev. Cell* 16.3 (Mar. 2009), pp. 374–385.

[89] J. C. Schmidt, H. Arthanari, A. Boeszoermenyi, N. M. Dashkevich, E. M. Wilson-Kubalek, N. Monnier, M. Markus, M. Oberer, R. A. Milligan, M. Bathe, G. Wagner, E. L. Grishchuk, and I. M. Cheeseman. "The kinetochore-bound Ska1 complex tracks depolymerizing microtubules and binds to curved protofilaments". In: *Dev. Cell* 23.5 (Nov. 2012), pp. 968–980.

[90] A. Hanisch, H. H. Sillje, and E. A. Nigg. "Timely anaphase onset requires a novel spindle and kinetochore complex comprising Ska1 and Ska2". In: *EMBO J.* 25.23 (Nov. 2006), pp. 5504–5515.

[91] T. N. Gaitanos, A. Santamaria, A. A. Jeyaprakash, B. Wang, E. Conti, and E. A. Nigg. "Stable kinetochore-microtubule interactions depend on the Ska complex and its new component Ska3/C13Orf3". In: *EMBO J.* 28.10 (May 2009), pp. 1442–1452.

[92] E. A. Foley, M. Maldonado, and T. M. Kapoor. "Formation of stable attachments between kinetochores and microtubules depends on the B56-PP2A phosphatase". In: *Nat. Cell Biol.* 13.10 (Oct. 2011), pp. 1265–1271.

[93] G. M. Alushin, V. H. Ramey, S. Pasqualato, D. A. Ball, N. Grigorieff, A. Musacchio, and E. Nogales. "The Ndc80 kinetochore complex forms oligomeric arrays along microtubules". In: *Nature* 467.7317 (Oct. 2010), pp. 805–810.

[94] D. Cimini, X. Wan, C. B. Hirel, and E. D. Salmon. "Aurora kinase promotes turnover of kinetochore microtubules to reduce chromosome segregation errors". In: *Curr. Biol.* 16.17 (Sept. 2006), pp. 1711–1718.

[95] Y. W. Chan, A. A. Jeyaprakash, E. A. Nigg, and A. Santamaria. "Aurora B controls kinetochore-microtubule attachments by inhibiting Ska complex-KMN network interaction". In: *J. Cell Biol.* 196.5 (Mar. 2012), pp. 563–571.

[96] S. Hua, Z. Wang, K. Jiang, Y. Huang, T. Ward, L. Zhao, Z. Dou, and X. Yao. "CENP-U cooperates with Hec1 to orchestrate kinetochore-microtubule attachment". In: *J. Biol. Chem.* 286.2 (Jan. 2011), pp. 1627–1638.

[97] D. Cimini, B. Moree, J. C. Canman, and E. D. Salmon. "Merotelic kinetochore orientation occurs frequently during early mitosis in mammalian tissue cells and error correction is achieved by two different mechanisms". In: *J. Cell. Sci.* 116.Pt 20 (Oct. 2003), pp. 4213–4225.

[98] S. Santaguida and A. Musacchio. "The life and miracles of kinetochores". In: *EMBO J.* 28.17 (Sept. 2009), pp. 2511–2531.

[99] R. B. Nicklas and C. A. Koch. "Chromosome micromanipulation. 3. Spindle fiber tension and the reorientation of mal-oriented chromosomes". In: *J. Cell Biol.* 43.1 (Oct. 1969), pp. 40–50.

[100] X. Li and R. B. Nicklas. "Mitotic forces control a cell-cycle checkpoint". In: *Nature* 373.6515 (Feb. 1995), pp. 630–632.

[101] R. B. Nicklas, M. S. Campbell, S. C. Ward, and G. J. Gorbsky. "Tension-sensitive kinetochore phosphorylation in vitro". In: *J. Cell. Sci.* 111 (Pt 21) (Nov. 1998), pp. 3189–3196.

[102] G. Vader, J. J. Kauw, R. H. Medema, and S. M. Lens. "Survivin mediates targeting of the chromosomal passenger complex to the centromere and midbody". In: *EMBO Rep.* 7.1 (Jan. 2006), pp. 85–92.

[103] M. Carmena, M. Wheelock, H. Funabiki, and W. C. Earnshaw. "The chromosomal passenger complex (CPC): from easy rider to the godfather of mitosis". In: *Nat. Rev. Mol. Cell Biol.* 13.12 (Dec. 2012), pp. 789–803.

[104] C. Ditchfield, V. L. Johnson, A. Tighe, R. Ellston, C. Haworth, T. Johnson, A. Mortlock, N. Keen, and S. S. Taylor. "Aurora B couples chromosome alignment with anaphase by targeting BubR1, Mad2, and Cenp-E to kinetochores". In: *J. Cell Biol.* 161.2 (Apr. 2003), pp. 267–280.

[105] S. Hauf, R. W. Cole, S. LaTerra, C. Zimmer, G. Schnapp, R. Walter, A. Heckel, J. van Meel, C. L. Rieder, and J. M. Peters. "The small molecule Hesperadin reveals a role for Aurora B in correcting kinetochore-microtubule attachment and in maintaining the spindle assembly checkpoint". In: *J. Cell Biol.* 161.2 (Apr. 2003), pp. 281–294.

[106] M. A. Lampson, K. Renduchitala, A. Khodjakov, and T. M. Kapoor. "Correcting improper chromosome-spindle attachments during cell division". In: *Nat. Cell Biol.* 6.3 (Mar. 2004), pp. 232–237.

[107] T. U. Tanaka, N. Rachidi, C. Janke, G. Pereira, M. Galova, E. Schiebel, M. J. Stark, and K. Nasmyth. "Evidence that the Ipl1-Sli15 (Aurora kinase-INCENP) complex promotes chromosome bi-orientation by altering kinetochore-spindle pole connections". In: *Cell* 108.3 (Feb. 2002), pp. 317–329.

[108] S. Santaguida, A. Tighe, A. M. D'Alise, S. S. Taylor, and A. Musacchio. "Dissecting the role of MPS1 in chromosome biorientation and the spindle checkpoint through the small molecule inhibitor reversine". In: *J. Cell Biol.* 190.1 (July 2010), pp. 73–87.

[109] T. J. Maresca and E. D. Salmon. "Intrakinetochore stretch is associated with changes in kinetochore phosphorylation and spindle assembly checkpoint activity". In: *J. Cell Biol.* 184.3 (Feb. 2009), pp. 373–381.

[110] Y. Yamagishi, T. Honda, Y. Tanno, and Y. Watanabe. "Two histone marks establish the inner centromere and chromosome bi-orientation". In: *Science* 330.6001 (Oct. 2010), pp. 239–243.

[111] S. A. Kawashima, Y. Yamagishi, T. Honda, K. Ishiguro, and Y. Watanabe. "Phosphorylation of H2A by Bub1 prevents chromosomal instability through localizing shugoshin". In: *Science* 327.5962 (Jan. 2010), pp. 172–177.

[112] M. S. van der Waal, A. T. Saurin, M. J. Vromans, M. Vleugel, C. Wurzenberger, D. W. Gerlich, R. H. Medema, G. J. Kops, and S. M. Lens. "Mps1 promotes rapid centromere accumulation of Aurora B". In: *EMBO Rep.* 13.9 (Sept. 2012), pp. 847–854.

[113] S. J. Suijkerbuijk, M. Vleugel, A. Teixeira, and G. J. Kops. "Integration of kinase and phosphatase activities by BUBR1 ensures formation of stable kinetochore-microtubule attachments". In: *Dev. Cell* 23.4 (Oct. 2012), pp. 745–755.

[114] P. Xu, E. A. Raetz, M. Kitagawa, D. M. Virshup, and S. H. Lee. "BUBR1 recruits PP2A via the B56 family of targeting subunits to promote chromosome congression". In: *Biol Open* 2.5 (May 2013), pp. 479–486.

[115] R. Li and A. W. Murray. "Feedback control of mitosis in budding yeast". In: *Cell* 66.3 (Aug. 1991), pp. 519–531.

[116] M. A. Hoyt, L. Totis, and B. T. Roberts. "S. cerevisiae genes required for cell cycle arrest in response to loss of microtubule function". In: *Cell* 66.3 (Aug. 1991), pp. 507–517.

[117] B. T. Roberts, K. A. Farr, and M. A. Hoyt. "The Saccharomyces cerevisiae checkpoint gene BUB1 encodes a novel protein kinase." In: *Mol Cell Biol.* 14.12 (1994), pp. 8282–8291.

[118] E. Weiss and M. Winey. "The Saccharomyces cerevisiae spindle pole body duplication gene MPS1 is part of a mitotic checkpoint". In: *J. Cell Biol.* 132.1-2 (Jan. 1996), pp. 111–123.

[119] S. Biggins, F. F. Severin, N. Bhalla, I. Sassoon, A. A. Hyman, and A. W. Murray. "The conserved protein kinase Ipl1 regulates microtubule binding to kinetochores in budding yeast". In: *Genes Dev.* 13.5 (Mar. 1999), pp. 532–544.

[120] V. B. Indjeian, B. M. Stern, and A. W. Murray. "The centromeric protein Sgo1 is required to sense lack of tension on mitotic chromosomes". In: *Science* 307.5706 (Jan. 2005), pp. 130–133.

[121] G. Varetti and A. Musacchio. “The spindle assembly checkpoint”. In: *Curr. Biol.* 18.14 (July 2008), R591–595.

[122] P. Lara-Gonzalez, F. G. Westhorpe, and S. S. Taylor. “The spindle assembly checkpoint”. In: *Curr. Biol.* 22.22 (Nov. 2012), R966–980.

[123] G. Fang, H. Yu, and M. W. Kirschner. “Direct binding of CDC20 protein family members activates the anaphase-promoting complex in mitosis and G1”. In: *Mol. Cell* 2.2 (Aug. 1998), pp. 163–171.

[124] E. R. Kramer, C. Gieffers, G. Holzl, M. Hengstschlager, and J. M. Peters. “Activation of the human anaphase-promoting complex by proteins of the CDC20/Fizzy family”. In: *Curr. Biol.* 8.22 (Nov. 1998), pp. 1207–1210.

[125] L. H. Hwang, L. F. Lau, D. L. Smith, C. A. Mistrot, K. G. Hardwick, E. S. Hwang, A. Amon, and A. W. Murray. “Budding Yeast Cdc20: A Target of the Spindle Checkpoint”. In: *Science* 279.5353 (1998), pp. 1041–1044.

[126] S. H. Kim, D. P. Lin, S. Matsumoto, A. Kitazono, and T. Matsumoto. “Fission yeast Slp1: an effector of the Mad2-dependent spindle checkpoint”. In: *Science* 279.5353 (Feb. 1998), pp. 1045–1047.

[127] M. Glotzer, A. W. Murray, and M. W. Kirschner. “Cyclin is degraded by the ubiquitin pathway”. In: *Nature* 349.6305 (Jan. 1991), pp. 132–138.

[128] A. Yamamoto, V. Guacci, and D. Koshland. “Pds1p, an inhibitor of anaphase in budding yeast, plays a critical role in the APC and checkpoint pathway(s)”. In: *J. Cell Biol.* 133.1 (Apr. 1996), pp. 99–110.

[129] H. Funabiki, H. Yamano, K. Kumada, K. Nagao, T. Hunt, and M. Yanagida. “Cut2 proteolysis required for sister-chromatid seperation in fission yeast”. In: *Nature* 381.6581 (May 1996), pp. 438–441.

[130] S. L. Holloway, M. Glotzer, R. W. King, and A. W. Murray. “Anaphase is initiated by proteolysis rather than by the inactivation of maturation-promoting factor”. In: *Cell* 73.7 (July 1993), pp. 1393–1402.

[131] V. Sudakin, D. Ganoth, A. Dahan, H. Heller, J. Hershko, F. C. Luca, J. V. Ruderman, and A. Hershko. “The cyclosome, a large complex containing cyclin-selective ubiquitin ligase activity, targets cyclins for destruction at the end of mitosis”. In: *Mol. Biol. Cell* 6.2 (Feb. 1995), pp. 185–197.

[132] V. Sudakin, G. K. Chan, and T. J. Yen. “Checkpoint inhibition of the APC/C in HeLa cells is mediated by a complex of BUBR1, BUB3, CDC20, and MAD2”. In: *J. Cell Biol.* 154.5 (Sept. 2001), pp. 925–936.

[133] A. Kulukian, J. S. Han, and D. W. Cleveland. “Unattached kinetochores catalyze production of an anaphase inhibitor that requires a Mad2 template to prime Cdc20 for BubR1 binding”. In: *Dev. Cell* 16.1 (Jan. 2009), pp. 105–117.

[134] W. C. Chao, K. Kulkarni, Z. Zhang, E. H. Kong, and D. Barford. “Structure of the mitotic checkpoint complex”. In: *Nature* 484.7393 (Apr. 2012), pp. 208–213.

[135] K. G. Hardwick, R. C. Johnston, D. L. Smith, and A. W. Murray. "MAD3 Encodes a Novel Component of the Spindle Checkpoint Which Interacts with Bub3p, Cdc20p, and Mad2p". In: *J Cell Biol.* 148.5 (2000), pp. 871–882.

[136] D. T. Lau and A. W. Murray. "Mad2 and Mad3 cooperate to arrest budding yeast in mitosis". In: *Curr. Biol.* 22.3 (Feb. 2012), pp. 180–190.

[137] J. Nilsson, M. Yekezare, J. Minshull, and J. Pines. "The APC/C maintains the spindle assembly checkpoint by targeting Cdc20 for destruction". In: *Nat. Cell Biol.* 10.12 (Dec. 2008), pp. 1411–1420.

[138] J. S. Han, A. J. Holland, D. Fachinetti, A. Kulukian, B. Cetin, and D. W. Cleveland. "Catalytic assembly of the mitotic checkpoint inhibitor BubR1-Cdc20 by a Mad2-induced functional switch in Cdc20". In: *Mol. Cell* 51.1 (July 2013), pp. 92–104.

[139] P. Lara-Gonzalez, M. I. F. Scott, M. Diez, O. Sen, and S. S. Taylor. "BubR1 blocks substrate recruitment to the APC/C in a KEN-box-dependent manner". In: *J Cell Sci.* 124.24 (2011), pp. 4332–4345.

[140] D. Izawa and J. Pines. "Mad2 and the APC/C compete for the same site on Cdc20 to ensure proper chromosome segregation". In: *J. Cell Biol.* 199.1 (Oct. 2012), pp. 27–37.

[141] J. L. Burton and M. J. Solomon. "Mad3p, a pseudosubstrate inhibitor of APCCdc20 in the spindle assembly checkpoint". In: *Genes Dev.* 21.6 (Mar. 2007), pp. 655–667.

[142] I. T. Foe, S. A. Foster, S. K. Cheung, S. Z. DeLuca, D. O. Morgan, and D. P. Toczyski. "Ubiquitination of Cdc20 by the APC occurs through an intramolecular mechanism". In: *Curr. Biol.* 21.22 (Nov. 2011), pp. 1870–1877.

[143] S. A. Foster and D. O. Morgan. "The APC/C subunit Mnd2/Apc15 promotes Cdc20 autoubiquitination and spindle assembly checkpoint inactivation". In: *Mol. Cell* 47.6 (Sept. 2012), pp. 921–932.

[144] C. L. Rieder, R. W. Cole, A. Khodjakov, and G. Sluder. "The checkpoint delaying anaphase in response to chromosome monoorientation is mediated by an inhibitory signal produced by unattached kinetochores". In: *J. Cell Biol.* 130.4 (Aug. 1995), pp. 941–948.

[145] A. Musacchio and E. D. Salmon. "The spindle-assembly checkpoint in space and time". In: *Nat. Rev. Mol. Cell Biol.* 8.5 (May 2007), pp. 379–393.

[146] J. Maciejowski, K. A. George, M. E. Terret, C. Zhang, K. M. Shokat, and P. V. Jallepalli. "Mps1 directs the assembly of Cdc20 inhibitory complexes during interphase and mitosis to control M phase timing and spindle checkpoint signaling". In: *J. Cell Biol.* 190.1 (July 2010), pp. 89–100.

[147] M. Maldonado and T. M. Kapoor. "Constitutive Mad1 targeting to kinetochores uncouples checkpoint signalling from chromosome biorientation". In: *Nat. Cell Biol.* 13.4 (Apr. 2011), pp. 475–482.

[148] R. Fraschini, A. Beretta, L. Sironi, A. Musacchio, G. Lucchini, and S. Piatti. "Bub3 interaction with Mad2, Mad3 and Cdc20 is mediated by WD40 repeats and does not require intact kinetochores". In: *EMBO J.* 20.23 (Dec. 2001), pp. 6648–6659.

[149] E. M. Kim and D. J. Burke. "DNA damage activates the SAC in an ATM/ATR-dependent manner, independently of the kinetochore". In: *PLoS Genet.* 4.2 (Feb. 2008), e1000015.

[150] L. A. Malureanu, K. B. Jeganathan, M. Hamada, L. Wasilewski, J. Davenport, and J. M. van Deursen. "BubR1 N terminus acts as a soluble inhibitor of cyclin B degradation by APC/C(Cdc20) in interphase". In: *Dev. Cell* 16.1 (Jan. 2009), pp. 118–131.

[151] A. De Antoni, C. G. Pearson, D. Cimini, J. C. Canman, V. Sala, L. Nezi, M. Mapelli, L. Sironi, M. Faretta, E. D. Salmon, and A. Musacchio. "The Mad1/Mad2 complex as a template for Mad2 activation in the spindle assembly checkpoint". In: *Curr. Biol.* 15.3 (Feb. 2005), pp. 214–225.

[152] S. S. Taylor, E. Ha, and F. McKeon. "The Human Homologue of Bub3 Is Required for Kinetochore Localization of Bub1 and a Mad3/Bub1-related Protein Kinase". In: *J Cell Biol.* 142.1 (1998), pp. 1–11.

[153] R. H. Chen. "BubR1 is essential for kinetochore localization of other spindle checkpoint proteins and its phosphorylation requires Mad1". In: *J. Cell Biol.* 158.3 (Aug. 2002), pp. 487–496.

[154] L. Sironi, M. Melixetian, M. Faretta, E. Prosperini, K. Helin, and A. Musacchio. "Mad2 binding to Mad1 and Cdc20, rather than oligomerization, is required for the spindle checkpoint". In: *EMBO J.* 20.22 (Nov. 2001), pp. 6371–6382.

[155] L. Sironi, M. Mapelli, S. Knapp, A. De Antoni, K. T. Jeang, and A. Musacchio. "Crystal structure of the tetrameric Mad1-Mad2 core complex: implications of a 'safety belt' binding mechanism for the spindle checkpoint". In: *EMBO J.* 21.10 (May 2002), pp. 2496–2506.

[156] X. Luo, Z. Tang, J. Rizo, and H. Yu. "The Mad2 spindle checkpoint protein undergoes similar major conformational changes upon binding to either Mad1 or Cdc20". In: *Mol. Cell* 9.1 (Jan. 2002), pp. 59–71.

[157] X. Luo, Z. Tang, G. Xia, K. Wassmann, T. Matsumoto, J. Rizo, and H. Yu. "The Mad2 spindle checkpoint protein has two distinct natively folded states". In: *Nat. Struct. Mol. Biol.* 11.4 (Apr. 2004), pp. 338–345.

[158] M. Mapelli, L. Massimiliano, S. Santaguida, and A. Musacchio. "The Mad2 conformational dimer: structure and implications for the spindle assembly checkpoint". In: *Cell* 131.4 (Nov. 2007), pp. 730–743.

[159] J. Davenport, L. D. Harris, and R. Goorha. "Spindle checkpoint function requires Mad2-dependent Cdc20 binding to the Mad3 homology domain of BubR1". In: *Exp. Cell Res.* 312.10 (June 2006), pp. 1831–1842.

[160] V. Vanoosthuyse, J. C. Meadows, S. J. van der Sar, J. B. Millar, and K. G. Hardwick. "Bub3p facilitates spindle checkpoint silencing in fission yeast". In: *Mol. Biol. Cell* 20.24 (Dec. 2009), pp. 5096–5105.

[161] I. Primorac and A. Musacchio. "Panta rhei: the APC/C at steady state". In: *J. Cell Biol.* 201.2 (Apr. 2013), pp. 177–189.

[162] Z. Tang, R. Bharadwaj, B. Li, and H. Yu. "Mad2-Independent inhibition of APCCdc20 by the mitotic checkpoint protein BubR1". In: *Dev. Cell* 1.2 (Aug. 2001), pp. 227–237.

[163] Z. Tang, H. Shu, D. Oncel, S. Chen, and H. Yu. "Phosphorylation of Cdc20 by Bub1 Provides a Catalytic Mechanism for APC/C Inhibition by the Spindle Checkpoint". In: *Mol. Cell* 16.3 (2004), pp. 387–397.

[164] J. Zich, A. M. Sochaj, H. M. Syred, L. Milne, A. G. Cook, H. Ohkura, J. Rappsilber, and K. G. Hardwick. "Kinase activity of fission yeast Mph1 is required for Mad2 and Mad3 to stably bind the anaphase promoting complex". In: *Curr. Biol.* 22.4 (Feb. 2012), pp. 296–301.

[165] E. M. King, N. Rachidi, N. Morrice, K. G. Hardwick, and M. J. Stark. "Ipl1p-dependent phosphorylation of Mad3p is required for the spindle checkpoint response to lack of tension at kinetochores". In: *Genes Dev.* 21.10 (May 2007), pp. 1163–1168.

[166] A. T. Saurin, M. S. van der Waal, R. H. Medema, S. M. Lens, and G. J. Kops. "Aurora B potentiates Mps1 activation to ensure rapid checkpoint establishment at the onset of mitosis". In: *Nat Commun* 2 (2011), p. 316.

[167] W. Nijenhuis, E. von Castelmur, D. Littler, V. De Marco, E. Tromer, M. Vleugel, M. H. van Osch, B. Snel, A. Perrakis, and G. J. Kops. "A TPR domain-containing N-terminal module of MPS1 is required for its kinetochore localization by Aurora B". In: *J. Cell Biol.* 201.2 (Apr. 2013), pp. 217–231.

[168] M. Vleugel, M. Omerzu, V. Groenewold, M. A. Hadders, S. M. Lens, and G. J. Kops. "Sequential multisite phospho-regulation of KNL1-BUB3 interfaces at mitotic kinetochores". In: *Mol. Cell* 57.5 (Mar. 2015), pp. 824–835.

[169] G. V. Caldas, K. F. DeLuca, and J. G. DeLuca. "KNL1 facilitates phosphorylation of outer kinetochore proteins by promoting Aurora B kinase activity". In: *J. Cell Biol.* 203.6 (Dec. 2013), pp. 957–969.

[170] R. B. Schittenhelm, R. Chaleckis, and C. F. Lehner. "Intrakinetochore localization and essential functional domains of Drosophila Spc105". In: *EMBO J.* 28.16 (Aug. 2009), pp. 2374–2386.

[171] V. Krenn, K. Overlack, I. Primorac, S. van Gerwen, and A. Musacchio. "KI motifs of human Knl1 enhance assembly of comprehensive spindle checkpoint complexes around MELT repeats". In: *Curr. Biol.* 24.1 (Jan. 2014), pp. 29–39.

[172] N. London, S. Ceto, J. A. Ranish, and S. Biggins. "Phosphoregulation of Spc105 by Mps1 and PP1 regulates Bub1 localization to kinetochores". In: *Curr. Biol.* 22.10 (May 2012), pp. 900–906.

[173] Y. Yamagishi, C. H. Yang, Y. Tanno, and Y. Watanabe. "MPS1/Mph1 phosphorylates the kinetochore protein KNL1/Spc7 to recruit SAC components". In: *Nat. Cell Biol.* 14.7 (July 2012), pp. 746–752.

[174] L. A. Shepperd, J. C. Meadows, A. M. Sochaj, T. C. Lancaster, J. Zou, G. J. Buttrick, J. Rappsilber, K. G. Hardwick, and J. B. Millar. "Phosphodependent recruitment of Bub1 and Bub3 to Spc7/KNL1 by Mph1 kinase maintains the spindle checkpoint". In: *Curr. Biol.* 22.10 (May 2012), pp. 891–899.

[175] I. Primorac, J. R. Weir, E. Chiroli, F. Gross, I. Hoffmann, S. van Gerwen, A. Ciliberto, and A. Musacchio. “Bub3 reads phosphorylated MELT repeats to promote spindle assembly checkpoint signaling”. In: *Elife* 2 (2013), e01030.

[176] V. Vanoosthuyse, R. Valsdottir, J. P. Javerzat, and K. G. Hardwick. “Kinetochore targeting of fission yeast Mad and Bub proteins is essential for spindle checkpoint function but not for all chromosome segregation roles of Bub1p”. In: *Mol. Cell. Biol.* 24.22 (Nov. 2004), pp. 9786–9801.

[177] V. L. Johnson, M. I. Scott, S. V. Holt, D. Hussein, and S. S. Taylor. “Bub1 is required for kinetochore localization of BubR1, Cenp-E, Cenp-F and Mad2, and chromosome congression”. In: *J. Cell. Sci.* 117.Pt 8 (Mar. 2004), pp. 1577–1589.

[178] P. E. Rischitor, K. M. May, and K. G. Hardwick. “Bub1 is a fission yeast kinetochore scaffold protein, and is sufficient to recruit other spindle checkpoint proteins to ectopic sites on chromosomes”. In: *PLoS ONE* 2.12 (2007), e1342.

[179] K. Overlack, I. Primorac, M. Vleugel, V. Krenn, S. Maffini, I. Hoffmann, G. J. P. L. Kops, and A. Musacchio. “A molecular basis for the differential roles of Bub1 and BubR1 in the spindle assembly checkpoint”. In: *eLife* 4 (2015). Ed. by S. C. Harrison.

[180] G. Zhang, T. Lischetti, D. G. Hayward, and J. Nilsson. “Distinct domains in Bub1 localize RZZ and BubR1 to kinetochores to regulate the checkpoint”. In: *Nat Commun* 6 (2015), p. 7162.

[181] D. M. Brady and K. G. Hardwick. “Complex formation between Mad1p, Bub1p and Bub3p is crucial for spindle checkpoint function”. In: *Curr. Biol.* 10.11 (June 2000), pp. 675–678.

[182] S. Kim, H. Sun, D. R. Tomchick, H. Yu, and X. Luo. “Structure of human Mad1 C-terminal domain reveals its involvement in kinetochore targeting”. In: *Proc. Natl. Acad. Sci. U.S.A.* 109.17 (Apr. 2012), pp. 6549–6554.

[183] C. Klebig, D. Korinth, and P. Meraldi. “Bub1 regulates chromosome segregation in a kinetochore-independent manner”. In: *J Cell Biol.* 185.5 (2009), pp. 841–858.

[184] G. J. Kops, Y. Kim, B. A. Weaver, Y. Mao, I. McLeod, J. R. Yates, M. Tagaya, and D. W. Cleveland. “ZW10 links mitotic checkpoint signaling to the structural kinetochore”. In: *J. Cell Biol.* 169.1 (Apr. 2005), pp. 49–60.

[185] L. Hewitt, A. Tighe, S. Santaguida, A. M. White, C. D. Jones, A. Musacchio, S. Green, and S. S. Taylor. “Sustained Mps1 activity is required in mitosis to recruit O-Mad2 to the Mad1-C-Mad2 core complex”. In: *J. Cell Biol.* 190.1 (July 2010), pp. 25–34.

[186] N. Jelluma, T. B. Dansen, T. Sliedrecht, N. P. Kwiatkowski, and G. J. Kops. “Release of Mps1 from kinetochores is crucial for timely anaphase onset”. In: *J Cell Biol.* 191.2 (2010), pp. 281–290.

[187] J. Espeut, D. K. Cheerambathur, L. Krenning, K. Oegema, and A. Desai. “Microtubule binding by KNL-1 contributes to spindle checkpoint silencing at the kinetochore”. In: *J. Cell Biol.* 196.4 (Feb. 2012), pp. 469–482.

[188] G. Zhang, T. Lischetti, and J. Nilsson. "A minimal number of MELT repeats supports all the functions of KNL1 in chromosome segregation". In: *J. Cell. Sci.* 127.Pt 4 (Feb. 2014), pp. 871–884.

[189] A. Espert, P. Uluocak, R. N. Bastos, D. Mangat, P. Graab, and U. Gruneberg. "PP2A-B56 opposes Mps1 phosphorylation of Knl1 and thereby promotes spindle assembly checkpoint silencing". In: *J. Cell Biol.* 206.7 (Sept. 2014), pp. 833–842.

[190] D. A. Starr, B. C. Williams, T. S. Hays, and M. L. Goldberg. "ZW10 helps recruit dynactin and dynein to the kinetochore". In: *J. Cell Biol.* 142.3 (Aug. 1998), pp. 763–774.

[191] E. R. Griffis, N. Stuurman, and R. D. Vale. "Spindly, a novel protein essential for silencing the spindle assembly checkpoint, recruits dynein to the kinetochore". In: *J. Cell Biol.* 177.6 (June 2007), pp. 1005–1015.

[192] R. Karess. "Rod-Zw10-Zwilch: a key player in the spindle checkpoint". In: *Trends Cell Biol.* 15.7 (July 2005), pp. 386–392.

[193] M. Mapelli, F. V. Filipp, G. Rancati, L. Massimiliano, L. Nezi, G. Stier, R. S. Hagan, S. Confalonieri, S. Piatti, M. Sattler, and A. Musacchio. "Determinants of conformational dimerization of Mad2 and its inhibition by p31comet". In: *EMBO J.* 25.6 (Mar. 2006), pp. 1273–1284.

[194] F. G. Westhorpe, A. Tighe, P. Lara-Gonzalez, and S. S. Taylor. "p31comet-mediated extraction of Mad2 from the MCC promotes efficient mitotic exit". In: *J. Cell. Sci.* 124.Pt 22 (Nov. 2011), pp. 3905–3916.

[195] K. Wang, B. Sturt-Gillespie, J. C. Hittle, D. Macdonald, G. K. Chan, T. J. Yen, and S. T. Liu. "Thyroid hormone receptor interacting protein 13 (TRIP13) AAA-ATPase is a novel mitotic checkpoint-silencing protein". In: *J. Biol. Chem.* 289.34 (Aug. 2014), pp. 23928–23937.

[196] S. J. Suijkerbuijk, T. J. van Dam, G. E. Karagöz, E. von Castelmur, N. C. Hubner, A. M. Duarte, M. Vleugel, A. Perrakis, S. G. Rüdiger, B. Snel, and G. J. Kops. "The Vertebrate Mitotic Checkpoint Protein BUBR1 Is an Unusual Pseudokinase". In: *Dev. Cell* 22.6 (2012), pp. 1321–1329.

[197] M. Vleugel, E. Hoogendoorn, B. Snel, and G. J. Kops. "Evolution and Function of the Mitotic Checkpoint". In: *Dev. Cell* 23.2 (2012), pp. 239–250.

[198] P. Meraldi and P. K. Sorger. "A dual role for Bub1 in the spindle checkpoint and chromosome congression". In: *EMBO J.* 24.8 (Apr. 2005), pp. 1621–1633.

[199] S. D'Arcy, O. R. Davies, T. L. Blundell, and V. M. Bolanos-Garcia. "Defining the molecular basis of BubR1 kinetochore interactions and APC/C-CDC20 inhibition". In: *J. Biol. Chem.* 285.19 (May 2010), pp. 14764–14776.

[200] D. Lu, J. Y. Hsiao, N. E. Davey, V. A. Van Voorhis, S. A. Foster, C. Tang, and D. O. Morgan. "Multiple mechanisms determine the order of APC/C substrate degradation in mitosis". In: *J Cell Biol.* 207.1 (2014), pp. 23–39.

[201] B. D. Fiore, N. E. Davey, A. Hagting, D. Izawa, J. Mansfeld, T. J. Gibson, and J. Pines. "The ABBA Motif Binds APC/C Activators and Is Shared by APC/C Substrates and Regulators". In: *Dev. Cell* 32.3 (2015), pp. 358–372.

[202] L. A. Diaz-Martinez, W. Tian, B. Li, R. Warrington, L. Jia, C. A. Brautigam, X. Luo, and H. Yu. "The Cdc20-binding Phe Box of the Spindle Checkpoint Protein BubR1 Maintains the Mitotic Checkpoint Complex During Mitosis". In: *J. Biol. Chem.* 290.4 (2015), pp. 2431–2443.

[203] N. A. Larsen, J. Al-Bassam, R. R. Wei, and S. C. Harrison. "Structural analysis of Bub3 interactions in the mitotic spindle checkpoint". In: *Proc. Natl. Acad. Sci. U.S.A.* 104.4 (2007), pp. 1201–1206.

[204] H. Sharp-Baker and R. H. Chen. "Spindle checkpoint protein Bub1 is required for kinetochore localization of Mad1, Mad2, Bub3, and CENP-E, independently of its kinase activity". In: *J. Cell Biol.* 153.6 (June 2001), pp. 1239–1250.

[205] S. Elowe, K. Dulla, A. Uldschmid, X. Li, Z. Dou, and E. A. Nigg. "Uncoupling of the spindle-checkpoint and chromosome-congression functions of BubR1". In: *J. Cell. Sci.* 123.Pt 1 (Jan. 2010), pp. 84–94.

[206] S. S. Taylor, D. Hussein, Y. Wang, S. Elderkin, and C. J. Morrow. "Kinetochore localisation and phosphorylation of the mitotic checkpoint components Bub1 and BubR1 are differentially regulated by spindle events in human cells". In: *J Cell Sci.* 114.24 (2001), pp. 4385–4395.

[207] T. Kiyomitsu, H. Murakami, and M. Yanagida. "Protein Interaction Domain Mapping of Human Kinetochore Protein Blinkin Reveals a Consensus Motif for Binding of Spindle Assembly Checkpoint Proteins Bub1 and BubR1". In: *Mol. Cell. Biol.* 31.5 (2011), pp. 998–1011.

[208] V. Krenn, A. Wehenkel, X. Li, S. Santaguida, and A. Musacchio. "Structural analysis reveals features of the spindle checkpoint kinase Bub1-kinetochore subunit Knl1 interaction". In: *J. Cell Biol.* 196.4 (2012), pp. 451–467.

[209] M. Vleugel, E. Tromer, M. Omerzu, V. Groenewold, W. Nijenhuis, B. Snel, and G. J. Kops. "Arrayed BUB recruitment modules in the kinetochore scaffold KNL1 promote accurate chromosome segregation". In: *J. Cell Biol.* 203.6 (Dec. 2013), pp. 943–955.

[210] M. Vleugel, T. A. Hoek, E. Tromer, T. Sliedrecht, V. Groenewold, M. Omerzu, and G. J. Kops. "Dissecting the roles of human BUB1 in the spindle assembly checkpoint". In: *J. Cell. Sci.* 128.16 (Aug. 2015), pp. 2975–2982.

[211] N. London and S. Biggins. "Mad1 kinetochore recruitment by Mps1-mediated phosphorylation of Bub1 signals the spindle checkpoint". In: *Genes Dev.* 28.2 (Jan. 2014), pp. 140–152.

[212] M. W. Moyle, T. Kim, N. Hattersley, J. Espeut, D. K. Cheerambathur, K. Oegema, and A. Desai. "A Bub1-Mad1 interaction targets the Mad1-Mad2 complex to unattached kinetochores to initiate the spindle checkpoint". In: *J. Cell Biol.* 204.5 (Mar. 2014), pp. 647–657.

[213] Z. Rahmani, M. E. Gagou, C. Lefebvre, D. Emre, and R. E. Karess. "Separating the spindle, checkpoint, and timer functions of BubR1". In: *J. Cell Biol.* 187.5 (Nov. 2009), pp. 597–605.

[214] J. Kang, M. Yang, B. Li, W. Qi, C. Zhang, K. M. Shokat, D. R. Tomchick, M. Machius, and H. Yu. "Structure and Substrate Recruitment of the Human Spindle Checkpoint Kinase Bub1". In: *Mol. Cell* 32.3 (2008), pp. 394–405.

[215] D. Perera, V. Tilston, J. A. Hopwood, M. Barchi, R. P. Boot-Handford, and S. S. Taylor. "Bub1 maintains centromeric cohesion by activation of the spindle checkpoint". In: *Dev. Cell* 13.4 (Oct. 2007), pp. 566–579.

[216] G. Manning, D. B. Whyte, R. Martinez, T. Hunter, and S. Sudarsanam. "The protein kinase complement of the human genome". In: *Science* 298.5600 (Dec. 2002), pp. 1912–1934.

[217] S. S. Taylor and A. P. Kornev. "Protein kinases: evolution of dynamic regulatory proteins". In: *Trends Biochem. Sci.* 36.2 (Feb. 2011), pp. 65–77.

[218] Y. Mao, A. Abrieu, and D. W. Cleveland. "Activating and Silencing the Mitotic Checkpoint through CENP-E-Dependent Activation/Inactivation of BubR1". In: *Cell* 114.1 (2003), pp. 87–98.

[219] Y. Mao, A. Desai, and D. W. Cleveland. "Microtubule capture by CENP-E silences BubR1-dependent mitotic checkpoint signaling". In: *J. Cell Biol.* 170.6 (Sept. 2005), pp. 873–880.

[220] J. Zhang, S. Ahmad, and Y. Mao. "BubR1 and APC/EB1 cooperate to maintain metaphase chromosome alignment". In: *J. Cell Biol.* 178.5 (Aug. 2007), pp. 773–784.

[221] Y. Guo, C. Kim, S. Ahmad, J. Zhang, and Y. Mao. "CENP-E–dependent BubR1 autophosphorylation enhances chromosome alignment and the mitotic checkpoint". In: *J. Cell Biol.* 198.2 (July 2012), pp. 205–217.

[222] S. Elowe, S. Hummer, A. Uldschmid, X. Li, and E. A. Nigg. "Tension-sensitive Plk1 phosphorylation on BubR1 regulates the stability of kinetochore microtubule interactions". In: *Genes Dev.* 21.17 (Sept. 2007), pp. 2205–2219.

[223] H. Huang, J. Hittle, F. Zappacosta, R. S. Annan, A. Hershko, and T. J. Yen. "Phosphorylation sites in BubR1 that regulate kinetochore attachment, tension, and mitotic exit". In: *J. Cell Biol.* 183.4 (Nov. 2008), pp. 667–680.

[224] Z. Lin, L. Jia, D. R. Tomchick, X. Luo, and H. Yu. "Substrate-Specific Activation of the Mitotic Kinase Bub1 through Intramolecular Autophosphorylation and Kinetochore Targeting". In: *Structure* 22.11 (2014), pp. 1616–1627.

[225] R. M. Ricke, K. B. Jeganathan, L. Malureanu, A. M. Harrison, and J. M. van Deursen. "Bub1 kinase activity drives error correction and mitotic checkpoint control but not tumor suppression". In: *J. Cell Biol.* 199.6 (2012), pp. 931–949.

[226] C. D. Warren, D. M. Brady, R. C. Johnston, J. S. Hanna, K. G. Hardwick, and F. A. Spencer. "Distinct chromosome segregation roles for spindle checkpoint proteins". In: *Mol. Biol. Cell* 13.9 (Sept. 2002), pp. 3029–3041.

[227] S. Yamaguchi, A. Decottignies, and P. Nurse. "Function of Cdc2p-dependent Bub1p phosphorylation and Bub1p kinase activity in the mitotic and meiotic spindle checkpoint". In: *EMBO J.* 22.5 (Mar. 2003), pp. 1075–1087.

[228] J. Fernius and K. G. Hardwick. "Bub1 kinase targets Sgo1 to ensure efficient chromosome biorientation in budding yeast mitosis". In: *PLoS Genet.* 3.11 (Nov. 2007), e213.

[229] H. Liu, L. Jia, and H. Yu. "Phospho-H2A and cohesin specify distinct tension-regulated Sgo1 pools at kinetochores and inner centromeres". In: *Curr. Biol.* 23.19 (Oct. 2013), pp. 1927–1933.

[230] T. S. Kitajima, S. Hauf, M. Ohsugi, T. Yamamoto, and Y. Watanabe. “Human Bub1 defines the persistent cohesion site along the mitotic chromosome by affecting Shugoshin localization”. In: *Curr. Biol.* 15.4 (Feb. 2005), pp. 353–359.

[231] H. Liu, Q. Qu, R. Warrington, A. Rice, N. Cheng, and H. Yu. “Mitotic Transcription Installs Sgo1 at Centromeres to Coordinate Chromosome Segregation”. In: *Mol. Cell* 59.3 (Aug. 2015), pp. 426–436.

[232] C. G. Riedel, V. L. Katis, Y. Katou, S. Mori, T. Itoh, W. Helmhart, M. Galova, M. Petronczki, J. Gregan, B. Cetin, I. Mudrak, E. Ogris, K. Mechtler, L. Pelletier, F. Buchholz, K. Shirahige, and K. Nasmyth. “Protein phosphatase 2A protects centromeric sister chromatid cohesion during meiosis I”. In: *Nature* 441.7089 (May 2006), pp. 53–61.

[233] Z. Tang, H. Shu, W. Qi, N. A. Mahmood, M. C. Mumby, and H. Yu. “PP2A is required for centromeric localization of Sgo1 and proper chromosome segregation”. In: *Dev. Cell* 10.5 (May 2006), pp. 575–585.

[234] Y. Boyarchuk, A. Salic, M. Dasso, and A. Arnaoutov. “Bub1 is essential for assembly of the functional inner centromere”. In: *J. Cell Biol.* 176.7 (Mar. 2007), pp. 919–928.

[235] M. Huse and J. Kuriyan. “The conformational plasticity of protein kinases”. In: *Cell* 109.3 (May 2002), pp. 275–282.

[236] B. Nolen, S. Taylor, and G. Ghosh. “Regulation of protein kinases; controlling activity through activation segment conformation”. In: *Mol. Cell* 15.5 (Sept. 2004), pp. 661–675.

[237] A. Asghar, A. Lajeunesse, K. Dulla, G. Combes, P. Thebault, E. A. Nigg, and S. Elowe. “Bub1 autophosphorylation feeds back to regulate kinetochore docking and promote localized substrate phosphorylation”. In: *Nat Commun* 6 (2015), p. 8364.

[238] R.-H. Chen, A. Shevchenko, M. Mann, and A. W. Murray. “Spindle Checkpoint Protein Xmad1 Recruits Xmad2 to Unattached Kinetochores”. In: *J. Cell Biol.* 143.2 (1998), pp. 283–295.

[239] T. Hiratsuka. “New ribose-modified fluorescent analogs of adenine and guanine nucleotides available as substrates for various enzymes”. In: *Biochim. Biophys. Acta* 742.3 (Feb. 1983), pp. 496–508.

[240] Q. Ni, J. Shaffer, and J. A. Adams. “Insights into nucleotide binding in protein kinase A using fluorescent adenosine derivatives”. In: *Protein Sci.* 9.9 (Sept. 2000), pp. 1818–1827.

[241] R. C. Edgar. “MUSCLE: multiple sequence alignment with high accuracy and high throughput”. In: *Nucleic Acids Res.* 32.5 (2004), pp. 1792–1797.

[242] H. Ashkenazy, E. Erez, E. Martz, T. Pupko, and N. Ben-Tal. “ConSurf 2010: calculating evolutionary conservation in sequence and structure of proteins and nucleic acids”. In: *Nucleic Acids Res.* 38.suppl 2 (2010), W529–W533.

[243] L. A. Kelley and M. J. Sternberg. “Protein structure prediction on the Web: a case study using the Phyre server”. In: *Nat Protoc* 4.3 (2009), pp. 363–371.

[244] D. T. Jones. “Protein secondary structure prediction based on position-specific scoring matrices1”. In: *J. Mol. Biol.* 292.2 (1999), pp. 195–202.

[245] T. S. Walter, C. Meier, R. Assenberg, K. F. Au, J. Ren, A. Verma, J. E. Nettleship, R. J. Owens, D. I. Stuart, and J. M. Grimes. "Lysine methylation as a routine rescue strategy for protein crystallization". In: *Structure* 14.11 (Nov. 2006), pp. 1617–1622.

[246] O. Kleifeld, A. Doucet, A. Prudova, U. auf dem Keller, M. Gioia, J. N. Kizhakkedathu, and C. M. Overall. "Identifying and quantifying proteolytic events and the natural N terminome by terminal amine isotopic labeling of substrates". In: *Nat Protoc* 6.10 (Oct. 2011), pp. 1578–1611.

[247] R. Gassmann, A. Carvalho, A. J. Henzing, S. Ruchaud, D. F. Hudson, R. Honda, E. A. Nigg, D. L. Gerloff, and W. C. Earnshaw. "Borealin: a novel chromosomal passenger required for stability of the bipolar mitotic spindle". In: *J. Cell Biol.* 166.2 (July 2004), pp. 179–191.

[248] N. Jelluma, A. B. Brenkman, N. J. van den Broek, C. W. Cruijsen, M. H. van Osch, S. M. Lens, R. H. Medema, and G. J. Kops. "Mps1 phosphorylates Borealin to control Aurora B activity and chromosome alignment". In: *Cell* 132.2 (Jan. 2008), pp. 233–246.

[249] E. Bourhis, A. Lingel, Q. Phung, W. J. Fairbrother, and A. G. Cochran. "Phosphorylation of a borealin dimerization domain is required for proper chromosome segregation". In: *Biochemistry* 48.29 (July 2009), pp. 6783–6793.

[250] A. M. Waterhouse, J. B. Procter, D. M. A. Martin, M. Clamp, and G. J. Barton. "Jalview Version 2 A multiple sequence alignment editor and analysis workbench". In: *Bioinformatics* 25.9 (2009), pp. 1189–1191.

[251] V. M. Bolanos-Garcia, T. Lischetti, D. Matak-Vinkovi?, E. Cota, P. J. Simpson, D. Y. Chirgadze, D. R. Spring, C. V. Robinson, J. Nilsson, and T. L. Blundell. "Structure of a Blinkin-BUBR1 complex reveals an interaction crucial for kinetochore-mitotic checkpoint regulation via an unanticipated binding Site". In: *Structure* 19.11 (Nov. 2011), pp. 1691–1700.

[252] J. M. Murphy et al. "A robust methodology to subclassify pseudokinases based on their nucleotide-binding properties". In: *Biochem. J.* 457.2 (2014), pp. 323–334.

[253] T. Kruse, G. Zhang, M. S. Larsen, T. Lischetti, W. Streicher, T. Kragh Nielsen, S. P. Bjørn, and J. Nilsson. "Direct binding between BubR1 and B56-PP2A phosphatase complexes regulate mitotic progression". In: *J. Cell. Sci.* 126.Pt 5 (Mar. 2013), pp. 1086–1092.

[254] A. S. Shaw, A. P. Kornev, J. Hu, L. G. Ahuja, and S. S. Taylor. "Kinases and pseudokinases: lessons from RAF". In: *Mol. Cell. Biol.* 34.9 (May 2014), pp. 1538–1546.

[255] W. Qi and H. Yu. "KEN-Box-dependent Degradation of the Bub1 Spindle Checkpoint Kinase by the Anaphase-promoting Complex/Cyclosome". In: *J. Biol. Chem.* 282.6 (2007), pp. 3672–3679.

[256] T. W. Seeley, L. Wang, and J. Y. Zhen. "Phosphorylation of human MAD1 by the BUB1 kinase in vitro". In: *Biochem. Biophys. Res. Commun.* 257.2 (Apr. 1999), pp. 589–595.

[257] P. Creixell, A. Palmeri, C. J. Miller, H. J. Lou, C. C. Santini, M. Nielsen, B. E. Turk, and R. Linding. "Unmasking Determinants of Specificity in the Human Kinome". In: *Cell* 163.1 (2015), pp. 187–201.

[258] Y. Hashimoto, S. Zhang, S. Zhang, Y.-R. Chen, and G. Blissard. "Correction: BTI-Tnao38, a new cell line derived from Trichoplusia ni, is permissive for AcMNPV infection and produces high levels of recombinant proteins". In: *BMC Biotechnology* 12.1 (2012), p. 12.

[259] J. Painter and E. A. Merritt. "Optimal description of a protein structure in terms of multiple groups undergoing TLS motion". In: *Acta Cryst. D Biol. Cryst.* 62.Pt 4 (Apr. 2006), pp. 439–450.

[260] Z. Zhang and A. G. Marshall. "A universal algorithm for fast and automated charge state deconvolution of electrospray mass-to-charge ratio spectra". In: *J. Am. Soc. Mass Spectrom.* 9.3 (Mar. 1998), pp. 225–233.

[261] J. Cox and M. Mann. "MaxQuant enables high peptide identification rates, individualized p.p.b.-range mass accuracies and proteome-wide protein quantification". In: *Nat. Biotechnol.* 26.12 (Dec. 2008), pp. 1367–1372.

[262] Schrödinger, LLC. "The PyMOL Molecular Graphics System, Version 1.3r1". Aug. 2010.

[263] S. McNicholas, E. Potterton, K. S. Wilson, and M. E. M. Noble. "Presenting your structures: the *CCP*4*mg* molecular-graphics software". In: *Acta Cryst. Sec. D* 67.4 (Apr. 2011), pp. 386–394.

[264] D. J. Fitzgerald, P. Berger, C. Schaffitzel, K. Yamada, T. J. Richmond, and I. Berger. "Protein complex expression by using multigene baculoviral vectors". In: *Nat. Methods* 3.12 (Dec. 2006), pp. 1021–1032.

[265] S. Trowitzsch, C. Bieniossek, Y. Nie, F. Garzoni, and I. Berger. "New baculovirus expression tools for recombinant protein complex production". In: *J. Struct. Biol.* 172.1 (Oct. 2010), pp. 45–54.

[266] P. N. Dyer, R. S. Edayathumangalam, C. L. White, Y. Bao, S. Chakravarthy, U. M. Muthurajan, and K. Luger. "Reconstitution of nucleosome core particles from recombinant histones and DNA". In: *Meth. Enzymol.* 375 (2004), pp. 23–44.

[267] A. Guse, C. J. Fuller, and A. F. Straight. "A cell-free system for functional centromere and kinetochore assembly". In: *Nat Protoc* 7.10 (Oct. 2012), pp. 1847–1869.

[268] U. K. Laemmli. "Cleavage of structural proteins during the assembly of the head of bacteriophage T4". In: *Nature* 227.5259 (Aug. 1970), pp. 680–685.

[269] P. H. Brown and P. Schuck. "Macromolecular size-and-shape distributions by sedimentation velocity analytical ultracentrifugation". In: *Biophys. J.* 90.12 (June 2006), pp. 4651–4661.

[270] J. B. Fenn, M. Mann, C. K. Meng, S. F. Wong, and C. M. Whitehouse. "Electrospray ionization for mass spectrometry of large biomolecules". In: *Science* 246.4926 (Oct. 1989), pp. 64–71.

[271] J. Rappsilber, M. Mann, and Y. Ishihama. "Protocol for micro-purification, enrichment, pre-fractionation and storage of peptides for proteomics using StageTips". In: *Nat Protoc* 2.8 (2007), pp. 1896–1906.

[272] A. Michalski, E. Damoc, J.-P. Hauschild, O. Lange, A. Wieghaus, A. Makarov, N. Nagaraj, J. Cox, M. Mann, and S. Horning. "Mass Spectrometry-based Proteomics Using Q Exactive, a High-performance Benchtop Quadrupole Orbitrap Mass Spectrometer". In: *Mol. Cell. Proteomics* 10.9 (2011).

[273] J. V. Olsen, B. Macek, O. Lange, A. Makarov, S. Horning, and M. Mann. "Higher-energy C-trap dissociation for peptide modification analysis". In: *Nat. Methods* 4.9 (Sept. 2007), pp. 709–712.

[274] F. Herzog, A. Kahraman, D. Boehringer, R. Mak, A. Bracher, T. Walzthoeni, A. Leitner, M. Beck, F.-U. Hartl, N. Ban, L. Malmström, and R. Aebersold. "Structural Probing of a Protein Phosphatase 2A Network by Chemical Cross-Linking and Mass Spectrometry". In: *Science* 337.6100 (2012), pp. 1348–1352.

[275] A. Maiolica, D. Cittaro, D. Borsotti, L. Sennels, C. Ciferri, C. Tarricone, A. Musacchio, and J. Rappsilber. "Structural Analysis of Multiprotein Complexes by Cross-linking, Mass Spectrometry, and Database Searching". In: *Mol. Cell. Proteomics* 6.12 (2007), pp. 2200–2211.

[276] W. Kabsch. "*XDS*". In: *Acta Cryst. Sec. D* 66.2 (Feb. 2010), pp. 125–132.

[277] A. J. McCoy, R. W. Grosse-Kunstleve, P. D. Adams, M. D. Winn, L. C. Storoni, and R. J. Read. "*Phaser* crystallographic software". In: *J. Appl. Crystallogr.* 40.4 (Aug. 2007), pp. 658–674.

[278] P. D. Adams, P. V. Afonine, G. Bunkóczi, V. B. Chen, I. W. Davis, N. Echols, J. J. Headd, L.-W. Hung, G. J. Kapral, R. W. Grosse-Kunstleve, A. J. McCoy, N. W. Moriarty, R. Oeffner, R. J. Read, D. C. Richardson, J. S. Richardson, T. C. Terwilliger, and P. H. Zwart. "*PHENIX*: a comprehensive Python-based system for macromolecular structure solution". In: *Acta Cryst. Sec. D* 66.2 (Feb. 2010), pp. 213–221.

[279] P. Emsley and K. Cowtan. "*Coot*: model-building tools for molecular graphics". In: *Acta Cryst. Sec. D* 60.12 Part 1 (Dec. 2004), pp. 2126–2132.

[280] P. Emsley, B. Lohkamp, W. G. Scott, and K. Cowtan. "Features and development of *Coot*". In: *Acta Cryst. Sec. D* 66.4 (Apr. 2010), pp. 486–501.

[281] V. B. Chen, W. B. Arendall III, J. J. Headd, D. A. Keedy, R. M. Immormino, G. J. Kapral, L. W. Murray, J. S. Richardson, and D. C. Richardson. "*MolProbity*: all-atom structure validation for macromolecular crystallography". In: *Acta Cryst. Sec. D* 66.1 (Jan. 2010), pp. 12–21.

[282] I. W. Davis, A. Leaver-Fay, V. B. Chen, J. N. Block, G. J. Kapral, X. Wang, L. W. Murray, W. B. Arendall, J. Snoeyink, J. S. Richardson, and D. C. Richardson. "MolProbity: all-atom contacts and structure validation for proteins and nucleic acids". In: *Nucleic Acids Res.* 35.suppl 2 (2007), W375–W383.

Acknowledgements

Foremost, I would like to express my sincere gratitude to my advisor Prof. Andrea Musacchio for the opportunity to join his laboratory as a PhD student, for continuous support of my research, for his patience, enthusiasm, and discussions. I would like to thank the other members of my internal advisory committee, Prof. Roger Goody and Dr. Alex Bird for the scientific guidance they provided through the course of the research project. Finally, I would like to thank Prof. Daniel Rauh for taking the time to serve as the second evaluator of my thesis.

A very special thanks goes out to all past and present members of Department I at the MPI Dortmund, for fruitful scientific discussions, sharing reagents and technical knowhow. I am most grateful for an excellent working atmosphere that extends beyond the walls of the laboratory, therefore enriches and motivates even working weekends.
In particular, I must acknowledge Doro Vogt, Marion Pesenti, Charlotte Smith, Ivana Primorac, Anika Altenfeld, Maria Thanasoula and Alex Faesen for the kind provision of countless proteins. Appreciation also goes out to John Weir, Ingrid Vetter and Arthur Porfetye for all of their patience and explanations regarding X-ray crystallography and technical expertise in crystallogenesis as well as everyone who went to the synchrotron to measure crystals and collect datasets. I am deeply indebted to Franz Herzog for the great collaboration and exceptional support on cross-linking and mass spectrometry, Franziska Müller and Tanja Bange for the readiness and dedicated analysis of phosphorylation sites on numerous proteins. Thanks are due to Arsen Petrovic who generously and superbly served as a guide through the jungle of analytical ultracentrifugation, Federica Basilico and Doro Vogt for invaluable time and effort put in introducing me to the world of nucleosome reconstitution. I wish to thank Alex Faesen for contibuting to precious ideas and stimulating discussions, Sascha Gentz for peptide synthesis, the DPF (Astrid Sander, Tina Rogowsky) for insect cell protein purification. In conclusion, I recognise that this thesis would not have been possible without the many volunteering proofreaders, inside and outside of the laboratory.
My sincere thanks goes to Antje Peukert who was always very supportive in removing bureaucratic barriers throughout my time as a graduate student and especially Christa Hornemann for the times of critical need in which her assistance helped to follow the way through to the end.
I would also like to thank my fellow friends Anika Altenfeld, Stefan Baumeister, Kathrin Estel, Arthur Porfetye, and specifically Kerstin Klare for our joint lunch ventures, exchanges of knowledge, (guitar) skills, and venting of frustration during our concurrent theses, which all considerably added to enriching the experience. Along the same lines, I am immensely grateful for the time spent with Federica Basilico and Charlotte Smith, both excellent exercising company. Additionally, I am filled with gratitude and pride regarding the numerous projects, Charlotte and I tackled during (cr)afternoons.
I wish to thank my family and friends, in particular my parents and brother, the former and current members of the Doppelkopf gang, Steffi and Matthias for the support they provided me through the years and without whose love, encouragement, distractions and editing assistance, I would not have finished this thesis.

Affidavit (Eidesstattliche Erklärung)

Eidesstattliche Versicherung (Affidavit)

BREIT, Claudia — Name, Vorname (Surname, first name)

154810 — Matrikel-Nr. (Enrolment number)

Belehrung:

Wer vorsätzlich gegen eine die Täuschung über Prüfungsleistungen betreffende Regelung einer Hochschulprüfungsordnung verstößt, handelt ordnungswidrig. Die Ordnungswidrigkeit kann mit einer Geldbuße von bis zu 50.000,00 € geahndet werden. Zuständige Verwaltungsbehörde für die Verfolgung und Ahndung von Ordnungswidrigkeiten ist der Kanzler/die Kanzlerin der Technischen Universität Dortmund. Im Falle eines mehrfachen oder sonstigen schwerwiegenden Täuschungsversuches kann der Prüfling zudem exmatrikuliert werden, § 63 Abs. 5 Hochschulgesetz NRW.

Die Abgabe einer falschen Versicherung an Eides statt ist strafbar.

Wer vorsätzlich eine falsche Versicherung an Eides statt abgibt, kann mit einer Freiheitsstrafe bis zu drei Jahren oder mit Geldstrafe bestraft werden, § 156 StGB. Die fahrlässige Abgabe einer falschen Versicherung an Eides statt kann mit einer Freiheitsstrafe bis zu einem Jahr oder Geldstrafe bestraft werden, § 161 StGB.

Die oben stehende Belehrung habe ich zur Kenntnis genommen:

Official notification:

Any person who intentionally breaches any regulation of university examination regulations relating to deception in examination performance is acting improperly. This offence can be punished with a fine of up to EUR 50,000.00. The competent administrative authority for the pursuit and prosecution of offences of this type is the chancellor of the TU Dortmund University. In the case of multiple or other serious attempts at deception, the candidate can also be unenrolled, Section 63, paragraph 5 of the Universities Act of North Rhine-Westphalia.

The submission of a false affidavit is punishable.

Any person who intentionally submits a false affidavit can be punished with a prison sentence of up to three years or a fine, Section 156 of the Criminal Code. The negligent submission of a false affidavit can be punished with a prison sentence of up to one year or a fine, Section 161 of the Criminal Code.

I have taken note of the above official notification.

Dortmund, im November 2015 — Ort, Datum (Place, date)

Unterschrift (Signature)

Titel der Dissertation:
(Title of the thesis):

Biochemical studies of spindle assembly checkpoint components

Ich versichere hiermit an Eides statt, dass ich die vorliegende Dissertation mit dem Titel selbstständig und ohne unzulässige fremde Hilfe angefertigt habe. Ich habe keine anderen als die angegebenen Quellen und Hilfsmittel benutzt sowie wörtliche und sinngemäße Zitate kenntlich gemacht.
Die Arbeit hat in gegenwärtiger oder in einer anderen Fassung weder der TU Dortmund noch einer anderen Hochschule im Zusammenhang mit einer staatlichen oder akademischen Prüfung vorgelegen.

I hereby swear that I have completed the present dissertation independently and without inadmissible external support. I have not used any sources or tools other than those indicated and have identified literal and analogous quotations.

The thesis in its current version or another version has not been presented to the TU Dortmund University or another university in connection with a state or academic examination.*

*Please be aware that solely the German version of the affidavit ("Eidesstattliche Versicherung") for the PhD thesis is the official and legally binding version.

Dortmund, im November 2015 — Ort, Datum (Place, date)

Unterschrift (Signature)